

UCSF

UC San Francisco Electronic Theses and Dissertations

Title

Familial Cortical Myoclonus Caused by Mutation in NOL3

Permalink

<https://escholarship.org/uc/item/35r3d8kq>

Author

Russell, Jonathan Foster

Publication Date

2013

Peer reviewed|Thesis/dissertation

Familial Cortical Myoclonus Caused by Mutation in *NOL3*

by

Jonathan Foster Russell

DISSERTATION

Submitted in partial satisfaction of the requirements for the degree of

DOCTOR OF PHILOSOPHY

in

Biomedical Sciences

in the

Copyright 2013

by

Jonathan Foster Russell

I dedicate this dissertation to Mom and Dad, for their adamant love and support

No man has earned the right to intellectual ambition until he has learned to lay his course by a star which he has never seen—to dig by the divining rod for springs which he may never reach. In saying this, I point to that which will make your study heroic. For I say to you in all sadness of conviction, that to think great thoughts you must be heroes as well as idealists. Only when you have worked alone – when you have felt around you a black gulf of solitude more isolating than that which surrounds the dying man, and in hope and in despair have trusted to your own unshaken will – then only will you have achieved. Thus only can you gain the secret isolated joy of the thinker, who knows that, a hundred years after he is dead and forgotten, men who never heard of him will be moving to the measure of his thought—the subtle rapture of a postponed power, which the world knows not because it has no external trappings, but which to his prophetic vision is more real than that which commands an army.

-Oliver Wendell Holmes, Jr.

ACKNOWLEDGMENTS

I am humbled by the efforts of many, many others who were essential for this work. To be provided the privilege of pursuing truth as a profession requires the stars to align. For me, they have.

I wish to thank my thesis advisor, Louis J. Ptáček, M.D., for his mentorship. During the course of my interviews with about 50 MSTP faculty members across the country, the most challenging interview I had was with Louis! It didn't scare me off, though: I appreciated the intensity of his questions and the direction of the science, and I was eager to join the lab. Louis took me under his wing as a neophyte first-year medical student, and he has provided me with priceless advice and encouragement over the last four years.

I have benefitted immensely from the help of many members of the laboratory, viz.: S.Y. (Christin) Chong, Ph.D., Mary Heng, Ph.D., Lorna Kategaya, Ph.D., Sehoon Keum, Ph.D., Mary Lange, Hsien-Yang Lee, Ph.D., Emily Quinn, Jenise C. Wong, M.D., Ph.D., Linda Zhang, and Ying Zhang. Zachery Kornberg aided me with the linkage and Sanger sequencing. I could not have performed the FACS experiments without Philip Kurien, M.D. The biochemistry expertise of William (Casey) Hallows, Ph.D., was critical. Perhaps more importantly, he was a fun guy to eat lunch with daily. I am especially indebted to Shen-Yi (Bruce) Howng, Ph.D., for serving as my scientific sounding board, and for his friendship. Over the past few years I spent many (most?) of my waking hours working alongside Bruce. There may never again be a time in my life when I have the freedom and environs for such frequent, deep, freewheeling discussions. I will always cherish them.

I am grateful to the many UCSF faculty members who took time out of their incredibly busy lives to generously offer their mentorship. I thank Daniel H. Lowenstein, M.D., Scott A. Oakes, M.D., and Anthony Wynshaw-Boris, M.D., Ph.D., for their service and helpful advice during my qualifying exam. Kevin M. Shannon, M.D., directed the MSTP and provided invaluable experimental suggestions and career advice during my dissertation committee meetings. Kevin also repeatedly demonstrated that he could beat me in golf. Finally, Robert L. Nussbaum, M.D., has guided my development for five years: first as my MSTP advisor, then as my BMS advisor, then as chair of my qualifying exam committee, and ultimately as chair of my dissertation committee. His scientific insight, ethical standards, and moral support were all far beyond the call of duty. I am willing to bet that faculty advisors underestimate the influence of a meeting that takes place each quarter and may only last an hour. More than once I entered Bob's office deep in the throes of graduate school despondency, and yet he found a way to buoy my spirits. This was, as they say, nontrivial. His creed – to never lose sight of our patients, for they are the reason we do science – has become mine.

Many others at UCSF were critical to this work, including Jana Toutolmin and Catherine Norton in the MSTP office, and Lisa Magargal et al. in the BMS office. MacKenzie A. Howard, Ph.D. and Scott C. Baraban, Ph.D., helped with electrophysiological characterization of *NOL3* knockout mice. Jonathan Trinidad, Ph.D., assisted with mass spectrometry experiments.

I was lucky to benefit from numerous collaborations outside of UCSF. Jamie L. Steckley, M.D., Angelika F.G. Hahn, M.D., and their colleagues at London Health Science University and other universities in Canada phenotyped the patients and col-

lected DNA samples. Giovanni Coppola, M.D., Daniel H. Geschwind, M.D., Ph.D., and others at UCLA performed targeted sequencing. Joe Quadrilatero, Ph.D., of the University of Waterloo generously shared *Nol3* knockout mice. Peter Kuffa and Gabriel Nunez, Ph.D., of the University of Michigan shared human *NOL3* cDNA constructs. Kinya Ishikawa, M.D., Ph.D., of Tokyo Medical and Dental University dug through his freezers and transcribed the sequences of many primer sequences for the *BEAN*, *tk2*, and *FLJ27243* genes. The *Nol3* knockin mouse was generated through collaborations with inGenious Targeting Laboratory, Inc., and with Caiying Guo, Ph.D., of the Howard Hughes Medical Institute Janelia Farm Research Campus. The proteomic screen was done in collaboration with Applied Biomics. It goes without saying that we are forever indebted to the patients and their families for their participation.

Graduate school is just one stop of many on my educational journey, and I would be remiss to omit important teachers and mentors at prior junctions. They have influenced me greatly. They include Tas Anthony, Margaret Shullaw, and James Ruebush at Iowa City West High School; Alejandro Aballay, Ph.D., David Brady, Ph.D., Kevin DeLapp, Ph.D., Kylie A. Haskins, Ph.D., V. Louise Roth, Ph.D., and Thomas P. Witelski, Ph.D., at Duke University; and Louise Aronson, M.D., and Don Ganem, M.D., at UCSF School of Medicine.

Personal financial support was provided by the UCSF MSTP (funded by NIH NIGMS grant T32GM07618 and the UCSF School of Medicine), and later by NIH NINDS grant F31NS077533. The research itself was funded by NIH grants NS044379 and U54 RR19481, by the Sandler Fund for Neurogenetics, and by the Howard Hughes Medical Institute. In the stress generated by interminable grant applications, we often

lose sight of the fact that, historically, it is a very recent phenomenon for anyone other than a select group of aristocrats to have the wherewithal to conduct meaningful scientific research. I am grateful to be born in this age and for the resources that modern society chooses to allocate for research. That they go towards science rather than guns or butter underscores our responsibility to conduct our research nobly.

Lastly, I wish to express my heartfelt dependence upon my friends and especially my family. My fiancée has offered unyielding support throughout the ecstasy and agony of graduate school. Her love, loyalty, good cheer, and unconditional kindness made it less agony, mostly ecstasy. My grandparents have loved and provided for me in innumerable ways. My brother, sister, sister-in-law, nephews, and niece were all constant sources of joy and encouragement. Most importantly, I have always been able to count on my parents. I can be a trying child, yet they are a wellspring of emotional, financial, and moral ballast. They instilled in us a thirst for knowledge that cannot be slaked, ethical standards requiring constant vigilance, and a love for man that necessitates improving his lot. These principles have impelled this work. For these reasons, I dedicate this dissertation to them.

ABSTRACT

Familial Cortical Myoclonus Caused by Mutation in *NOL3*

Jonathan Foster Russell

Many neurologic diseases cause discrete episodic impairment. Study of the genes and mechanisms underlying these diseases has informed our understanding of the nervous system. Here we describe a novel episodic neurologic disorder, which we term familial cortical myoclonus (FCM). FCM is characterized by adult onset, slowly progressive, multifocal, cortical myoclonus, inherited as an autosomal dominant trait. On the basis of clinical, electrophysiological, and genetic data, FCM is nosologically distinct. We utilized genome-wide single nucleotide polymorphism genotyping, microsatellite linkage, and massively parallel sequencing to identify a mutation in the gene *nucleolar protein 3* (*NOL3*) that likely causes FCM. *NOL3* is thought to bind to pro-apoptotic proteins and thereby repress apoptosis, but our extensive experimentation did not replicate these claims. In vitro, the *NOL3* mutation leads to post-translational modification of *NOL3* protein. We could not pinpoint the identity of the modification, but did find that this process is regulated by phosphorylation at residue T114. Finally, a proteomic screen for novel binding partners identified two candidates that modulate neuronal/astroglial differentiation. We hypothesize that the *NOL3* mutation abrogates these interactions to cause FCM. This hypothesis will be tested with *Nol3* mutant mice that we generated. In total, this work defines a novel episodic neurologic phenotype and the associated mutation, calls into question some of the published functions of *NOL3*, and presents an alternative mechanism that may explain the pathophysiology of FCM.

TABLE OF CONTENTS

Chapter I

An Overview of Episodic Neurologic Disorders..... 1

Chapter II

Familial Cortical Myoclonus, a Novel Movement Disorder..... 57

Chapter III

Identification of a Mutation in *NOL3*..... 86

Chapter IV

Functional Characterization of the *NOL3* Mutation..... 127

Chapter V

Conclusion..... 212

LIST OF TABLES

Chapter I

Table 1. Diagnosis of complex episodic disorders.....	9
---	---

Chapter II

Table 1. Clinical characteristics in 11 affected family members.....	72
--	----

Chapter III

Table 1. Genome-wide SNP array.....	103
Table 2. Three putative shared regions identified by SNP IBD analysis.....	104
Table 3. Critical region pairwise LOD analysis.....	108
Table 4. Targeted DNA capture and massively parallel sequencing reads (A) and variants (B).....	110
Table 5. Novel non-synonymous coding variants in critical region identified by targeted DNA capture and massively parallel sequencing.....	113

Chapter IV

Table 1. Primers used for cloning mutant <i>NOL3</i> constructs.....	141
Table 2. Novel <i>NOL3</i> binding partners identified by co-immunoprecipitation and differential two-dimensional gel electrophoresis.....	185

Appendices

Appendix 1. Microsatellite markers and primers for linkage analysis.....	220
Appendix 2. Critical region contains 113 known or predicted genes.....	222
Appendix 3. Primers for Sanger sequencing select candidate genes in critical region.....	226
Appendix 4. <i>NOL3</i> primers.....	231
Appendix 5. Detailed characterization of knockin mouse generation.....	232

LIST OF FIGURES

Chapter I

Figure 1. The landscape of episodic neurologic disorders.....	4
Figure 2. Channelopathy mechanisms.....	11
Figure 3. Beyond the channelopathy paradigm: mechanisms of synaptopathy and circuitopathy.....	21

Chapter II

Figure 1. Extended family pedigree.....	69
Figure 2. Somatosensory evoked potentials in the familial cortical myoclonus family.....	74
Figure 3. Functional magnetic resonance imaging in the familial cortical myoclonus family.....	74
Figure 4. Additional patients with a history of cortical myoclonus that may be familial.....	76

Chapter III

Figure 1. Microsatellite linkage genotyping methodology.....	95
Figure 2. Genome-wide SNP mapping identified 3 candidate linkage regions.....	104
Figure 3. Genetic and physical map positions of microsatellite markers....	105
Figure 4. Pedigree with chromosome 16q21-22.1 haplotypes.....	106
Figure 5. Fine mapping of critical region.....	107
Figure 6. Coverage (post-duplicate removal) by massively parallel sequencing over the entire region on chromosome 16 (top) and by coding sequence of each gene (bottom).....	111
Figure 7. Alignment of short sequence reads (post-duplicate removal) over the <i>NOL3 E21Q</i> sequence variant.....	112
Figure 8. Sanger sequencing chromatographs (electropherograms) confirmed cosegregation of the NM_001185058.1:c.61G>C variant, predicted to cause an <i>E21Q</i> mutation in <i>NOL3</i>	113

Chapter IV

Figure 1. Overview of published functions of <i>NOL3</i>	129
Figure 2. <i>NOL3</i> protein contains a C-terminal proline(P)/ glutamate(E) domain, and an N-terminal caspase activation recruitment domain (CARD).....	131

Figure 3. NOL3 amino acid sequence is highly conserved across species...	154
Figure 4. Alignment of amino acid sequences of human genes containing CARDS.....	156
Figure 5. NOL3 protein secondary structure predictions.....	157
Figure 6. In silico homology modelling of WT and E21Q NOL3 protein structure predicts that E21Q alters the electrostatic surface potential of NOL3.....	158
Figure 7. Expression of <i>Nol3</i> RNA in the murine brain.....	159
Figure 8. <i>Nol3</i> may be more highly expressed in oligodendrocytes than astrocytes.....	160
Figure 9. Expression of <i>Nol3</i> in various murine brain cell types.....	161
Figure 10. <i>NOL3</i> RNA expression during development in humans.....	162
Figure 11. <i>NOL3</i> RNA is expressed at comparable levels in various human brain regions.....	163
Figure 12. The <i>E21Q</i> mutation does not affect cytoplasmic expression of NOL3-FLAG in SK-N-SH cells, a cell line of neuronal origin....	165
Figure 13. Neither WT nor E21Q NOL3-FLAG localize to mitochondria in HEK293 cells.....	166
Figure 14. NOL3 ^{E21Q} -FLAG exhibits altered post-translational modification in HEK293 cells.....	167
Figure 15. NOL3-FLAG protein is present at equal levels in <i>WT</i> and <i>E21Q</i> stable cell lines.....	168
Figure 16. In vitro phosphatase treatment does not remove mutant- enriched upper band.....	169
Figure 17. <i>T114A</i> mutation abrogates formation of upper band in mutant (<i>E21Q</i>) background.....	171
Figure 18. Coomassie staining demonstrates robust purification of NOL3-FLAG prior to mass spectrometry analysis.....	173
Figure 19. T114 is hyper-phosphorylated in both mutant upper and lower bands, relative to WT.....	173
Figure 20. FACS double stain approach for apoptosis analysis.....	178
Figure 21. Expression of either <i>WT</i> or <i>E21Q NOL3</i> predisposes HEK293 cells to apoptosis at baseline.....	180
Figure 22. Quantification of FACS data confirms that <i>NOL3</i> expression predisposes to apoptosis at baseline.....	181
Figure 23. Putative pro-apoptotic binding partners do not interact with NOL3.....	182
Figure 24. Two-dimensional gel electrophoresis of co- immunoprecipitates obtained from Vehicle or <i>WT NOL3</i> HEK293 cells.....	184
Figure 25. Somatosensory evoked potentials in aged <i>Nol3</i> ^{-/-} (KO) and <i>Nol3</i> ^{+/+} (WT) littermate control mice.....	187
Figure 26. Generation of mice with knockin allele or conditional knockout allele at the <i>Nol3</i> locus.....	189

CHAPTER I

An Overview of Episodic Neurologic Disorders

SUMMARY

Many neurologic diseases cause discrete episodic impairment in contrast with progressive deterioration. The symptoms of these episodic disorders exhibit striking variety. Herein we review what is known of the phenotypes, genetics, and pathophysiology of episodic neurologic disorders. Of these, most are genetically complex, with unknown or polygenic inheritance. Four are very common: transient ischemic attack, syncope, epilepsy, and migraine. Many other symptomatically similar disorders are complex and rare, as exemplified by episodic disorders with autoimmune etiology. In contrast, a fascinating panoply of episodic disorders exhibit Mendelian inheritance. We classify episodic Mendelian disorders according to the primary neuroanatomical location affected: skeletal muscle, cardiac muscle, neuromuscular junction, peripheral nerve, or central nervous system (CNS). Most known Mendelian mutations alter genes that encode membrane-bound ion channels. These mutations cause ion channel dysfunction, which ultimately leads to altered membrane excitability as manifested by episodic disease. Other Mendelian disease genes encode proteins essential for ion channel trafficking or stability. In fact, autoimmune episodic disorders share the pathophysiological endpoint of ion channel dysfunction. These observations have cemented the “channelopathy” paradigm, in which episodic disorders are conceptualized as disorders of ion channels. However, we expand upon this paradigm to propose that dysfunction at the synaptic and neuronal circuit levels may underlie some episodic neurologic entities.

INTRODUCTION

Whereas many diseases of the nervous system cause progressive deterioration, a sizable fraction of them are predominantly episodic in nature. In this subset of disorders, a patient's neurologic function is impaired during an episode (also known as an attack). Although some patients may suffer from superimposed, chronic neurologic dysfunction, between attacks patients are usually completely normal. Episodes are often triggered by mundane stimuli, such as hunger, fatigue, emotions, stress, exercise, diet, temperature, or hormones. Why these commonplace stimuli trigger episodes of neurologic impairment in some patients but not others is poorly understood.

Many episodic neurologic disorders exist, encompassing a protean range of symptoms. These may include weakness, stiffness, paralysis, arrhythmia, pain, ataxia, migraine, involuntary movements, and seizures. The vast majority of episodic neurologic disorders exhibit complex inheritance—that is, disease seems to develop primarily owing to environmental influences rather than genetic ones. In this review, we briefly address the complex disorders that are commonly encountered in clinical practice: transient ischemic attack, syncope, epilepsy, and migraine (**Figure 1**). Aside from these four diseases, which are complex and common, there exist a myriad of symptomatically similar diseases that are complex but rare. Of these, many are in fact progressive neurologic disorders that happen to feature episodic symptoms but are not primarily episodic in nature. However, others are indeed primarily episodic. In this chapter, we focus on those complex, rare disorders with autoimmune etiology because they have provided substantial pathophysiological insight. [CONTINUED, p. 5]

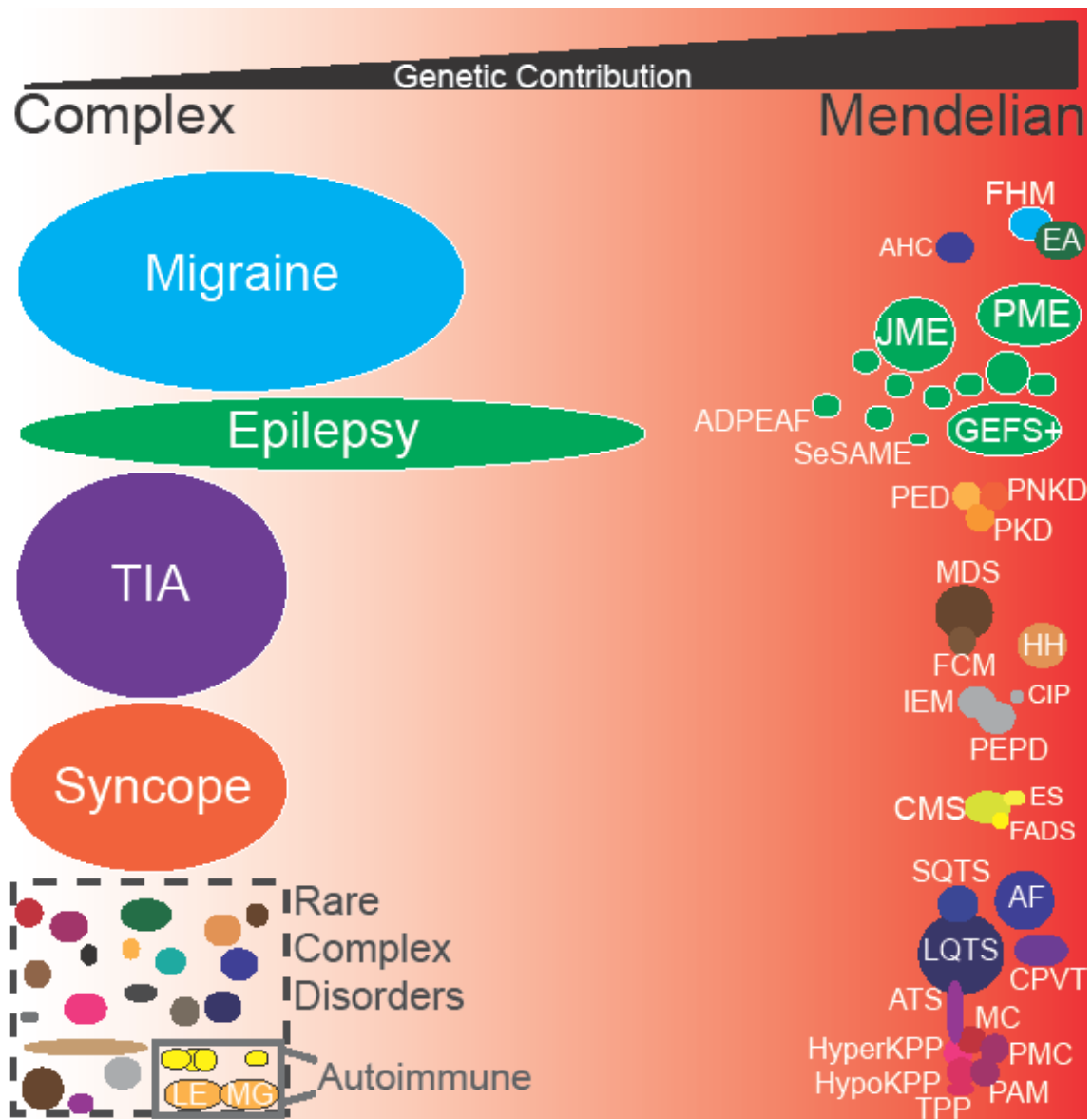


Figure 1. The landscape of episodic neurologic disorders.

There are many episodic neurologic disorders, with a vast range in genetic contribution and prevalence. Prevalence is depicted in crude approximation by the size of each ellipse. This fascinating group includes four common complex disorders (left), many rare complex disorders including autoimmune (lower left), and many rare Mendelian forms (right). Some Mendelian phenotypes exhibit profound similarity to particular complex disorders, as depicted by identical coloration (e.g., light green for idiopathic epilepsy and for Mendelian epilepsy syndromes). Often, Mendelian phenotypes share phenotypic and/or genetic characteristics, as depicted by overlap and/or similar coloration of each corresponding ellipse. Some complex disorders seem to have a substantial genetic contribution, particularly epilepsy, but most of the complex inheritance remains unexplained (middle). Abbreviations: ADPEAF, autosomal dominant partial epilepsy with auditory features; AF, atrial fibrillation; ATS, Andersen-Tawil syndrome; AHC, alternating hemiplegia of childhood; CIP, congenital insensitivity to pain; CMS, congenital myasthenic syndromes; CPVT, catecholaminergic polymorphic ventricular tachycardia; EA, epi-

sodic ataxia; ES, Escobar syndrome; FADS, fetal akinesia deformation sequence; FCM, familial cortical myoclonus; FHM, familial hemiplegic migraine; GEFS+, generalized epilepsy with febrile seizures plus; HH, hereditary hyperekplexia; HyperKPP, hyperkalemic periodic paralysis; HypoKPP, hypokalemic periodic paralysis; IEM, inherited erythromelalgia; JME, juvenile myoclonic epilepsy; LE, Lambert-Eaton myasthenic syndrome; LQTS, long QT syndrome; MC, myotonia congenita; MDS, myoclonus dystonia syndrome; MG, myasthenia gravis; PAM, potassium-aggravated myotonia; PED, paroxysmal exercise-induced dyskinesia; PEPD, paroxysmal extreme pain disorder; PKD, paroxysmal kinesigenic dyskinesia; PMC, paramyotonia congenita; PME, progressive myoclonic epilepsy; PNKD, paroxysmal non-kinesigenic dyskinesia; SeSAME, seizures, sensorineural deafness, ataxia, mental retardation, and electrolyte imbalance; SQTS, short QT syndrome; TIA, transient ischemic attack; TPP, thyrotoxic periodic paralysis.

For the same reason, the remaining bulk of this chapter focuses on episodic neurologic disorders that are Mendelian (**Figure 1**). Each is rare. For these disorders, single gene mutations are sufficient to cause disease. However, even in these genetic diseases, environmental factors can still be important in triggering attacks. Over the past two decades, medical geneticists have extensively clarified the known phenotypes, identified many novel phenotypes, and pinpointed scores of disease genes. In many cases, disease gene discovery has directly led to pathophysiological insight and, in a few cases, even novel treatments. We organize these diverse disorders on the basis of the primary neuroanatomical location affected: skeletal muscle, cardiac muscle, neuromuscular junction (NMJ), peripheral nerve, or CNS. As much as is possible given practical constraints, for each disorder we review the clinical presentation, genetics, and pathophysiology, with particular emphasis on new discoveries and unanswered questions. Finally, in the concluding section we present our view of the field's urgent challenges.

COMPLEX DISORDERS

Complex episodic neurologic disorders develop primarily due to environmental factors, although in most disorders some evidence indicates polygenic inheritance, which remains largely undeciphered (Poduri & Lowenstein 2011, Shyti et al. 2011, Della-Morte et al. 2012). Complex episodic disorders are very common in aggregate. This group includes a legion of causes that are each individually rare, such as autoimmune episodic disorders (see below). Also, four complex disorders are commonly encountered in clinical practice: transient ischemic attack, syncope, epilepsy, and migraine (**Figure 1**).

Four Common Complex Disorders

A transient ischemic attack (TIA) results from diminished cerebral perfusion that causes abrupt, focal neurological symptoms in a pattern corresponding to the compromised vascular distribution (Della-Morte et al. 2012). Cerebral hypoperfusion usually arises from platelet emboli or thrombi that transiently lodge in a cerebral artery but are dislodged before permanent neurologic injury develops; by definition, TIA symptoms resolve within 24 hours. Despite prompt resolution, TIAs typically recur over the course of days to weeks with a stereotypic symptom cluster. These patients should be promptly evaluated and treated, usually by addressing the source of emboli or by anticoagulation, to decrease the risk of progression to ischemic stroke (Della-Morte et al. 2012).

Transient cerebral hypoperfusion also results in syncope (i.e., fainting; Gauer 2011). Causes of hypoperfusion include orthostatic hypotension, neurovascular disease, decreased cardiac output (usually from arrhythmia), and neural reflexes. For example, a classic scenario is an unpleasant stimulus, such as a noisome odor, triggering a vasovagal

reflex of bradycardia and hypotension that leads to syncope. The clinical history and premonitory symptoms – fading vision, nausea, pallor, sweating, etc. – are typically diagnostic. Syncopal patients occasionally exhibit brief, mild myoclonic limb jerks or incontinence but are fully oriented upon awakening, distinguishing syncope from the postictal confusion of a true seizure.

Epilepsy is defined as recurrent seizures, which result from episodic cortical hyperexcitability. Generalized hyperexcitability manifests as unconsciousness, tonic-clonic convulsions, cyanosis, reactive hyperventilation, excessive salivation, and postictal confusion. In comparison, when hyperexcitability involves a focal neurologic region, the symptoms reflect the affected cortical region and vary widely depending on the particular epilepsy syndrome (Berg et al. 2010, Berg & Scheffer 2011). Epilepsy has manifold pathophysiologies, primarily structural, metabolic, neurodegenerative, idiopathic, and genetic (including some Mendelian forms; see below and **Figure 1**). Interestingly, seizures can be triggered by stressors such as infection, psychosomatic trauma, or menses.

The final common complex disorder is migraine. Migraine is characterized by episodic severe headache accompanied by nausea, photophobia, and phonophobia. Many patients experience prodromal symptoms hours to days before headache, which vary widely, and about one-quarter of patients experience aura, commonly visual, which immediately precedes the headache. The pathophysiology of migraine remains hotly disputed but probably involves both alterations in cortical excitability (i.e., cortical spreading depression) as well as transient vasoconstriction followed by vasodilatation of cere-

bral and meningeal vessels (Dodick 2008). Like epilepsy, migraine is commonly triggered by stressors (Haut et al. 2006).

A Myriad of Rare Complex Disorders

Episodic neurologic symptoms also occur in a wide range of complex disorders, each of which is individually rare (**Figure 1**). Many are diseases of progressive deterioration that happen to feature episodic symptoms, whereas others are primarily episodic in nature, after which the patient returns to normal baseline. For a given clinical finding, the differential diagnosis is typically extensive (**Table 1**). For example, myoclonus is a component of more than 200 disorders that span the spectrum of neurologic disease: structural malformations, infections, storage disorders, spinocerebellar degenerations, dementias, metabolic derangements, toxin/drug exposures, post-hypoxia, malabsorption (Celiac's disease), various epilepsy syndromes, and many more (Caviness & Brown 2004). The differential diagnosis can be just as broad for other episodic presentations (**Table 1**). Usually the diagnosis is suggested by the entire clinical history and examination rather than by episodic symptoms per se. If a diagnosis remains elusive, there is an increased probability of an autoimmune or Mendelian cause.

Table 1. Diagnosis of complex episodic disorders.

Episodic neurologic symptoms occur in a variety of complex disorders. The differential diagnosis for a given finding can be very broad. Select episodic presentations are provided along with references containing diagnostic approaches. We have omitted other presentations, such as arrhythmia, ataxia, hemiplegia, pain, paralysis, stiffness, and weakness.

Presentation	Reference(s) with diagnostic approach
Dyskinesia	Fahn et al. 2011
Exaggerated startle	Dreissen et al. 2012
Migraine	Haut et al. 2006
Myoclonus	Caviness & Brown 2004
Ophthalmic disorder	Sheffield & Stone 2011
Seizures	Berg et al. 2010, Berg et al. 2011
Sleep disorder	Sehgal & Mignot 2011
Syncope	Gauer 2011
TIA	Della-Morte et al. 2012

Rare complex disorders with autoimmune etiologies have provided especial insight into pathophysiology (Vincent et al. 2006, Kleopa 2011). Classically, these autoimmune episodic disorders are caused by autoantibodies against ion channels (**Figure 2A**). For example, ion channels at the NMJ are the targets of autoantibodies that cause muscle weakness in Lambert-Eaton myasthenic syndrome (LEMS) and myasthenia gravis (MG) (Vincent et al. 2006). Clinically, LEMS is characterized by proximal muscle weakness and autonomic dysfunction, whereas MG patients exhibit striking fatigability, particularly of ocular muscles. Both LEMS and MG must be distinguished from congenital myasthenic syndromes (see below), which also present with weakness but are juvenile onset and Mendelian rather than autoimmune in etiology. LEMS is caused by autoantibodies against presynaptic voltage-gated calcium channels, whereas MG is usually caused by autoantibodies against the nicotinic acetylcholine receptor (AChR) on the motor end plate. Recent work has tied AChR-seronegative MG to autoantibodies against

muscle-specific tyrosine kinase (MuSK) (Hoch et al. 2001) or low-density lipoprotein receptor-related protein 4 (Lpr4) (Higuchi et al. 2011, Pevzner et al. 2012). Neither of these targets are ion channels; instead, they function to promote postsynaptic clustering of the AChR channel (**Figure 2C**).

A compelling, recently elucidated example of autoantibodies interfering with targets other than ion channels to cause episodic disease is stiff-man syndrome (SMS). SMS is characterized by extreme muscle cramps superimposed upon progressive, fluctuating muscle rigidity and stiffness. Tragically, these symptoms are so severe that they often cause joint deformities, skeletal fractures, and even muscle rupture. Cramp attacks are triggered by movement, unanticipated somatosensory stimuli, stress, and strong emotions. Solimena et al. (1988) showed that 80% of patients develop auto-antibodies against glutamic acid decarboxylase (GAD) autoantibodies, but anti-GAD antibody infusion into model animals does not passively transfer SMS symptoms. Recently, Geis et al. (2010) achieved passive transfer in rats by infusing anti-amphiphysin antibodies collected from human SMS patients. Furthermore, anti-amphiphysin antibodies were internalized into CNS GABAergic neurons where they inhibited GABA (gamma-aminobutyric acid) release. This work demonstrates that SMS is caused by autoantibodies directed not against ion channels but rather against intracellular, pre-synaptic targets (**Figure 2C**). It seems likely that other autoimmune or “idiopathic” disorders may be caused by autoantibodies targeting intracellular, synaptic, or even non-neuronal targets (Lennon et al. 2005). [CONTINUED, p. 12]

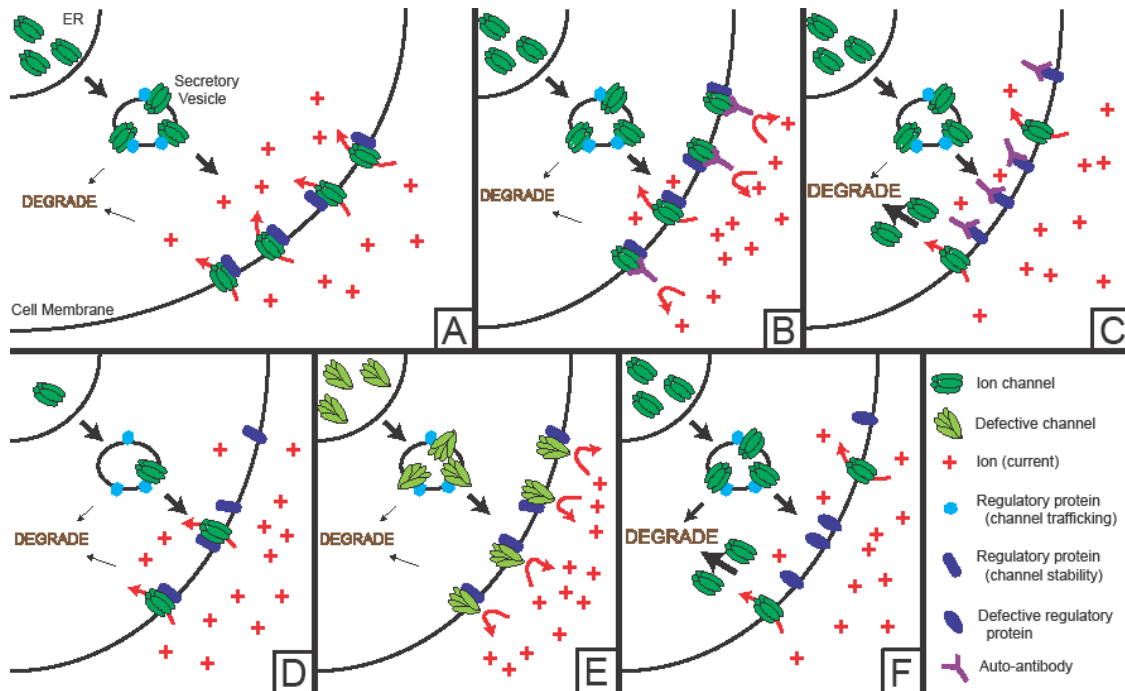


Figure 2. Channelopathy mechanisms.

(A) Normally, ion channels are trafficked from the endoplasmic reticulum (ER) via secretory vesicles to the cell membrane, where they conduct ions across the membrane to control cellular membrane potential and hence excitability.

(B) Many autoimmune episodic neurologic disorders are caused by autoantibodies binding to ion channels, which causes defective channel function, such as decreased ion permeability (shown here).

(C) Investigators have recently associated numerous autoimmune episodic disorders with autoantibodies against targets other than channels. These autoantibodies bind to channel-associated regulatory proteins, thereby indirectly causing defective channel function. Shown here are autoantibodies against a regulatory protein that stabilizes the channel at the membrane. Inhibition of this regulatory protein by autoantibody binding results in decreased channel stability, so more channels are degraded and overall current is decreased.

(D-E) Most episodic neurologic disorders that exhibit Mendelian inheritance are caused by mutations in ion channel genes. There are many different possible effects of mutations, including absent or decreased expression (D), defective trafficking or stability leading to premature degradation, decreased ion permeability (E), increased ion permeability, and altered channel kinetics (e.g., delayed inactivation).

(F) Aside from mutations in ion channels themselves, recent work has identified mutations in genes that do not encode channels. Like the targets of some autoantibodies (C), these genes encode regulatory proteins that bind to channels and are critical for channel stability and localization. When mutated, defective regulatory proteins result in aberrant channel trafficking or stability, premature channel degradation, and hence decreased current.

For panels B-F, see text for examples.

Another example of an autoimmune episodic disorder is Isaac's syndrome (neuromyotonia). Isaac's syndrome is a disorder of motor nerve hyperexcitability that can present with hyperhidrosis and a range of muscle symptoms including fasciculations, cramps, stiffness, myokymia (quivering), and pseudomyotonia (slow relaxation). For many years, Isaac's syndrome and two related disorders, Morvan's syndrome and limbic encephalitis, were thought to result from autoantibodies against voltage-gated potassium channels (Vincent et al. 2006). However, the data were mixed. Dalmau and colleagues recently presented strong evidence that these disorders are instead caused by autoantibodies against the Caspr2-Lgi1 complex, which associates with voltage-gated potassium channels on the motor nerve (Lai et al. 2010, Lancaster et al. 2011, Irani et al. 2012, Loukaides et al. 2012). These findings further illustrate an emerging understanding that in addition to targeting channels directly (**Figure 2B**), autoantibodies may target channel-associated regulatory proteins to cause channel dysfunction indirectly (**Figure 2C**).

MENDELIAN DISORDERS

General Characteristics

Although each is individually rare, many distinct episodic disorders exhibit Mendelian inheritance. Despite very strong genetic contributions, these diseases share striking similarity with the complex disorders discussed above in that patients are often completely normal between attacks, and attacks are often triggered by commonplace environmental stimuli.

We have organized the Mendelian episodic disorders on the basis of the focus of pathology within the nervous system: skeletal muscle, cardiac muscle, NMJ, peripheral nerve, or CNS (**Figure 1**). Most are juvenile onset and autosomal dominant. The vast majority of known disease genes encode ion channels, which has led to use of the term “channelopathies” to describe this group of disorders (**Figure 2**; Kullmann 2010, Ryan & Ptáček 2010). However, this usage is a misnomer for two reasons. First, complex episodic disorders can also result from channel dysfunction, as exemplified by the autoimmune diseases discussed above. Second, some non-neurologic Mendelian diseases are caused by mutations in ion channels (Benoit et al. 2010). Thus, the term “channelopathy” should be reserved for any disorder, complex or Mendelian, neurologic or non-neurologic, caused by channel dysfunction.

Most Mendelian channelopathies affect primarily a single organ system, presumably because a typical ion channel is expressed in one cell type or a limited number of cell types. The exact pathophysiology depends on the mutation severity (e.g., missense or nonsense) and on the type of channel that is mutated (Kullman 2010, Ryan & Ptáček 2010). Missense mutations are often gain-of-function, causing increased ion flux. How-

ever, missense mutations can certainly cause loss-of-function (**Figure 2E**), and dominant-negative mechanisms are also common because some channels are composed of subunits encoded by separate genes that homo- or hetero-multimerize into a functional channel. Nonsense (truncation) mutations are almost always loss-of-function or dominant-negative (**Figure 2D**). Although exceptions abound, generally mutations in sodium channel genes cause gain-of-function, whereas potassium and chloride channel mutations cause loss-of-function. Sodium, potassium, and chloride channels usually cause myocyte or neuronal dysfunction. In contrast, AChR, GABA_A receptor, glycine receptor, and calcium channel mutations typically disrupt synaptic transmission. In any case, in the peripheral nervous system (PNS) the ultimate pathophysiology rests on whether the mutation renders the affected cell hypoexcitable or hyperexcitable. In the CNS, pathophysiology rests on whether inhibitory or excitatory neurons are preferentially affected, thereby resulting in a net hypoexcitable or hyperexcitable network (**Figure 3B**).

Skeletal Muscle

Primary skeletal muscle disorders were the first episodic disorders for which causative mutations were identified (Ptáček et al. 1991, Rojas et al. 1991, McClatchey et al. 1992, Ptáček et al. 1992). These entities were central to establishing the “channelopathy” paradigm, as all known disease genes encode ion channels. The molecular and cellular pathophysiology has been thoroughly elucidated, and in some cases this insight has led to clinical trials and successful treatments (Tawil et al. 2000). Each disorder falls on a spectrum ranging from muscle hyperexcitability to hypoexcitability. Hyperexcit-

able muscle presents clinically as myotonia: after contraction, the muscle is slow to relax. In contrast, hypoexcitable muscle presents clinically as weakness or paralysis.

Myotonia congenita (MC) constitutes the far hyperexcitable end of the spectrum. Patients suffer stiffness, particularly after prolonged inactivity, which is relieved by repetitive muscle activity (Lossin & George 2008). Mutations in *CLCN1*, the skeletal muscle chloride channel, cause MC in either autosomal dominant (Thomsen disease) or autosomal recessive (Becker disease) forms (Koch et al. 1992). Myotonia in Becker disease tends to be more severe and can even be accompanied by episodic weakness.

Like Becker disease, paramyotonia congenita (PMC) is characterized by both myotonia and weakness (Jurkat-Rott et al. 2010). PMC can be distinguished from MC because PMC patients exhibit “paradoxical myotonia”, in which myotonia is exacerbated by exercise and can transition to weakness (whereas myotonia in MC is relieved by exercise). Also, PMC attacks are prominently triggered by cold and mostly affect the upper extremities and face. PMC is caused by mutations in *SCN4A*, a skeletal muscle voltage-gated sodium channel (Ptáček et al. 1992). Different *SCN4A* mutations cause potassium-aggravated myotonia (PAM) (Ptáček et al. 1994b), in which myotonia is instead triggered by potassium. However, in PAM the myotonia never transitions to weakness (Jurkat-Rott et al. 2010).

On the opposite, hypoexcitable end of the spectrum are hyperkalemic periodic paralysis (HyperKPP) and hypokalemic periodic paralysis (HypoKPP) (Jurkat-Rott et al. 2010). Patients suffer from episodes of weakness or paralysis, triggered by exercise or stress. During attacks, HypoKPP patients are always hypokalemic, whereas HyperKPP patients are often normokalemic. However, for purposes of diagnosis HyperKPP attacks

can be induced by a potassium load. Aside from serum potassium levels, the periodic paralyses are clinically distinguishable because HypoKPP never causes myotonia, whereas HyperKPP causes myotonia early in an attack before evolving to weakness/paralysis. Both HyperKPP and HypoKPP patients can develop progressive fixed weakness in those muscles prone to paralytic attacks. Like PMC and PAM, HyperKPP and HypoKPP are caused by mutations in *SCN4A* (Ptáček et al. 1991, Bulman et al. 1999), which highlights the relatedness of these disorders. Other cases of HypoKPP are caused by mutations in *CACNA1S*, which encodes a skeletal muscle voltage-gated calcium channel (Ptáček et al. 1994a). Genotype-phenotype correlations and pathophysiological mechanisms are reviewed elsewhere (Raja Rayan & Hanna 2010).

A variant of HypoKPP is thyrotoxic periodic paralysis (TPP) (Jurkat-Rott et al. 2010). TPP patients suffer weakness/paralysis in attacks triggered by thyrotoxicosis. TPP usually afflicts young adult males of Asian ancestry. Ryan et al. (2010) recently demonstrated that some TPP cases are caused by mutations in *KCNJ18*, encoding a skeletal muscle potassium channel. *KCNJ18* mutations have since been discovered in a few patients with non-familial HypoKPP but normal thyroid function, called “sporadic periodic paralysis” (Cheng et al. 2011). However, *KCNJ18* mutations account for only one-fourth to one-third of TPP cases. We have sequenced many known ion channels in *KCNJ18*-mutation negative TPP patients but found no mutations (L.J. Ptáček, unpublished observations), and the genetic basis underlying these cases remains to be elucidated.

Finally, periodic paralysis (either HypoKPP or HyperKPP) is observed in Andersen-Tawil syndrome (ATS) (Tristani-Firouzi & Etheridge 2010). ATS is a pleiotropic disorder: periodic paralysis may be accompanied by neurocognitive deficits,

skeletal dysmorphisms, and, of paramount clinical importance, long QT syndrome (see below). ATS is caused by mutations in *KCNJ2*, another potassium channel (Plaster et al. 2001). *KCNJ2* mutations are found in only 60% of ATS families, suggesting the existence of at least one additional disease gene.

Cardiac Muscle

Numerous Mendelian diseases feature episodic dysfunction of cardiac muscle. These include atrial fibrillation and four ventricular arrhythmias: long QT syndrome, short QT syndrome, Brugada syndrome, and catecholaminergic polymorphic ventricular tachycardia. Most of the disease genes encode ion channels, but some do not. For example, atrial fibrillation (AF) can be caused by autosomal dominant mutations in five potassium channel genes (*KCNA5*, *KCNE2*, *KCNE5*, *KCNJ2*, *KCNQ1*) and three sodium channel genes (*SCN1B*, *SCN2B*, *SCN5A*) (Mahida et al. 2011). However, monogenic AF can also be caused by mutations in *GJA5*, *NPPA*, or *NUP155*, which encode a gap junction protein, atrial natriuretic peptide, and a nucleoporin, respectively. Pathophysiological mechanisms for these non-ion channel genes are not known (Mahida et al. 2011).

A well-known ventricular arrhythmia, long QT syndrome (LQTS) is defined by an elongated QT interval per EKG. This electrical abnormality reflects delayed cardiomyocyte repolarization, which predisposes to torsades de pointes arrhythmia that manifests clinically as palpitations, syncope, or sudden cardiac death. LQTS presents in four clinical subtypes: Andersen-Tawil syndrome (see above), Romano-Ward syndrome (most common), Jervell and Lange-Nielsen syndrome (includes congenital deafness), and Timothy syndrome (includes cardiac malformations, syndactyly, and autism spectrum

disorders) (McBride & Garg 2010). Like AF, LQTS is genetically heterogeneous, with 13 known genes, including six potassium channel genes (*KCNE1*, *KCNE2*, *KCNH2*, *KCNJ2*, *KCNJ5*, *KCNQ1*), two sodium channel genes (*SCN4B*, *SCN5A*), one calcium channel gene (*CACNA1C*), and four genes not encoding channels: *AKAP9*, *ANK2*, *CAV3*, and *SNTA1*. Mutations in the four non-channel genes seem to disrupt trafficking or stability of cardiomyocyte ion channels (**Figure 2F**; Mohler et al. 2003, Vatta et al. 2006, Chen et al. 2007, Ueda et al. 2008).

Patients with short QT syndrome (SQTS) suffer from a shortened QT interval that, like LQTS, predisposes to ventricular arrhythmia and sudden cardiac death. SQTS is caused by autosomal dominant mutations in three potassium channel genes (*KCNH2*, *KCNJ2*, *KCNQ1*), two of which are also LQTS genes (McBride & Garg 2010). Thus, SQTS and LQTS constitute a spectrum ranging from prolonged to delayed cardiomyocyte repolarization. SQTS can also present in concert with Brugada syndrome (BS) – defined by elevation of the ST segment in select EKG leads – in patients with mutations in *CACNA1C* and *CACNB2*, which encode calcium channel subunits. Alternatively, isolated BS results from mutations in three sodium channel genes (*SCN1B*, *SCN3B*, *SCN5A*), one potassium channel gene (*KCNE3*), and *GPD1L*, which encodes a protein that regulates *SCN5A* phosphorylation and thereby modulates sodium current density (**Figure 2F**; Valdivia et al. 2009, McBride & Garg 2010).

Finally, another important cause of sudden cardiac death in children is catecholaminergic polymorphic ventricular tachycardia (CPVT). In CPVT, the catecholaminergic surge associated with strong emotions or exercise can trigger ventricular tachycardia. The four disease genes, *RYR2*, *CASQ2*, *TRDN*, and *CALM1*, encode essential components

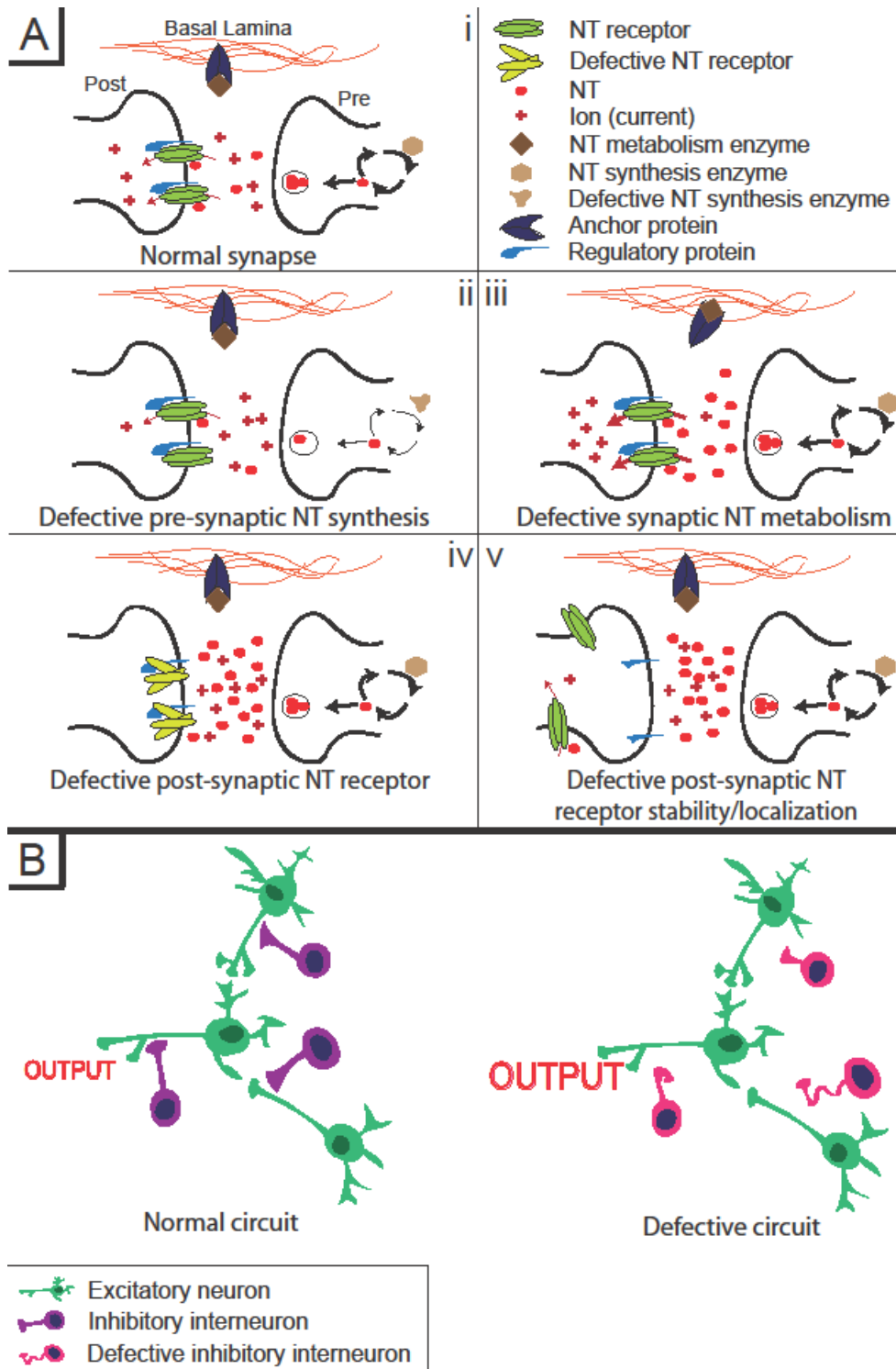
of cardiomyocyte calcium signaling (McBride & Garg 2010, Nyegaard et al. 2012, Roux-Buisson et al. 2012). Recently, Watanabe et al. (2009) elegantly identified flecainide as a potent inhibitor of arrhythmias in a CPVT mouse model. This work was validated in human trials (van der Werf et al. 2011), suggesting an effective treatment for this otherwise lethal disease.

Neuromuscular Junction

Mendelian disorders of the neuromuscular junction (NMJ) are known as congenital myasthenic syndromes (CMS). CMS are distinguished from the complex, autoimmune NMJ disorders LEMS and MG (see above), because CMS cannot be treated by immunosuppression. Although CMS subtypes are clinically and genetically heterogeneous, they are usually characterized by episodic ocular and respiratory weakness (Barisic et al. 2011). Weakness results from impaired neuromuscular transmission.

Most CMS subtypes are autosomal recessive, caused by mutations in 1 of 14 known genes. The subtypes/genes are classified by the NMJ component that is primarily affected: pre-synaptic, synaptic, or post-synaptic (**Figure 3A**; Barisic et al. 2011). Pre-synaptic CMS features prominent episodic apnea, and is caused by mutations in *CHAT*, encoding an enzyme critical for acetylcholine synthesis (**Figure 3A, part ii**). Synaptic CMS can be caused by mutations in *COLQ* (Mihaylova et al. 2008) and *LAMB2* (Maselli et al. 2009), which encode proteins that anchor acetylcholinesterase to the basal lamina (**Figure 3A, part iii**). The most common type of CMS, by far, is post-synaptic CMS, usually caused by defects in acetylcholine receptor (AChR) subunit genes *CHRNA1*, *CHRNB1*, *CHRND*, and *CHRNE* (**Figure 3A, part iv**). Mutations in another AChR

subunit gene, *CHRNG*, cause Escobar syndrome (ES), characterized by joint contractures, pterygia (webbing), and in utero CMS-like respiratory distress that resolves by birth (Hoffmann et al. 2006). Finally, rare cases of post-synaptic CMS are caused by mutations in non-AChR genes, namely *AGRN*, *DOK7*, *GFPT1*, *MUSK*, and *RAPSN*. These genes constitute a molecular pathway essential for AChR aggregation and positioning on the post-synaptic membrane (**Figure 3A, part v**; Barisic et al. 2011). Mutations in some of these genes (*CHRNA1*, *CHRNBI*, *CHRND*, *DOK7*, and *RASPN*) cause fetal akinesia deformation sequence (FADS), a perinatal lethal syndrome characterized by developmental anomalies like pterygia, as well as fetal akinesia. Given the clinical and genetic overlap, FADS is considered an extreme phenotype on a continuum that includes ES and CMS. Identifying which gene is mutated in a CMS patient is critical because certain genetic subtypes respond robustly to otherwise toxic medications (Barisic et al. 2011). About half of CMS cases await genetic diagnosis, suggesting a fruitful area for human genetics to provide further insights into synaptic physiology.



synaptic cleft, where it activates post-synaptic (Post) NT receptors that then pass current. Regulatory proteins modulate NT receptor stability and localization. NT is metabolized in the synaptic cleft by enzymes that can be anchored to the pre-synaptic cell, the post-synaptic cell, or the basal lamina (depicted). Defects in these processes can alter synaptic transmission and excitability, as exemplified by defective neuromuscular junction (NMJ) synaptic transmission in the congenital myasthenic syndromes (CMS). CMS can be caused by mutations in a NT synthesis enzyme (ii), mutations in proteins that anchor a NT metabolism enzyme to the basal lamina (iii), mutations in the NT receptor itself (iv), and mutations in proteins that regulate NT receptor stability/localization (v). Although this pathophysiology has been heretofore demonstrated only for one type of synapse – the NMJ in CMS – other episodic disorders of the CNS are likely caused by dysfunction of higher-order synapses. Additional mechanisms of synaptopathy are conceivable, such as defects in synaptic vesicle release.

(B) Another potential mechanism of episodic disease is defective regulation at the circuit level, i.e., “circuitopathy”. For example, one type of defective circuit is exemplified by GEFS+ (generalized epilepsy with febrile seizures plus), which is caused by *SCN1A* mutations that result in decreased GABAergic inhibition by interneurons. Certainly many other types of defective circuits are possible, but whether they can cause episodic neurologic disease is not yet known.

Peripheral Nerve

Recent studies have shown that mutations in *SCN9A* cause an intriguing trio of pain perception disorders. *SCN9A* encodes a sodium channel that is specifically expressed in those peripheral sensory neurons that function as nociceptors. Mutations lead to aberrant excitability of nociceptive nerves and thus alter the patient’s sensitivity to painful stimuli. Autosomal dominant, gain-of-function mutations cause hypersensitivity to pain in two disorders: inherited erythromelalgia (IEM) and paroxysmal extreme pain disorder (PEPD) (Yang et al. 2004, Fertleman et al. 2006). Burning pain occurs in discrete episodes, accompanied by erythema and swelling. IEM affects the extremities and is commonly triggered by exercise, heat, or dietary components, whereas PEPD affects submandibular, ocular, and rectal areas and is triggered by perianal stimulation (e.g., bowel movements).

Autosomal recessive, loss-of-function *SCN9A* mutations cause the opposite phenotype: congenital insensitivity to pain (CIP), characterized by complete absence of pain sensation (Cox et al. 2006). Although ostensibly appealing, patients with CIP suffer substantial injuries and early deaths because of inadvertent trauma. Early studies suggested that CIP patients are otherwise normal, but Weiss et al. (2011) recently demonstrated that the patients cannot smell; moreover, mice with olfactory sensory neuron-specific *SCN9A* knockout also exhibit anosmia (Weiss et al. 2011). Nevertheless, the specificity and degree of pain relief achieved by genetic inactivation of this channel make it a promising target for developing drugs to treat pain (Clare 2010).

Central Nervous System

A smorgasbord of Mendelian episodic disorders afflict the CNS, with diverse symptoms depending on which region of the CNS is affected. For example, the cerebellum is the focus of pathology in episodic ataxia (EA). EA is distinguished by attacks of ataxia (imbalance and incoordination) without impaired consciousness (Jen et al. 2007, Jen 2008). Sometimes, attacks include weakness or are superimposed on progressive ataxia. Seven subtypes (EA1-EA7) vary in associated symptoms, such as myokymia, nystagmus, tinnitus, vertigo, and hemiplegic migraine. Most subtypes share exertion, emotions, and startle as triggers. Each is autosomal dominant, with mutations in *KCNA1* (EA1), *CACNA1A* (EA2), *CACNB4* (EA5), and *SLC1A3* (EA6). Despite demonstrated linkage, the genes for EA3, EA4, and EA7 have proven elusive. *KCNA1* and *CACNA1A/CACNB4* encode subunits of potassium and calcium channels, respectively, that are highly expressed in Purkinje cells of the cerebellum (Tomlinson et al. 2009), and

indeed, mice expressing mutant channels exhibit aberrant Purkinje cell activity (Jen et al. 2007). The EA6 gene, *SLC1A3*, encodes a glutamate reuptake transporter expressed in cerebellar astrocytes (Jen et al. 2005), but how mutant *SLC1A3* alters cerebellar output remains unknown.

EA2 features migraine, so it is also termed familial hemiplegic migraine (FHM) type 1. FHM patients suffer from attacks of headache with hemiplegia during aura. Whereas FHM1 is associated with ataxia, two other subtypes, FHM2 and FHM3, are not. For all subtypes, inheritance is autosomal dominant. FHM2 is caused by mutations in *ATPIA2* (De Fusco et al. 2003), which encodes a sodium-potassium ATPase. FHM3 patients carry mutations in the sodium channel *SCN1A* (Dichgans et al. 2005). Knockin mouse models for both FHM1 and FHM2 have increased susceptibility to cortical spreading depression (CSD) (Tottene et al. 2009, Leo et al. 2011), in keeping with the theory that aberrant cortical excitability is at least partially responsible for migraine pathophysiology (see above).

A related disorder is alternating hemiplegia of childhood (AHC), characterized by recurrent attacks of hemiplegia (Neville & Ninan 2007). AHC often presents with concomitant epilepsy and developmental delay. As a very rare, sporadic disorder, the etiology of AHC has long remained a mystery, but Heinzen et al. (2012) recently showed that AHC is caused by *de novo* mutations in *ATPIA3*, another sodium-potassium ATPase gene. The mechanism linking sodium-potassium ATPases and hemiplegia in FHM2 and AHC is not clear. Distinct *ATPIA3* mutations cause a quite dissimilar phenotype, autosomal dominant rapid-onset dystonia-parkinsonism (de Carvalho Aguiar et al. 2004).

Some families exhibit autosomal dominant migraine without hemiplegia. So far two genes have been proposed. The first, *KCNK18*, a potassium channel, was mutated in a single large family and tracked with the phenotype in nine affected individuals (Lafreniere et al. 2010). Moreover, the mutant subunit suppressed wild-type channel function in vitro through a dominant negative effect (Lafreniere et al. 2010). However, the same group (Andres-Enguix et al. 2012) later discovered *KCNK18* variants in unaffected controls, variants that also completely abrogate wild-type channel function. How to reconcile these data? One possibility is that *KCNK18* mutation alone is not sufficiently causative and that the single affected family carries additional migraine susceptibility variants. However, it is extremely unlikely that another locus would cosegregate with the phenotype in the large family (nine affected individuals), which suggests that either the *KCNK18* linkage region itself contains additional susceptibility variants or that *KCNK18* is not causally related to the phenotype. On balance, it is our view that *KCNK18* mutations are likely not causative, although we would happily recant upon identification of additional affected families with *KCNK18* mutations. A stronger case can be made for the second candidate gene, *CSNK1D*, which encodes a kinase, because two independent families carry distinct mutations (Brennan et al. 2013). These mutations alter nearby residues that reside in the highly conserved kinase domain, and were shown in vitro to disrupt kinase activity (Xu et al. 2005, Brennan et al. 2013). Furthermore, a mutant mouse model exhibits increased peripheral allodynia, cortical spreading depression, and arterial dilation, all physiological markers of migraine (Brennan et al. 2013). In any case, the overlapping, well-characterized phenotypes of these three families strongly argue for the existence of Mendelian migraine that is distinct

from FHM and distinct from migraine with complex inheritance (Eriksen et al. 2004). Heretofore unnamed, we propose the term autosomal dominant migraine (ADM) for this disorder.

Hereditary hyperekplexia (HH) is a disorder of the brain stem, featuring an exaggerated startle reaction (Dreissen et al. 2012). Most patients exhibit stiffness at birth that lasts through infancy. Stiffness is exacerbated by handling and is so pronounced that the baby can be held vertically or horizontally without a change in posture. Consciousness is always preserved. Although prolonged stiffness resolves after infancy, throughout the rest of their lives patients suffer from stiffness for a few seconds after an exaggerated startle reaction to unexpected stimuli. HH inheritance can be autosomal dominant, autosomal recessive or sporadic, and is usually caused by mutations in *GLRA1* (Shiang et al. 1993). *GLRA1* encodes a subunit of the glycine receptor located in the postsynaptic membrane of glycinergic neurons (**Figure 3A, part iv**; Dreissen et al. 2012). Less commonly, patients carry mutations in *SCL6A5* (which encodes a presynaptic glycine transporter) (Rees et al. 2006), or, very rarely, mutations in *GLRB*, *GPHN*, or *ARHGEF9* (all encode postsynaptic glycinergic proteins). These mutations decrease the inhibition exerted by glycinergic neurons in the spinal cord and brainstem, resulting in excessive excitation as reflected by stiffness and exaggerated startle (Dreissen et al. 2012).

Another fascinating group of episodic disorders are the paroxysmal dyskinesias. In these diseases, excessive excitation manifests as attacks of involuntary movements that can include dystonia (sustained contractions), athetosis (writhing), and chorea (small dance-like movements) (Bhatia 2011). There are three Mendelian paroxysmal dys-

kinesias: paroxysmal exercise-induced dyskinesia (PED), paroxysmal non-kinesigenic dyskinesia (PNKD), and paroxysmal kinesigenic dyskinesia (PKD). All three are autosomal dominant with juvenile onset.

PED is usually triggered by exercise and causes dystonia in the heavily exercised muscles. The PED gene, *SLC2A1*, encodes the main glucose transporter in the brain (Suls et al. 2008, Weber et al. 2008). Mutations impair glucose import into the brain such that the increased energy demand after exercise renders the basal ganglia hypoglycemic. However, this defect must not be specific to the basal ganglia seeing as PED often presents with concomitant neurologic illness that may include hemiplegic migraine, developmental delay, and especially epilepsy. Indeed, De Vivo disease, which is also caused by *SLC2A1* mutations, features severe, global developmental delay and epilepsy; PED may not be appreciable (De Vivo et al. 1991, Seidner et al. 1998). Diagnosis of any phenotype along this PED-De Vivo spectrum is critical because the ketogenic diet is a highly effective treatment (Leen et al. 2010). Ketone bodies use a different transporter to enter the CNS and thereby provide an alternative energy source.

In contrast with PED, PKD attacks are often triggered by startle or sudden movements (hence “kinesigenic”) (Bhatia 2011). PNKD attacks are, by definition, not triggered by movement. Instead, PNKD is induced by ethanol, caffeine, or stress. In both PKD and PNKD, hormones play a role: PKD attacks peak in puberty but decrease in pregnancy, and PNKD attacks increase with menses. However, the exact role of hormones in the genesis of attacks is unclear. PNKD is caused by mutations in the gene *PNKD*, which encodes an enzyme that seems to modulate dopamine release in the striatum in response to ethanol, caffeine, and redox status (Lee et al. 2004, Rainier et al.

2004, Lee et al. 2012b). One hypothesis is that *PNKD* mutations, which alter protein stability and cleavage (Ghezzi et al. 2009, Shen et al. 2011), are gain-of-function, rendering a patient more susceptible to stimuli that trigger dopamine dysregulation in the basal ganglia (Lee et al. 2012b).

Numerous groups recently identified the PKD disease gene, *PRRT2* (Chen et al. 2011, Wang et al. 2011, Heron et al. 2012, Lee et al. 2012a, Li et al. 2012). Within affected families, there is remarkable pleiotropy; some patients suffer from episodic ataxia or hemiplegic migraine (Cloarec et al. 2012, Gardiner et al. 2012, Marini et al. 2012), and others from benign, afebrile infantile epilepsy prior to PKD onset [termed infantile convulsions with choreoathetosis (ICCA)] (Cloarec et al. 2012, Heron et al. 2012, Lee et al. 2012a). In fact, some patients suffer from benign familial infantile epilepsy (BFIE) that resolves in infancy and is never succeeded by PKD (Heron et al. 2012). Given the phenotypic and genetic overlap of these disorders, we have proposed the term PKD/infantile convulsions (PKD/IC) for the diagnosis of any *PRRT2* mutation-positive patient with BFIE, PKD, or both (ICCA) (Cloarec et al. 2012, Lee et al. 2012a). *PRRT2* encodes a transmembrane protein that lacks characteristic ion channel motifs, and its function is not known. Lee et al. (2012a) found that mutations disrupt in vitro binding of *PRRT2* to SNAP-25, a synaptic protein integral for neurotransmitter release. However, *PRRT2* predominantly localizes to axons rather than to dendritic processes (Lee et al. 2012a), and it is a widespread misconception that individual protein-protein interactions are critical to physiological function (Gillis & Pavlidis 2012). Nevertheless, one possible unifying hypothesis is that PKD and *PNKD* are both disorders of synaptic regulation (**Figure 3A**), although this certainly remains unproven.

Another Mendelian movement disorder is marked by the primary symptom of myoclonus. Myoclonus is defined as sudden, brief, involuntary movements, i.e., twitches. Myoclonus is commonly a component of epilepsy, but in this disorder seizures do not occur. The disorder, myoclonus dystonia syndrome (MDS), is characterized by juvenile onset myoclonus and/or dystonia (Nardocci et al. 2008, Roze et al. 2008). MDS patients suffer severe psychiatric comorbidity, especially depression, although MDS symptoms are clearly ameliorated by ethanol, so depression may simply be a by-product of self-medication by intoxication. MDS is caused by autosomal dominant mutations in *SGCE* (Zimprich et al. 2001), which, like *PRRT2*, encodes a non-ion channel transmembrane protein. Although *SGCE* was cloned in 2001, there has been almost no mechanistic insight since, and its function continues to be obscure.

The broadest category of inherited episodic CNS disorders is composed of the Mendelian epilepsy syndromes (Poduri & Lowenstein 2011). An illustrative example is generalized epilepsy with febrile seizures plus (GEFS+). Whereas febrile seizures are common and typically benign in young children, their persistence after age six defines GEFS+. Most GEFS+ cases are genetically complex, but about 10% are autosomal dominant. So far, all known disease genes encode ion channels, including three voltage-gated sodium channel genes (*SCN1A*, *SCN1B*, *SCN2A*) and two GABA_A receptor (GABA_AR) subunit genes: *GABRG2* and *GABRD* (Wallace et al. 1998, Escayg et al. 2000, Baulac et al. 2001, Sugawara et al. 2001, Dibbens et al. 2004). Thirteen additional loci have been linked to GEFS+ and await gene identification (Morar et al. 2011, Poduri & Lowenstein 2011). Mutations in *SCN1A* are most common. In fact, other *SCN1A* mutations cause more severe phenotypes along the GEFS+ continuum: severe myoclonic epilepsy of

infancy (SMEI, also known as Dravet syndrome), borderline SMEI, and intractable epilepsy of childhood (IEC) (Stafstrom 2009). *SCN1A* knockout and knockin mice die young from epilepsy, and their hippocampal GABAergic interneurons are hypoexcitable, leading to a net hyperexcitable state (**Figure 3B**; Yu et al. 2006, Martin et al. 2010). Given that GEFS+ can also be caused by mutations in GABA_AR subunits, interneuron dysfunction is likely a common mechanism underlying the entire GEFS+ continuum, although to our knowledge this hypothesis remains to be tested in *GABRG2* and *GABRD* knockout mice.

Predictably, many other Mendelian epilepsy syndromes are caused by mutations in ion channels. These phenotypes and the associated genes are extensively reviewed elsewhere (Helbig et al. 2008, Mantegazza et al. 2010, Nicita et al. 2012). The known genes include two GABA_AR subunits, two AChR subunits, the brain glucose transporter, a sodium-potassium ATPase, four potassium channels, one calcium channel subunit, one chloride channel, and one sodium channel. Two other sodium channel genes, *SCN3A* and *SCN8A*, have been associated with childhood epilepsy (Holland et al. 2008, Estacion et al. 2010, Veeramah et al. 2012), but mutations were each detected in only a single patient; therefore, definitive assignment of these genes will require the discovery of distinct mutations in additional patients.

Recent work has demonstrated that mutations in non-channel genes can cause Mendelian epilepsy. For example, patients with a phenotype along the GEFS+ spectrum who lack an *SCN1A* mutation and are female sometimes harbor *PCDH19* mutations (Depienne et al. 2009, Depienne et al. 2011). *PCDH19* encodes a calcium-dependent cell adhesion protein (Morishita & Yagi 2007). Two fascinating unanswered questions are,

how do mutations in a cell adhesion protein cause epilepsy, and why do these mutations cause disease only in females?

Another well-characterized epilepsy syndrome caused by mutations in a non-channel gene is autosomal dominant partial epilepsy with auditory features (ADPEAF). The disease gene is *LGII* (Kalachikov et al. 2002). Interestingly, *Lgi1* associates with voltage-gated potassium channels, and autoantibodies to the *Lgi1*-*Caspr2* complex are associated with the autoimmune, peripheral nerve disorder known as Isaac's syndrome (see above). How *LGII* mutations cause temporal lobe epilepsy without any peripheral nerve hyperexcitability is not clear, and in fact *Lgi1* function is essentially unknown. Recent work suggests that *Lgi1* inhibits seizure-induced trafficking of potassium channels in thalamocortical neurons (**Figure 2C**; Smith et al. 2012), but it also seems to function in remodeling of synapses and sensory axons (Zhou et al. 2009, Zhou et al. 2012), and it is unclear how these findings can be reconciled into a unifying hypothesis.

Yet another non-channel epilepsy gene, *EFHC1*, is mutated in one subset of juvenile myoclonic epilepsy (JME) (Suzuki et al. 2004). *EFHC1* encodes a microtubule-associated protein that regulates cell division and neuronal migration during cortical development (de Nijs et al. 2009). In fact, a cornucopia of genes that function in neuronal migration are mutated in Mendelian syndromes that feature epilepsy as one symptom along with dramatic, radiologically evident malformations of cortical development (Andrade 2009, Barkovich et al. 2012). For example, severe mutations in a gene essential for interneuron migration, *ARX*, cause gross cortical malformations, but milder mutations result in less severe phenotypes such as early infantile epileptic encephalopathy or even isolated mental retardation (Kitamura et al. 2002, Stromme et al. 2002, Shoubridge

et al. 2010). Likewise, severe infantile epilepsy phenotypes are caused by mutations in *CDKL5*, *STXBP1*, and *TBC1D24*, which are non-channel genes that are clearly essential for normal brain development, although their exact function remains unknown (Weaving et al. 2004, Saitsu et al. 2008, Corbett et al. 2010, Falace et al. 2010). On the basis of these data, it seems likely that many complex cases of epilepsy – which have a substantial genetic contribution (**Figure 1**) – may result from a constellation of more subtle, genetically influenced defects in cortical development.

One last class of Mendelian epilepsies is progressive myoclonic epilepsy (PME): juvenile onset, myoclonic epilepsy in association with neurodegeneration, dementia, and early death (Ramachandran et al. 2009). There are many PME subtypes and causative genes, mostly encoding lysosomal proteins (Ramachandran et al. 2009). Some clinical variants also feature substantial pathology outside the CNS, such as action myoclonus-renal failure (AMRF) syndrome (Badhwar et al. 2004). A similar disorder, deemed SeSAME syndrome (Seizures, Sensorineural deafness, Ataxia, Mental retardation, and Electrolyte imbalance), is caused by mutations in the potassium channel *KCNJ10* (Bockenbauer et al. 2009, Scholl et al. 2009). Epilepsy in SeSAME syndrome is less severe, does not progress, and is not accompanied by neurodegeneration, so it does not qualify as a PME subtype. We highlight it here to emphasize a somewhat unusual case in which ion channel mutations cause dramatic pleiotropy in diverse organ systems.

Finally, primary episodic sleep disorders, a few of which are Mendelian, are reviewed elsewhere (Sehgal & Mignot 2011, Zhang et al. 2011). Mendelian ophthalmic disorders are extraordinarily diverse and have been very well characterized; however,

they are usually progressive rather than episodic, as reviewed by Sheffield & Stone (2011).

BEYOND THE CHANNELOPATHY PARADIGM

We have highlighted the immense progress made in characterizing the phenotypes, genetics, and pathophysiology of episodic neurologic disorders. In our view, four main objectives should be the focus of future work.

The first two objectives are broadly applicable to human genetics. First, we should identify all Mendelian phenotypes and disease genes. This goal is realistic given the advent of inexpensive, high-throughput sequencing (Gonzaga-Jauregui et al. 2012). Many sporadic or seemingly idiopathic cases of severe, stereotyped disorders are likely the result of mutations that are remarkably straightforward to detect via exome sequencing (Choi et al. 2009, Bamshad et al. 2011). On the other hand, many of the disorders described above were characterized in large families with highly significant linkage, and yet, cloning of the disease genes at linked loci remained elusive for years, often because of the sheer number of candidate genes within the critical regions. This problem is now easily circumvented by high-throughput sequencing (e.g., Lee et al. 2012a).

However, there will be challenges. Foremost among them is evaluating whether a rare variant is truly causative. Numerous “disease genes” have been assigned on the basis of a single affected patient carrying a variant (Holland et al. 2008, Veeramah et al. 2012). Although this data certainly represents grounds for functional investigation, the gold standard should continue to be allelic heterogeneity. In fact, every human carries hundreds of rare, novel variants (Tennessen et al. 2012), so even using the identification of two rare variants in the same gene from a large collection of patients to claim causality may be unwarranted (O’Roak et al. 2012, Sanders et al. 2012). Instead, large families with the statistical power to detect linkage will remain valuable because linkage con-

strains the pool of rare variants that must be considered for causality. Even when the evidence includes a highly penetrant phenotype, large families, linkage, and allelic heterogeneity, some mutations are not sufficient to cause disease in unrelated patients (Klassen et al. 2011). The sobering reality is that determining the causal relationships between mutations and Mendelian diseases may take many years to unravel.

The second main objective is to identify genetic risk factors for related, genetically complex disorders (**Figure 1**). It was hoped that genome-wide association studies (GWAS) would provide an unbiased method for doing so; however, except for a few remarkable early findings (Hageman et al. 2005, Duerr et al. 2006), despite extensive patient collections the calculated effect sizes have been very small. Consequently, the overwhelming majority of GWAS associations have been insufficient to induce researchers to pursue functional biological investigation, or when investigated are found to have no functional effect. It remains an open question whether high-throughput sequencing will prove fruitful where GWAS was not, although we remain hopeful. In our view, one possibility merits serious consideration: the null hypothesis. Perhaps the “missing heritability” (Eichler et al. 2010) is not missing after all but has instead been grossly overestimated by inherently biased measures of heritability. Only time will tell. Given this history, we are puzzled as to why more resources are not directed toward the tried-and-true approach of applying our comprehension of rare Mendelian disorders to understand pathophysiology of related complex diseases, as exemplified by Goldstein & Brown’s (2009) elucidation of familial hypercholesterolemia, which sparked development of the blockbuster statin drugs. This approach has seemingly fallen out of favor. In this regard, episodic neurologic disorders are particularly tantalizing because Mendelian forms exhib-

it very specific symptoms and symptom clusters (e.g., congenital insensitivity to pain) that may allow for pharmacological treatments with minimal side effects.

A third goal is to understand why these disorders are episodic in nature. Typically, patients appear to be normal between attacks and yet suffer extreme dysfunction during an attack. Moreover, attacks are triggered by precipitants that are routinely encountered by affected patients and unaffected patients alike, and even in affected patients these precipitants do not always trigger an attack. The link between the precipitant and an attack is clear for some disorders, such as the primary skeletal muscle disorders in which altered extracellular ion concentrations affect myocyte excitability. Another well-characterized example is PED, in which exercise depletes blood glucose to cause CNS hypoglycemia and hence dyskinesia. However, other triggers remain baffling. For example, strong emotion is a common trigger, but how do psychological factors trigger neurological dysfunction? No one knows.

Finally, the fourth objective is to expand on the channelopathy paradigm (**Figure 3**). Although more mutations in ion channels will likely be found, it has become evident that many genes that do not encode channels can be mutated to cause episodic disorders. For some, the effect of gene mutation is easily tied to changes in excitability, such as when the genes encode proteins essential for ion channel trafficking, stability, or function (**Figure 2F**). However, as we have repeatedly noted, for many genes the link to cellular excitability remains poorly understood. We propose that rather than disease genes affecting excitability in a cell-intrinsic way (e.g., ion channel expression or localization on the cell membrane), a compelling area for future study is the role of disease genes in modulating excitability at the synaptic level. This concept of a “synaptopathy” is certainly

not new, since the congenital myasthenic syndromes have long been known to be disorders of synaptic regulation (**Figure 3A**). However, the concept of synaptopathy has, to date, been restricted to the NMJ (**Figure 3A**), and it seems probable that higher synapses may be dysfunctional in episodic disorders of the CNS. We cannot help but speculate that the lessons learned by investigating synaptic function in Mendelian episodic disorders may apply to various complex disorders such as autism that are known synaptopathies (Grabrucker et al. 2011).

Likewise, disordered regulation of excitability at the circuit level (“circuitopathy”) likely contributes to episodic disorders of the CNS (**Figure 3B**). For example, *SCN1A* mutations in GEFS+, in which sodium channel dysfunction results in aberrant interneurons, can be conceptualized as a channelopathy or a circuitopathy because ion channels and also neuronal circuits are defective. Many other types of aberrant circuits are possible, and we anticipate that some non-channel genes, especially those implicated in brain development and/or mutated in Mendelian epilepsy syndromes, cause disease by altering circuit wiring.

In summary, the past two decades have borne witness to the description of many novel episodic neurologic phenotypes, the identification of causative mutations, and the elucidation of underlying pathophysiology. On all three fronts – syndromes, genes, and mechanisms – much work remains. With the widespread application of high-throughput genomic technology, we expect progress to continue apace. In time, we expect that these fronts will be conquered and the spoils will redound in the form of novel treatments for these tragic diseases. We owe as much to our patients.

REFERENCES

- Andrade DM. 2009. Genetic basis in epilepsies caused by malformations of cortical development and in those with structurally normal brain. *Hum Genet* 126:173-93
- Andres-Enguix I, Shang L, Stansfeld PJ, Morahan JM, Sansom MSP, et al. 2012. Functional analysis of missense variants in the TRESK (KCNK18) K⁺ channel. *Sci Rep* 2:237
- Badhwar A, Berkovic S, Dowling JP, Gonzales M, Narayanan S, et al. 2004. Action myoclonus-renal failure syndrome: characterisation of a unique cerebro-renal disorder. *Brain* 127:2173-82
- Bamshad MJ, Ng SB, Bigham AW, Tabor HK, Emond MJ, et al. 2011. Exome sequencing as a tool for Mendelian disease gene discovery. *Nat Rev Genet* 12:745-55
- Barisic N, Chaouch A, Muller JS, Lochmuller H. 2011. Genetic heterogeneity and pathophysiological mechanisms in congenital myasthenic syndromes. *Eur J Paediatr Neurol* 15:189-96
- Barkovich AJ, Guerrini R, Kuzniecky RI, Jackson GD, Dobyns WB. 2012. A developmental and genetic classification for malformations of cortical development: update 2012. *Brain* 135:1348-69
- Baulac S, Huberfeld G, Gourfinkel-An I, Mitropoulou G, Beranger A, et al. 2001. First genetic evidence of GABA(A) receptor dysfunction in epilepsy: a mutation in the gamma2-subunit gene. *Nat Genet* 28:46-48

- Benoit G, Machuca E, Heidet L, Antignac C. 2010. Hereditary kidney diseases: highlighting the importance of classical Mendelian phenotypes. *Ann N Y Acad Sci* 1214:83-93
- Berg AT, Berkovic SF, Brodie MJ, Buchhalter J, Cross JH, et al. 2010. Revised terminology and concepts for organization of seizures and epilepsies: Report of the ILAE Commission on Classification and Terminology, 2005-2009. *Epilepsia* 51: 676-85
- Berg AT, Scheffer IE. 2011. New concepts in classification of the epilepsies: entering the 21st century. *Epilepsia* 52:1058-62
- Bhatia KP. 2011. Paroxysmal dyskinesias. *Mov Disord* 26:1157-65
- Bockenbauer D, Feather S, Stanescu HC, Bandulik S, Zdebik AA, et al. 2009. Epilepsy, ataxia, sensorineural deafness, tubulopathy, and KCNJ10 mutations. *N Engl J Med* 360:1960-70
- Brennan KC, Bates EA, Shapiro RE, Zyuzin J, Hallows WC, et al. 2013. Casein kinase I δ mutations in familial migraine and advanced phase sleep syndrome. *Manuscript submitted.*
- Bulman DE, Scoggan KA, van Oene MD, Nicolle MW, Hahn AF, et al. 1999. A novel sodium channel mutation in a family with hypokalemic periodic paralysis. *Neurology* 53:1932-36
- Caviness J, Brown P. 2004. Myoclonus: current concepts and recent advances. *Lancet Neurol* 3:598-607

- Chen L, Marquardt ML, Tester DJ, Sampson KJ, Ackerman MJ, et al. 2007. Mutation of an A-kinase-anchoring protein causes long-QT syndrome. *Proc Natl Acad Sci U S A* 104:20990-95
- Chen WJ, Lin Y, Xiong ZQ, Wei W, Ni W, et al. 2011. Exome sequencing identifies truncating mutations in PRRT2 that cause paroxysmal kinesigenic dyskinesia. *Nat Genet* 43:1252-55
- Cheng CJ, Lin SH, Lo YF, Yang SS, Hsu YJ, et al. 2011. Identification and functional characterization of Kir2.6 mutations associated with non-familial hypokalemic periodic paralysis. *J Biol Chem* 286:27425-35
- Choi M, Scholl UI, Ji W, Liu T, Tikhonova IR, et al. 2009. Genetic diagnosis by whole exome capture and massively parallel DNA sequencing. *Proc Natl Acad Sci U S A* 106:19096-101
- Clare JJ. 2010. Targeting voltage-gated sodium channels for pain therapy. *Expert Opin Investig Drugs* 19:45-62
- Cloarec R, Bruneau N, Rudolf G, Massacrier A, Salmi M, et al. 2012. PRRT2 links infantile convulsions and paroxysmal dyskinesia with migraine. *Neurology* 79:2097-2103
- Corbett MA, Bahlo M, Jolly L, Afawi Z, Gardner AE, et al. 2010. A focal epilepsy and intellectual disability syndrome is due to a mutation in TBC1D24. *Am J Hum Genet* 87:371-75
- Cox JJ, Reimann F, Nicholas AK, Thornton G, Roberts E, et al. 2006. An SCN9A channelopathy causes congenital inability to experience pain. *Nature* 444:894-98

- de Carvalho Aguiar P, Sweadner KJ, Penniston JT, Zaremba J, Liu L, et al. 2004. Mutations in the Na⁺/K⁺-ATPase alpha3 gene ATP1A3 are associated with rapid-onset dystonia parkinsonism. *Neuron* 43:169-75
- De Fusco M, Marconi R, Silvestri L, Atorino L, Rampoldi L, et al. 2003. Haploinsufficiency of ATP1A2 encoding the Na⁺/K⁺ pump alpha2 subunit associated with familial hemiplegic migraine type 2. *Nat Genet* 33:192-96
- de Nijs L, Leon C, Nguyen L, Loturco JJ, Delgado-Escueta AV, et al. 2009. EFHC1 interacts with microtubules to regulate cell division and cortical development. *Nat Neurosci* 12:1266-74
- De Vivo DC, Trifiletti RR, Jacobson RI, Ronen GM, Behmand RA, et al. 1991. Defective glucose transport across the blood-brain barrier as a cause of persistent hypoglycorrhachia, seizures, and developmental delay. *N Engl J Med* 325:703-9
- Della-Morte D, Guadagni F, Palmirotta R, Testa G, Caso V, et al. 2012. Genetics of ischemic stroke, stroke-related risk factors, stroke precursors and treatments. *Pharmacogenomics* 13:595-613
- Depienne C, Bouteiller D, Keren B, Cheuret E, Poirier K, et al. 2009. Sporadic infantile epileptic encephalopathy caused by mutations in PCDH19 resembles Dravet syndrome but mainly affects females. *PLoS Genet* 5:e1000381
- Depienne C, Trouillard O, Bouteiller D, Gourfinkel-An I, Poirier K, et al. 2011. Mutations and deletions in PCDH19 account for various familial or isolated epilepsies in females. *Hum Mutat* 32:E1959-75

- Dibbens LM, Feng HJ, Richards MC, Harkin LA, Hodgson BL, et al. 2004. GABRD encoding a protein for extra- or peri-synaptic GABAA receptors is a susceptibility locus for generalized epilepsies. *Hum Mol Genet* 13:1315-19
- Dichgans M, Freilinger T, Eckstein G, Babini E, Lorenz-Depiereux B, et al. 2005. Mutation in the neuronal voltage-gated sodium channel SCN1A in familial hemiplegic migraine. *Lancet* 366:371-77
- Dodick DW. 2008. Examining the essence of migraine—is it the blood vessel or the brain? A debate. *Headache* 48:661-67
- Dreissen YEM, Bakker MJ, Koelman JHTM, Tijssen MAJ. 2012. Exaggerated startle reactions. *Clin Neurophysiol* 123:34-44
- Duerr RH, Taylor KD, Brant SR, Rioux JD, Silverberg MS, et al. 2006. A genome-wide association study identifies IL23R as an inflammatory bowel disease gene. *Science* 314:1461-63
- Eichler EE, Flint J, Gibson G, Kong A, Leal SM, et al. 2010. Missing heritability and strategies for finding the underlying causes of complex disease. *Nat Rev Genet* 11:446-50
- Eriksen MK, Thomsen LL, Andersen I, Nazim F, Olesen J. 2004. Clinical characteristics of 362 patients with familial migraine with aura. *Cephalalgia* 24:564-75
- Escayg A, MacDonald BT, Meisler MH, Baulac S, Huberfeld G, et al. 2000. Mutations of SCN1A, encoding a neuronal sodium channel, in two families with GEFS+. *Nat Genet* 24:343-45

- Estacion M, Gasser A, Dib-Hajj SD, Waxman SG. 2010. A sodium channel mutation linked to epilepsy increases ramp and persistent current of Nav1.3 and induces hyperexcitability in hippocampal neurons. *Exp Neurol* 224:362-68
- Fahn S. 2011. Classification of movement disorders. *Mov Disord* 26:947-57
- Falace A, Filipello F, La Padula V, Vanni N, Madia F, et al. 2010. TBC1D24, an ARF6-interacting protein, is mutated in familial infantile myoclonic epilepsy. *Am J Hum Genet* 87:365-70
- Fertleman CR, Baker MD, Parker KA, Moffatt S, Elmslie FV, et al. 2006. SCN9A mutations in paroxysmal extreme pain disorder: allelic variants underlie distinct channel defects and phenotypes. *Neuron* 52:767-74
- Gardiner AR, Bhatia KP, Stamelou M, Dale RC, Kurian MA, et al. 2012. PRRT2 gene mutations: from paroxysmal dyskinesia to episodic ataxia and hemiplegic migraine. *Neurology* 79:2115-21
- Gauer RL. 2011. Evaluation of syncope. *Am Fam Physician* 84:640-50
- Geis C, Weishaupt A, Hallermann S, Grunewald B, Wessig C, et al. 2010. Stiff person syndrome-associated autoantibodies to amphiphysin mediate reduced GABAergic inhibition. *Brain* 133:3166-80
- Ghezzi D, Viscomi C, Ferlini A, Gualandi F, Mereghetti P, et al. 2009. Paroxysmal non-kinesigenic dyskinesia is caused by mutations of the MR-1 mitochondrial targeting sequence. *Hum Mol Genet* 18:1058-64
- Gillis J, Pavlidis P. 2012. "Guilt by association" is the exception rather than the rule in gene networks. *PLoS Comput Biol* 8:e1002444

- Goldstein JL, Brown MS. 2009. The LDL receptor. *Arterioscler Thromb Vasc Biol* 29:431-38
- Gonzaga-Jauregui C, Lupski JR, Gibbs RA. 2012. Human genome sequencing in health and disease. *Annu Rev Med* 63:35-61
- Grabrucker AM, Schmeisser MJ, Schoen M, Boeckers TM. 2011. Postsynaptic ProSAP/Shank scaffolds in the cross-hair of synaptopathies. *Trends Cell Biol* 21:594-603
- Hageman GS, Anderson DH, Johnson LV, Hancox LS, Taiber AJ, et al. 2005. A common haplotype in the complement regulatory gene factor H (HF1/CFH) predisposes individuals to age-related macular degeneration. *Proc Natl Acad Sci U S A* 102:7227-32
- Haut SR, Bigal ME, Lipton RB. 2006. Chronic disorders with episodic manifestations: focus on epilepsy and migraine. *Lancet Neurol* 5:148-57
- Heinzen EL, Swoboda KJ, Hitomi Y, Gurrieri F, Nicole S, et al. 2012. De novo mutations in ATP1A3 cause alternating hemiplegia of childhood. *Nature Genet* 44:1030-4
- Helbig I, Scheffer IE, Mulley JC, Berkovic SF. 2008. Navigating the channels and beyond: unraveling the genetics of the epilepsies. *Lancet Neurol* 7:231-45
- Heron SE, Grinton BE, Kivity S, Afawi Z, Zuberi SM, et al. 2012. PRRT2 mutations cause benign familial infantile epilepsy and infantile convulsions with choreoathetosis syndrome. *Am J Hum Genet* 90:152-60

- Higuchi O, Hamuro J, Motomura M, Yamanashi Y. 2011. Autoantibodies to low-density lipoprotein receptor-related protein 4 in myasthenia gravis. *Ann Neurol* 69:418-22
- Hoch W, McConville J, Helms S, Newson-Davis J, Melms A, et al. 2001. Autoantibodies to the receptor tyrosine kinase MuSK in patients with myasthenia gravis without acetylcholine receptor antibodies. *Nat Med* 7:365-68
- Hoffmann K, Muller JS, Stricker S, Megarbane A, Rajab A, et al. 2006. Escobar syndrome is a prenatal myasthenia caused by disruption of the acetylcholine receptor fetal gamma subunit. *Am J Hum Genet* 79:303-12
- Holland KD, Kearney JA, Glauser TA, Buck G, Keddache M, et al. 2008. Mutation of sodium channel SCN3A in a patient with cryptogenic pediatric partial epilepsy. *Neurosci Lett* 433:65-70
- Irani SR, Pettingill P, Kleopa KA, Schiza N, Waters P, et al. 2012. Morvan syndrome: clinical and serological observations in 29 cases. *Ann Neurol* 72:241-55
- Jen JC, Wan J, Palos TP, Howard BD, Baloh RW. 2005. Mutation in the glutamate transporter EAAT1 causes episodic ataxia, hemiplegia, and seizures. *Neurology* 65:529-34
- Jen JC, Graves TD, Hess EJ, Hanna MG, Griggs RC, et al. 2007. Primary episodic ataxias: diagnosis, pathogenesis and treatment. *Brain* 130:2484-93
- Jen JC. 2008. Hereditary episodic ataxias. *Ann N Y Acad Sci* 1142:250-53
- Jurkat-Rott K, Lerche H, Weber Y, Lehmann-Horn F. 2010. Hereditary channelopathies in neurology. *Adv Exp Med Biol* 686:305-34

- Kalachikov S, Evgrafov O, Ross B, Winawer M, Barker-Cummings C, et al. 2002. Mutations in LGI1 cause autosomal-dominant partial epilepsy with auditory features. *Nat Genet* 30:335-41
- Kitamura K, Yanazawa M, Sugiyama N, Miura H, Iizuka-Kogo A, et al. 2002. Mutation of ARX causes abnormal development of forebrain and tests in mice and X-linked lissencephaly with abnormal genitalia in humans. *Nat Genet* 32:359-69
- Klassen T, Davis C, Goldman A, Burgess D, Chen T, et al. 2011. Exome sequencing of ion channel genes reveals complex profiles confounding personal risk assessment in epilepsy. *Cell* 145:1036-48
- Kleopa KA. 2011. Autoimmune channelopathies of the nervous system. *Curr Neuroparmacol* 9:458-67
- Koch MC, Steinmeyer K, Lorenz C, Ricker K, Wolf F, et al. 1992. The skeletal muscle chloride channel in dominant and recessive human myotonia. *Science* 257:797-800
- Kullman DM. 2010. Neurological channelopathies. *Annu Rev Neurosci* 33:151-72
- Lafreniere RG, Zameel Cader M, Poulin J-F, Andres-Enguix I, Simoneau M, et al. 2010. A dominant-negative mutation in the TRESK potassium channel is linked to familial migraine with aura. *Nat Med* 16:1157-60
- Lai M, Huijbers MG, Lancaster E, Graus F, Bataller L, et al. 2010. Investigation of LGI1 as the antigen in limbic encephalitis previously attributed to potassium channels: a case series. *Lancet Neurol* 9:776-85
- Lancaster E, Huijbers MG, Bar V, Boronat A, Wong A, et al. 2011. Investigations of caspr2, an autoantigen of encephalitis and neuromyotonia. *Ann Neurol* 69:303-11

- Lee HY, Huang Y, Bruneau N, Roll P, Roberson ED, et al. 2012a. Mutations in the gene PRRT2 cause paroxysmal kinesigenic dyskinesia with infantile convulsions. *Cell Rep* 1:2-12
- Lee HY, Nakayama J, Xu Y, Fan X, Karouani M, et al. 2012b. Dopamine dysregulation in a mouse model of paroxysmal nonkinesigenic dyskinesia. *J Clin Invest* 122:507-18
- Lee HY, Xu Y, Huang Y, Ahn AH, Auburger GW, et al. 2004. The gene for paroxysmal non-kinesigenic dyskinesia encodes an enzyme in a stress response pathway. *Hum Mol Genet* 13:3161-70
- Leen WG, Klepper J, Verbeek MM, Leferink M, Hofste T, et al. 2010. Glucose transporter-1 deficiency syndrome: the expanding clinical and genetic spectrum of a treatable disorder. *Brain* 133:655-70
- Lennon VA, Kryzer TJ, Pittock SJ, Verkman AS, Hinson SR. 2005. IgG marker of optic-spinal multiple sclerosis binds to the aquaporin-4 water channel. *J Exp Med* 202:473-77
- Leo L, Gherardini L, Barone V, De Fusco M, Pietrobon D, et al. 2011. Increased susceptibility to cortical spreading depression in the mouse model of familial hemiplegic migraine type 2. *PLoS Genet* 7:e1002129
- Li J, Zhu X, Wang X, Sun W, Feng B, et al. 2012. Targeted genomic sequencing identifies PRRT2 mutations as a cause of paroxysmal kinesigenic choreoathetosis. *J Med Genet* 49:76-78
- Lossin C, George AL Jr. 2008. Myotonia congenita. *Adv Genet* 63:25-55

- Loukaides P, Schiza N, Pettingill P, Palazis L, Vounou E, et al. 2012. Morvan's syndrome associated with antibodies to multiple components of the voltage-gated potassium channel complex. *J Neurol Sci* 312:52-56
- Mahida S, Lubitz SA, Rienstra M, Milan DJ, Ellinor PT. 2011. Monogenic atrial fibrillation as pathophysiological paradigms. *Cardiovasc Res* 89:692-700
- Mantegazza M, Rusconi R, Scalmani P, Avanzini G, Franceschetti S. 2010. Epileptogenic ion channel mutations: from bedside to bench and, hopefully, back again. *Epilepsy Res* 92:1-29
- Marini C, Conti V, Mei D, Battaglia D, Lettori D, et al. 2012. PRRT2 mutations in familial infantile seizures, paroxysmal dyskinesia, and hemiplegic migraine. *Neurology* 79:2109-14
- Martin MS, Dutt K, Papale LA, Dube CM, Dutton SB, et al. 2010. Altered function of the SCN1A voltage-gated sodium channel leads to gamma-aminobutyric acidergic (GABAergic) interneuron abnormalities. *J Biol Chem* 285:9823-34
- Maselli RA, Ng JJ, Anderson JA, Cagney O, Arredondo J, et al. 2009. Mutations in LAMB2 causing a severe form of synaptic congenital myasthenic syndrome. *J Med Genet* 46:203-8
- McBride KL, Garg V. 2010. Impact of Mendelian inheritance in cardiovascular disease. *Ann N Y Acad Sci* 1214:122-37
- McClatchey AI, McKenna-Yasek D, Cros D, Worthen HG, Kuncel RW, et al. 1992. Novel mutations in families with unusual and variable disorders of the skeletal muscle sodium channel. *Nat Genet* 2:148-52
- Mihaylova V, Muller JS, Vilchez JJ, Salih MA, Kabiraj MM, et al. 2008. Clinical and

- molecular genetic findings in COLQ-mutant congenital myasthenic syndromes.
Brain 131:747-59
- Mohler PJ, Schott JJ, Gramolini AO, Dilly KW, Guatimosim S, et al. 2003. Ankyrin-B mutation causes type 4 long-QT cardiac arrhythmia and sudden cardiac death.
Nature 421:634-39
- Morar B, Zhelyazkova S, Azmanov DN, Radionova M, Angelicheva D, et al. 2011. A novel GEFS+ locus on 12p13.33 in a large Roma family. *Epilepsy Res* 97:198-207
- Morishita H, Yagi T. 2007. Protocadherin family: diversity, structure, and function.
Curr Opin Cell Biol 19:584-92
- Nardocci N, Zorzi G, Barzaghi C, Zibordi F, Ciano C, et al. 2008. Myoclonus-dystonia syndrome: clinical presentation, disease course, and genetic features in 11 families. *Mov Disord* 23:28-34
- Neville BG, Ninan M. 2007. The treatment and management of alternating hemiplegia of childhood. *Dev Med Child Neurol* 49:777-80
- Nicita F, De Liso P, Danti FR, Papetti L, Ursitti F, et al. 2012. The genetics of monogenic idiopathic epilepsies and epileptic encephalopathies. *Seizure* 21:3-11
- Nyegaard M, Overgaard MT, Sondergaard MT, Vranas M, Behr ER, et al. 2012. Mutations in calmodulin cause ventricular tachycardia and sudden cardiac death.
Am J Hum Genet 91:703-12
- O’Roak BJ, Vives L, Girirajan S, Karakoc E, Krumm N, et al. 2012. Sporadic autism exomes reveal a highly interconnected protein network of de novo mutations.
Nature 485:246-50

- Pevzner A, Schoser B, Peters K, Cosma NC, Karakatsani A, et al. 2012. Anti-LRP4 autoantibodies in AchR- and MuSK-antibody-negative myasthenia gravis. *J Neurol* 259:427-35
- Plaster NM, Tawil R, Tristani-Firouzi M, Canun S, Bendahhou S, et al. 2001. Mutations in Kir2.1 cause the developmental and episodic electrical phenotypes of Andersen's syndrome. *Cell* 105:511-19
- Poduri A, Lowenstein D. 2011. Epilepsy genetics – past, present, and future. *Curr Opin Genet Dev* 21:325-32
- Ptáček LJ, George AL Jr, Barchi RL, Griggs RC, Riggs JE, et al. 1992. Mutations in an S4 segment of the adult skeletal muscle sodium channel cause paramyotonia congenita. *Neuron* 8:891-97
- Ptáček LJ, George AL Jr, Griggs RC, Tawil R, Kallen RG, et al. 1991. Identification of a mutation in the gene causing hyperkalemic periodic paralysis. *Cell* 67:1021-27
- Ptáček LJ, Tawil R, Griggs RC, Engel AG, Layzer RB, et al. 1994a. Dihydropyridine receptor mutations cause hypokalemic periodic paralysis. *Cell* 77:863-68
- Ptáček LJ, Tawil R, Griggs RC, Meola G, McManis P, et al. 1994b. Sodium channel mutations in acetazolamide-responsive myotonia congenita, paramyotonia congenita, and hyperkalemic periodic paralysis. *Neurology* 44:1500-3
- Rainier S, Thomas D, Tokarz D, Ming L, Bui M, et al. 2004. Myofibrillogenesis regulator 1 gene mutations cause paroxysmal dystonic choreoathetosis. *Arch Neurol* 61:1025-29
- Raja Rayan DL, Hanna MG. 2010. Skeletal muscle channelopathies: nondystrophic myotonias and periodic paralysis. *Curr Opin Neurol* 23:466-76

- Ramachandran N, Girard JM, Turnbull J, Minassian BA. 2009. The autosomal recessively inherited progressive myoclonus epilepsies and their genes. *Epilepsia* 50(Suppl 5):29-36
- Rees MI, Harvey K, Pearce BR, Chung SK, Duguid IC, et al. 2006. Mutations in the gene encoding GlyT2 (SLC6A5) define a presynaptic component of human startle disease. *Nat Genet* 38:801-6
- Rojas CV, Wang JZ, Schwartz LS, Hoffman EP, Powell BR, et al. 1991. A Met-to-Val mutation in the skeletal muscle Na⁺ channel alpha-subunit in hyperkalaemic periodic paralysis. *Nature* 354:387-89
- Roux-Buisson N, Cacheux M, Fourest-Lieuvain A, Fauconnier J, Brocard J, et al. 2012. Absence of triadin, a protein of the calcium release complex, is responsible for cardiac arrhythmia with sudden death in humans. *Hum Mol Genet* 21:2759-67
- Roze E, Apartis E, Clot F, Dorison N, Thobois S, et al. 2008. Myoclonus-dystonia: clinical and electrophysiologic pattern related to SGCE mutations. *Neurology* 70:1010-16
- Ryan DP, da Silva MR, Soong TW, Fontaine B, Donaldson MR, et al. 2010. Mutations in potassium channel Kir2.6 cause susceptibility to thyrotoxic hypokalemic periodic paralysis. *Cell* 140:88-98
- Ryan DP, Ptáček LJ. 2010. Episodic neurological channelopathies. *Neuron* 68:282-92
- Saitou H, Kato M, Mizuguchi T, Hamada K, Osaka H, et al. 2008. De novo mutations in the gene encoding STXBP1 (MUNC18-1) cause early infantile epileptic encephalopathy. *Nat Genet* 40:782-88

- Sanders J, Murtha MT, Gupta AR, Murdoch JD, Raubeson MJ, et al. 2012. De novo mutations revealed by whole-exome sequencing are strongly associated with autism. *Nature* 485:237-41
- Scholl UI, Choi M, Liu T, Ramaekers VT, Hausler MG, et al. 2009. Seizures, sensorineural deafness, ataxia, mental retardation, and electrolyte imbalance (SeSAME syndrome) caused by mutations in KCNJ10. *Proc Natl Acad Sci U S A* 106:5842-47
- Sehgal A, Mignot E. 2011. Genetics of sleep and sleep disorders. *Cell* 146:194-207
- Seidner G, Alvarez MG, Yeh JI, O'Driscoll KR, Klepper J, et al. 1998. GLUT-1 deficiency syndrome caused by haploinsufficiency of the blood-brain barrier hexose carrier. *Nat Genet* 18:188-91
- Sheffield VC, Stone EM. 2011. Genomics and the eye. *N Engl J Med* 364: 1932-42
- Shen Y, Lee HY, Rawson J, Ojha S, Babbitt P, et al. 2011. Mutations in PNKD causing paroxysmal dyskinesia alters protein cleavage and stability. *Hum Mol Genet* 20:2322-32
- Shiang R, Ryan SG, Zhu YZ, Hahn AF, O'Connell P, et al. 1993. Mutations in the alpha 1 subunit of the inhibitory glycine receptor cause the dominant neurologic disorder, hyperekplexia. *Nat Genet* 5:351-58
- Shoubridge C, Fullston T, Gecz J. 2010. ARX spectrum disorders: making inroads into the molecular pathology. *Hum Mutat* 31:889-900
- Shyti R, de Vries B, van den Maagdenberg A. 2011. Migraine genes and the relation to gender. *Headache* 51:880-90

- Smith SE, Xu L, Kasten MR, Anderson MP. 2012. Mutant LGI1 inhibits seizure-induced trafficking of Kv4.2 potassium channels. *J Neurochem* 120:611-21
- Solimena M, Folli F, Denis-Donini S, Comi GC, Pozza G, et al. 1988. Autoantibodies to glutamic acid decarboxylase in a patient with stiff-man syndrome, epilepsy, and type I diabetes mellitus. *N Engl J Med* 318:1012-20
- Stafstrom CE. 2009. Severe epilepsy syndromes of early childhood: the link between genetics and pathophysiology with a focus on SCN1A mutations. *J Child Neurol* 24:S15-23
- Strømme P, Mangelsdorf ME, Shaw MA, Lower KM, Lewis SM, et al. 2002. Mutations in the human ortholog of *Aristaless* cause X-linked mental retardation and epilepsy. *Nat Genet* 30:441-45
- Sugawara T, Tsurubuchi Y, Agarwala KL, Ito M, Fukuma G, et al. 2001. A missense mutation of the Na⁺ channel alpha II subunit gene *Na(v)1.2* in a patient with febrile and afebrile seizures causes channel dysfunction. *Proc Natl Acad Sci U S A* 98:6384-89
- Suls A, Dedeken P, Goffin K, Van Esch H, Dupont P, et al. 2008. Paroxysmal exercise-induced dyskinesia and epilepsy is due to mutations in *SLC2A1*, encoding the glucose transporter GLUT1. *Brain* 131:1831-44
- Suzuki T, Delgado-Escueta AV, Aguan K, Alonso ME, Shi J, et al. 2004. Mutations in *EFHC1* cause juvenile myoclonic epilepsy. *Nat Genet* 36:842-49
- Tawil R, McDermott MP, Brown R Jr, Shapiro BC, Ptáček LJ, et al. 2000. Randomized trials of dichlorphenamide in the periodic paralyses. Working Group on Periodic Paralysis. *Ann Neurol* 47:46-53

- Tennessen JA, Bigham AW, O'Connor TD, Fu W, Kenny EE, et al. 2012. Evolution and functional impact of rare coding variation from deep sequencing of human exomes. *Science* 337:64-69
- Tomlinson SE, Hanna MG, Kullmann DM, Tan SV, Burke D. 2009. Clinical neurophysiology of the episodic ataxias: insights into ion channel dysfunction in vivo. *Clin Neurophysiol* 120:1768-76
- Tottene A, Conti R, Fabbro A, Vecchia D, Shapovalova M, et al. 2009. Enhanced excitatory transmission at cortical synapses as the basis for facilitated spreading depression in Ca(v)2.1 knockin migraine mice. *Neuron* 61:762-73
- Tristani-Firouzi M, Etheridge SP. 2010. Kir 2.1 channelopathies: the Andersen-Tawil syndrome. *Pflugers Arch* 460:289-94
- Ueda K, Valdivia C, Medeiros-Domingo A, Tester DJ, Vatta M, et al. 2008. Syntrophin mutation associated with long QT syndrome through activation of the nNOS-SCN5A macromolecular complex. *Proc Natl Acad Sci U S A* 105:9355-60
- Valdivia CR, Ueda K, Ackerman MJ, Makielski JC. 2009. GPD1L links redox state to cardiac excitability by PKC-dependent phosphorylation of the sodium channel SCN5A. *Am J Physiol Heart Circ Physiol* 297:H1446-52
- van der Werf C, Kannankeril PJ, Sacher F, Krahn AD, Viskin S, et al. 2011. Flecainide therapy reduces exercise-induced ventricular arrhythmias in patients with catecholaminergic polymorphic ventricular tachycardia. *J Am Coll Cardiol* 57:2244-54

- Vatta M, Ackerman MJ, Ye B, Makielski JC, Ughanze EE, et al. 2006. Mutant caveolin-3 induces persistent late sodium current and is associated with long-QT syndrome. *Circulation* 114:2104-12
- Veeramah KR, O'Brien JE, Meisler MH, Cheng X, Dib-Hajj SD, et al. 2012. De novo pathogenic SCN8A mutation identified by whole-genome sequencing of a family quartet affected by infantile epileptic encephalopathy and SUDEP. *Am J Hum Genet* 90:502-10
- Vincent A, Lang B, Kleopa KA. 2006. Autoimmune channelopathies and related neurological disorders. *Neuron* 52:123-38
- Wallace RH, Wang DW, Singh R, Scheffer IE, George AL Jr, et al. 1998. Febrile seizures and generalized epilepsy associated with a mutation in the Na⁺-channel beta1 subunit gene SCN1B. *Nat Genet* 19:366-70
- Wang JL, Cao L, Li XH, Hu ZM, Li JD, et al. 2011. Identification of PRRT2 as the causative gene of paroxysmal kinesigenic dyskinesias. *Brain* 134:3493-3501
- Watanabe H, Chopra N, Laver D, Hwang HS, Davies SS, et al. 2009. Flecainide prevents catecholaminergic polymorphic ventricular tachycardia in mice and humans. *Nat Med* 15:380-3
- Weaving LS, Christodoulou J, Williamson SL, Friend KL, McKenzie OL, et al. 2004. Mutations of CDKL5 cause a severe neurodevelopmental disorder with infantile spasms and mental retardation. *Am J Hum Genet* 75:1079-93
- Weber YG, Storch A, Wuttke TV, Brockmann K, Kempfle J, et al. 2008. GLUT1 mutations are a cause of paroxysmal exertion-induced dyskinesias and induce hemolytic anemia by a cation leak. *J Clin Invest* 118:2157-68

- Weiss J, Pyrski M, Jacobi E, Bufe B, Willnecker V, et al. 2011. Loss-of-function mutations in sodium channel Nav1.7 cause anosmia. *Nature* 472:186-90
- Xu Y, Padiath QS, Shapiro RE, Jones CR, Wu SC, et al. 2005. Functional consequences of a CK1delta mutation causing familial advanced sleep phase syndrome. *Nature* 434:640-44
- Yang Y, Wang Y, Li S, Xu Z, Li H, et al. 2004. Mutations in SCN9A, encoding a sodium channel alpha subunit, in patients with primary erythralgia. *J Med Genet* 41:171-74
- Yu FH, Mantegazza M, Westenbroek RE, Robbins CA, Kalume F, et al. 2006. Reduced sodium current in GABAergic interneurons in a mouse model of severe myoclonic epilepsy in infancy. *Nat Neurosci* 9:1142-49
- Zhang L, Jones CR, Ptáček LJ, Fu YH. 2011. The genetics of the human circadian clock. *Adv Genet* 74: 231-47
- Zhou YD, Lee S, Jin Z, Wright M, Smith SE, Anderson MP. 2009. Arrested maturation of excitatory synapses in autosomal dominant lateral temporal lobe epilepsy. *Nat Med* 15:1208-14
- Zhou YD, Zhang D, Ozkaynak E, Wang X, Kasper EM, et al. 2012. Epilepsy gene LGI1 regulates postnatal developmental remodeling of retinogeniculate synapses. *J Neurosci* 32:903-10
- Zimprich A, Grabowski M, Asmus F, Naumann M, Berg D, et al. 2001. Mutations in the gene encoding epsilon-sarcoglycan cause myoclonus-dystonia syndrome. *Nat Genet* 29:66-69

CHAPTER II

Familial Cortical Myoclonus, a Novel Movement Disorder

SUMMARY

Myoclonus is characterized by sudden, brief involuntary movements, and its presence is debilitating. The differential diagnosis of myoclonus is extensive, but in only two autosomal dominant disorders, familial adult myoclonic epilepsy (FAME) and myoclonus dystonia syndrome (MDS), does myoclonus predominate. We identified 11 members of a large, Canadian Mennonite family suffering from adult onset, slowly progressive, disabling, multifocal myoclonus. Somatosensory evoked potentials indicated a cortical origin of the myoclonus. There were no associated seizures. In total, this family's phenotype is not consistent with any previously described syndrome, including FAME or MDS. We propose that familial cortical myoclonus (FCM) is a novel movement disorder. We also identified seven patients from five kindreds who suffered from cortical myoclonus that may be familial; however, their inheritance was not clear, and the phenotypes were not consistent with the index family, so we concluded that none of these patients have FCM. We anticipate that this work will enhance diagnosis in patients with myoclonus. Furthermore, genetic analysis of the FCM family to identify the underlying mutation may provide insight into the pathophysiology of this peculiar disorder.

INTRODUCTION

Myoclonus is characterized by sudden, brief, shock-like involuntary movements (Caviness & Brown 2004, Kojovic et al. 2011). These movements can result from involuntary muscle contractions (“positive myoclonus”) or from involuntary muscle relaxations (“negative myoclonus”). Myoclonic movements are simple, in contrast with chorea (movements that are complex and brief) or dystonia (movements that are complex and sustained). Unlike a tic, myoclonus cannot be voluntarily suppressed. On gross examination it may be difficult to differentiate high-frequency myoclonus from tremor or a clonic seizure, both of which involve rhythmic alternating contraction of agonist and antagonist muscles. In contrast, myoclonic jerks are arrhythmic or solitary and do not alternately afflict muscle pairs. (However, myoclonus may be one component of a seizure, as noted below.) Myoclonic movements can differ substantially between patients in their distribution (focal, segmental, multifocal, hemi, or generalized), temporal pattern (continuous or intermittent), and activation (“spontaneous myoclonus” occurs at rest, whereas “stimulus-sensitive myoclonus” occurs in response to various stimuli; e.g., action myoclonus is triggered by voluntary movement). Depending on which muscles are affected and the frequency of attacks, myoclonus can be severely debilitating.

In Chapter I we introduced the differential diagnosis for myoclonus. It is extremely broad, spanning the spectrum of neurologic disease: structural malformations, infections, storage disorders, spinocerebellar degenerations, dementias, metabolic derangements, toxin/drug exposures, post-hypoxia, malabsorption (Celiac’s disease), various epilepsy syndromes, and many more (Caviness & Brown 2004, Kojovic et al. 2011, Lozsadi 2012). Organizing such a heterogeneous collection of disorders is challenging.

One approach is to classify the myoclonus into four categories: physiologic, symptomatic, epileptic, or essential. Physiologic myoclonus, such as hiccups or hypnagogic jerks, is widespread and benign. The second type, symptomatic myoclonus, can occur secondary to a multifarious array of neurologic illnesses (see list in preceding paragraph). The third type is epileptic myoclonus, in which myoclonus occurs as just one component of a chronic seizure disorder, although very rarely, myoclonus can be the sole outward manifestation of epilepsy (discussed below). Finally, in essential myoclonus the myoclonus is the predominant or only clinical finding.

Another scheme groups myoclonus by the level of the nervous system from which it is thought to originate. The terminal step in myoclonus is inappropriate contraction of skeletal muscle. This inappropriate contraction arises from hyperexcitability of the nervous system at any point along the normal pathway for propagation of motor output – from the cerebral cortex, to the subcortex, to the spine, to the peripheral nervous system. The focus of hyperexcitability is called the “myoclonus generator”. In identifying the generator, clinical details are helpful (Kojovic et al. 2011, Lozsadi 2012) but electrophysiological examination is the standard of care (Shibasaki & Hallett 2005, Cassim & Houdayer 2006). If electromyography (EMG) demonstrates shorter bursts, it reflects a higher-level generator (e.g., cortical myoclonus has bursts of <50ms). In contrast, longer bursts indicate a lower-level generator (e.g., a spinal or peripheral origin of the myoclonus).

Relative to cortical myoclonic jerks, subcortical jerks are typically more sustained (around 500ms), but this may not always be the case. To distinguish between the two, EMG is paired with electroencephalography (EEG). EMG-EEG is measured over time in

response to sensory stimulation by way of electrical shocks at the median nerve. After around 100 jerks are detected by EMG, the EEG traces corresponding to one second before and one second after those jerks are averaged into a composite trace. This technique is known as jerk-locked back averaging (JLBA), and the cortical responses are known as somatosensory evoked potentials (SSEPs) (Shibasaki & Hallett 2005, Cassim & Houdayer 2006). In cortical myoclonus, the SSEPs over the parietal P25-N33 complex, corresponding to the somatosensory cortex, exhibit amplitude of at least 10 times greater than normal. Typically, the cutoff for labeling such traces as “giant SSEPs” is 8.6 μ V (Shibasaki & Hallett 2005). This test very effectively distinguishes cortical myoclonus (giant SSEPs) from subcortical myoclonus and also spinal or peripheral myoclonus, which all are associated with normal SSEPs. Giant SSEPs reflect a hyperexcitable somatosensory cortex, corresponding to the enhanced stimulus-sensitivity in cortical myoclonus. Various sensory stimuli, such as action, posture, touch, or emotion, can serve as triggers. Hyperexcitability of the somatosensory cortex can be corroborated by functional MRI (fMRI): the primary somatic sensory cortex (SI) contralateral to the myoclonic muscle(s) is found to have increased blood flow thought to correspond to neuronal activity (Shibasaki & Hallett 2005, Cassim & Houdayer 2006).

Typically, electrophysiological examination is not required for diagnosing myoclonus because symptomatic myoclonus predominates and a diagnosis is suggested by the holistic clinical picture (Caviness & Brown 2004, Borg 2006, Kojovic et al. 2011). The same is true for epileptic myoclonus. Essential myoclonus, in which myoclonus is the major or lone clinical finding, has a more limited differential diagnosis. Sporadic cases in the elderly may be primary progressive myoclonus of aging (Alvarez & Caviness

2008, Katschnig et al. 2011). In neonates one should consider benign neonatal sleep myoclonus (Maurer et al. 2010), which was thought to be sporadic but in fact may be hereditary (Afawi et al. 2012). A family history of myoclonus can be instructive, as two hereditary disorders constitute the vast majority of essential myoclonus: familial adult myoclonic epilepsy, and myoclonus dystonia syndrome.

Familial adult myoclonic epilepsy (FAME) is also known as benign adult familial myoclonic epilepsy (BAFME) or familial cortical myoclonic tremor with epilepsy (FCMTE), among other monikers. FAME is technically epileptic myoclonus rather than essential myoclonus, but it may be considered to be essential myoclonus because the myoclonus is sometimes the only detectable symptom (Striano et al. 2005). Classically, FAME is an adult onset disorder, but at least two very large families exhibit juvenile onset (Gardella et al. 2006, Crompton et al. 2012). Symptoms range from finger tremor-like myoclonus to postural limb tremor-like myoclonus to generalized tonic-clonic seizures (Crompton et al. 2012). Likely, many mild cases of FAME are misdiagnosed as essential tremor (Louis 2001, Bain 2007, Louis et al. 2008). Classic FAME does not include dementia, although it may include decreased cognition (Van Rootselaar et al. 2005). One severe variant, called FAME3, is distinguished by dementia along with prominent ataxia, cerebellar atrophy, early disability, and death (Carr et al. 2007). The myoclonus in FAME is provoked by stress, emotion, fatigue, and touch (Van Rootselaar et al. 2005), reflecting cortical myoclonus. Giant SSEPs are observed. FAME inheritance is autosomal dominant, with linkage to chromosomes 8q23.3-q24.11 (Mikami et al. 1999, Plaster et al. 1999, Mori et al. 2011), 2p11.1-p12.2 (Guerrini et al. 2001, Crompton et al. 2012), 5p15.31-p15 (Depienne et al. 2010), and 3q26.32-q28 (Yeetong et

al. 2012). Despite over ten years of extensive study, the disease genes residing in the FAME critical regions have not been identified.

The second hereditary essential myoclonus disorder is myoclonus dystonia syndrome (MDS). MDS is typically characterized by myoclonic jerks of the arms and axial musculature, along with mild dystonia (often cervical dystonia or writer's cramp) (Nardocci et al. 2008, Kinugawa et al. 2009, Muller 2009). Symptoms are clearly ameliorated with alcohol and exacerbated by muscle activation, posture, or psychological stress. However, MDS is not considered stimulus-sensitive, and SSEPs are normal, indicating a subcortical origin (Shibasaki & Hallett 2005, Cassim & Houdayer 2006). Cognition is normal. There is pronounced psychiatric comorbidity, including depression, anxiety, and obsessive-compulsive disorder (Saunders-Pullman et al. 2002), but the prevalence of these conditions may relate to frequent self-medication by intoxication. Onset occurs in childhood or adolescence, and the course is variable, from progression to spontaneous remission. MDS is inherited in an autosomal dominant fashion, with reduced penetrance and variable expressivity. Most cases are caused by mutations in the epsilon sarcoglycan (*SGCE*) gene on chromosome 7q21.3 (Zimprich et al. 2001, Nardocci et al. 2008, Roze et al. 2008). Some cases are caused by microdeletions spanning the *SGCE* gene (Han et al. 2008). There is also strong evidence for a second locus, chromosome 18p11 (Grimes et al. 2002; Han et al. 2007), as well as for additional locus heterogeneity (Valente et al. 2003, Schule et al. 2004, Orth et al. 2007, Groen et al. 2011). A few exceptional cases of MDS include one *SGCE* mutation-positive family with onset in middle age (Wong et al. 2010); myoclonus dystonia plus syndrome, characterized by MDS and short stature, microcephaly, and mental retardation, caused by

a 7q21 microdeletion encompassing the *SGCE* gene and others nearby (Saugier-Weber et al. 2010); and MDS-like symptoms observed in concert with cerebrotendinous xanthomatosis (Lagarde et al. 2012), ataxia-telangiectasia (Saunders-Pullman et al. 2012), and tyrosine hydroxylase deficiency (Stamelou et al. 2012). Importantly, studies have demonstrated via normal SSEPs that the myoclonus is subcortical in all known *SGCE* mutation-positive and mutation-negative cases of MDS (Li et al. 2008, Marelli et al. 2008).

SGCE encodes a membrane protein thought to function in the dystrophin-glycoprotein complex (DGC), but there is little data to support the hypothesis that *SGCE* functions in a DGC-like complex in the brain (Waite et al. 2012). The other sarcoglycans, *sarcoglycan alpha*, *beta*, *gamma*, and *delta*, are mutated in limb girdle muscular dystrophy (LGMD) (Ozawa et al. 2005), but patients with MDS and mutations in *SGCE* do not have LGMD, and patients with LGMD do not have MDS, as would be expected if *SGCE* were functioning together with the other sarcoglycans. Since MDS pathology is specific to the brain, one possibility is that *SGCE* has a different function in the CNS. Ritz et al. (2010) identified a *SGCE* isoform expressed exclusively in brain, but it is unclear whether this isoform differs functionally from other *SGCE* isoforms. Investigations of the *SGCE* knockout mouse, which recapitulates some aspects of the MDS phenotype, have been largely uninformative at the molecular and cellular level (Yokoi et al. 2006, 2010, 2011). It has been twelve years since *SGCE* was pinpointed, yet the pathophysiology of MDS is entirely unknown.

We have identified a family with a phenotype that is clinically and electrophysiologically distinct from other familial disorders in which myoclonus is prominent, including FAME and MDS. Affected members of the large family suffer from autosomal

dominant, slowly progressive, multifocal, cortical myoclonus evoked by somatosensory stimuli. Their myoclonus is not associated with seizures or other neurological deficits aside from mild cerebellar ataxia late in the course of the illness. Here we present the family's phenotype as assessed by history, neurological examination, electrophysiology, and imaging. Familial cortical myoclonus without epilepsy or other neurological deficits has not been described. Thus, we propose that this family exhibits a novel movement disorder, which we have termed familial cortical myoclonus (FCM).

METHODS

This study was approved by the University of Western Ontario Health Sciences Research Ethics Board, and by the University of California, San Francisco Institutional Review Board. All family members provided written informed consent. Thirty-five family members underwent personal interview and complete neurological examination. An individual was identified as affected with myoclonus if the patient reported symptoms of recurrent sudden, involuntary rapid movements of the face, extremities, or body; or if myoclonus was observed upon examination.

Nine of 11 affected individuals, and 12 unaffected relatives (**Figure 1**), underwent SSEP studies. SSEPs were performed by stimulating the median nerve at the wrist with electric shocks delivered at a rate of 5.1Hz as a square wave pulse of 0.2ms duration. An SSEP was determined to be “giant” if the P25-N33 amplitude difference was greater than 8.6 μ V, as defined by Shibasaki & Hallett (2005). Jerk-locked back averaging was not performed as this technique was not available to us and family members were residing in multiple locations across Canada. Instead, multiple representative traces for each patient were averaged to arrive at the values in **Table 1**.

Several family members were investigated with multiple EEGs and computed tomography (CT) or magnetic resonance imaging (MRI) of the brain. Also, the proband (both on and off clonazepam treatment) and her unaffected son underwent fMRI.

Ten affected patients and 25 unaffected relatives donated DNA for genetic studies. DNA was extracted from whole blood according to standard protocols. The quantity and quality of DNA was determined on a NanoDrop ND-1000 UV-Vis Spectrophotometer (Nanodrop Technologies, Wilmington, DE). DNA stocks were stored in a

locked refrigerator at 4°C, and DNA aliquots were stored at -20°C. Analysis of the DNA samples is presented in Chapter III.

We searched for additional families or individuals with similar symptoms to the index family. Clinical data and DNA samples from these patients – 7 individuals from 5 kindreds – were provided by the following collaborators: Steven Frucht, M.D., of Mount Sinai School of Medicine; Leon Dure, M.D., of the University of Alabama at Birmingham School of Medicine; and Kailash Bhatia, M.D., of University College London Institute of Neurology.

RESULTS

Family Heritage

The family (**Figure 1**) is of Mennonite heritage having emigrated from Ukraine through Holland to western Canada (Puffenberger 2003).

Case Reports

The proband (arrow in **Figure 1**) was a 64 year old female who had suffered sudden, involuntary jerking movements in her hands since her teens. The jerks were elicited by action or inadvertent touch. She tended to stumble when walking over uneven ground. At the age of 16 she developed sudden, unexplained falls with preserved consciousness. Falls were also triggered by sudden movement, for example when she rushed to answer the phone. At age 48 she had sustained a fall and head injury triggered by a sudden turning of her head. Over time the jerks became more frequent and widespread, so that she opted for treatment with clonazepam which ameliorated her symptoms. She reported no cognitive symptoms, ataxia, or seizures, and, apart from myoclonus, the neurologic examination was normal. Multifocal myoclonus occurred at rest and with activity in her face and upper extremities when examined off clonazepam. EEG and MRI of the head were unremarkable on several occasions. Median nerve SSEP studies showed giant amplitude P25-N33 cortical response at age 48 (20.3 μ V) and age 60 (11.3 μ V). Brain fMRI demonstrated hyperactivation in the contralateral SI cortex with hand rubbing compared to the study of her unaffected son (**Figure 3**), further supporting the concept of a cortical origin of the myoclonus. Motor and visual activation maps did not differ from controls. [CONTINUED, p. 70]

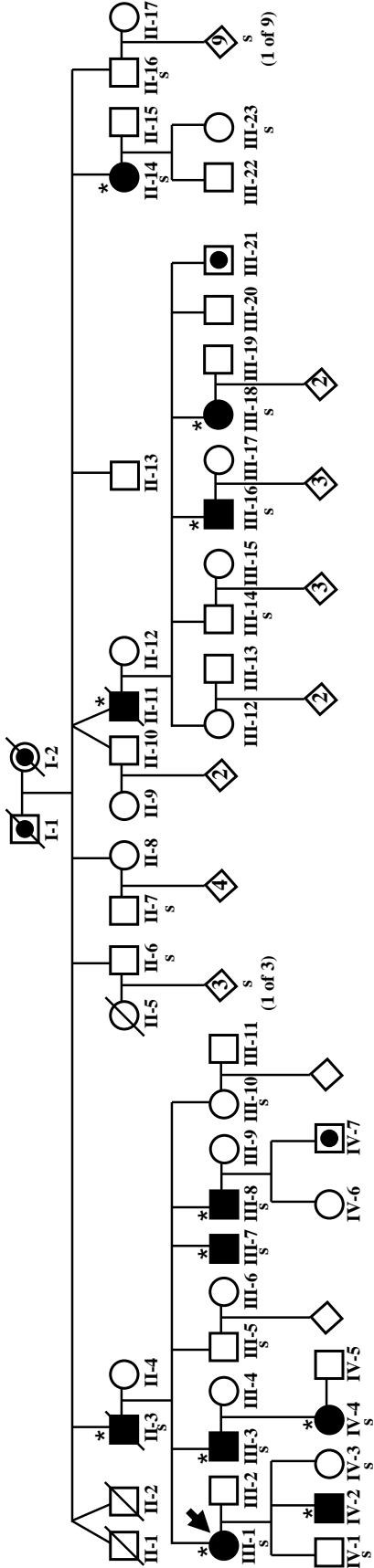


Figure 1. Extended family pedigree.

Dots denote patients with unknown phenotype. Diamonds indicate unaffected progeny with gender masked to preserve anonymity; the number inside diamond denotes multiple unaffected progeny. Asterisks mark patients that carry the *NOL3* mutation. S indicates that SSEP was performed on that patient. One asterisk has been omitted from a carrier to preserve anonymity, and some additional family members (including one unaffected patient who was analyzed by SSEP) were omitted altogether.

The excessive cortical activation in the proband was markedly suppressed by the prescription of clonazepam which had successively alleviated the myoclonus.

The father of the proband (II-3 in **Figure 1**) began to have sudden falls with preserved consciousness at age 50. Triggers included walking over uneven ground or sudden head movements. He also described sudden jerky movements in his limbs. Symptoms were most prominent in the morning and improved after eating lunch. He developed jerking in the extremities in response to exertion, emotional stress, fatigue or sleep deprivation. There was no history of seizures or dystonia. Examination at age 77 revealed intermittent myoclonus in all four limbs, occurring spontaneously or with touch. Myoclonus was prominent upon testing of deep tendon reflexes. There was mild difficulty with heel-shin testing and a slightly wide-based gait. Treatment with clonazepam thrice daily at a dose of 0.5mg significantly reduced myoclonus. However, falls progressed and by age 85 he was confined to a wheelchair, unable to care for himself, and resided in a nursing home. EEG was normal, whereas SSEP studies demonstrated giant cortical responses at 69.4 μ V.

A third affected patient, the proband's youngest brother (III-8 in **Figure 1**), was a 52 year old male who first became aware of sudden jerking movements in his arms while playing baseball in his mid-twenties. He would experience sudden jerking movements of the arms when he reached out to catch the ball. He developed sudden falls if he was touched inadvertently, and would be unable to protect himself with his hands. He also tended to fall if he was walking on uneven ground and had to make a sudden corrective movement. Symptoms were increased with fatigue, exertion, stress, or emotional extremes. Myoclonus was more prominent early in the morning prior to eating breakfast.

He thought drinking caffeine or alcohol worsened his symptoms. Treatment with valproate at 250mg two or three times daily provided excellent symptom control. His neurologic examination showed intermittent diffuse multifocal myoclonus which was worse with action. Finger-nose and heel-shin testing were normal, but he had difficulty with tandem gait. Stance and gait were wide-based. Median nerve SSEPs showed giant amplitude cortical responses (42.9 μ V).

Summary of Clinical Findings

We identified a large Canadian Mennonite family with a history of myoclonus. In total, 11 family members (7 male, 4 female) exhibited stimulus-evoked, multifocal myoclonus throughout the face, arms and legs (**Table 1**). Onset ranged from the second to the seventh decade. Inheritance was autosomal dominant. Myoclonus was the most prominent and disabling clinical feature in all patients. Myoclonus was triggered by action, sudden movements, and/or by inadvertent somatosensory stimuli, but not by light, noise, or startle. Symptoms reportedly were aggravated by fatigue, exertion, sleep deprivation, emotion, and hunger. Five individuals observed that their symptoms were alleviated by a diet of frequent small meals taken throughout the day. Alcohol reportedly had no effect except in one individual in whom myoclonus was ameliorated and in another in whom myoclonus was exacerbated by alcohol. Most (8 of 11) individuals had sustained multiple sudden falls without loss of consciousness that were provoked either by sudden movements or by walking on uneven ground. Patients could not prevent these falls, nor could they protect themselves, and thus they often sustained severe injuries. Generally, they could get up immediately after and [CONTINUED, p. 73]

Table 1. Clinical characteristics in 11 affected family members.

Abbreviations are: +, presence, -, absence; F, face; FNT, finger nose test; LE, lower extremity; UE, upper extremity. IDs refer to **Figure 1**.

ID	Age of Onset	Myoclonus					Alcohol effect	Falls	Speech disturbance	Other	Effective treatment	Median SSEPs (μ V)	
		action	touch	motions	insomnia	fatigue, exertion							lack of food
II-3	50	+	+	+	+	+	UE, LE	none	+	-	mild ataxia	clonazepam	69.4
II-11	50s	+	+	+	+	+	F, UE, LE	none	+	-	multi-infarct dementia	valproate	not done
II-14	60s	+	+	+	+	+	UE, LE	none	+	-	action tremor		79.1
III-1	late teens	+	+	+	+	+	F, UE, LE	none	+	+		clonazepam	20.3
III-3	30s	+	+	+	+	+	UE, LE	decreased	+	-	mild ataxia	clonazepam, valproate	39.4
III-7	40s	+	+	+	+	+	F, UE	none	-	-			55.0
III-8	18	+	+	+	+	+	UE, LE	increased	+	-	mild ataxia	valproate	42.9
III-16	40	+	+	+	+	+	UE, LE	none	+	-	mild ataxia		refused
III-18	40	+	+	+	+	+	UE	none	-	-			21.8
IV-2	20	+	+	+	+	+	F, UE, LE	none	+	+			giant, data unavailable
IV-4	late 20s	+	+	+	+	+	UE, LE	none	-	+			21.2

function with normal strength.

Myoclonus became progressively more frequent and widespread over decades and thereby interfered with activities of daily living. Older patients became wheelchair-dependent. Four showed signs of mild cerebellar limb and gait ataxia late in the course of their illness. There were no signs of cognitive decline, spasticity, or dystonia apart from one individual who had several strokes and developed multi-infarct dementia, likely independent of the myoclonus, which had been present for many years. Moreover, overt seizures were not observed, nor was there a history of psychiatric illness or treatment with psychotropic medication. Myoclonus was effectively suppressed in five patients by treating with either clonazepam or valproic acid (**Table 1**).

SSEP studies, using median nerve electrical depolarization as the stimulus, and recording electrodes to measure ensuing brain electrical activity (see **Introduction**), were performed. SSEPs in 9 of 9 affected patients showed giant cortical responses (**Figure 2A**). All 12 unaffected relatives who were tested with SSEPs had normal cortical evoked responses of low amplitude (**Figure 2B**). As noted above, fMRI of the brain revealed excessive activation of the contralateral SI cortex in the proband, as compared to her unaffected son (**Figure 3**). Finally, repeated EEG recordings in several affected family members were always normal, with no epileptiform activity; thus, the infrequent falls were unlikely to be caused by seizures. [CONTINUED, p. 75]

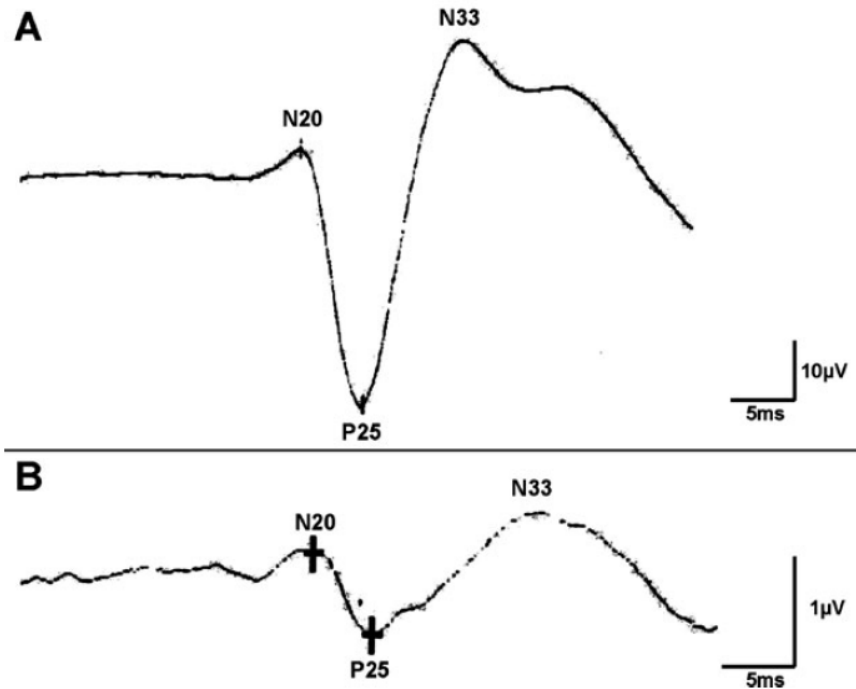


Figure 2. Somatosensory evoked potentials in the familial cortical myoclonus family.

Somatosensory evoked potential waveforms were measured following electrical stimulation of the median nerve at the wrist in a representative (A) affected (II-3 in **Figure 1**; 69.4 μ V) and (B) unaffected (1.1 μ V) family member.

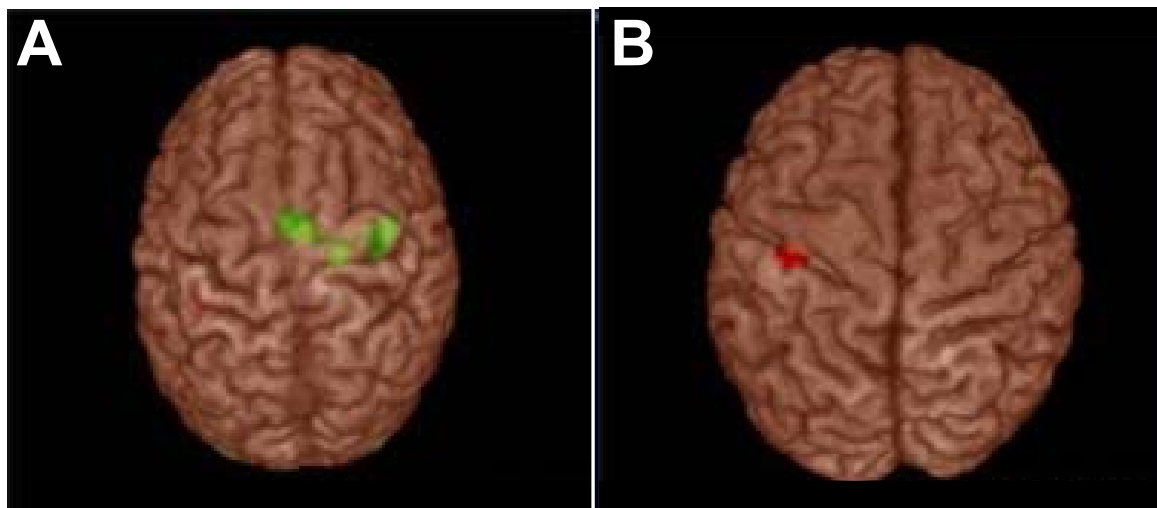


Figure 3. Functional magnetic resonance imaging in the familial cortical myoclonus family.

Brain imaging demonstrated unusually high activation of the contralateral somatosensory cortex in response to hand rubbing in the affected proband (A; III-1 in **Figure 1**) as compared to her unaffected son (B; IV-1).

Search for Additional Patients and Kindreds with Familial Cortical Myoclonus

We canvassed movement disorder specialists and neurogeneticists around the globe in an effort to identify additional individuals and kindreds with the same or a similar phenotype. We identified 7 subjects from 5 kindreds suffering from cortical myoclonus that may be familial (**Figure 4**).

Patient 45141 was a Puerto Rican man with myoclonus, ET-like tremor, and orthostatic tremor. The myoclonus responded to valproate and levetiracetam. Cognition was normal. Inheritance was reportedly autosomal dominant, but we were unable to obtain clinical information or DNA from his affected brother.

Kindred K50197 was an African American family with prominent myoclonus. The myoclonus was somewhat stimulus-sensitive. Again, cognition was normal and inheritance was reported to be autosomal dominant. No additional information or DNA samples were available.

Patient 101287 was a 9 year old female with a six year history of myoclonus. Myoclonus was triggered by action. For example, she had trouble drinking or holding plates. On exam, she had a pattern of irregularly irregular myoclonic jerks, primarily affecting the upper extremities. Myoclonus resolved in sleep but then persisted throughout the daytime and worsened when she was distracted. EEG and MRI were normal. She had resulted from a birth complicated by placenta previa but subsequently attained normal developmental milestones. She was otherwise healthy and intelligent. Attempts to treat her myoclonus with phenobarbital, levetiracetam, valproate, and lamotrigine were ineffective. Her family history was negative for movement disorders.

For the remaining three patients, apart from a history of cortical myoclonus that may be familial and had resisted diagnosis, clinical data were not available.

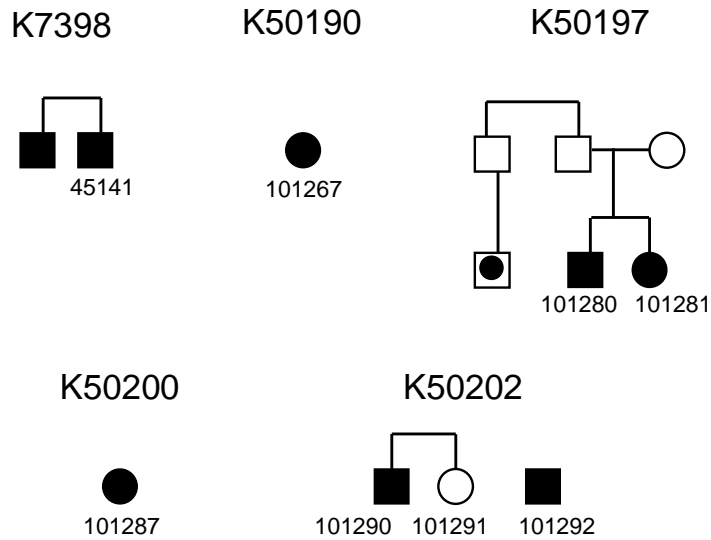


Figure 4. Additional patients with a history of cortical myoclonus that may be familial.

Dot denotes patient with unknown phenotype. Anonymized patient numbers indicate those patients for whom DNA was obtained and analyzed (see Chapter III). The relationship of patient 101292 to the remainder of kindred K50202 is not known.

DISCUSSION

We have described a large family suffering from autosomal dominant, adult onset, slowly progressive, multifocal myoclonus. All affected patients exhibited giant SSEPs (**Figure 2**), which are the sine qua non of cortical myoclonus (Caviness & Brown 2004, Shibasaki & Hallett 2005, Kojovic et al. 2011). A cortical origin of the myoclonus is corroborated by the fMRI measurement of excessive activation in the contralateral somatosensory cortex (**Figure 3**; see **Introduction**). The myoclonus was well controlled in many affected family members by clonazepam or valproate (**Table 1**), but nevertheless became progressively more frequent and ultimately debilitating. There were no other neurological symptoms or signs apart from mild ataxia late in the course of the illness. In our view, the ataxia is likely unrelated to the myoclonus because many years had elapsed prior to ataxia onset, and it was restricted to patients of advanced age, for whom ataxia is a common finding.

This family's illness went undiagnosed for more than a decade after coming to clinical attention. Many diagnoses were entertained. Cortical myoclonus is dominantly inherited in epileptic disorders such as FAME (see **Introduction**). However, the clinical presentation of FAME is distinct from that observed in our family, where myoclonus was slowly progressive and became disabling late in the course of the illness, and overt seizures were not observed. The presentation in this family is also not consistent with a progressive myoclonic epilepsy syndrome (see Chapter I), because there were neither seizures nor progressive dementia. The phenotype would be more consistent with the syndrome of progressive myoclonic ataxia defined by infrequent seizures and little or no cognitive dysfunction (Marseilles Consensus Group 1990), although ataxia was mild and

occurred late in the illness, and we could not detect even infrequent seizures. Another possible diagnosis is hereditary hyperekplexia, an autosomal dominant disorder characterized by an excessive startle reaction (see Chapter I). However, hereditary hyperekplexia is clinically distinct and neurophysiologically marked by hyperexcitability of brain stem origin; giant SSEP cortical responses are not observed (Dreissen et al. 2012).

The presentation in this family also differs from MDS (see **Introduction**), which is, to our knowledge, the sole hereditary essential myoclonus syndrome hitherto described. MDS is characterized by juvenile onset essential myoclonus, dystonia, and psychiatric comorbidity (Nardocci et al. 2008, Roze et al. 2008), whereas in this family myoclonus was adult onset and not accompanied by dystonia or psychiatric comorbidity. Furthermore, in MDS the symptoms are clearly ameliorated by alcohol, which was not the case in this family. Finally, in MDS the myoclonus is of subcortical origin and is not stimulus-sensitive; giant SSEPs are never observed (Li et al. 2008, Marelli et al. 2008).

Hence, by exclusion we conclude that this family represents the first report of a nosologically distinct disorder. This syndrome consists of autosomal dominant, adult onset, slowly progressive, multifocal, cortical myoclonus, without associated dystonia or seizures. We propose for this disorder the term familial cortical myoclonus (FCM).

Identifying additional patients and families with the same or a similar phenotype would bolster the claim that FCM constitutes a novel phenotype. To this end, we found 7 subjects from 5 kindreds suffering from cortical myoclonus that may be familial (**Figure 4**). However, the clinical phenotypes of the 7 subjects were not identical to the FCM family, and none of the 5 kindreds exhibited parent-to-child transmission characteristic of

dominant inheritance. We made further attempts to identify additional FCM patients, which are described in Chapter III.

We anticipate that the characterization of FCM will enhance diagnosis in patients with myoclonus. Furthermore, as has been true for many other Mendelian diseases (Chapter I), description of this phenotype provides the opportunity to identify the causative mutation (Chapter III) and to elucidate pathophysiology (Chapter IV) that may be more broadly applicable to other types of myoclonus or even related diseases of neuronal hyperexcitability.

REFERENCES

- Afawi Z, Bassan H, Heron S, Oliver K, Straussberg R, et al. 2012. Benign neonatal sleep myoclonus: an autosomal dominant form not allelic to KCNQ2 or KCNQ3. *J Child Neurol* 27:1260-63
- Alvarez M, Caviness JN. 2008. Primary progressive myoclonus of aging. *Mov Disord* 23:1658-64
- Bain PG. 2007. Tremor. *Parkinsonism Relat Disord* 13(Suppl 3):S369-74
- Borg M. 2006. Symptomatic myoclonus. *Neurophysiol Clin* 36:309-18
- Carr JA, van der Walt PE, Nakayama J, Fu YH, Corfield V, et al. 2007. FAME 3: a novel form of progressive myoclonus and epilepsy. *Neurology* 68:1382-89
- Cassim F, Houdayer E. 2006. Neurophysiology of myoclonus. *Neurophysiol Clin* 36:281-91
- Caviness J, Brown P. 2004. Myoclonus: current concepts and recent advances. *Lancet Neurol* 3:598-607
- Crompton DE, Sadleir LG, Bromhead CJ, Bahlo M, Bellows ST, et al. 2012. Familial adult myoclonic epilepsy: recognition of mild phenotypes and refinement of the 2q locus. *Arch Neurol* 69:474-81
- Depienne C, Magnin E, Bouteiller D, Stevanin G, Saint-Martin C, et al. 2010. Familial cortical myoclonic tremor with epilepsy: the third locus (FCMTE3) maps to 5p. *Neurology* 74:2000-3
- Dreissen YEM, Bakker MJ, Koelman JHTM, Tijssen MAJ. 2012. Exaggerated startle reactions. *Clin Neurophysiol* 123:34-44
- Gardella E, Tinuper P, Marini C, Guerrini R, Parrini E, et al. 2006. Autosomal dominant

- early-onset cortical myoclonus, photic-induced myoclonus, and epilepsy in a large pedigree. *Epilepsia* 47:1643-49
- Grimes DA, Han F, Lang AE, St George-Hyssop P, Racacho L, et al. 2002. A novel locus for inherited myoclonus-dystonia on 18p11. *Neurology* 59:1183-86
- Groen J, van Rootselaar AF, van der Salm SM, Bloem BR, Tijssen M. 2011. A new familial syndrome with dystonia and lower limb action myoclonus. *Mov Disord* 26:896-900
- Guerrini R, Bonanni P, Patrignani A, Brown P, Parmeggiani L, et al. 2001. Autosomal dominant cortical myoclonus and epilepsy (ADCME) with complex partial and generalized seizures: A newly recognized epilepsy syndrome with linkage to chromosome 2p11.1-q12.2. *Brain* 124:2459-75
- Han F, Racacho L, Lang AE, Bulman DE, Grimes DA. 2007. Refinement of the DYT15 locus in myoclonus-dystonia. *Mov Disord* 22:888-92
- Han F, Racacho L, Yang H, Read T, Suchowersky O, et al. 2008. Large deletions account for an increasing number of mutations in SGCE. *Mov Disord* 23:456-60
- Katschnig P, Massano J, Edwards MJ, Schwingenschuh P, Cordivari C, et al. 2011. Late-onset asymmetric myoclonus: an emerging syndrome. *Mov Disord* 26:1744-48
- Kinugawa K, Vidailhet M, Clot F, Apartis E, Grabli D, et al. 2009. Myoclonus-dystonia: an update. *Mov Disord* 24:479-89
- Kojovic M, Cordivari C, Bhatia K. 2011. Myoclonic disorders: a practical approach for diagnosis and treatment. *Ther Adv Neurol Disord* 4:47-62
- Lagarde J, Roze E, Apartis E, Pothalil D, Sedel F, et al. 2012. Myoclonus and dystonia

- in cerebrotendinous xanthomatosis. *Mov Disord* 27:1805-10
- Li J, Cunic D, Paradiso G, Gunraj C, Pal PK, et al. 2008. Electrophysiological features of myoclonus-dystonia. *Mov Disord* 23:2055-61
- Louis ED. 2001. Clinical practice. Essential tremor. *N Engl J Med* 345:887-91
- Louis ED, Vonsattel JP. 2008. The emerging neuropathology of essential tremor. *Mov Disord* 23:174-82
- Lozsadi D. 2012. Myoclonus: a pragmatic approach. *Pract Neurol* 12:215-24
- Marelli C, Canafoglia L, Zibordi F, Ciano C, Visani E, et al. 2008. A neurophysiological study of myoclonus in patients with DYT11 myoclonus-dystonia syndrome. *Mov Disord* 23:2041-48
- Marseilles Consensus Group. 1990. Classification of progressive myoclonic epilepsies and related disorders. *Ann Neurol* 28:113-16
- Maurer VO, Rizzi M, Bianchetti MG, Ramelli GP. 2010. Benign neonatal sleep myoclonus: a review of the literature. *Pediatrics* 125:e919-24
- Mikami M, Yasuda T, Terao A, Nakamura M, Ueno S, et al. 1999. Localization of a gene for benign adult familial myoclonic epilepsy to chromosome 8q23.3-q24.1. *Am J Hum Genet* 65:745-51
- Mori S, Nakamura M, Yasuda T, Ueno S, Kaneko S, et al. 2011. Remapping and mutation analysis of benign adult familial myoclonic epilepsy in a Japanese pedigree. *J Hum Genet* 56:742-47
- Muller U. 2009. The monogenic primary dystonias. *Brain* 132:2005-25
- Nardocci N, Zorzi G, Barzaghi C, Zibordi F, Ciano C, et al. 2008. Myoclonus-dystonia

- syndrome: clinical presentation, disease course, and genetic features in 11 families. *Mov Disord* 23:28-34
- Orth M, Djarmati A, Baumer T, Winkler S, Grunewald A, et al. 2007. Autosomal dominant myoclonus-dystonia and Tourette syndrome in a family without linkage to the SGCE gene. *Mov Disord* 22:2090-96
- Ozawa E, Mizuno Y, Hagiwara Y, Sasaoka T, Yoshida M. 2005. Molecular and cell biology of the sarcoglycan complex. *Muscle Nerve* 32:563-76
- Plaster NM, Uyama E, Uchino M, Ikeda T, Flanigan KM, et al. 1999. Genetic localization of the familial adult myoclonic epilepsy (FAME) gene to chromosome 8q24. *Neurology* 53:1180-83
- Puffenberger EG. 2003. Genetic heritage of the Old Order Mennonites of southeastern Pennsylvania. *Am J Med Genet C Semin Med Genet* 121C:18-31
- Ritz K, van Schaik BD, Jakobs ME, van Kampen AH, Aronica E, et al. 2011. SGCE isoform characterization and expression in human brain: implications for myoclonus-dystonia pathogenesis? *Eur J Hum Genet* 19:438-44
- Roze E, Apartis E, Clot F, Dorison N, Thobois S, et al. 2008. Myoclonus-dystonia: clinical and electrophysiological pattern related to SGCE mutations. *Neurology* 70:1010-16
- Saugier-Veber P, Doummar D, Barthez MA, Czernecki V, Drouot N, et al. 2010. Myoclonus dystonia plus syndrome due to a novel 7q21 microdeletion. *Am J Med Genet A* 152A:1244-49
- Saunders-Pullman R, Raymond D, Stoessl AJ, Hobson D, Nakamura K, et al. 2012.

- Variant ataxia-telangiectasia presenting as primary-appearing dystonia in Canadian Mennonites. *Neurology* 78:649-57
- Saunders-Pullman R, Shriberg J, Heiman G, Raymond D, Wendt K, et al. 2002. Myoclonus dystonia: possible association with obsessive-compulsive disorder and alcohol dependence. *Neurology* 58:242-45
- Schule B, Kock N, Svetel M, Dragasevic N, Hedrich K, et al. 2004. Genetic heterogeneity in ten families with myoclonus-dystonia. *J Neurol Neurosurg Psychiatry* 75:1181-85
- Shibasaki H, Hallett M. 2005. Electrophysiological studies of myoclonus. *Muscle Nerve* 31:157-74
- Stamelou M, Mencacci NE, Cordivari C, Batla A, Wood NW, et al. 2012. Myoclonus-dystonia syndrome due to tyrosine hydroxylase deficiency. *Neurology* 79:435-41
- Striano P, Zara F, Striano S. 2005. Autosomal dominant cortical tremor, myoclonus and epilepsy: many syndromes, one phenotype. *Acta Neurol Scand* 111:211-17
- Valente EM, Misbahuddin A, Brancati F, Placzek MR, Garavaglia B, et al. 2003. Analysis of the epsilon-sarcoglycan gene in familial and sporadic myoclonus-dystonia: evidence for genetic heterogeneity. *Mov Disord* 18:1047-51
- Van Rootselaar AF, van Schaik IN, van den Maagdenberg AM, Koelman JH, Callenbach PM, et al. 2005. Familial cortical myoclonic tremor with epilepsy: a single syndromic classification for a group of pedigrees bearing common features. *Mov Disord* 20:665-73
- Waite A, Brown SC, Blake DJ. 2012. The dystrophin-glycoprotein complex in brain development and disease. *Trends Neurosci* 35:487-96

- Wong SH, Steiger MJ, Lerner AJ, Fletcher NA. 2010. Hereditary myoclonus dystonia (DYT11): a novel SGCE gene mutation with intrafamilial phenotypic heterogeneity. *Mov Disord* 25:956-57
- Yeetong P, Ausavarat S, Bhidayasiri R, Piravej K, Pasutharnchat N, et al. 2012. A newly identified locus for benign adult familial myoclonic epilepsy on chromosome 3q26.32-3q28. *Eur J Hum Genet* epub doi: 10.1038/ejhg.2012.133
- Yokoi F, Dang MT, Li J, Li Y. 2006. Myoclonus, motor deficits, alterations in emotional responses and monoamine metabolism in epsilon-sarcoglycan deficient mice. *J Biochem* 140:141-46
- Yokoi F, Dang MT, Zhou T, Li Y. 2012. Abnormal nuclear envelopes in the striatum and motor deficits in DYT11 myoclonus-dystonia mouse models. *Hum Mol Genet* 21:916-25.
- Yokoi F, Yang G, Li J, DeAndrade MP, Zhou T, et al. 2010. Earlier onset of motor deficits in mice with double mutations in Dyt1 and Sgce. *J Biochem* 148:459-66
- Zimprich A, Grabowski M, Asmus F, Naumann M, Berg D, et al. 2001. Mutations in the gene encoding epsilon-sarcoglycan cause myoclonus-dystonia syndrome. *Nat Genet* 29:66-69

CHAPTER III

Identification of a Mutation in *NOL3*

SUMMARY

We analyzed DNA from 35 members of a family suffering from familial cortical myoclonus (FCM). We used unbiased, genome-wide SNP genotyping to pinpoint three putative linkage regions. Two were excluded by classic microsatellite linkage analysis, and the third, chromosome 16q21-22.1, was linked. This critical region was subjected to targeted DNA capture followed by massively parallel sequencing. In combination with Sanger sequencing, we sequenced all known or predicted coding sequence. This analysis revealed only a single cosegregating, novel, non-synonymous mutation, which resides in the gene *nucleolar protein 3 (NOL3)*. To date we have been unable to identify additional *NOL3* mutations. Nevertheless, substantial evidence indicates that *NOL3* is the FCM disease gene.

INTRODUCTION

In Chapter II we presented clinical and electrophysiological data that familial cortical myoclonus (FCM) is a nosologically distinct movement disorder. Since FCM inheritance is autosomal dominant, we sought to identify the causative mutation. We utilized multiple overlapping methodologies: genome-wide single nucleotide polymorphism (SNP) mapping, microsatellite linkage analysis, massively parallel sequencing (MPS), and Sanger sequencing. Microsatellite linkage and Sanger sequencing have been mainstays of human genetics for many years (Strachan & Read 2010). In comparison, SNP mapping and MPS are relatively new techniques. As such, they each merit an introduction.

Linkage analysis is the first step in dissecting the genomic transmission of a Mendelian trait. The concept of linkage analysis is to search for identical-by-descent (IBD) regions within affected members of a family. It has been quite successful in identifying the mutations underlying many Mendelian disorders (Strachan & Read 2010). Until recently, microsatellite markers were used for linkage analysis because they are abundant, highly polymorphic, and relatively easy to genotype. However, one often runs against the power limit because of insufficient number of samples, ambiguity of genomic information, and/or phenotypic heterogeneity. To overcome these limitations and to exploit the rapid genotyping capability of SNP arrays, Giovanni Coppola et al., our collaborators at UCLA, have developed a mapping algorithm that identifies IBD regions using high density SNP data. Similar methods have been reported in the literature, mostly addressing families with autosomal recessive inheritance (Lencz et al. 2007, Shojaee et al. 2008). This approach is logically similar to genomic mismatch scanning (Nelson et al.

1993, Cheung & Nelson 1998). The analytical principle is based on the fact that in regions where subjects share a DNA fragment by descent, they must always share an allele at SNPs therein. Conversely, in regions where they do not share a fragment, there will be frequent occurrences of SNPs for which they do not share an allele, i.e., one sample is AA genotype and the other is BB genotype. By scanning for these counter-evidence AA versus BB SNPs, we delineate the boundaries of possible IBD fragments. The resulting blocks are compatible with an underlying IBD fragment, and if they are substantially larger (measured in centimorgan size) than the genomic background level of block sizes that represent population-level IBD, it becomes more likely that such a block represents true IBD, and thus it becomes a candidate linkage region for the disease in question. With a pedigree relating the individuals it is possible to assign an odds ratio comparable to the LOD score of traditional linkage analysis.

Whereas SNP genotyping has supplanted classic microsatellite linkage as the initial genome-wide scan to localize a mutation, identifying the mutation within that locus can still be challenging. Before thorough genomic maps, geneticists relied upon a grabbag of laborious tricks for gene identification (Strachan & Read 2010). After completion of the Human Genome Project (Lander et al. 2001) but prior to 2009, the candidate gene approach reigned supreme. A researcher attempting to identify a mutation would use the genome map to list the genes within the linked locus. He would then rank these candidate genes on the basis of known association with disease, sequence homology, expression patterns, and so on. Then, for each coding exon he would design primers, perform polymerase chain reaction (PCR), Sanger sequence the resulting amplicons, and compare the patient's sequence to the reference sequence (or an unaffected relative).

This process was repeated iteratively until a novel variant was identified. The next step was to confirm that the variant cosegregated with the phenotype in the family and that it was not present in a large cohort of controls. Finally, the researcher would sequence that same gene in other families with the same or similar phenotypes, in hopes of identifying additional alleles. This “allelic heterogeneity” is the gold standard of genetics, for if independent mutational events lead to the same phenotype, the most parsimonious explanation is that mutations in that gene cause the phenotype. Needless to say, identifying mutations using this approach – particularly if a priori the disease gene was not ranked highly on the candidate gene list – often required herculean effort. In some instances it was truly a Sisyphean task, as evidenced by the many loci with strong evidence of linkage that have resisted gene identification. For example, our laboratory has spent fourteen years searching for the causative mutation within a locus for familial adult myoclonic epilepsy (Plaster et al. 1999), to no avail. Another group has replicated the same locus (Mikami et al. 1999) and also failed to identify the disease gene (Mori et al. 2011).

This all changed in 2009 with the application of massively parallel sequencing (MPS) to disease gene discovery (Choi et al. 2009, Ng et al. 2010). (MPS is often referred to as next-generation sequencing [NGS], a term which we eschew because of its imprecision.) MPS enables the sequencing and analysis of billions and even trillions of base pairs in a rapid, accurate manner. For a geneticist attempting to identify a novel disease gene, this technology can substantially hasten the process. Since 2009 it has been widely adopted and repeatedly demonstrated its worth (Gonzaga-Jauregui et al. 2012).

There exist a number of ingenious methods for MPS, too many to present here (Metzker 2010). Briefly, we will describe the method we used. A patient’s genomic

DNA is sheared and adaptors are ligated to the resulting fragments. The ligated fragments are then electrophoresed to select fragments of a desired size (in our case, 200-300 base pairs). Purified fragments are then amplified by adaptor-mediated PCR. The next step is critical. All 200-300bp fragments can be sequenced, but often the experimental question dictates that the sequencing is done in a targeted manner—there is no use sequencing regions of the genome that cannot contain the mutation. For example, more than 90% of Mendelian mutations occur in protein-coding sequence, so it is logical to first focus on sequencing all coding sequence (the “exome”). On the other hand, suppose that linkage information pinpointed a particular locus (the “critical region”). In that case, there is no sense in sequencing any genomic regions other than the coding sequence within the critical region. Targeting the exome requires an array consisting of oligonucleotides tiled over the exome that have been prefabricated on a glass slide; targeting a critical region requires a custom array containing a subset of the exome array. The 200-300bp fragments are washed over the array, and those fragments that hybridize to the array are “captured” whereas other fragments are eluted. The captured fragments are purified and then sequenced simultaneously using the Illumina methodology (Metzker 2010). This entire process is known as targeted DNA capture and MPS, or, in the case of sequencing the exome, whole exome sequencing.

What of whole genome sequencing (WGS)? In our opinion, WGS, although rapidly becoming commonplace, is largely a waste of money. Each base-pair sequenced carries with it a finite cost, and the functional significance – or lack thereof, the ENCODE project (ENCODE Project Consortium et al. 2012) notwithstanding – of the vast majority of the genome is currently not known. Since coverage (both breadth and depth) of

sequence is critical for mutation discovery, rather than probe regions of the genome where the mutation cannot possibly reside it seems more prudent to ensure adequate coverage of the exome (or critical region). As always, there are caveats, such as the search for mutations in noncoding or unannotated sequence, or if adequate coverage of the exome can be achieved using the money saved by omitting array hybridization. Certainly in time the cost of WGS will be outstripped by the resources required for designing a custom array and performing targeted capture. However, that day has not yet arrived, and thus we opted for targeted capture of the critical region followed by MPS.

METHODS

All nucleotide positions are in reference to NCBI *Homo sapiens* genome build 37.1 (www.ncbi.nlm.nih.gov/genome/guide/human).

Determination of IBD Segments by SNP Mapping

We utilized the GeneChip Human Mapping 250K Nsp array (Affymetrix, Santa Clara, CA). This array covers ~250,000 SNPs across the genome, per subject. The genotyping accuracy of the Affymetrix 250K chip reported by the manufacturer is estimated to be 99.5%. In order to account for the estimated error rate, we adopted a window-cleaning function to remove isolated breaks. This algorithm identifies breaks within a pairwise comparison and removes isolated, singular breaks that are otherwise consistent with IBD in a surrounding specified number of SNP calls.

In regions where two affected individuals share an interval of DNA from a common ancestor, the two individuals will have long contiguous intervals of genotypes that are compatible with one allele being shared. Identifying these shared intervals became technically possible with the development of high density SNP genotyping technology. Genotyping large number of SNPs across the genome is now easy and cost effective, and it provides us with polymorphism data at a very high resolution. When using a 250K SNP panel, the practical mean resolution of IBD block detection comes down to 1-2cM even after factoring in the linkage disequilibrium between SNPs. Given this resolution, the IBD blocks inherited by distantly related individuals are likely to be significantly larger and readily detectable even after 10 generations (Chapman & Thompson 2003).

Rather than precisely distinguish and delineate the patterns of shared IBD per se, our goal is to reduce the search space for the causative alleles to a single or few IBD regions of reasonable size for the complete determination of targeted coding sequences through use of targeted capture followed by MPS.

Linkage Using Microsatellite Markers

We performed linkage analysis using microsatellite short tandem repeat markers for the three putative linkage regions on chromosomes 11, 16, and 17 (**Table 2**). All family members for whom DNA was collected (10 affected, 25 unaffected) were genotyped using microsatellites identified via the UCSC Genome Browser (www.genome.ucsc.edu) (**Appendix 1**). Microsatellites were interspersed every ~500kb throughout each putative linkage region. For fine mapping we selected additional microsatellites interspersed at smaller distances. At each marker we performed PCR with microsatellite-specific M13-forward and reverse primers, and the universal M13 primer (Schuelke 2000) tagged with WellRed D3 fluorescent label (Integrated DNA Technologies, San Diego, CA). PCR conditions were 94°C 5min; 30 cycles of 94°C 30sec, 55°C 45sec, 72°C 45sec; 14 cycles of 94°C 30sec, 53°C 45sec, 72°C 45sec; 72°C 10min; using a 2720 Thermal Cycler (Applied Biosystems, Carlsbad, CA). All PCR reactions were performed in 15µL reactions containing ~20ng template DNA, 1µM WellRed D3 M13 primer, .1µM M13 F primer, 1µM R primer, 2µM dNTPs (Qiagen, Valencia, CA), 1x PCR buffer (Qiagen), 0.5µL TAQ (Qiagen), and double distilled H₂O (ddH₂O). Fluorescently-labelled PCR products were separated by capillary electrophoresis using the CEQ8000 Genetic Analysis System (Beckman Coulter, Brea, CA)

(Figure 1). Genotypes for each family member at each marker were manually compiled and analyzed for evidence of linkage.

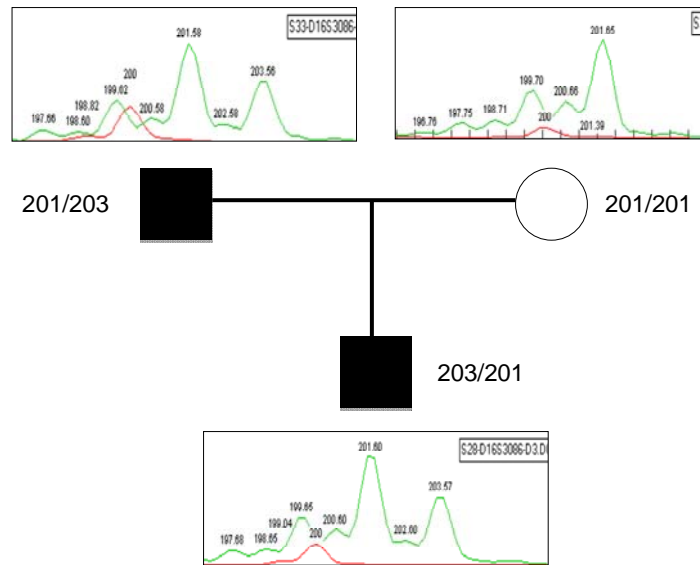


Figure 1. Microsatellite linkage genotyping methodology.

Shown is an example of a pedigree and the CEQ8000 Genome Analyzer traces obtained for each subject. Each subject’s genomic DNA was PCR’d using microsatellite-specific M13-forward and reverse primers, as well as the universal M13 primer tagged with a fluorescent label. PCR amplicons were electrophoresed and the base pair (bp) length was measured by the Genome Analyzer (denoted by the numbers above peaks). A heterozygous subject (201/203) has two large peaks, whereas a homozygous subject (201/201) has a single large peak. A difference of two bp, or multiples thereof, corresponds to microsatellite alleles of different length. Smaller peaks that occur prior to a large one are background (presumably due to polymerase slippage).

To confirm the statistical significance of linkage, pairwise LOD scores were calculated using Superlink (Fishelson & Geiger 2002, Silberstein et al. 2006). Assumptions were an autosomal dominant mode of inheritance with 90% penetrance and 0% phenocopy rate; disease mutant gene frequency of 0.0001; and uniform distribution of allele frequencies. Non-Mendelian inheritance of markers (see **Figure 4**) were not compatible

with the Superlink algorithm and were therefore replaced with null values. To ensure robustness, LOD scores were found to be stable across order-of-magnitude variations in the calculation parameters (**Table 3**).

Targeted DNA Capture and Massively Parallel Sequencing

Based on our initial IBD analysis and the linkage mapping, for reasons enumerated in the **Introduction** we focused on the critical region on chromosome 16. We designed a capture library to target the coding sequence of every RefSeq gene contained within the region from chr16:66,648,792 – 72,221,807 on the UCSC hg19 reference build. (Only one predicted gene resides between the southern border of the critical region at 65,206,293 and the southern border [66,648,792] of the sequence assayed by targeted capture. This gene, *LOC283867*, was bidirectionally Sanger sequenced to rule out presence of a variant; see below.) The coding exons from all aligned RefSeq transcripts in the region were merged into single, non-overlapping intervals before excluding repeat-masked regions (RepeatMasker 3.2.7; www.repeatmasker.org), and were expanded by up to 300bp on either side to ensure coverage of all coding sequence and splice junctions. These regions were submitted to Agilent's eArray (<http://earray.chem.agilent.com>), generating a final capture library design that consisted of 25,710 120-mer probes targeting a total of 875,805bp amongst 1,150 distinct regions of the reference genome, with an average tiling density of 4x.

Library construction and hybrid-selection was performed according to manufacturers' protocols. Briefly, a total of 1.5µg of DNA was diluted in 100µL of TE buffer and sonicated to a median fragment size of 200bp using an S2 instrument (Covaris, Woburn,

MA). The fragmented DNA was filled, end-polished, and A-tailed, followed by ligation of adapters. After several rounds of amplification, the library was size-selected by excision of 200-300bp fragments visualized with DNA Star on a 4% Nu Sieve Gel (Lonza, Rockland, ME). All adapter and amplification oligos were purchased from IDT (Coralville, IA) with additional modifications as specified in Bentley et al. (2008).

Quality and fragment distribution was assessed using a BioAnalyzer DNA 1000 Chip (Agilent Technologies, Santa Clara, CA). The samples were then hybridized to the SureSelect capture library for 24hrs. The captured sample library was purified and prepared for sequencing exactly as described in the Agilent SureSelect PE Protocol.

Single-end library sequencing was performed using a Genome Analyzer IIX (Illumina, San Diego, CA), yielding over 15,000,000 76bp reads on target (**Table 4A**). Alignment to the human genome was done using Burrows-Wheeler aligner with default settings (Li & Durbin 2009), and variants were called using the Genome Analysis Tool Kit (McKenna et al. 2010), and annotated using ANNOVAR (<http://www.openbioinformatics.org/annovar>). Capture efficiency was ~75% as defined by reads falling within 100bp of targeted sequence (**Table 4A**). Mean per-base coverage (including duplicate reads) was 634x, covering 98.9% of the target region (**Table 4A**). After duplicate read removal, average per-base coverage was 15x (**Table 4A**). Variant call sites exhibited significant overlap with DBSNP 132, at 95.23%, and are summarized in **Table 4B**.

We identified 7 novel non-synonymous variants for further follow up. Although upon first inspection there appears to be a high false positive rate of variants identified by MPS (4 of 7, **Table 5**), in our experience this false positive rate is substantially inflated because it represents called variants of a novel subset which are not representative of the

callset in general. Although insertion-deletion (indel) variants are more difficult to detect by single-end sequencing vis-à-vis paired-end sequencing, we nonetheless detected a rich library of indel variants dispersed throughout the target region. However, none of the detected indels resided in coding sequence (data not shown).

Sanger Sequencing of Additional Coding Sequences Not Assayed by MPS

We sequenced all known or predicted exons that were covered by MPS at less than 10x coverage post-duplicate removal; however, even at less than 10x coverage post-duplicate removal, the chance of not detecting a heterozygous variant given our average per-base coverage of 634x is slight (Choi et al. 2009). Nevertheless, for each locus we Sanger sequenced PCR amplicons obtained from two affected and one unaffected family member. All primers (**Appendix 3**) were designed to span the exons and splice junctions of candidate genes using the Primer3 program (www.frodo.wi.mit.edu), with genomic sequence obtained from the UCSC Genome Browser.

Also, because a penta-nucleotide repeat insertion in non-coding sequence was previously reported by Sato et al. (2009) in association with spinocerebellar ataxia type 31, to rule out this locus we utilized primers (primers 12-23, **Appendix 3**) that were tiled over the entire region from 66,514,116 – 66,520,026 which harbors the penta-nucleotide repeat insertion.

Except for those primers noted below, the following conditions were used: 94°C 3min; 10 cycles of 94°C 20sec, 62°C 30sec (touchdown step with 0.5°C decrease in annealing temperature each cycle), 72°C 1min; 38 cycles of 94°C 20sec, 58°C 30sec, 72°C 1min; 72°C 10min; using a 2720 Thermal Cycler. All PCR reactions were

performed in 15 μ L reactions containing ~20ng template DNA, 1 μ M F primer, 1 μ M R primer, 2 μ M dNTPs (Qiagen), 1x PCR buffer (Qiagen), 0.5 μ L TAQ (Qiagen), and ddH₂O. Amplicons were separated by gel electrophoresis to confirm amplification and proper size, purified using the QIAquick PCR Purification Kit (Qiagen), then bidirectionally sequenced using the F or R primer in turn. Sequencing was performed by Quintara Biosciences (Albany, CA) and analyzed with Sequencher software v4.8 (Gene Codes Corp., Ann Arbor, MI).

Many of these genes were excluded from targeted DNA capture because they are highly repetitive or GC-rich, so select loci required extensive PCR optimization. The following primer pairs (**Appendix 3**) required gel-purification using QIAquick Gel Extraction Kit (Qiagen) due to nonspecific amplification: 2, 6, 11, 13, 21, 22, 25, 28, 32, 37, 45, 46, 51, 55, 61, 68, 70. For primers 6-39, PCR reactions were performed in 50 μ L reactions containing ~20ng template DNA, 0.2 μ M F primer, 0.2 μ M R primer, 1x TaKaRa buffer, 1 unit TaKaRa Taq, 0.2mM TaKaRa dNTP mixture, and ddH₂O (TaKaRa reagents from TaKaRa Bio, Otsu, Shiga, Japan); conditions were 94°C 5min; 40 cycles of 94°C 30sec, 56°C 30sec, 72°C 90sec; 72°C 10min. Primers 6 and 48 required the same conditions except that instead of 1x TaKaRa buffer, 1x GC buffer II and 1x GC buffer I (TaKaRa Bio Inc.), respectively, were substituted. Primer 45 required conditions of 94°C 3min; 10 cycles of 94°C 20sec, 62°C 30sec (touchdown step), 72°C 1min; 45 cycles of 94°C 20sec, 58°C 30sec, 72°C 1min; 72°C 10min. Primer 46 required conditions of 94°C 3min; 45 cycles of 94°C 20sec, 61°C 30sec, 72°C 1min; 72°C 10min. Primer 61 required a 2min extension time with the standard cycling conditions.

Sanger Sequencing of *NOL3* in Cases and Controls

To detect the *E21Q* variant we performed bidirectional Sanger sequencing of exon 2 of *NOL3* in all affected and unaffected family members for whom DNA was collected (10 affected, 25 unaffected). This analysis (**Figure 8**) confirmed that the *E21Q* variant cosegregates with the affected status and the linked haplotype. To rule out *E21Q* as simply a rare variant, we sequenced an in-house collection of 252 Caucasian control subjects. We detected no variants at this locus in any of the 504 control chromosomes.

In collaboration with a number of movement disorder specialists and neuro-geneticists around the globe, we identified 7 patients from 5 kindreds suffering from cortical myoclonus that may be familial (see Chapter II). We bidirectionally Sanger sequenced the 5'UTR, coding, splice junction, and 3'UTR sequence of *NOL3* in all of these patients and their unaffected relatives for whom we obtained DNA. This analysis identified no novel variants.

We undertook further efforts to identify additional *NOL3* alleles. We collaborated with Samuel Berkovic, M.D., of the University of Melbourne. His group sequenced all *NOL3* coding sequence, splice junctions, and UTRs in their collection of patients with FAME, benign neonatal sleep myoclonus (Maurer et al. 2010, Afawi et al. 2012), and undiagnosed myoclonus. Additionally, we presented this work at the American Society for Human Genetics annual meeting (San Francisco, 2012), where Mark LeDoux, M.D., of the University of Tennessee explained that he may know of a family with FCM (see **Results**).

For these experiments, *NOL3* genomic and mRNA sequence was obtained from NCBI Genome Build 37.1 and primers were designed using Primer3 (**Appendix 4**). All

PCR reactions were performed in 15 μ L reactions containing ~20ng template DNA, 1 μ M F primer, 1 μ M R primer, 2 μ M dNTPs (Qiagen), 1x PCR buffer (Qiagen), 0.5 μ L TAQ (Qiagen), and ddH₂O. Amplicons were electrophoresed, purified, and sequenced with either F or R primer, as described above.

Database Analyses for *NOL3 E21Q* Variant

To ensure that the *E21Q* variant was not simply a rare variant, we combed genomic databases for the presence of *NOL3* variants in healthy controls. The *E21Q* variant was not present in dbSNP (www.ncbi.nlm.nih.gov/projects/SNP) or in 1,094 genomes from multiple ethnicities studied in the 1000 Genomes Project (www.browsers.1000genomes.org). Review of the Database of Genomic Variants (<http://projects.tcag.ca/variation>) for copy number variants revealed a 3.5kb duplication spanning *NOL3* in Yoruban controls (Matsuzaki et al. 2009) and a 155kb deletion spanning *NOL3* and 15 adjacent genes in an Asian control (Park et al. 2010).

Large-scale Screen for *NOL3 E21Q* Variant

To assess the prevalence of the *NOL3 E21Q* mutation in the general population, we screened a large series of controls obtained from NIMH using MassArray (Sequenom, San Diego, CA). Control subjects from the National Institute of Mental Health Schizophrenia Genetics Initiative (NIMH-GI), data and biomaterials are being collected by the “Molecular Genetics of Schizophrenia II” (MGS-2) collaboration. The investigators and co-investigators are: ENH/Northwestern University, Evanston, IL, MH059571, Pablo V. Gejman, M.D. (Collaboration Coordinator; PI), Alan R. Sanders, M.D.; Emory

University School of Medicine, Atlanta, GA, MH59587, Farooq Amin, M.D. (PI); Louisiana State University Health Sciences Center, New Orleans, LA, MH067257, Nancy Buccola (PI); University of California-Irvine, Irvine, CA, MH60870, William Byerley, M.D. (PI); Washington University, St. Louis, MO, MH060879, C. Robert Cloninger, M.D. (PI); University of Iowa, Iowa City, IA, MH59566, Raymond Crowe, M.D. (PI), Donald Black, M.D.; University of Colorado, Denver, CO, MH059565, Robert Freedman, M.D. (PI); University of Pennsylvania, Philadelphia, PA, MH061675, Douglas Levinson, M.D. (PI); University of Queensland, Queensland, Australia, MH059588, Bryan Mowry, M.D. (PI); Mt. Sinai School of Medicine, New York, NY, MH59586, Jeremy Silverman, Ph.D. (PI).

A SNP Genotyping Assay using Sequenom iPLEX Gold Technology (Sequenom, San Diego, CA, USA) was executed according to manufacturer's instructions. Spectro chip arrays were spotted with a nanodispenser, and a Sequenom MALDI-TOF spectrophotometer was used to read the array. The SpectroAquire and MassARRAY Typer Software packages (Sequenom) were used for interpretation and Typer analyzer v.3.4.0.1 8 was used to review and analyze all data. Only high-level calls (Conservative and Moderate, according to the Sequenom software) were considered for further analyses.

We screened a total of 4,246 samples from the NIMH reference control set. We confirmed the presence of the mutation in all of the affected family members from the FCM index family, consistent with their inclusion as positive controls. We did not detect the *NOL3 E21Q* sequence variant in any of the 4,246 controls.

RESULTS

To identify the mutation underlying FCM, ten affected and two unaffected family members (marked by asterisks in **Figure 4**) were genotyped by genome-wide SNP mapping. Mapping using identity-by-descent analysis, a statistical technique for analyzing SNP data to identify chromosomal regions of shared haplotypes, was conducted as described above (**Table 1**). We assumed that the two unaffected individuals were not carriers of the disease allele based on rigorous clinical evaluation, their advanced age at examination, and because they had unaffected progeny. Our original ten-way comparison including only affecteds yielded four primary regions of interest. We then used genotyping information from the two unaffecteds in order to exclude one region. This left three candidate regions on chromosomes 11, 16, and 17 (**Table 2, Figure 2**).

Table 1. Genome-wide SNP array.

Abbreviations are: F, female; M, male; MCR, mean call rate; MDR, mean detection rate. The pedigree IDs correspond to **Figure 4**.

Pedigree ID	Gender	SNP Call	AA Call	AB Call	BB Call	MCR	MDR
II-3	M	97.68%	38.62%	24.17%	37.22%	96.40%	99.32%
II-4	F	96.23%	38.84%	23.70%	37.46%	92.71%	98.59%
II-7	M	96.84%	38.44%	24.65%	36.92%	95.92%	99.18%
II-9	F	97.40%	38.28%	24.71%	37.01%	96.53%	99.11%
III-2	F	95.26%	38.58%	24.49%	36.93%	92.68%	98.38%
III-3	M	96.55%	38.33%	24.80%	36.87%	94.43%	98.98%
III-6	M	96.18%	38.22%	25.07%	36.71%	94.73%	99.26%
III-7	M	96.09%	38.67%	23.96%	37.37%	93.37%	98.74%
III-11	M	96.05%	38.37%	24.83%	36.80%	93.98%	98.78%
III-12	F	96.60%	37.52%	26.44%	36.04%	95.01%	98.79%
IV-2	M	97.27%	38.07%	25.29%	36.65%	96.05%	99.32%
IV-3	F	95.02%	38.43%	24.97%	36.60%	91.71%	98.35%

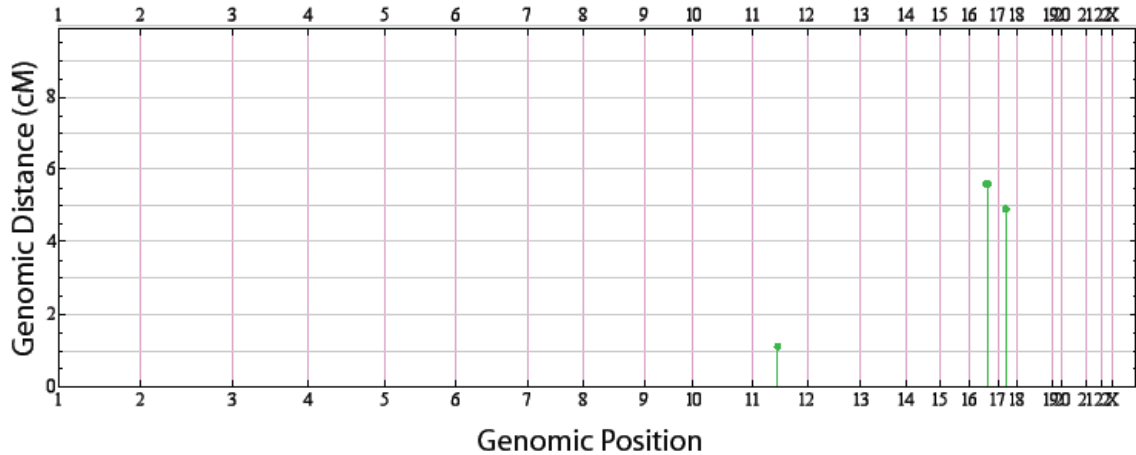


Figure 2. Genome-wide SNP mapping identified 3 candidate linkage regions. Identity-by-descent block size (cM) is plotted against genomic position. Blocks that were not identical-by-descent have been omitted. IBD blocks are in green. cM denotes centimorgan.

Table 2. Three putative shared regions identified by SNP IBD analysis.

All positions refer to NCBI Build 37.1. Abbreviations: Chr, chromosome; cM, centimorgan; Mb, megabase.

Likelihood	Chr	Position (SNP)		Size		
		start	end	Mb	cM	SNPs
1	16	65,306,450 (rs9302570)	73,346,034 (rs6564635)	8.04	5.62	449
2	17	34,461,903 (rs2376468)	36,194,230 (rs6607302)	1.73	4.92	93
3	11	63,874,943 (rs683996)	65,917,084 (rs801741)	2.04	1.12	60

We then sought to confirm these putative linkage regions using microsatellite linkage analysis. For the candidate regions on chromosomes 11 and 17, none of the microsatellite markers cosegregated with the disease phenotype, and setting phase enabled us to rule out linkage to these regions (data not shown). In contrast, ten microsatellite markers on chromosome 16q21-16q22.1 cosegregated with the disease phenotype (**Figures 3-5**). We performed fine mapping by selecting and genotyping additional

microsatellites (**Figure 5**). Fine mapping ceased when we found that no additional annotated genes resided between marker 16.16 (65,206,293) and marker 16.3 (65,285,223), and when we had exhausted all informative microsatellites between marker 16.19 (70,564,103) and marker 16.21 (70,779,308).

Of note, patient IV-5 carried the mutant haplotype but was asymptomatic when examined at age 26. SSEP was not performed, but given the late onset of the phenotype and IV-5's inheritance of what was otherwise a 100% penetrant haplotype, we assumed IV-5 was a carrier. [CONTINUED, p. 107]

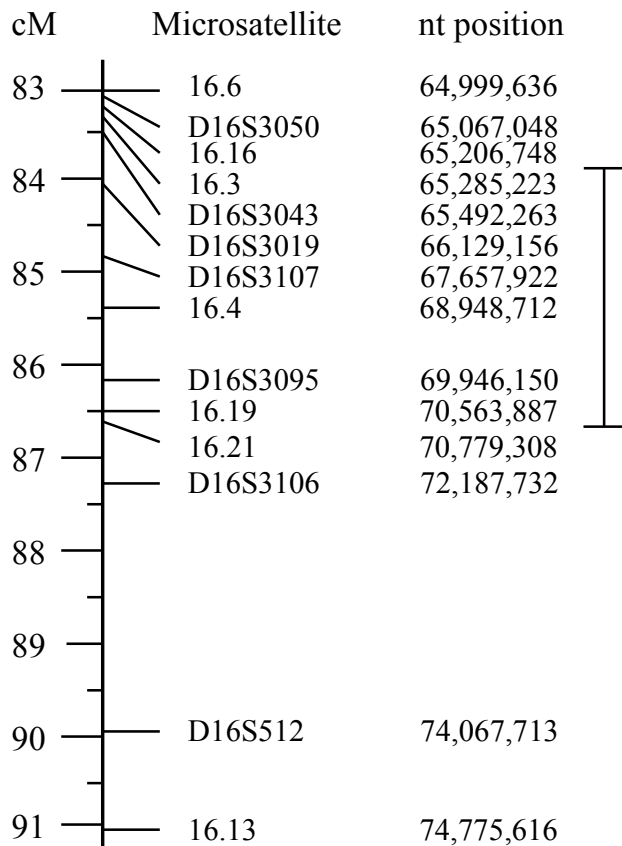


Figure 3. Genetic and physical map positions of microsatellite markers.

All distances are based on the deCODE map and NCBI 37.1. The bar represents the critical region.

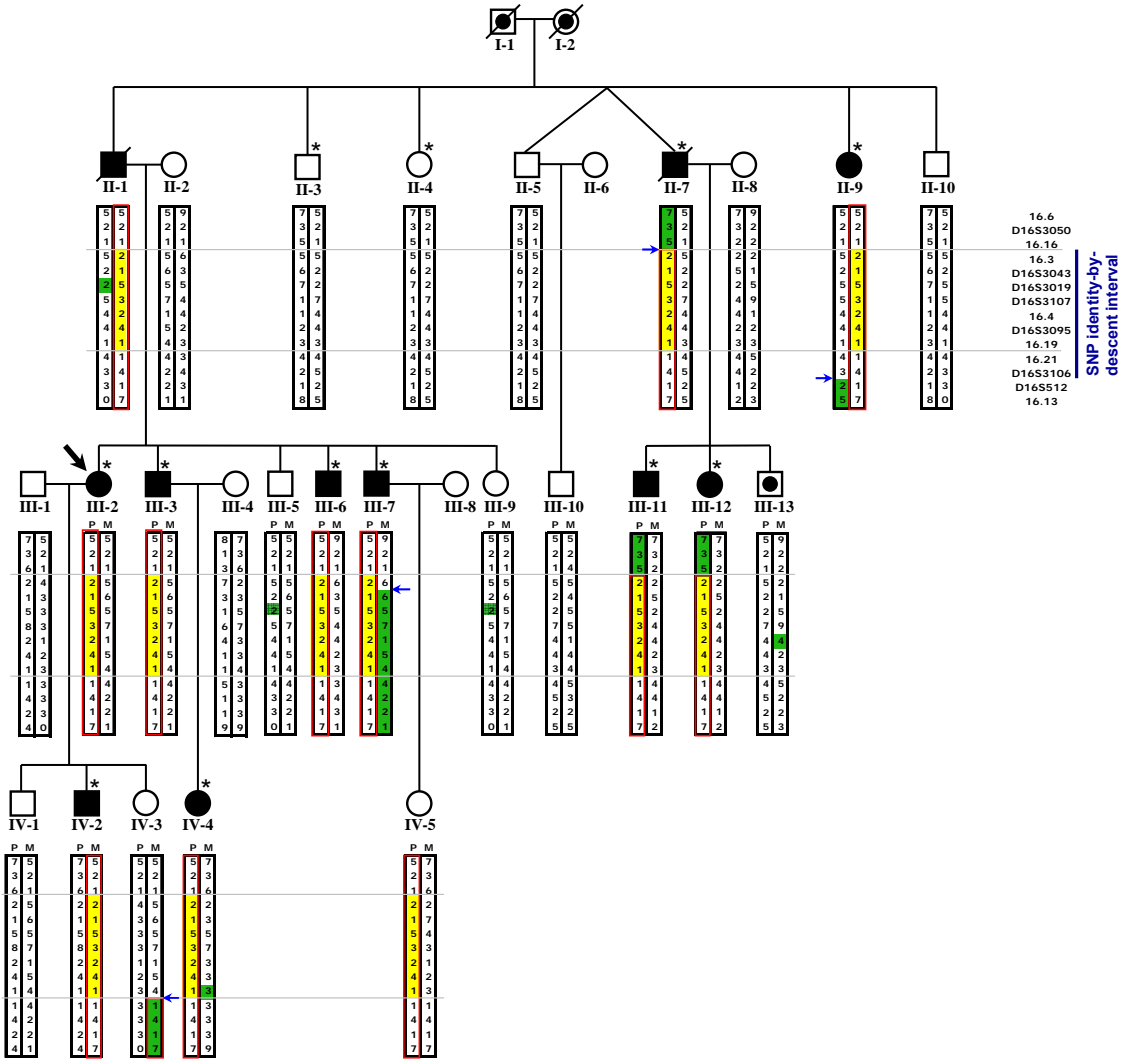


Figure 4. Pedigree with chromosome 16q21-22.1 haplotypes.

Each microsatellite allele for a given marker is denoted by a different integer value. Red boxes enclose the mutant haplotype. Yellow highlighting indicates the critical region of the mutant haplotype. Blue arrows denote recombination events. Alleles are highlighted in green if they differ from the remainder of that haplotype, because of either a recombination or non-Mendelian inheritance (II-1 and progeny, III-13, IV-4; likely due to spontaneous repeat contraction/expansion). II-1 and II-7 are now deceased but were examined prior to death. IV-3 was an asymptomatic adult with normal somatosensory evoked potentials (SSEP). The dot (III-13) denotes unknown phenotype; he refused SSEP. IV-5 was an asymptomatic 26 year old at examination (refused SSEP), and is predicted to be a carrier, although incomplete penetrance is possible. Forty-two relatives were omitted to preserve anonymity. Asterisks denote subjects who were genotyped for genome-wide SNP identity-by-descent mapping.

Marker	Start	Stop
16.6	64,999,636	64,999,785
D16S3050	65,067,048	65,067,207
16.16	65,206,748	65,206,293
16.3	65,285,223	65,285,462
D16S3043	65,492,263	65,492,559
D16S3019	66,129,156	66,129,455
D16S3086	66,935,898	66,936,081
D16S3107	67,657,922	67,658,221
16.4	68,948,712	68,948,927
D16S3141	69,105,838	69,106,120
D16S3095	69,946,150	69,946,411
16.1	70,306,725	70,306,969
16.19	70,563,887	70,564,103
16.21	70,779,308	70,779,507
16.5	70,860,578	70,860,745
D16S752	71,335,127	71,335,354
D16S3106	72,187,732	72,188,021
D16S3139	72,711,582	72,711,821
D16S3066	73,329,816	73,330,063
D16S512	74,067,713	74,067,915
D16S3115	74,530,429	74,530,674
16.13	74,775,616	74,775,846

The mutant haplotype at these markers was absent in II-7 and his progeny.

Recombination event

The mutant haplotype at these markers was present in all affected individuals, and absent in all unaffected individuals (except IV-5).

Recombination event

The mutant haplotype at these markers was present in IV-3, who was asymptomatic and had normal SSEP.

Figure 5. Fine mapping of critical region.
Positions are via NCBI 37.1

We were able to delineate the northern (centromeric) border of the critical region because three markers (16.6, D16S3050, 16.16) exhibited cosegregation with the disease phenotype in all family members except for patient II-7 and his progeny, reflecting an obligate recombination event between 16.16 (65,206,293) and 16.3 (65,285,223) (**Figures 4, 5**). We delineated the southern (telomeric) border of the critical region because 9 microsatellite markers (16.21, 16.5, ..., D16S3115, 16.13), while shared by all affected individuals, were also present in patient IV-3 (**Figures 4, 5**). IV-3 had an asymptomatic history like IV-5, but IV-3 also underwent SSEP which was normal. While we could not

definitively rule out incomplete penetrance or delayed onset, we deemed IV-3 to be unaffected and thereafter focused our efforts on the 5.57Mb region between markers 16.16 and 16.21 on chromosome 16q21-22.1 (**Figures 4, 5**). The SNP IBD analysis had suggested that the southern border was 73,346,034 (**Table 2**); however, that analysis only compared sequence similarity among ten affected patients and did not utilize unaffected patient genotypes to rule out the region from 70,779,308 – 73,346,034 that, shared among both affected patients and unaffected IV-3, must therefore not contain the disease gene. Thus, conservatively including the spaces between informative markers, we concluded that the disease gene must reside in a 5.57Mb region on chromosome 16q21-22.1 (65,206,293 – 70,779,308). The peak pairwise LOD score was 4.54 (**Table 3**). A LOD score above 3.0 is the cutoff for strong statistical significance (Strachan & Read 2010). A LOD of 4.54 reflects the probability that this degree of linkage would occur by chance is about one in 35,000.

Table 3. Critical region pairwise LOD analysis.

Marker	Recombination Fraction						
	0	0.01	0.05	0.1	0.2	0.3	0.4
16.6	-4.4841	-0.8611	-0.1713	0.0744	0.179	0.1013	-0.0016
D16S3050	-3.7385	-0.1594	0.4065	0.535	0.4714	0.2731	0.076
16.16	-3.7918	-0.156	0.4098	0.538	0.4736	0.2741	0.076
16.3	4.0454	4.0032	3.801	3.4917	2.734	1.8139	0.7571
D16S3043	4.0641	4.0221	3.8203	3.5114	2.7539	1.8324	0.7694
D16S3019	3.0811	3.027	2.8051	2.5146	1.8838	1.1746	0.4097
D16S3107	4.0641	4.0221	3.8204	3.5114	2.7539	1.8324	0.7697
16.4	4.5448	4.4691	4.1588	3.7526	2.8708	1.8783	0.7787
D16S3095	1.7068	1.6997	1.6419	1.523	1.1889	0.7741	0.3384
16.19	1.78	1.7715	1.7068	1.5779	1.2171	0.7657	0.2987
16.21	3.0451	3.0443	2.9821	2.8111	2.2671	1.5186	0.6135
D16S3106	3.0641	3.0635	3.0017	2.8311	2.2873	1.5373	0.6263
D16S512	1.4037	1.4315	1.4866	1.4696	1.261	0.8894	0.3905
16.13	3.0641	3.0634	3.0017	2.8311	2.2873	1.5373	0.6249

The 5.57Mb critical region contained 113 known or predicted candidate genes (**Appendix 2**). We considered all predicted open reading frames to be candidate genes. Of particular a priori interest were 7 solute carrier genes; *neuritin 1-like (NRNIL)*, similar to *neuritin*, a gene that promotes motor neuron axon arborization; and *syntrophin beta 2 (SNTB2)*, which encodes a component of the dystrophin glycoprotein complex implicated in myoclonus dystonia syndrome (see Chapter II).

To identify putative disease-causing variants, we performed targeted capture of the critical region in one affected patient (the proband) followed by MPS (see **Introduction**; Gnirke et al. 2009). Mean coverage over 98.9% of targeted base-pairs was 634x (**Table 4**). A number of GC-rich or highly repetitive exons were absent from the arrays used for targeted DNA capture, or were present on the arrays but sequenced at less than 10x coverage (post-duplicate removal), so we individually Sanger sequenced all of these exons (**Appendix 3**). Thus, all known or predicted coding sequences (including splice junctions) in the critical region were either bidirectionally Sanger sequenced or sequenced at mean per-base coverage of 634x (**Table 4**). The sensitivity to detect heterozygous variants via MPS approaches 100% at per-base coverage of 20x or greater (Choi et al. 2009), so our complementary sequencing approaches are very likely to have identified all coding variants in the critical region. [CONTINUED, p. 112]

Table 4. Targeted DNA capture and massively parallel sequencing reads (A) and variants (B).

(A)

Probed bases	2,032,106bp	
Targeted bases	873,213bp	
Total number of aligned reads	22,421,614	
Reads with single alignment	19,563,230	87.30%
Singular alignments within target region (+/- 100bp)	16,717,268	74.60%
Reads on target region	15,621,205	69.70%
Average target sequence enrichment (absolute)	118.7 Mb	634x
Average target enrichment (duplicates removed)	29.7 Mb	15x
Proportion of exons covered	98.9%	
Target covered (non-duplicate reads)	Depth	Proportion of target regions
	20x	36.24%
	5x	69.60%
	1x	98.90%

(B)

Variants	672				
Heterozygous	468 (70%)	Intergenic	386	Synonymous	77
Homozygous	204 (30%)	Intronic	146	Non-synonymous	68
dbSNP132	640 (95%)	Exonic	140	UTR	80
Total	672		672		

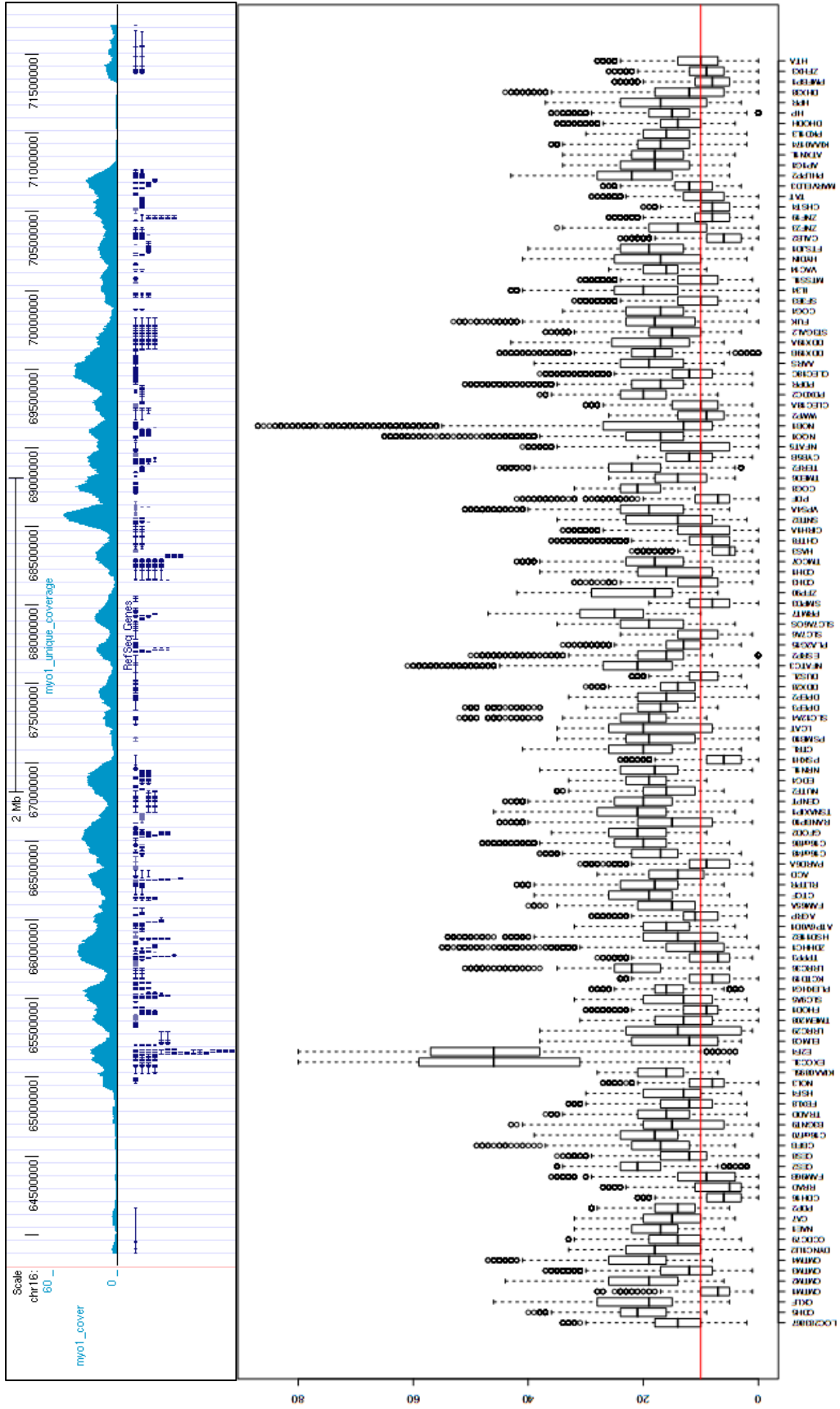


Figure 6. Coverage (post-duplicate removal) by massively parallel sequencing over the entire region on chromosome 16 (top) and by coding sequence of each gene (bottom).

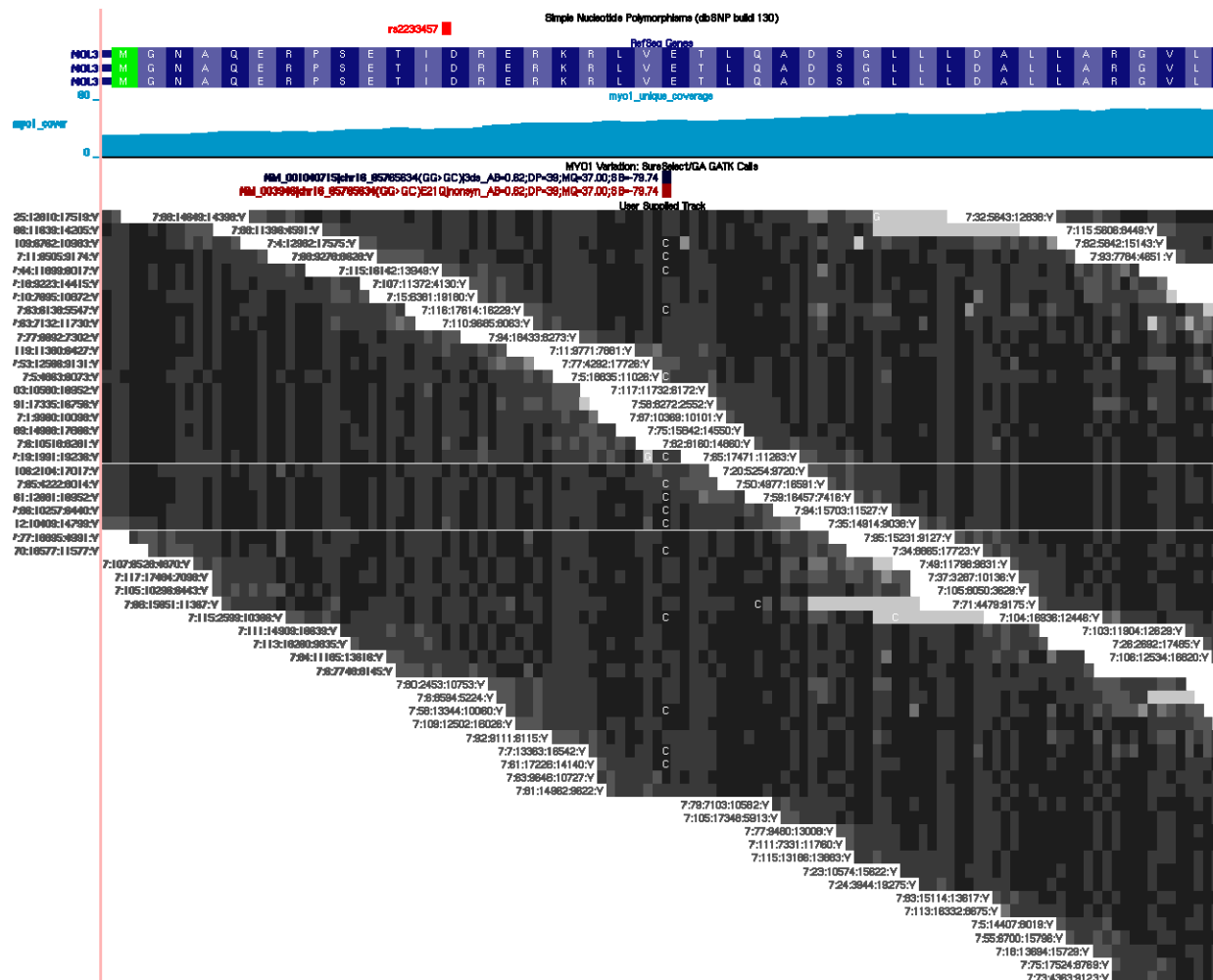


Figure 7. Alignment of short sequence reads (post-duplicate removal) over the *NOL3* *E21Q* sequence variant.

Seven variants met our quality criteria as putative disease-causing variants (Table 5), but only one variant cosegregated with affected status, was not present in any genome database or in controls, and was predicted to cause an amino acid change. This variant was NM_001185058.1:c.61G>C in the gene *nucleolar protein 3* (*NOL3*), predicted to cause an *E21Q* missense mutation (Figures 7, 8). This variant is not present in any SNP database or in 1,094 genomes from multiple ethnicities studied in the 1000 Genomes Project. Furthermore, we did not detect this variant upon Sanger sequencing 252 unrelated

Caucasian control subjects, and it was absent from an additional 4,246 normal controls analyzed by Sequenom MassArray (Gabriel et al. 2009). Thus, having exhaustively sequenced all coding sequences in the critical region and identified only a single novel, non-synonymous coding variant, *E21Q*, which is extremely rare (absent from more than 10,000 control chromosomes), we conclude that the *NOL3* mutation is likely causative of this family's clinical presentation.

Table 5. Novel non-synonymous coding variants in critical region identified by targeted DNA capture and massively parallel sequencing.

Positions are via NCBI 37.1. Although at first inspection there appears to be a high false positive rate, in our experience this is substantially inflated because it represents called variants of a novel subset which are not representative of the callset in general.

Gene	Position	Base Change	AA Change	Follow up
<i>NOL3</i>	67,208,133	G→C	E21Q	cosegregates, and absent in 0 of 252 unrelated controls
<i>EXOC3L</i>	67,218,411	C→T	R716H	absent from all databases and 0 of 180 control exomes, but present in 3 of 140 unrelated controls
<i>PLEKHG4</i>	67,316,179	C→A	Q394K	false positive
<i>DPEP3</i>	68,009,705	C→G	A502G	false positive
<i>PRMT7</i>	68,349,938	A→G	E19G	false positive
<i>TMCO7</i>	69,117,433	G→A	V1052I	did not cosegregate
<i>TMED6</i>	69,385,563	C→G	D32H	false positive

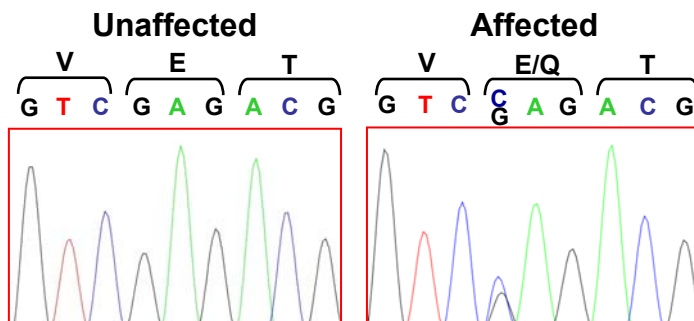


Figure 8. Sanger sequencing chromatographs (electropherograms) confirmed cosegregation of the NM_001185058.1:c.61G>C variant, predicted to cause an *E21Q* mutation in *NOL3*.

Identifying additional *NOL3* alleles that are associated with FCM or FCM-like phenotypes (i.e., allelic heterogeneity) would support the conclusion that *NOL3* mutation causes FCM. As described in Chapter II, we identified 7 subjects from 5 kindreds suffering from cortical myoclonus that may be familial. We Sanger sequenced all coding sequence, splice junctions, and UTRs of *NOL3* in these patients, but did not observe any *NOL3* variants. However, none of these 7 patients had phenotypes that were identical to the FCM family, and none of the 5 kindreds exhibited parent-to-child transmission characteristic of dominant inheritance. We further sequenced *NOL3* in a collection of patients with FAME, undiagnosed myoclonus, or benign neonatal sleep myoclonus, which may be autosomal dominant (Maurer et al. 2010, Afawi et al. 2012). None of these patients had *NOL3* mutations. In a promising development, we recently became aware that Mark LeDoux of the University of Tennessee, a dystonia geneticist and movement disorder specialist, has phenotyped (but never published) a large family from Mississippi with adult onset, autosomal dominant, highly penetrant myoclonus, including with giant SSEPs. His group is currently taking DNA samples to sequence *NOL3* in the Mississippi family.

DISCUSSION

We used SNP mapping, linkage, and targeted MPS to identify a mutation in *NOL3*. Although to date we have been unable to identify additional FCM kindreds with mutations in *NOL3*, we have presented substantial evidence that *NOL3* is the disease gene underlying FCM. We sequenced all known or predicted splice junctions and coding sequences within the critical region at 634x average coverage and detected only a single novel variant, the *E21Q* mutation in *NOL3*, which cosegregated with the phenotype. This mutation was absent in more than 10,000 control chromosomes. Given the deluge of sequencing data recently deposited in public databases, the absence of the *E21Q* mutation in these databases constitutes additional evidence that it is extremely rare and therefore likely causative of this family's phenotype.

Nevertheless, we do concede the possibility that *E21Q* is a private variant that is linked to the actual disease mutation but is not itself causative. There are numerous plausible explanations. For example, the causative mutation could reside in coding sequence within the critical region that is currently not annotated, or in noncoding sequence within the critical region, such as an untranslated region, promoter, or intronic branch site (see Chapter IV). Alternatively, the causative mutation may not have been detected due to systematic sequencing error. We sought to mitigate this shortcoming by identifying coding sequences that were not sequenced adequately by MPS and then carefully Sanger sequencing them, but one can never be sure that mistakes were not made. Another possibility is that FCM is caused by a synonymous variant that, instead of modifying the amino acid sequence, alters mRNA stability or expression; to our knowledge, causative synonymous variants are always identified by sequencing an disease gene that has already-

y been established—pinpointing a disease gene by way of a synonymous index mutation would be very difficult. Finally, we cannot exclude the possibility of a copy number variant (CNV) causing FCM, although we did not detect any CNVs by massively parallel sequencing, and prior studies have detected both heterozygous duplications and deletions spanning *NOL3* in normal subjects (see **Methods**), which strongly argues against this scenario.

However remote these possibilities, there are two parallel lines of investigation to definitively demonstrate that *NOL3* is the FCM disease gene. The first is characterization of a knockin mouse model harboring an *E21Q* mutation (see Chapter IV). The second is identification of independent *NOL3* alleles that cause FCM or FCM-like phenotypes such as familial adult myoclonic epilepsy (FAME), *SGCE* mutation-negative myoclonus dystonia syndrome (MDS), or perhaps even idiopathic generalized epilepsy. Unfortunately, our efforts to date – sequencing patients with undiagnosed myoclonus, FAME, or benign neonatal sleep myoclonus – have been fruitless. We are heartened by the recent news that the LeDoux group has phenotyped a large family from Mississippi with adult onset, autosomal dominant, highly penetrant myoclonus, including with giant SSEPs, an electrophysiological characteristic that distinguishes FCM from two very similar autosomal dominant conditions (see Chapter II). To our knowledge, this family is the first dead ringer for the FCM phenotype, so we anticipate that they will carry an independent *NOL3* mutation. It may instead be the case that the Mississippi family is distantly related to the FCM index family. If so, we expect that they will carry the same critical region haplotype and *E21Q* mutation; this would raise the LOD score but would not establish allelic heterogeneity.

On a somewhat tangential note, one approach we considered to attain allelic heterogeneity was searching for *NOL3* mutations in natural animal models of inherited myoclonus. Inherited myoclonus has been described in dogs (Fox et al. 1984), horses (Gundlach et al. 1993), lambs (Blignaut et al. 2011), and, most prominently, Hereford calves (Harper et al. 1986). It is thought that the myoclonus in these species results from mutations in *Gla1*, which encodes a glycine receptor subunit, though this has only been demonstrated for calves (Pierce et al. 2001). This mechanism is analogous to that of hereditary hyperekplexia in humans (see Chapters I, II). Indeed, the myoclonus in these species more closely resembles hereditary hyperekplexia than FCM: it is juvenile onset, autosomal recessive, and lower motor neuron in pathology. It would be worthwhile to sequence *NOL3* in those species without evident glycine receptor abnormalities, but we were unable to obtain their DNA.

The genetic analysis presented in this chapter strengthens the conclusion that FCM constitutes a novel phenotype. This conclusion was put forth in Chapter II on the basis of clinical data. As detailed therein, the autosomal dominant myoclonus observed in the index family could conceivably be misdiagnosed as FAME or MDS. However, our linkage data ruled out all known FAME loci (Mikami et al. 1999, Plaster et al. 1999, Guerrini et al. 2001, Depienne et al. 2010, Crompton et al. 2012, Yeetong et al. 2012). Moreover, we excluded linkage to known MDS chromosomal regions (Zimprich et al. 2001, Grimes et al. 2002, Han et al. 2007), and we sequenced but found no mutations in the *SGCE* gene. In concert with the clinical dissimilarity (see Chapter II), the evidence for a novel locus in this family bolsters the contention that FCM is a novel phenotype.

A substantial strength of this work is that exons which were not covered to at least 10x depth by MPS were subsequently Sanger sequenced. Given the GC-rich and/or highly repetitive nature of many of these exons, which likely explains why they were not amenable to MPS, the manual PCR and sequencing of these exons proved tedious. Had we been lucky enough to quickly identify independent *NOL3* alleles, this step would not have been necessary. However, another *NOL3* allele did not readily present itself, and this step was most certainly necessary. In the absence of allelic heterogeneity, if an exon is not sequenced it simply cannot be excluded, and any assignment of a disease gene should be considered preliminary. We stress it here because many groups fail to do likewise (e.g., Veeramah et al. 2012). In our view, the failure to do so is a misapplication of a powerful technology.

In fact, even if MPS is properly applied and two or more mutations are identified in a gene, that gene may still not be the disease gene! Every human carries hundreds of rare, novel variants (Tennessen et al. 2012, Fu et al. 2013), so if the exome is sequenced in a large cohort, just by chance one may observe multiple mutations in the same gene that are not truly causative. If that large cohort consists of patients with a particular disorder, one could erroneously conclude that the implicated gene affects the pathology of that disorder. We expect this fallacy to be rife in the next few years in the field of complex genetics, as larger and larger samples of patients are sequenced for causative rare variants (O’Roak et al. 2012, Sanders et al. 2012). For Mendelian traits, large families will remain valuable because they enable the statistical power of linkage to dictate the subset of the rare variants identified by MPS that can be considered for causality. Even when linkage from a large family with a stereotyped, highly penetrant phenotype is used

to identify a mutation, and the causality has been validated by allelic heterogeneity and functional experiments, some unrelated persons may carry the exact same mutation and be unaffected (Klassen et al. 2011). Even Mendelian mutations are not deterministic.

Some complex geneticists are attempting to do something similar, by using MPS to search for rare variants in loci suggested by genome-wide association studies (GWAS). Setting aside our fundamental objections to GWAS (see Chapter I), this approach is nonetheless logically inconsistent. GWAS are not designed nor powered to detect loci harboring rare variants. GWAS is based on the hypothesis that common diseases result from common variants, whereas MPS is based on the hypothesis that common diseases result from rare variants. To utilize GWAS loci to constrain the MPS-identified variants that are considered for causality is to conflate two diametrically opposed hypotheses. It may well be true that certain loci are home to both causative common variants and causative rare variants, but is this substantially more likely than the alternative scenario in which the causative variants, common and rare, are interspersed throughout the genome? In effect, this approach simply provides tenuous cover to discard the vast majority of the variants identified by MPS, because right now we have no idea what to make of them.

Hence, although MPS provides a powerful way to rapidly sequence much of the exome or genome, it is not foolproof. Methods of localizing a mutation, such as genome-wide SNP array genotyping and microsatellite linkage, remain powerful. It should be noted that methods are being developed for SNP and microsatellite linkage using whole-genome sequencing data (Nielsen et al. 2011). In time, this application will enable both linkage and candidate mutation identification to be done in one fell swoop, providing a justification for the establishment of whole genome sequencing as the standard (see

Introduction). For the time being, however, MPS retains the following weaknesses: regions of low or no coverage; sequencing or data annotation methodologies that may systematically miss particular mutations, such as indels (e.g., Lee et al. 2012a); difficulty prioritizing noncoding variants that may be functionally relevant but are incredibly plentiful; inability to prioritize coding sequences that are included in genome databases but are not currently annotated as part of the exome; and inability to assess sequences in gaps in the human genome map, of which there are almost 300 (Garber et al. 2009). While MPS is no doubt a revolutionary technology, we believe that the field has been subject to a certain degree of hype. There are considerable limitations to MPS that should be weighed carefully when designing experiments and interpreting results, and even seemingly airtight genetic cases should be functionally validated in vitro and in vivo.

Notwithstanding these limitations, we utilized MPS to identify a *NOL3* mutation that likely causes FCM. This was guided by unbiased genome-wide SNP array genotyping and confirmatory microsatellite linkage to chromosome 16q21-22.1. Thus far we have been unable to identify additional *NOL3* alleles. In total, this work bolsters the assertion in Chapter II that FCM constitutes a novel movement disorder. Furthermore, knowledge of the mutation in *NOL3* raises hope that functional investigation of *NOL3* (Chapter IV) may shed light on neuronal membrane hyperexcitability and the pathophysiology of myoclonus and related disorders.

REFERENCES

- Afawi Z, Bassan H, Heron S, Oliver K, Straussberg R, et al. 2012. Benign neonatal sleep myoclonus: an autosomal dominant form not allelic to KCNQ2 or KCNQ3. *J Child Neurol* 27:1260-63
- Bentley D, Balasubramanian S, Swerdlow H, Smith GP, Milton J, et al. 2008. Accurate whole human genome sequencing using reversible terminator chemistry. *Nature* 456:53-59
- Blignaut DJ, Holm DE, Leask R, Stander N, Steyl JC. 2011. Congenital reflex myoclonus in two Merino cross lambs in South Africa. *Vet Rec* 169:684
- Chapman NH, Thompson EA. 2003. A model for the length of tracts of identity by descent in finite random mating populations. *Theoretical Population Biol* 64:141-150
- Cheung VG, Nelson SF. 1998. Genomic mismatch scanning identifies human genomic DNA shared identical by descent. *Genomics* 47:1-6
- Choi M, Scholl UI, Ji W, Liu T, Tikhonova IR, et al. 2009. Genetic diagnosis by whole exome capture and massively parallel DNA sequencing. *Proc Natl Acad Sci U S A* 106:19096-101
- Crompton DE, Sadleir LG, Bromhead CJ, Bahlo M, Bellows ST, et al. 2012. Familial adult myoclonic epilepsy: recognition of mild phenotypes and refinement of the 2q locus. *Arch Neurol* 69:474-81
- Depienne C, Magnin E, Bouteiller D, Stevanin G, Saint-Martin C, et al. 2010. Familial cortical myoclonic tremor with epilepsy: the third locus (FCMTE3) maps to 5p. *Neurology* 74:2000-3

- ENCODE Project Consortium, Dunham I, Kundaje A, Aldred SF, Collins PJ, et al. 2012. An integrated encyclopedia of DNA elements in the human genome. *Nature* 489:57-74
- Fishelson M, Geiger D. 2002. Exact genetic linkage computations for general pedigrees. *Bioinformatics* 18(Suppl 1):S189-198
- Fox JG, Averill DR, Hallett M, Schunk K. 1984. Familial reflex myoclonus in Labrador Retrievers. *Am J Vet Res* 45:2367-70
- Fu W, O'Connor TD, Jun G, Kang HM, Abecasis G, et al. 2013. Analysis of 6,516 exomes reveals the recent origin of most human protein-coding variants. *Nature* 493:216-20
- Gabriel S, Ziaugra L, Tabbaa D. 2009. SNP genotyping using the Sequenom MassARRAY iPLEX platform. *Curr Protoc Hum Genet* 60:2.12.1-2.12.18
- Garber M, Zody MC, Arachchi HM, Berlin A, Gnerre S, et al. 2009. Closing gaps in the human genome using sequencing by synthesis. *Genome Biol* 10:R60
- Gnirke A, Melkinov A, Maguire J, Rogov P, LeProust EM, et al. 2009. Solution hybrid selection with ultra-long oligonucleotides for massively parallel targeted sequencing. *Nat Biotechnol* 27:182-89
- Gonzaga-Jauregui C, Lupski JR, Gibbs RA. 2012. Human genome sequencing in health and disease. *Annu Rev Med* 63:35-61
- Grimes DA, Han F, Lang AE, St George-Hyssop P, Racacho L, et al. 2002. A novel locus for inherited myoclonus-dystonia on 18p11. *Neurology* 59:1183-86
- Guerrini R, Bonanni P, Patrignani A, Brown P, Parmeggiani L, et al. 2001. Autosomal

- dominant cortical myoclonus and epilepsy (ADCME) with complex partial and generalized seizures: A newly recognized epilepsy syndrome with linkage to chromosome 2p11.1-q12.2. *Brain* 124:2459-75
- Gundlach AL, Kortz G, Burazin TC, Madigan J, Higgins RJ. 1993. Deficit of inhibitor glycine receptors in spinal cord from Peruvian Pasos: evidence for an equine form of inherited myoclonus. *Brain Res* 628:263-70
- Han F, Racacho L, Lang AE, Bulman DE, Grimes DA. 2007. Refinement of the DYT15 locus in myoclonus-dystonia. *Mov Disord* 22:888-92
- Harper PA, Healy PJ, Dennis JA. 1986. Inherited congenital myoclonus of polled Hereford calves (so-called neuraxial oedema): a clinical, pathological and biochemical study. *Vet Rec* 119:59-62
- Klassen T, Davis C, Goldman A, Burgess D, Chen T, et al. 2011. Exome sequencing of ion channel genes reveals complex profiles confounding personal risk assessment in epilepsy. *Cell* 145:1036-48
- Lander ES, Linton LM, Birren B, Nusbaum C, Zody MC, et al. 2001. Initial sequencing and analysis of the human genome. *Nature* 409:860-921
- Lee HY, Huang Y, Bruneau N, Roll P, Roberson ED, et al. 2012. Mutations in the gene PRRT2 cause paroxysmal kinesigenic dyskinesia with infantile convulsions. *Cell Rep* 1:2-12
- Lencz T, Lambert C, Derosse P, Burdick KE, Morgan TV, et al. 2007. Runs of homozygosity reveal highly penetrant recessive loci in schizophrenia. *Proc Natl Acad Sci USA* 104:19942-19947

- Li H, Durbin R. 2009. Fast and accurate short read alignment with Burrows-Wheeler transform. *Bioinformatics* 25:1754-1760
- Matsuzaki H, Wang PH, Hu J, Rava R, Fu GK. 2009. High resolution discovery and confirmation of copy number variants in 90 Yoruba Nigerians. *Genome Biol* 10:R125
- Maurer VO, Rizzi M, Bianchetti MG, Ramelli GP. 2010. Benign neonatal sleep myoclonus: a review of the literature. *Pediatrics* 125:e919-24
- McKenna A, Hanna M, Banks E, Sivachenko A, Cibukskis K, et al. 2010. The Genome Analysis Toolkit: A MapReduce framework for analyzing next-generation DNA sequencing data. *Genome Res* 20:1297-1303
- Metzker ML. 2010. Sequencing technologies – the next generation. *Nat Rev Genet* 11:31-46
- Mikami M, Yasuda T, Terao A, Nakamura M, Ueno S, et al. 1999. Localization of a gene for benign adult familial myoclonic epilepsy to chromosome 8q23.3-q24.1. *Am J Hum Genet* 65:745-51
- Mori S, Nakamura M, Yasuda T, Ueno S, Kaneko S, et al. 2011. Remapping and mutation analysis of benign adult familial myoclonic epilepsy in a Japanese pedigree. *J Hum Genet* 56:742-47
- Nelson SF, McCusker JH, Sander MA, Kee Y, Modrich P, et al. 1993. Genomic mismatch scanning: a new approach to genetic linkage mapping. *Nat Genet* 4:11-18
- Nielsen R, Paul JS, Albrechtsen A, Song YS. 2011. Genotype and SNP calling from next-generation sequencing data. *Nat Rev Genet* 12:443-51

- Ng SB, Buckingham KJ, Lee C, Bigham AW, Tabor HK, et al. 2010. Exome sequencing identifies the cause of a Mendelian disorder. *Nat Genet* 42:30-35
- O’Roak BJ, Vives L, Girirajan S, Karakoc E, Krumm N, et al. 2012. Sporadic autism exomes reveal a highly interconnected protein network of de novo mutations. *Nature* 485:246-50
- Park H, Kim JI, Ju YS, Gokcumen O, Mills RE, et al. 2010. Discovery of common Asian copy number variants using integrated high-resolution array CGH and massively parallel DNA sequencing. *Nat Genet* 42:400-405
- Pierce KD, Handford CA, Morris R, Vafa B, Dennis JA, et al. 2001. A nonsense mutation in the alpha1 subunit of the inhibitory glycine receptor associated with bovine myoclonus. *Mol Cell Neurosci* 17:354-63
- Plaster NM, Uyama E, Uchino M, Ikeda T, Flanigan KM, et al. 1999. Genetic localization of the familial adult myoclonic epilepsy (FAME) gene to chromosome 8q24. *Neurology* 53:1180-83
- Sanders J, Murtha MT, Gupta AR, Murdoch JD, Raubeson MJ, et al. 2012. De novo mutations revealed by whole-exome sequencing are strongly associated with autism. *Nature* 485:237-41
- Sato N, Amino T, Kobayashi K, Asakawa S, Ishiguro T, et al. 2009. Spinocerebellar ataxia type 31 is associated with "inserted" penta-nucleotide repeats containing (TGGAA)_n. *Am J Hum Genet* 85:544-557
- Schuelke M. 2000. An economic method for the fluorescent labeling of PCR fragments. *Nat Biotechnol* 18:233-234

- Shojaee S, Sina F, Banihosseini SS, Kazemi MH, Kalhor R, et al. 2008. Genome-wide linkage analysis of a Parkinsonian-pyramidal syndrome pedigree by 500K SNP arrays. *Am J Hum Genet* 82:1375-1384
- Silberstein M, Tzemach A, Dovgolevsky N, Fishelson M, Schuster A, et al. 2006. Online system for faster multipoint linkage analysis via parallel execution on thousands of personal computers. *Am J Hum Genet* 78:922-935
- Strachan T, Read AP. 2010. *Human molecular genetics, 4th edition*. New York: Garland Science
- Tennessen JA, Bigham AW, O'Connor TD, Fu W, Kenny EE, et al. 2012. Evolution and functional impact of rare coding variation from deep sequencing of human exomes. *Science* 337:64-69
- Veeramah KR, O'Brien JE, Meisler MH, Cheng X, Dib-Hajj SD, et al. 2012. De novo pathogenic SCN8A mutation identified by whole-genome sequencing of a family quartet affected by infantile epileptic encephalopathy and SUDEP. *Am J Hum Genet* 90:502-10
- Yeetong P, Ausavarat S, Bhidayasiri R, Piravej K, Pasutharnchat N, et al. 2012. A newly identified locus for benign adult familial myoclonic epilepsy on chromosome 3q26.32-3q28. *Eur J Hum Genet* epub doi: 10.1038/ejhg.2012.133
- Zimprich A, Grabowski M, Asmus F, Naumann M, Berg D, et al. 2001. Mutations in the gene encoding epsilon-sarcoglycan cause myoclonus-dystonia syndrome. *Nat Genet* 29:66-69

CHAPTER IV

Functional Characterization of the *NOL3* Mutation

SUMMARY

Previously we identified a mutation in the gene *nucleolar protein 3 (NOL3)* that likely causes familial cortical myoclonus (FCM). Here we first review the *NOL3* literature, and then describe our experiments to functionally characterize the *NOL3* mutation. *NOL3* encodes a protein-protein interaction motif that facilitates binding to five pro-apoptotic binding partners. Consequently, *NOL3* functions to repress apoptosis. Most groups have focused on *NOL3* in cardiomyocytes because its expression appears to minimize ischemic cardiac injury. In contrast, the role of *NOL3* in the CNS is essentially unknown. We found that *NOL3* is broadly expressed in the murine and human brain. Despite extensive testing, we could not replicate the published *NOL3* binding partners. Moreover, we found that *NOL3* expression actually enhanced basal apoptosis. We sought to elucidate the effects of the *NOL3* mutation that was identified in FCM patients. We observed that the mutation alters post-translational modification (PTM) of *NOL3*. The exact identity of the PTM eluded us, but we did find that generation of this PTM is regulated by phosphorylation at T114 on *NOL3*. We also studied previously-generated *Nol3* knockout mice but did not detect a neurologic phenotype. Finally, we screened the proteome for novel binding partners of WT or mutant *NOL3*. We identified two candidates, HNRNPD and PRPF19, which are important for CNS development. These interactions were abrogated by the mutation, suggesting a hypothesis that will be tested using mutant knockin mice that we generated. In total, this work calls into question some of the published functions of *NOL3* and presents an alternative mechanism by which *NOL3* mutation may potentially cause FCM.

INTRODUCTION

In Chapter II we described a novel Mendelian phenotype, familial cortical myoclonus (FCM), and in Chapter III we identified a mutation in the gene *nucleolar protein 3* (*NOL3*) that likely causes FCM. We sought to investigate the molecular pathophysiology of *NOL3* mutation in FCM, not only in hopes of bolstering the claim that *NOL3* mutation causes FCM but also with the expectation that it may provide broader insight into *NOL3* function. We first review the published functions of *NOL3*, which are summarized in **Figure 1**.

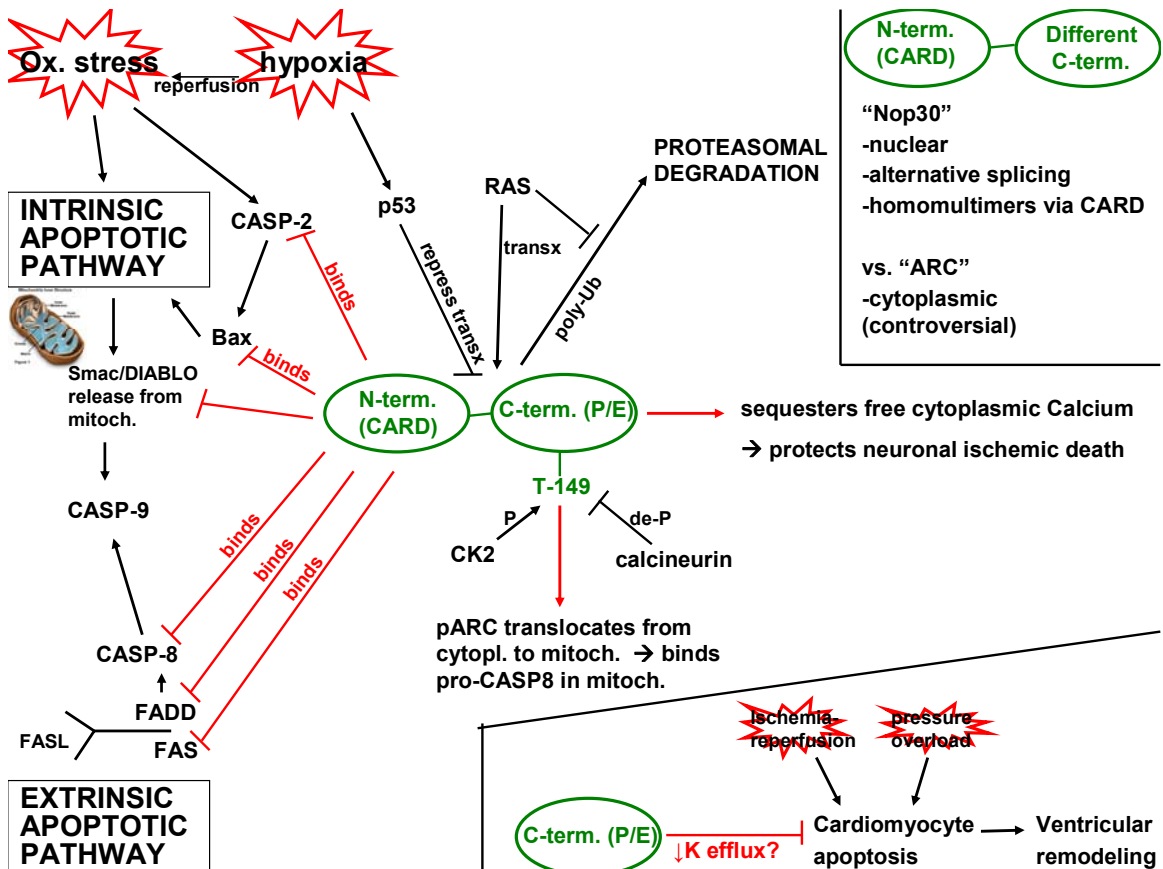


Figure 1. Overview of published functions of NOL3.

See text for details. Abbreviations: C-term., C-terminus; CARD, caspase activation recruitment domain; CASP, caspase; CK2, casein kinase 2; cytopl., cytoplasm; de-P, de-phosphorylation; K, potassium; mitoch., mitochondria; N-term., N-terminus; ox. stress, oxidative stress; P, phosphorylation; P/E, proline/glutamate-rich domain; poly-Ub, poly-ubiquitylation.

NOL3 was first identified in 1998 on the basis of sequence homology to a motif called a caspase activation recruitment domain (CARD) (Koseki et al. 1998). CARDS are one of six types of conserved protein motifs that are critical to apoptotic signalling (Reed et al. 2004). CARDS facilitate protein-protein interactions: a CARD on each of two interacting proteins bind to one another via complementary electrostatic surfaces (Chou et al. 1998). This protein binding regulates the activity of apoptotic proteins. For example, the namesakes of the CARD, caspases, are proteases that initiate or execute proteolytic cleavage cascades. Widespread proteolysis ravages the cellular machinery, causing cell death (Reed et al. 2004). Caspase activity is altered when the caspase CARD is bound to the CARD of another protein (Reed et al. 2004). The name of the domain, caspase activation recruitment, is a misnomer. Some proteins with CARDS inhibit caspases, and other CARDS activate apoptotic signaling proteins that are not caspases.

Five human proteins with CARDS have been crystallized (Chou et al. 1998, Vaughn et al. 1999, Zhou et al. 1999, Renatus et al. 2001, Hiller et al. 2003, Manon et al. 2007, Srimathi et al. 2008, de Alba 2009). Each CARD contains a bundle of 6 alpha-helices (Reed et al. 2004). Many CARDS can homodimerize, and, as noted above, all are thought to heterodimerize via complementary electrostatic interactions. Each CARD consists of a hydrophobic core surrounded by acidic (negatively charged) or basic (positively charged) residues (Chou et al. 1998). The positive residues of one CARD interact with the negative residues of the other CARD, and vice versa. These interactions are highly specific depending on the particular CARD-CARD interaction (Chou et al. 1998, Zhou et al. 1999).

NOL3 encodes a 206 amino acid protein containing an N-terminal CARD. The C-terminus consists of a proline(P)/glutamate(E)-rich domain (Koseki et al. 1998) (**Figure 2**). Little is known about the function of the P/E domain. On the other hand, based on the presence of the CARD, a logical hypothesis was that *NOL3* regulates apoptosis. Indeed, Koseki et al. (1998) found that *NOL3* binds Caspase-2 and Caspase-8. *NOL3* did not bind Caspase-1, -3, or -9, in keeping with the specificity of CARD-CARD heterodimerization interactions. The authors further showed that *NOL3* overexpression in cell culture blocks apoptosis. They concluded that *NOL3* protein-protein interactions function to repress apoptosis. For this reason, *NOL3* is often referred to as *apoptosis repressor with CARD domain (ARC)*.

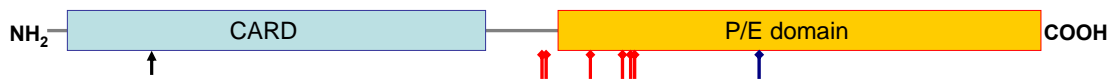


Figure 2. *NOL3* protein contains a C-terminal proline(P)/glutamate(E) domain, and an N-terminal caspase activation recruitment domain (CARD).

CARDS mediate protein-protein binding via electrostatic interactions. The *E21Q* mutation, identified in patients with FCM, is denoted by the black arrow. Known phosphoresidues are denoted by red diamondhead arrows; T149 is a well-characterized phosphoresidue (blue diamondhead arrow).

The seminal observation that *NOL3* inhibits apoptosis has been reinforced many times by multiple groups in the succeeding years. For example, Neuss et al. (2001) showed that oxidative stress leads to a decrease in *NOL3* expression, and oxidative stress-induced cell death could be suppressed by ectopic *NOL3* expression. Apart from the binding partners first identified, Caspase-2 and Caspase-8, both Gustafsson et al. (2004) and Nam et al. (2004) found that *NOL3* binds Bax. *NOL3* binding to Bax inhibited Bax

activation and translocation to mitochondria, which would ordinarily trigger apoptosis. Nam et al. (2004) also found that *NOL3* binds Fas and FADD to interfere with the normal pro-apoptotic Fas-FADD interaction. The *NOL3* CARD is both necessary and sufficient for these protein-protein interactions (**Figure 1**; Nam et al. 2004).

NOL3 is expressed in the heart, skeletal muscle, and brain (Koseki et al. 1998, Engidawork et al. 2001, Gulesserian et al. 2001, Shelke & Leeuwenburgh 2003), as well as smooth muscle in the pulmonary vasculature (Quadriatero et al. 2010, Zaiman et al. 2012). In the brain, it is not known which regions or cell types express *NOL3*. An early paper suggested that in cultured hippocampal neurons the GFP-tagged CARD domain of *NOL3* localizes to the cell body, whereas the C-terminal domain localizes to dendrites (Hong et al. 2003).

Early observations that *NOL3* is expressed in the heart and in skeletal muscle raised the exciting possibility that apoptotic repression by *NOL3* could be exploited to ameliorate cardiac or skeletal disorders characterized by inappropriate apoptosis. One such disorder is muscular dystrophy. Although it is not entirely clear whether the increased cell death of dystrophic pathology results from necrosis or apoptosis, it was certainly reasonable to hypothesize that overexpression of *NOL3* would alleviate dystrophic pathology (Abmayr et al. 2004). However, transgenic *NOL3* expression in mice had no effect.

Investigators have been more successful in cardiomyocytes. In contrast to dystrophic myocytes, it is much better established that cardiomyocytes undergo apoptosis due to ischemia in acute coronary syndromes. Apoptotic cardiomyocytes are then replaced by fibrotic tissue, which impairs cardiac function. Therefore, a suppressor of

cardiomyocyte apoptosis would make an attractive therapeutic target. Ekhterae et al. (2003) found that in cultured cardiomyocytes NOL3 represses apoptosis, possibly by blocking voltage-gated potassium channels (**Figure 1**). Gustafsson et al. (2004) suggested instead that NOL3 represses cardiomyocyte apoptosis by binding to Bax and preventing its activation. Still another group proposed that NOL3 interferes with cytochrome c release and Caspase-3 activation (Li et al. 2007). A separate group implicated spironolactone, a mineralocorticoid receptor antagonist, in blocking NOL3 degradation in cardiomyocytes, which would presumably protect against infarction (Loan Le et al. 2012). Finally, one laboratory has argued that phosphorylation of NOL3 enables repression of cardiomyocyte apoptosis. Li et al. (2002) produced evidence that NOL3 is phosphorylated at its threonine 149 (T149) residue (**Figure 2**). The paper stated that T149 phosphorylation was essential for NOL3 translocation from the cytoplasm to the mitochondria. Furthermore, it claimed that only the phosphorylated form of NOL3 could bind to Caspase-8 and thereby repress apoptosis. The same group later showed that the non-phosphorylatable version of NOL3 cannot bind Caspase-8 or FADD (Murtaza et al. 2008).

These observations were extended with *in vivo* models. Gustafsson et al. (2004) suffused rat hearts with either recombinant wild-type (WT) NOL3 or NOL3 with a point mutation in the CARD. To model an acute coronary syndrome, this study and others used ischemia-reperfusion, in which the heart is rendered ischemic (e.g., through aortic clamp) and then reperfused. Infarct size is then assessed. Gustafsson et al. (2004) found that WT NOL3 suppressed infarct size, but mutant NOL3 did not. Donath et al. (2006) took a genetic approach, performing ischemia-reperfusion experiments on *Nol3* knockout

mice. These mice had no gross behavioral or morphological deficits and no cardiac phenotype at baseline. However, after ischemia-reperfusion, knockout mice had larger infarcts and cardiomyopathy. Pyo et al. (2008) showed the converse by generating transgenic cardiac-specific *Nol3* overexpressing mice. These mice were resistant to ischemia-reperfusion injury. Curiously, Pyo et al. found that when cardiomyocytes from these mice were cultured, the C-terminal P/E domain of *NOL3* was sufficient for apoptotic repression. A second *Nol3* knockout mouse line was created by Zaiman et al. (2012). They observed that under conditions of chronic hypoxia, *Nol3* expression was upregulated and *Nol3*-deficient mice had increased cell death, decreased proliferation, and decreased vascular remodeling. Thus, *Nol3* inhibition of apoptosis acts to limit the damage of hypoxia-induced pulmonary hypertension.

There have been attempts to validate these mouse experiments in higher organisms such as rabbits (Bouma et al. 2010) and even sheep (Ekhterae et al. 2011). However, the data are weak. Similarly, Donath et al. (2006) claimed that *NOL3* protein is less abundant in hearts from human patients with end-stage congestive heart failure, and Zaiman et al. (2012) showed increased *NOL3* expression in biopsies from patients with pulmonary hypertension. In our view, their data is wholly unconvincing.

Another line of investigation has focused on *NOL3* in cancer. *NOL3* is clearly upregulated in cancer cell lines (Wang et al. 2005, Heikaus et al. 2008, Mercier et al. 2008, Rajandram et al. 2009). In cancer cells *NOL3* function seems to differ from its ordinary apoptotic function: in the nucleus of cancer cells, *NOL3* binds p53, preventing p53 tetramerization and triggering p53 export to the cytoplasm (**Figure 1**). This blocks p53 induction of apoptosis (Foo et al. 2007), allowing cancer cell growth to proceed un-

checked. *NOL3* is able to evade degradation in cancer cells due to RAS, which simultaneously activates *NOL3* transcription and prevents *NOL3* protein poly-ubiquitylation (Wu et al. 2010). In other cancer work, two groups suggested the involvement of *NOL3* in doxorubicin chemotherapy resistance (An et al. 2009, Wang et al. 2009), and Carter et al. (2011) found that *NOL3* expression has prognostic value for acute myeloid leukemia.

If *NOL3* inhibits cardiomyocyte apoptosis, it would be logical to hypothesize that it does the same in the CNS. This supposition is supported by a modicum of evidence. *NOL3* expression has been detected in the brains of rats, mice, and humans (Koseki et al. 1998, Engidawork et al. 2001, Gulesserian et al. 2001, Shelke & Leeuwenburgh 2003). In the mouse cortex, *Nol3* expression declines with age (Shelke & Leeuwenburgh 2003). *Nol3* expression also declines in cerebellar tissue after chronic alcohol intake (Ren et al. 2009). In ischemic primary cortical neuronal cultures, *Nol3* is upregulated, further suggesting a role in neuroprotection (Prasad et al. 2010). Hong et al. (2003) found that rat hippocampal neurons that are ischemic have decreased *Nol3* expression, but *Nol3* overexpression prevented ischemic neuronal death. Hong et al.'s is the lone experiment to show a functional consequence other than gene expression changes. Given the inconsistencies between Hong et al. and Prasad et al., with one observing *Nol3* upregulation and the other downregulation in response to ischemia, and both papers being plagued by technical weaknesses, the function of *NOL3* in the CNS remains essentially unknown.

One early paper used a human cDNA library expressed in yeast to identify an alternatively spliced *NOL3* isoform, termed *Nop30* (*nucleolar protein of 30 kDa*) (**Figure 1**; Stoss et al. 1999). *Nop30* and *NOL3* both contain an N-terminal CARD but differ in their C-terminus. Stoss et al. demonstrated that *Nop30* can homodimerize and also can

heterodimerize with NOL3. Moreover, the authors stated that Nop30 heterodimerizes with the splicing factor SRp30c, and the overexpression of *Nop30* affects RNA splicing. We doubt the biological relevance of these findings. They have never been replicated and the same group has never published again on *Nop30*. More damningly, the *Nop30* transcript has never been detected in vivo. However, although it seems likely that *Nop30* was a spurious finding, we cannot rule out a role for Nop30 and/or NOL3 in RNA processing.

Our hypothesis that FCM is caused by mutation in *NOL3*, a repressor of apoptosis, is strengthened by the known pathophysiology of Unverricht-Lundborg disease (ULD) (Kalviainen et al. 2008). Although ULD patients suffer extensive neurodegeneration, ULD is in some ways similar to FCM: ULD is a Mendelian disorder characterized by progressive myoclonic epilepsy with stimulus-sensitive myoclonus of the proximal extremities (Kalviainen et al. 2008). However, ULD differs from FCM in that ULD myoclonus is subcortical in origin (Kalviainen et al. 2008). Interestingly, ULD is caused by mutations in *cystatin-B* (*CSTB*), a gene which encodes an inhibitor of apoptosis (Joensuu et al. 2008). *CSTB* knockout mice have increased cerebellar apoptosis and hyperexcitable hippocampal slices, and suffer from myoclonic seizures as measured by gross observation and electrophysiologic monitoring (Lehtinen et al. 2009). Thus, there is precedent for mutation in an apoptosis repressor leading to neuronal hyperexcitability as manifested clinically by myoclonus.

In addition to the *CSTB* mouse, there is strong justification for studying myoclonus in mouse models. Espinosa et al. (2001) demonstrated that mice with potassium channel mutations exhibited myoclonus that was easily phenotyped by visual observa-

tion. Similarly, Suzuki et al. (2009) studied mice with null alleles in *Efhc1*, a gene that is mutated in humans with juvenile myoclonic epilepsy (see Chapter I). In *Efhc1* knockout mice they observed seizures and frequent spontaneous myoclonus.

We sought to elucidate the molecular pathophysiology by which *NOL3* mutation causes FCM. Since the mutation resides in a protein-protein interaction motif that, as detailed above, is known to be important for protein binding, we hypothesized that the mutation alters *NOL3* protein-protein interactions. In this chapter we present the experiments we undertook to test this hypothesis, along with other experiments that provide a basic characterization of *NOL3* in the brain.

METHODS

Amino Acid Alignment

Evolutionary conservation was investigated using NOL3 amino acid sequences from different organisms. Sequences were aligned with the ClustalW2 program (www.ebi.ac.uk/Tools/clustalw2/index.html). Identity and similarity between species was determined with BLASTp, using sequences obtained from NCBI Protein (<http://www.ncbi.nlm.nih.gov/protein>), including Human (*Homo sapiens*; NP_001171987.1), canine (*Canis lupus familiaris*; XP_853983.1), cattle (*Bos taurus*; NP_001077157.1), mouse (*Mus musculus*; NP_084428.1), and rat (*Rattus norvegicus*; NP_445968.2). NOL3 homologs from other species were identified by BLASTp (<http://blast.ncbi.nlm.nih.gov>) but were omitted from amino acid alignment (for example, *Pan troglodytes* NOL3 is 100% identical to human NOL3).

Interestingly, we were unable to identify homologs in *Caenorhabditis elegans*, *Drosophila melanogaster*, or *Danio rerio*. We also searched for NOL3 homologs in 9 additional species encompassing 4 reptile/bird genomes (*Anolis carolinesis*, i.e., green anole lizard; *Gallus gallus*, i.e., chicken; *Meleagris gallopavo*, i.e., turkey; *Taeniopygia guttata*, i.e., zebra finch), 1 amphibian (*Xenopus tropicalis*, i.e., frog), and 4 bony fish in addition to zebrafish (*Gadus morhua*, i.e., Atlantic cod; *Gasterosteus aculeatus*, i.e., stickleback; *Latimeria chalumnae*, i.e., West Indian Ocean coelacanth; *Takifugu rubripes*, i.e., Puffer fish). To ensure that negative results were not a consequence of ultra-stringent search parameters, we individually varied the following parameters: Expect Threshold from the standard value (10) to up to three orders of magnitude (100, 1,000, or 10,000); Matrix from the standard (BLOSUM62) to all other available matrices (PAM30,

PAM70, BLOSUM80, BLOSUM45); Gap Costs from the standard (Existence 11, Extension 1) to all other available conditions (Existence 9, Extension 2; Existence 8, Extension 2; Existence 7, Extension 2; Existence 12, Extension 1; Existence 10, Extension 1); and Compositional Adjustments from the standard value (Conditional compositional score matrix adjustment) to either Composition-based statistics or Universal compositional score matrix adjustment (the condition No adjustment was omitted because it revealed thousands of homology matches due to low stringency). The definition for homology was >50 alignment score, or e-value $<1e-10$; for comparison, under standard search parameters, a homology match to *Mus musculus*, a positive control, yielded >200 alignment score and an e-value of $2e-82$.

In Silico Homology Modelling

The crystal structure of NOL3 protein is not known, so to analyze the 3-dimensional structure we performed in silico homology modelling. We used the structure of the Nod1 CARD domain (PDB structure 2DBD) (Manon et al. 2007) as the template. Since the C-terminus of NOL3 is not homologous to any published structures, only the N-terminal CARD was modelled, viz. amino acids 10-83. We performed homology modelling using SWISS-MODEL (<http://swissmodel.expasy.org>), and analyzed resultant structures with UCSF Chimera software (www.cgl.ucsf.edu/chimera). We repeated the analysis with a different structure of the Nod1 CARD domain (PDB structure 2NZ7) (Srimathi et al. 2008) and obtained similar results (data not shown).

Other Bioinformatic Analyses

We predicted *NOL3* protein secondary structure using Jpred (www.compbio.dundee.ac.uk/www-jpred), I-TASSER (www.zhanglab.ccmb.med.umich.edu/I-TASSER), and PSIPRED (www.bioinf.cs.ucl.ac.uk/psipred). Potential splicing enhancers, splice branch points, and nuclear export sequences were predicted with RESCUE-ESE (www.genes.mit.edu/burgelab/rescue-ese), Human Splicing Finder (www.umd.be/HSF), and NetNES 1.1 (www.cbs.dtu.dk/services/netNES), respectively. We also used PolyPhen-2 (www.genetics.bwh.harvard.edu/pph2) to predict whether *E21Q* is a deleterious variant.

***NOL3* Constructs**

A pcDNA3.1 vector containing human *NOL3* cDNA sequence with a C-terminal FLAG-tag (the *E21Q* mutation is near the N-terminus) was kindly provided by Gabriel Nunez, Ph.D., and Peter Kuffa (University of Michigan) (Koseki et al. 1998). Site-directed mutagenesis to introduce the *E21Q* mutation was performed with the QuikChange II XL Mutagenesis kit (Agilent) using HPLC-purified primer 5'-GAAACG CCTGGTCCAGACGCTGCAGGC-3' and its antisense primer 5'-GCCTGCAGCGTCT GGACCAGGCGTTTC-3'. The manufacturer's instructions were followed, with the following refinements: for PCR, a 7min extension step was used to amplify the ~6kb pcDNA3.1; DpnI digestion was performed for 2h at 37°C; before transformation, PCR products were purified with QIAquick PCR Purification Kit (Qiagen). Colonies were cultured, and plasmid was isolated by QIAprep Plasmid Miniprep Kit (Qiagen) and then sequenced with the following primers: 5'-GGCGGTAGGCGTGTA-3', 5'-CGTCGCCG

TCCAGCTC-3', 5'-AGCACCCAGTCCGCCCTGAGC-3'. Mutation-positive clones were transformed and cultured, and ample plasmid was purified using QIAfilter Plasmid Maxi Kit (Qiagen). Purified plasmid was again Sanger sequenced to ensure correct sequence. Other *NOL3* mutant constructs were constructed using the same approach. The site-directed mu-tageneis primers used are listed in **Table 1**.

Table 1. Primers used for cloning mutant *NOL3* constructs.

Mutation	Primers
<i>S104A</i>	5'-GCTACCGGGACCGCGCCTATGACCCTCCAT-3' ATGGAGGGTCATAGGCGCGGTCCCGGTAGC
<i>T114A</i>	CAGGCCACTGGGCGCCGGAGGCA TGCCTCCGGCGCCCAGTGGCCTG
<i>T122A</i>	CCGGCTCGGGGGCCACATGCCCC GGGGCATGTGGCCCCCGAGCCGG
<i>T123A</i>	GCTCGGGGACCGCATGCCCCGGG CCCGGGGCATGCGGTCCCCGAGC
<i>T149A</i>	GTGCAATCCGGGGCCCCGGAGGAGC GCTCCTCCGGGGCCCCGGATTGCAC
<i>T114D</i>	GCCCAGGCCACTGGGATCCGGAGGCACCCGG CCGGGTGCCTCCGGATCCCAGTGGCCTGGGC
<i>C79A</i>	GGAGCTGCTACGCGCTGCCCAGCGTACC GGTACGCTGGGCAGCGCGTAGCAGCTCC
<i>K17R</i>	CCGCGAGCGGAGACGCCTGGTCCG CGACCAGGCGTCTCCGCTCGCGG
<i>K68R</i>	GGTGCAGGGCAGGGGCGAGGCCCG CGGGCCTCGCCCCTGCCCTGCACC
<i>K163R</i>	GCTGAGGCCTCTAGAGAGGCTGAACC GGTTCAGCCTCTCTAGAGGCCTCAGC

***NOL3* Expression in the CNS**

To determine the expression pattern of *NOL3* in the CNS, we utilized the mouse and human versions of the Allen Brain Atlas (Lein et al. 2007, Hawrylycz et al. 2012). For further analysis, including differential expression of *Nol3* by CNS cell type, we utilized BacTRAP (www.bactrap.org; Heiman et al. 2008), and supplementary data from

Sugino et al. (2006) and Cahoy et al. (2008). Data were analyzed and plotted with Microsoft Excel.

To assay expression of *NOL3* in human brain regions, we performed reverse transcriptase PCR on a RapidScan cDNA panel containing first-strand cDNA prepared from 12 human brain parts (AMSBio, Lake Forest, CA). *NOL3* was amplified using the following primers: 5'-GCCAGAGTACGAGGCATTGGATGC-3', 5'-CGGACTCGTCCCTTTCCTCGAAG-3'. This PCR yields a 647bp product from genomic DNA and a 491bp product from cDNA. We confirmed that each lane contained comparable amounts of cDNA by PCRing *beta-actin* (*ACTB*) with the following primers: 5'-CATGTACGTTGCTATCCAGGC-3', 5'-CTCCTTAATGTCACGCACGAT-3'.

We also used reverse transcriptase PCR to assay expression of *Nol3* in cultured primary oligodendrocytes and astrocytes from WT mice. We used the following primers for *Nol3*: 5'-CTCCGGCTCTTGTCTGGAT-3', 5'-GCGGAGTTCGAAGAAATG-3', yielding an RNA-specific product of 549bp. For a loading control, we PCRed *beta-actin* with the following primers: 5'-GGCTGTATTCCCCTCCATCG-3', 5'-CCAGTTGGTACAATGCCATGT-3' (product size of 154bp).

Generation of Stable Cell Lines and Transiently Transfected Cell Lines

Human embryonic kidney (HEK) 293 cells were obtained from American Type Culture Collection (catalog number CRL-1573, ATCC, Manassas, VA) and cultured in DMEM supplemented with 10% fetal bovine serum (FBS) in a 37°C incubator with 5% CO₂. Cells were transiently transfected with either FuGENE (Roche, Indianapolis, IN) or Lipofectamine 2000 reagent (Invitrogen, Carlsbad, CA) according to manufacturers'

instructions. Multiple, independent stable cell lines were generated by transfecting a 50% confluent culture, which was grown to confluency, split to a 15cm plate, and selected with G418 (Invitrogen) antibiotic at 400 μ g/mL. Each independent stable line was poly-clonal. Stable lines were maintained in DMEM containing 10% FBS and 200 μ g/mL G418. Lines expressing NOL3 protein at similar levels were identified by the following method: cells were washed with ice-cold PBS, scraped with a cold scraper, isolated by centrifugation, lysed with RIPA buffer (50mM Tris HCl pH 7.4, 150mM NaCl, 1mM EDTA, 1% Triton X-100, 1% Sodium deoxycholate, 0.1% SDS, 1 cOmplete protease inhibitor cocktail tablet (Roche) per 10 mL), sonicated, harvested for protein by 4°C centrifugation, and analyzed by Western blotting. Cell stocks were stored in liquid nitrogen and cell lysates at -20°C or -80°C.

The other cell lines used were HeLa (CCL-2) and COS7 (CRL-1651) courtesy of ATCC, and SK-N-SH (MA6210) from ATCC by way of the UCSF Cell Culture Facility.

Western Blots

SDS-PAGE (sodium dodecyl sulfate-polyacrylamide gel electrophoresis) was performed under standard conditions. Briefly, 4X SDS buffer (50mM Tris HCl pH 6.8, 2% SDS, 10% glycerol, 1% β -mercaptoethanol, 12.5mM EDTA, 0.02% bromophenol blue) was added 1:3 to each sample, and samples were then denatured by boiling for 5min at 95°C. Equal amounts of sample were loaded into a 12% Bis-Tris NUPAGE Gel (Invitrogen); electrophoresed using NUPAGE MOPS buffer (50mM MOPS, 50mM Tris Base, 0.1% SDS, 1mM EDTA, pH 7.7; Invitrogen) at 50mA for ~1hr; and transferred to a nitrocellulose membrane in transfer buffer (25mM Tris Base, 192mM glycine, 10%

methanol) at 100mA for ~1hr at 4°C. Membranes were blocked in Odyssey Blocking Buffer (LI-COR Biosciences, Lincoln, NE) for 5min at room temperature (RT), incubated with primary antibody/antibodies for 1hr at RT, washed thrice for 5min each with TBS-T (50mM Tris Base, 150mM NaCl, 0.05% Tween 20, pH 7.6), incubated with secondary antibody/antibodies for 1hr at RT, then again washed thrice for 5min each with TBS-T. The following antibodies were diluted in Odyssey Blocking Buffer: rabbit anti-FLAG clone F7425 (Sigma-Aldrich, St. Louis, MO) at 1:500; mouse anti-GAPDH clone MAB374 (Millipore, Billerica, MA) at 1:500; rabbit anti-NOL3 clone 160737 (Cayman Chemical, Ann Arbor, MI) at 1:500; and various IR-Dye Secondary Antibodies (LI-COR) at 1:10,000. Membranes were scanned and densitometry analyses were performed with the Odyssey Infrared Imaging System and accompanying software (LI-COR). Molecular weight was determined by co-loading Precision Plus Dual Color Standards (Bio-Rad, Hercules, CA). GAPDH served as loading control, and quantity of the lower molecular weight FLAG band served as an additional, internal loading control; also, total FLAG:GAPDH levels were ~1 (**Figure 15**). All experiments were performed at least thrice. Statistical analysis was a paired two-tailed t-test, using Microsoft Excel.

Investigations to Identify the Upper Band

Western blots were performed in the manner described above and were probed using the following antibodies: anti-phosphothreonine mAb clone 14B3 (Calbiochem, Darmstadt, Germany); anti-ubiquitin clone 6C1.17 (BD Pharmingen, San Jose, CA); and anti-ubiquitin clone P4D1 (Santa Cruz Biotechnology, Santa Cruz, CA). Phosphatase treatment was performed using calf intestinal alkaline phosphatase (New England

BioLabs, Ipswich, MA), protein phosphatase 1 (New England BioLabs), and potato acid phosphatase (Sigma Aldrich), all according to manufacturers' protocols. We also tinkered with the protocols by adding up to 10-fold additional phosphatase, and by incubating for variable intervals (1, 5, 10, 30, 60, and 120min). For in vivo phosphatase experiments, we treated HEK293 cells with 100 μ M, 1mM, or 10mM sodium fluoride or sodium orthovanadate (both from New England BioLabs), waited 20min, then harvested cell lysates and immunoblotted.

To test the hypothesis of palmitoylation, 100 μ L of protein lysate (1mg/mL) or of immunoprecipitated NOL3 was incubated with 5 μ L of 200mM TCEP(tris-2-carboxyethyl-phosphine)-HCl solution (Thermo Scientific, Rockford, IL) at 55°C for 1h. Then, 5 μ L from a 1M iodoacetamide solution (Sigma-Aldrich) was added and tubes were kept at RT for 1h in the dark. Samples were then processed for SDS-PAGE as described above.

For mass spectrometry experiments, we took care to avoid contamination. Lysate and IP samples were run by SDS-PAGE, and the gels were then stained with Coomassie blue dye for 1h at RT and destained with double distilled H₂O (ddH₂O) overnight at RT. The next day, we excised bands of interest. Samples were prepared and digested with trypsin as previously described (Trinidad et al. 2008). For some experiments, phosphorylated peptides were enriched using titanium dioxide as previously described (Trinidad et al. 2008). Tandem mass spectrometry (MS/MS) was carried out with an Orbitrap liquid chromatography/mass spectrometer (Thermo) at the UCSF Mass Spectrometry Facility. The data were analyzed using Protein Prospector as previously

described (Trinidad et al. 2008). For this work we relied heavily upon a collaboration with Jonathan Trinidad, Ph.D., of the Facility.

Co-immunoprecipitations

For our attempts at co-immunoprecipitations (co-IPs) of proteins that interact with NOL3 in the mouse brain, WT and *Nol3* knockout littermates were aged to one year. Mice were anesthetized with isoflurane and euthanized by cervical dislocation. Whole brain was dissected and stored overnight at -80°C. The next day, samples were thawed for 2min, upon which 3mL of tissue lysis buffer (5mM Tris-HCl pH 7.4, 1mM EDTA, 1% NP40, Roche cOmplete protease inhibitor, Roche PHOSStop phosphatase inhibitor) was added to a Dounce homogenizer along with the sample. Each sample was Dounce homogenized about 25 times until the solution was homogeneous by inspection. Solutions were transferred to 1.5mL eppendorf tubes, sonicated briefly, then centrifuged at 14,000rpm for 10min at 4°C. The supernatant was used for further co-IPs, IPs, and Western blots.

For co-IPs in HEK293 cells, dishes were grown to confluency, then placed on ice, rinsed twice gently with ice-cold PBS, and lysed using various buffers including RIPA (see above), NP40 (50mM Tris-HCl pH 7.4, 150mM NaCl, 1% NP-40, protease and phosphatase inhibitors), or gentler lysis buffer (50mM Tris-HCl pH 7.4, 150mM NaCl, 1mM EDTA, 1% Triton, protease and phosphatase inhibitors). The buffer and detached cells were placed into a 15mL conical and centrifuged at 1100rpm for 5min at 4°C. The supernatant at this step was the “input”—some was saved for later analysis. When using antibodies with lower affinity, samples were precleared by adding 50μL of protein A-

agarose (for rabbit monoclonal antibodies) or protein G-agarose (for mouse monoclonal antibodies) for every 1mL of lysate, rotated at 4°C for 1h, then centrifuged at 14,000rpm for 5min at 4°C. Samples were then centrifuged at 14,000rpm for 10min at 4°C, upon which the supernatant was removed. Primary antibody was added, typically 1-5µg of antibody per 1mg of 1mg/mL lysate, and incubated for variable intervals (from 1h to two days) on a circular rotator at 4°C. Samples were then centrifuged at 3000rpm for 1min at 4°C, thrice washed with ice-cold PBS, and centrifuged at 3000rpm for 1min at 4°C. Samples thus prepared were used for further treatments to study the upper band, such as in vitro phosphatase assays (see above). Otherwise, for co-IPs the pellets (along with the input samples, see above) were resuspended in 40µL of SDS sample buffer and run by SDS-PAGE as explicated above. For anti-FLAG IPs and co-IPs, we used EZView Red Anti-FLAG M2 affinity beads (Sigma-Aldrich). For immunoblotting of putative interacting proteins, we used the following primary antibodies: anti-Bax clone 2772 (Cell Signaling, Beverly, MA); anti-Bax clone 6A7 (Sigma-Aldrich); anti-Caspase-2 clone 3507 (Millipore); anti-Caspase-8 clone 12F5 (Enzo Life Sciences, Villeurbanne, France); anti-FADD clone 1F7 (Millipore); anti-Fas clone CH11 (Millipore); anti-MDM2 clone SMP14 (Santa Cruz Biotechnology); anti-PACSIN3 clone ab86077 (Abcam, Cambridge, MA); and anti-PNKP (Sigma-Aldrich). Primary antibodies were typically diluted at 1:1000, but for optimization purposes we performed serial dilutions and immunoblotted with antibody solutions as concentrated as 1:100.

For identification of novel binding partners, co-IPs corresponding to vector, *NOL3*^{WT}, or *NOL3*^{E21Q} cell lines were each labeled with a different fluorescent dye and simultaneously run on a 2-dimensional SDS-PAGE gel. DeCyder software was used to

identify and quantify gel spots with differential protein levels. Those spots which were more highly expressed in *NOL3*^{WT} or *NOL3*^{E21Q} cells than vector were excised and identified by standard tandem mass spectrometry. This work was done in collaboration with Applied Biomics (Hayward, CA).

Apoptosis Cell Imaging and FACS

For apoptosis imaging experiments we used either transiently transfected or stable HEK293 cell lines. Glass slides were coated with polylysine and washed thrice with distilled water, then seeded with cells. When appropriate, cells were transfected at least 5h later. The next day, or when cells reached 90% confluency, we added one of a variety of stimuli that induce apoptosis. These stimuli included anti-Fas agonist clone CH11 (Millipore), brefeldin A, and etoposide (both courtesy of Scott A. Oakes, M.D.). However, the majority of our experiments utilized staurosporine (STS, Sigma-Aldrich), a broad-spectrum kinase inhibitor, because many of the published experiments demonstrating a role for *NOL3* in repressing apoptosis utilized STS (e.g., Ekhterae et al. 2003). We experimented with a wide variety of STS concentrations (on a log scale) and incubation times (from 1h to 48h). After STS incubation, cells were washed thrice with PBS and fixed using 4% paraformaldehyde. Cells were again washed thrice with PBS, permeabilized with 0.2% Triton, and washed with PBS. We then executed various protocols to measure apoptosis. These included measurement of mitochondrial membrane permeability, nuclear fragmentation (Trypan Blue exclusion or Hoechst 33342), and especially chromosomal fragmentation using terminal deoxynucleotidyl transferase dUTP nick end labeling (TUNEL). For TUNEL assays, we used the DEADEnd Fluorometric

TUNEL System (Promega, Madison, WI) and included DNase treatment as a positive control. After TUNEL staining, cells were prepared for fluorescence microscopy as explicated below.

For fluorescence activated cell sorting (FACS) analysis of apoptosis, cells grown to 90% confluency were treated with 1 μ M STS for 5h at 37°C. We also tested a variety of confluencies (data not shown). After STS incubation, media was removed and cells were washed with PBS, upon which warm PBS containing 3% FBS and 1mM EDTA (PBS-FBS-EDTA) was added and pipetted up and down to gently detach cells from the plate. Cells in solution were added to a 15mL conical and kept on ice for the remainder of the protocol. The cells were centrifuged at 1000rpm for 3min at 4°C, the supernatant was removed, and 5mL of ice-cold PBS-FBS-EDTA was added to the cell pellet. The solution was passed through a 40 μ m filter and again 5mL of ice-cold PBS-FBS-EDTA was added. The solution was then transferred to a 15mL conical and centrifuged at 1000rpm for 3min at 4°C. The supernatant was removed, and cells were resuspended in 2mL of PBS-FBS. One-quarter of each sample was added to one of four 5mL polystyrene tubes, then stained with fluorescent markers. The markers used were 4',6'-diamidino-2-phenylindole (DAPI; Invitrogen) at a 1:10,000 dilution, propidium iodide (PI; Invitrogen) at a 1:50 dilution, and annexin V-fluorescein isothiocyanate (annexin V-FITC; BD Pharmingen) at a 1:100 dilution, all according to manufacturers' protocols. For each sample, one tube was left unstained, one tube was stained with DAPI (or, as it happened, PI), one tube was stained with annexin V, and one tube was stained with both PI and annexin V. We performed FACS with a UCSF Laboratory for Cell Analysis FACSCanto II flow cytometer (BD Biosciences, San Jose, CA). The settings were the

405nm laser and 450/50 filter for DAPI, and the 488nm laser with 670LP-655LP (PI) or 530/30-502LP (FITC) filters. Data was gathered using FACSDiva software (BD Biosciences) and subsequently analyzed with FlowJo v.10.0.5 (Tree Star, Portland, OR). The FACS plots in **Figure 21** depict data for 100,000 cells per condition.

Immunohistochemistry and Cell Imaging

For immunohistochemistry, cells were cultured in chamber slides or on polylysine-coated cover slips within 6-well dishes. To stain mitochondria, the cells were incubated with 300nM Mitotracker (Invitrogen) for 30min at 37°C. Cells were then washed thrice for 2min each in PBS, fixed with 4% paraformaldehyde for 15min at 37°C, washed thrice with PBS, permeabilized with 0.2% Triton, and washed with PBS. Slides were prepared using VECTASHIELD Hard-set mounting medium with DAPI (Vector Laboratories, Burlingame, CA). For immunohistochemistry sans Mitotracker, cells were simply washed with PBS, fixed, and permeabilized. For all immunohistochemistry, cells were blocked with 5% normal goat serum (NGS) in PBS for 1h at RT, then incubated with primary antibody (diluted 1:500 in 5% NGS blocking buffer) overnight at 4°C in a humidified chamber. The next day they were washed thrice for 5min with PBS, upon which secondary antibody (diluted 1:500 in blocking buffer) was added for 1.5h at RT in a humidified chamber. They were then washed thrice with PBS and slides were prepared using VECTASHIELD. The primary antibodies used were anti-FLAG clone M2 (Sigma-Aldrich) and anti-NOL3 (see above).

We imaged cells by fluorescence microscopy using a DM6000 FS (Leica, Wetzlar, Germany). Images were obtained with Image-Pro Plus software (Media-

Cybernetics, Rockville, MD). For confocal microscopy, we used the CSU22 spinning disk confocal microscope (Yokogawa, Tokyo, Japan) at the UCSF Nikon Imaging Center. With both microscopes we used the following lasers: 405nm for DAPI, 491nm for FITC, and 561nm for rhodamine (Mitotracker). Confocal images were taken using in-house software. All images were analyzed with ImageJ (www.rsweb.nih.gov/ij).

SSEP Studies in Mice

All mice were housed in the UCSF Laboratory Animal Resource Center (LARC) with approval of the Institutional Animal Care and Use Committee. All procedures throughout the study, including euthanasia, were performed in accordance with institutional, state, and federal regulations for the humane handling of animals. *Nol3* knockout (KO) mice were previously generated by Donath et al. (2006) and were a kind gift of Joe Quadrilatero, Ph.D., of the University of Waterloo. Mice were genotyped using the following primers: WT (5'-GATACCAGGAGATCTCTCAAATT-3', 5'-CAGCGCATCCAAGGCTTCGTAATC-3'), KO (5'-GATACCAGGAGATCTCTCAAATT-3', 5'-GATTGGGAAGACAATAGCAGGCATGC-3'). We used standard PCR reagents, except that unlike some genotyping protocols, the WT and KO PCR reactions were not combined into a single reaction. PCR was performed as follows: 93°C 2min; 55°C 1min; 65°C 3min; 29 cycles of 93°C 30sec, 55°C 30sec, 65°C 3min; 65°C 7min. The WT and KO bands were ~760bp and ~450bp, respectively.

Proof of principle for performing somatosensory evoked potentials (SSEPs) in mice was provided by Iuliano et al. (1994). Gross behavioral phenotyping to rule out myoclonus was performed similar to the protocol of Espinosa et al. (2001). For SSEPs,

Nol3 knockout (*Nol3*^{-/-}) and *WT* (*Nol3*^{+/+}) littermates were anesthetized with a mixture of ketamine and xylazine. A small incision was made in the scalp and the fascia cleaned away from the skull. A prefabricated electroencephalography (EEG) headmount (Pinnacle Technology, Lawrence, KS) was attached to the skull by four screws that penetrated through the skull to the dura. These screws were placed such that a pair straddled the somatosensory cortex of each hemisphere, and the screws served as cortical surface electrodes to monitor EEG activity in each hemisphere. The headmount included a pair of silver wire electrodes that were inserted subcutaneously over the trapezius muscles to record electromyographic (EMG) activity to detect movement and stimulus artifacts. The headmount was then linked to an amplifier (Pinnacle Technology) and EEG data was sampled at a rate of 400Hz.

SSEPs were evoked in anesthetized mice by stimulating the gastrocnemius muscle with a 2msec square current pulse delivered through a needle electrode. Suprathreshold stimuli evoked SSEPs that could be detected in the EEG of both hemispheres. SSEP threshold was roughly measured and stimulus strength was set to approximately 125% of threshold, which evoked a response to each stimulus. SSEP threshold was similar between genotypes (18-25mA). Fifteen to twenty SSEP sweeps were then recorded in response to the suprathreshold stimulus, averaged and normalized to peak amplitude. Mean SSEP time to peak, measured from the EMG stimulus artifact, and 10-90% rise time were calculated for each mouse.

Generation of *E21Q* Knockin Mutant Mice

Mice with a *Nol3* allele containing the *E21Q* mutation and three *LoxP* sites were generated as described in **Appendix 5**. In deciding where to place the third *LoxP* site, we utilized the following three splice acceptor prediction programs: Human Splicing Finder (URL above), Softberry (www.linux1.softberry.com/berry.phtml) and Fruitfly (www.fruitfly.org). The targeting vector was constructed in collaboration with ingenious Targeting Laboratory (Ronkonkoma, New York). Embryonic stem cell work was completed by the Howard Hughes Medical Institute Janelia Farm Research Campus core facility.

RESULTS

Evolutionary Conservation and Other Bioinformatic Analyses

First, we assessed *NOL3* evolutionary conservation. When we compared *NOL3* amino acid sequence across humans, dogs, cattle, mice, and rats, we observed extremely high conservation (**Figure 3**). For example, between humans and mice 88.4% of residues are identical and 93.2% are similar. Conservation is particularly pronounced for the CARD, including the region around E21, the residue mutated in FCM (**Figure 3**). Despite extensive searching, we were unable to identify homologs in *Drosophila*, *C. elegans*, or even “lower” vertebrate species such as *D. rerio* (zebrafish). However, as a positive control we did identify *NOL3* homologs in newly-sequenced vertebrate mammal

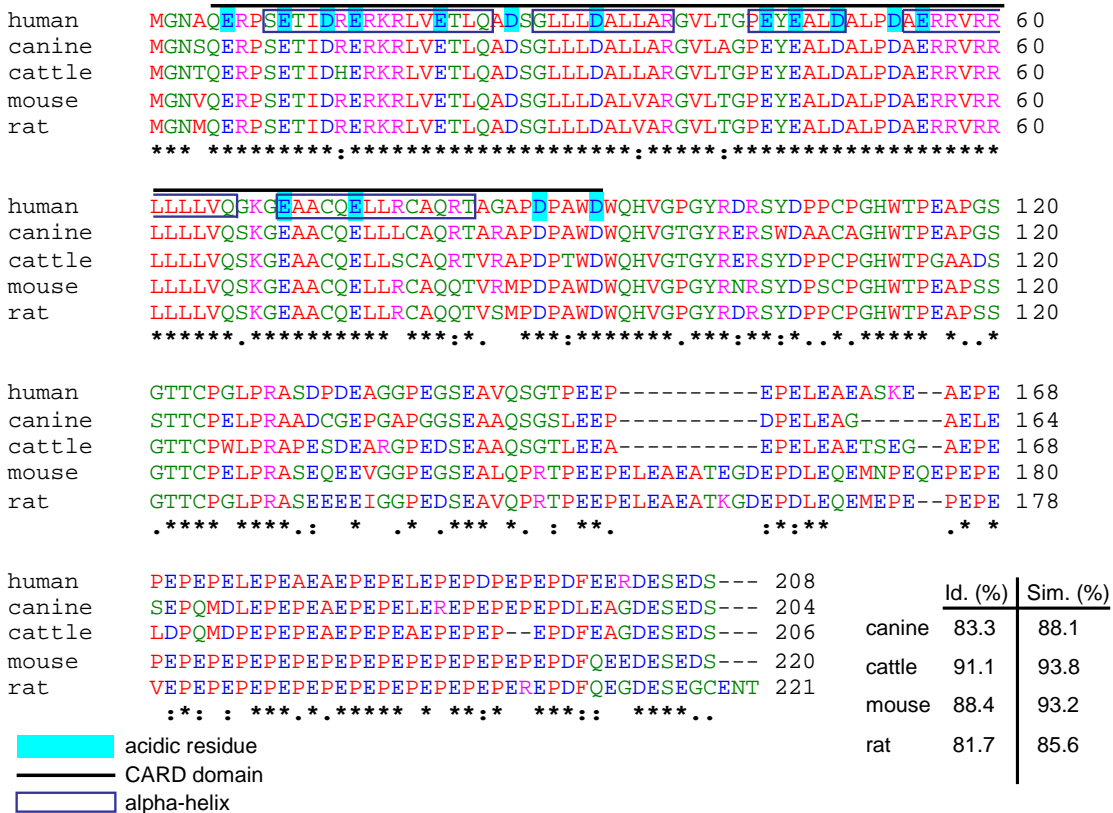


Figure 3. *NOL3* amino acid sequence is highly conserved across species.

genomes, including the giant panda (*Ailuropoda melanoleuca*), marmoset (*Callithrix jacchus*), and many other vertebrate mammals. For example, chimpanzee *NOL3* is 100% identical to human *NOL3*. We concluded that the *NOL3* gene is highly conserved but is restricted to higher vertebrates. The high degree of conservation suggests positive selection for *NOL3* function ever since its emergence in higher vertebrates. This is further supported by the observation that databases cataloguing variants from tens of thousands of human genomes contain only a handful of non-synonymous SNPs in *NOL3* coding sequence—presumably, *NOL3* mutations are likely to be deleterious to the organism and have been selected against.

We next attempted to identify *NOL3* homologs in the human proteome. Homology searching suggested three potential homologs (*testis anion transporter 1 isoform a*, *SLC family 26 member 8*, and *anion transporter/exchange-8*), but these genes were only modestly homologous to the *NOL3* P/E domain. There was no evident homology to the CARD. We were flummoxed that this approach failed to point to other proteins with CARDS. Six caspases contain CARDS, and CARDS are found in at least 22 other human genes (Reed et al. 2004). We performed peptide sequence alignment amongst human genes containing CARDS and were startled to observe strikingly low conservation (**Figure 4**). While *NOL3* may be more highly related to CARD genes than to randomly selected genes, the conservation is underwhelming, except for between *NOL3* and *CARD6* (**Figure 4**). Given the dissimilarity in amino acid sequence, we asked whether the *NOL3* CARD has the 6 or 7 antiparallel alpha-helices characteristic of the CARD motif (Reed et al. 2004). We used three separate secondary structure prediction programs, but none predicted more than 5 alpha-helices within the CARD, and one predicted

4 (Figure 5). Repeating the analysis with the *E21Q* mutation returned similar results (data not shown).

```

CASP-2      -----MHPDHQETLKKNRVVLAKQLLSELEHLLLEK--DIIT-LEMRELIQAK 77
CASP-9      -----MDEADRRLLRRCRLRLVEELQVDQLWDALLSR--ELFR-PHMIEDIQRA 46
CARD16      -----EKRRKLIHSMGEG---TINGLLDELLQT--RVLN-QEEMEKVKRE 46
CARD17      -----EKRRKQFIRSVGEG---TINGLLGELLELET--RVLS-QEIEIIVKCE 46
CARD18      -----KKRRIFIHSGVAG---TINALDCLLED--EVIS-QEDMNKVRDE 46
CASP-1      -----AKRRKQFINSVIG---TINGLLDELEK--RVLN-QEEMDKIKLA 46
CASP-4      -----KHPDKPLKVLEQLGKE---VLTEYLEKLVQS--NVLK-LKEEDKQKFN 46
CASP-5      NTDQKSTSVKKNHKKKTKMLEYLGKD---VLHG VFNYLAKH--DVLN-LKEEEKKKYY 104
CASP-12     -----PSNGVLVHMVKLLIKT---FLDGI FDDLMEN--NVLN-TDEIHLIGKC 47
NOD1        ----SESHPHIQLLKS NRLELVTHIRN----TQCLVDNLLKN--DYFS-AEDAEIVCAC 61
NOD2        ----GCEMCSEQEAFQAQRSQLVELLVSGSLEGFESVLDWLLSW--EVLS-WEDYEGFHLL 77
CARD11      -----EEDALWENVECNRHMSRYINPAKLTPYLRQC--KVIDEQDEDEVLNAP 64
CARD10      -----EEDALWERIEGVRHRLARALNPAKLTPYLRQC--RVIDEQDEEEVLSTY 69
ASC         -----
PYCARD      -----
CARD8       SHYCSVLFLSVNYLGGTFPGDICSEENQ-----IVSSYA--SKVCFEIEEDYKNRQ 55
NALP1      ASHVAQANLKLDDVSKIFPIAEIAEESSEPEVVPVELLCVPSPA--SQGDHLTKPLGTDDD 1078
BIRC2      TEEARFLTYHMWPLTFLSPSELARAGFYIIGPDRVACFACGG--KLSNWEPKDDAMSEH 240
BIRC3      NENARLLTFQTWPLTFLSPDLAKAGFYIIGPDRVACFACGG--KLSNWEPKDNAMSEH 225
CRADD      -----
RAIDD-2    -----
CARD14     -----ALDEETLWEMMESHRHRIVRCICPSRLTPYLRQA--KVLCLDEEEVLHSP 61
NLRC3      -----QGHGTGSPAEQVKALMDLLAGKSGSQSQAP--QALDRTPDAPLGPSCS 58
DLG5       GFDMAEGVNEPCFPDGCIFVTKVDKGSIADGRLRVNDWLLRI--NDVDL INKDKKQAIK 693
BCL10     -----MEPTAPSLTEEDL TEVKKDALENLRVYLCEK--IIAERHFHDLRAKKI 46
NLRC4      NREEVNIICCEKVEQDAARGI IHMLKKGSESCNLFKSLKEWNYPLFQDLNGQSLFHQT 93
APAF-1     AGCGKSVLAAEAVRDHSLLEGCFPGGVHWSVGKQDKSGLLMKLNLC'FRLDQDESFSQR 215
NOL3       -----MGNAQERPSETIDRERKRLVTLQADSGLLLDALLARGVLTGPYEALD 49
CARD6      -----MATESTPSEIIERERKLLLEILQHDPDSILD'TLTSRRLISEEYETLE 48
DDX58     -----MTTEQRRSLQAFQDYIRKTL'DPTYILSYMAPWFREEEVYIQAEKNKNG 49
IFIH1      ----VLDYLTFLPAEVKEQ'QRTVATSGNMQAVELLLSTLEKGVWHLGWTREFVEALRRT 86
MAVS       -----MPFAEDKTYKYICRNFSNFCNVDVVEILPYLPCLTARDQDRLRATC 46
QRICH1     -----MNNSLENTISFEIYIRVKARSVPQHRMKEFLDSLASKGPEALQEFQQTATT 51
RIPK2     -----MNGEAICSA'LPTIPYHKLADLRVLSRGASGTVSSARHADWRVQVAVKHLHIHT 53

```

Figure 4. Alignment of amino acid sequences of human genes containing CARDs. NOL3 sequence is highlighted in red. The E21 residue is highlighted in green.

Secondary structure is less relevant than tertiary structure because CARDs bind via surface electrostatic interactions. The *E21Q* mutation changes an acidic glutamate to a neutral glutamine residue, so a priori it seemed likely that the mutation alters the electrostatic surface potential of NOL3. The 3-dimensional protein structure of NOL3 has not been determined. In the absence of a known structure, the best way to approximate the structural effects of a mutation is via *in silico* homology modelling. This

splicing and cause disease (Burrows et al. 1998). We sequenced all FCM patients and putative FCM patients (see Chapter III), but they were all WT at these putative branch sites.

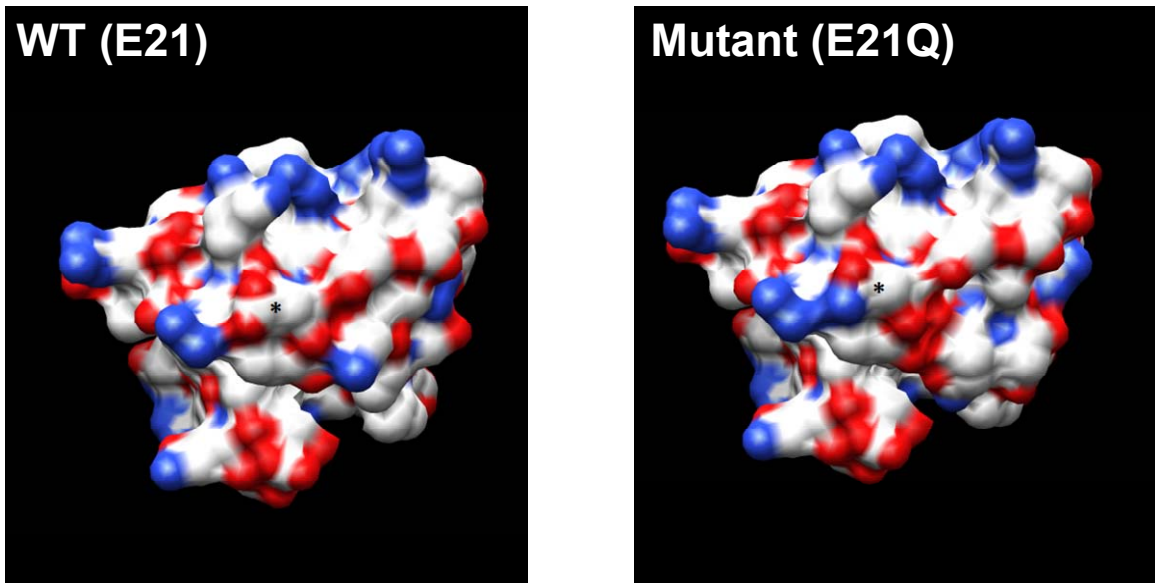


Figure 6. In silico homology modelling of WT and E21Q NOL3 protein structure predicts that E21Q alters the electrostatic surface potential of NOL3.

WT denotes wild-type; asterisk denotes amino acid 21; red denotes negative charge; blue denotes positive charge. The NOL3 CARD sequence was modelled based on homology to the structure of the CARD domain of Nod1. Structures were visualized with UCSF Chimera software.

***NOL3* Expression**

As noted above, the literature makes clear that *NOL3* is expressed in the brain (Koseki et al. 1998, Engidawork et al. 2001, Gulesserian et al. 2001, Shelke & Leeuwenburgh 2003, Abmayr et al. 2004). However, nothing is known about which particular brain regions or cell types express *NOL3*. This knowledge can be helpful in understanding pathophysiology (e.g., Lee et al. 2004). We examined expression in both mice and humans. For mice, we first utilized data that had been generated from high-through-

put projects. The Allen Brain Atlas data (Lein et al. 2007), generated by in situ hybridization, suggested diffuse moderate expression (**Figure 7**). *Nol3* was expressed at higher levels in the olfactory bulb, hippocampus, and hypothalamus (**Figure 7**). Our immunohistochemistry of *Nol3* protein in WT mouse brain agreed with these results (data not shown; see **Discussion**).

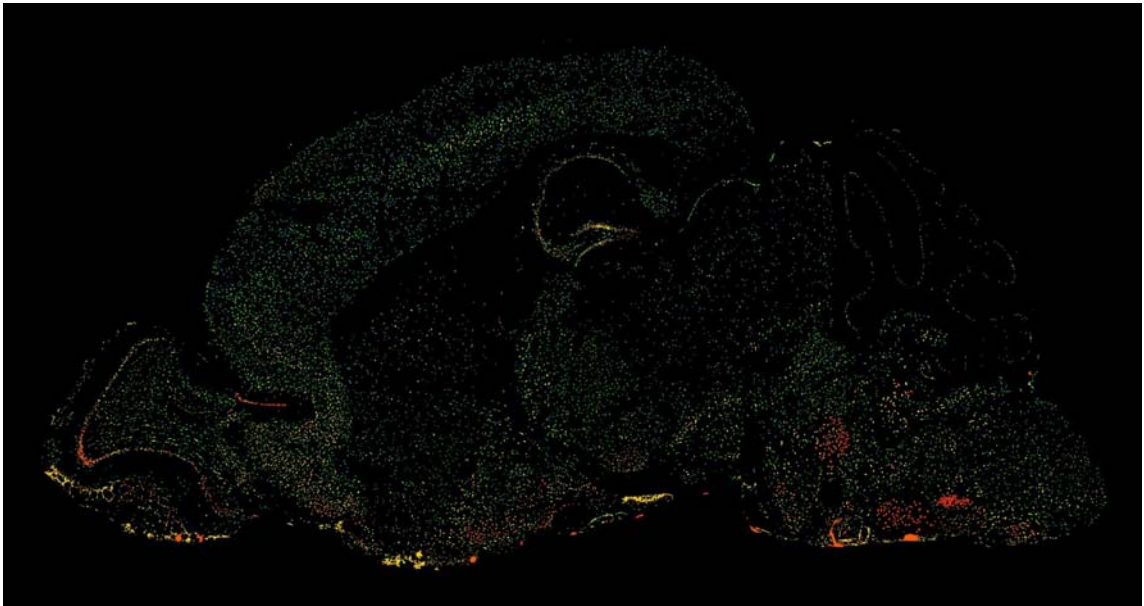


Figure 7. Expression of *Nol3* RNA in the murine brain.

Image generated by the murine Allen Brain Atlas (Lein et al. 2007). Red, yellow, and green denote high, intermediate, and low gene expression, respectively.

What about CNS cell type? Sugino et al. (2006) developed an elegant approach of labelling different neuronal populations with combinations of fluorescent proteins, enabling isolation and transcriptome profiling of each neuronal type. Their data did not indicate differential expression of *Nol3* by brain region, nor was *Nol3* enriched in glutamatergic or GABAergic neurons. However, their approach was restricted to neurons. Glia make up the vast majority of cells in the CNS, and it is becoming clear that they

serve many important roles (Molofsky et al. 2012). Cahoy et al. (2008) profiled expression in neurons, astrocytes, oligodendrocyte progenitor cells (OPCs), and oligodendrocytes. Again, *Nol3* expression was diffuse and relatively modest, albeit detectable. *Nol3* was ~3-fold enriched in oligodendrocytes and ~3-fold enriched in neurons, relative to astrocytes. In a separate experiment, we performed reverse transcriptase PCR of RNA from cultured oligodendrocytes or astrocytes, and observed *Nol3* enrichment in oligodendrocytes (**Figure 8**). This finding is preliminary because the RNA came from cultures generated with different WT mice, and the experiment was only performed once.

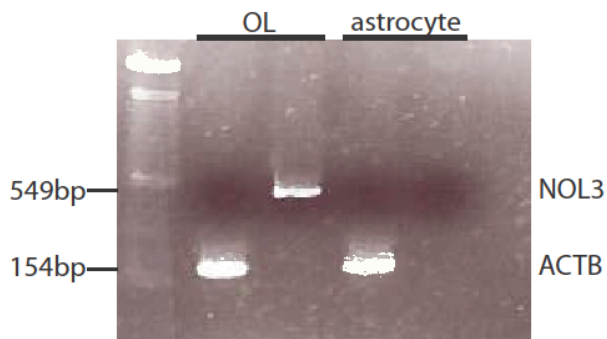


Figure 8. *Nol3* may be more highly expressed in oligodendrocytes than astrocytes. Reverse transcriptase PCR was performed on RNA from WT mouse primary cultured oligodendrocytes or astrocytes. We never attempted to repeat this admittedly crude experiment, so it is not definitive. ACTB denotes *beta-actin* (loading control); OL denotes oligodendrocyte.

Heiman et al. (2008) developed an ingenious method for transcriptional profiling in which various mouse lines each carry a different transgenic driver that promotes expression of a tagged ribosome. The tagged ribosome is then affinity purified and the associated RNAs are identified by microarray. For *Nol3*, they found increased expression in cholinergic neurons of the forebrain and basal ganglia, and in motoneurons of the brain

stem (**Figure 9**). Their data did not concord with Cahoy et al. or **Figure 8**, as Heiman et al. detected robust expression in cerebellar and cortical astrocytes (**Figure 9**).

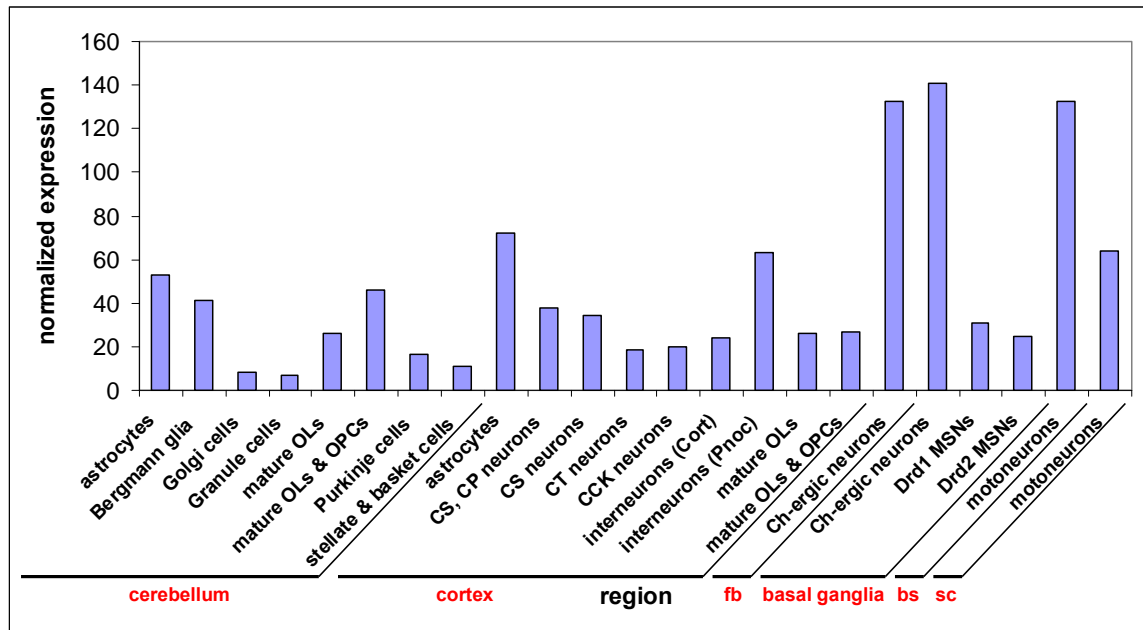


Figure 9. Expression of *Nol3* in various murine brain cell types. These data were generated by Heiman et al. 2008.

Of course, FCM is a disease of humans, so we studied *NOL3* expression in the human brain. According to the Human Protein Atlas (Uhlen et al. 2010), *NOL3* protein levels are high in cerebral cortical neurons and Purkinje cells, and moderate in hippocampal neurons, cortical and hippocampal glia, and cells in the granular and molecular layers of the cerebellum. This data is consistent with the human Allen Brain Atlas (Hawrylycz et al. 2012), which showed high expression in the locus cereleus, hypothalamus, globus pallidus, and cerebral cortical layers. The Atlas also indicated that *NOL3* expression is low during development and rises through childhood, leveling off at around age 30 (**Figure 10**). This finding could potentially explain the adult onset nature of the

disease—perhaps *NOL3* becomes more abundant and hence more functionally relevant as humans age. To move beyond high-throughput databases, we obtained a panel of human cDNA from ten regions of the brain and assayed *NOL3* expression by reverse-transcriptase PCR. This experiment is less sensitive than the techniques employed by the high-throughput projects, but more specific. It suggested that *NOL3* is expressed at roughly equal levels in various regions (**Figure 11**). In sum, in both mice and humans there is moderate expression of *NOL3* throughout the brain.

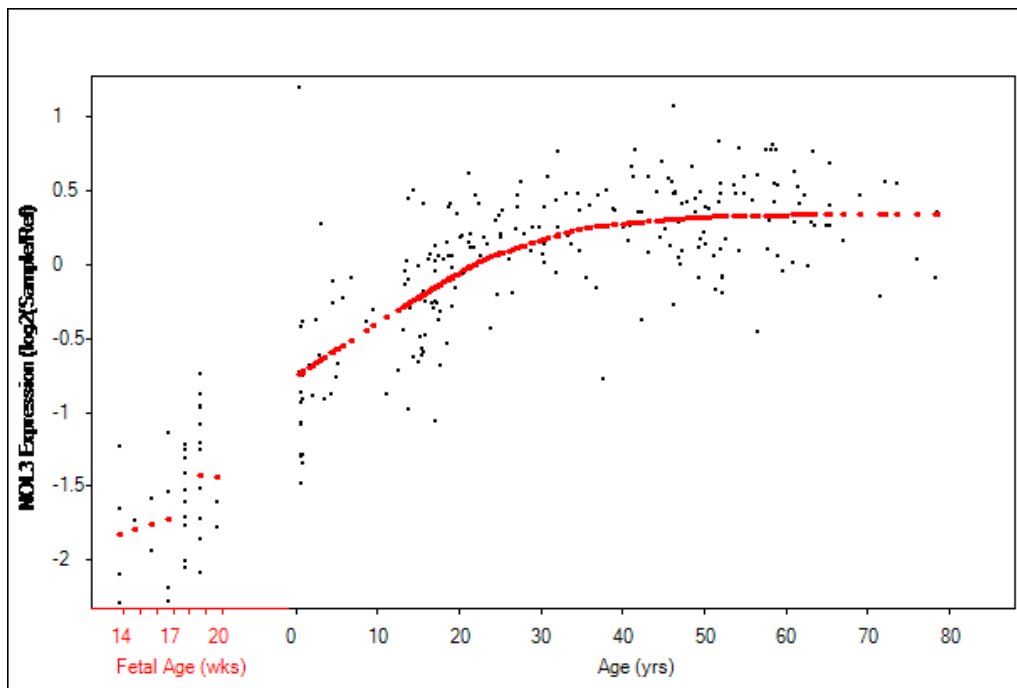


Figure 10. *NOL3* RNA expression during development in humans. These data were generated by the human Allen Brain Atlas (Hawrylycz et al. 2012).

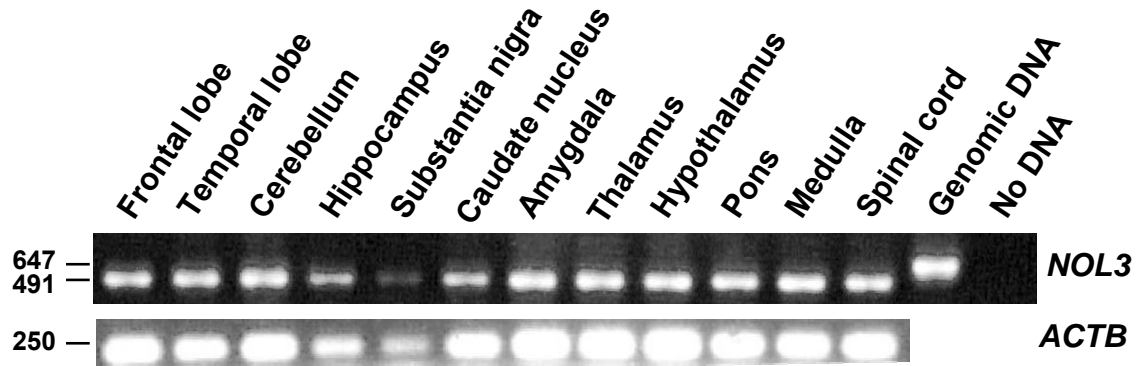


Figure 11. *NOL3* RNA is expressed at comparable levels in various human brain regions.

ACTB denotes *beta-actin* gene (loading control).

***NOL3* Subcellular Localization**

One common mechanism by which point mutations cause disease is by disrupting protein trafficking rather than protein function per se. Protein trafficking is assessed by examining subcellular localization. For WT *NOL3*, the literature conflicts. Some groups claim it has nuclear localization, which would be in keeping with the nomenclature *nucleolar protein 3* (Wang et al. 2005, Heikaus et al. 2008). Other groups state that *NOL3* is cytoplasmic (Stoss et al. 1999, Wang et al. 2005, Heikaus et al. 2008). Some evidence supports the idea that *NOL3* can be nuclear or cytoplasmic depending on the cell line, e.g., nuclear in most cancer cells and cytoplasmic in primary cultured rat neurons (Wang et al. 2005). Li et al. (2002) argued that *NOL3* ordinarily trafficks from the cytoplasm to mitochondria, and that a point mutation in the T149 residue prevented the mutant protein from entering the mitochondria. However, their images were low-resolution, scant, and not quantified.

In any case, because it is generally accepted that point mutations can disrupt trafficking, and there was some evidence, albeit controversial, that *NOL3* point mutations

disrupt trafficking, we hypothesized that the *E21Q* mutation might do likewise. We examined subcellular localization in HEK293 cells via fluorescence microscopy. Initially we transfected GFP-tagged *NOL3* (Wang et al. 2005), but we observed punctae characteristic of GFP tetramerization (data not shown), which is a well-described phenomenon that confounds any determination of subcellular localization (Rizzo et al. 2010). Though it may be ingrateful, we must note that since we used a construct kindly provided by Wang et al. (2005), their findings should be interpreted with caution.

To circumvent this problem, we expressed WT or E21Q *NOL3* with a FLAG epitope tag and performed immunohistochemistry against either the FLAG epitope or *NOL3* itself. We also co-stained with the mitochondrial dye Mitotracker, to test the claims of Li et al. (2002). Initial experiments did not reveal any appreciable differences between WT and E21Q (data not shown). The same was true in the cell line SK-N-SH, which is neuronal in origin (**Figure 12**). We confirmed this in HEK cells by high-resolution confocal microscopy. Confocal imaging demonstrated punctate staining of *NOL3* that did not overlap with mitochondria (**Figure 13**). We propose that the diffuse cytoplasmic expression observed by ordinary fluorescence microscopy in HEK and SK-N-SH (**Figure 12**) cells does not account for variation in *NOL3* localization in the z plane. When this was controlled for by confocal microscopy (which constrains fluorescence to one particular z plane at a time), the fluorescence was punctate. At this time we do not know whether these punctae reside in the cytoplasm or in non-mitochondrial, membrane-bound organelles. We abandoned this line of investigation because we are more interested in the pathophysiology of FCM – as reflected in differences between WT and

mutant NOL3 – rather than the subcellular localization per se. We concluded that the *E21Q* mutation does not affect protein trafficking. [CONTINUED, p. 166]

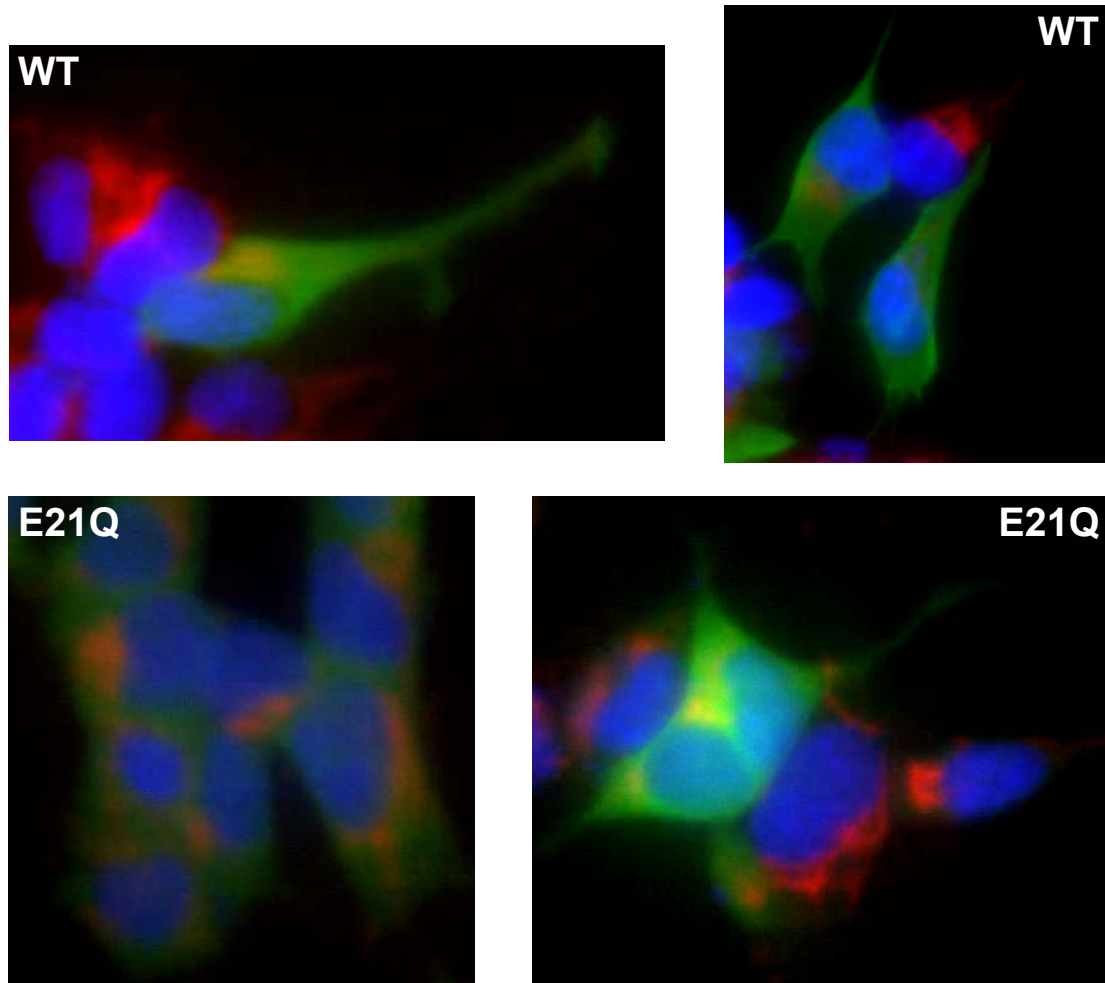


Figure 12. The *E21Q* mutation does not affect cytoplasmic expression of NOL3-FLAG in SK-N-SH cells, a cell line of neuronal origin.

Cells were transiently transfected and visualized with ordinary fluorescence microscopy. DAPI, FLAG, and Mitotracker are stained blue, green, and red, respectively. Shown are results using an antibody to FLAG; comparable results were obtained for NOL3 antibody. Comparable results were obtained in HEK cells. There was no green signal visible in cells transfected with empty vector (note that some adjacent cells not expressing the transgene have no green visible).

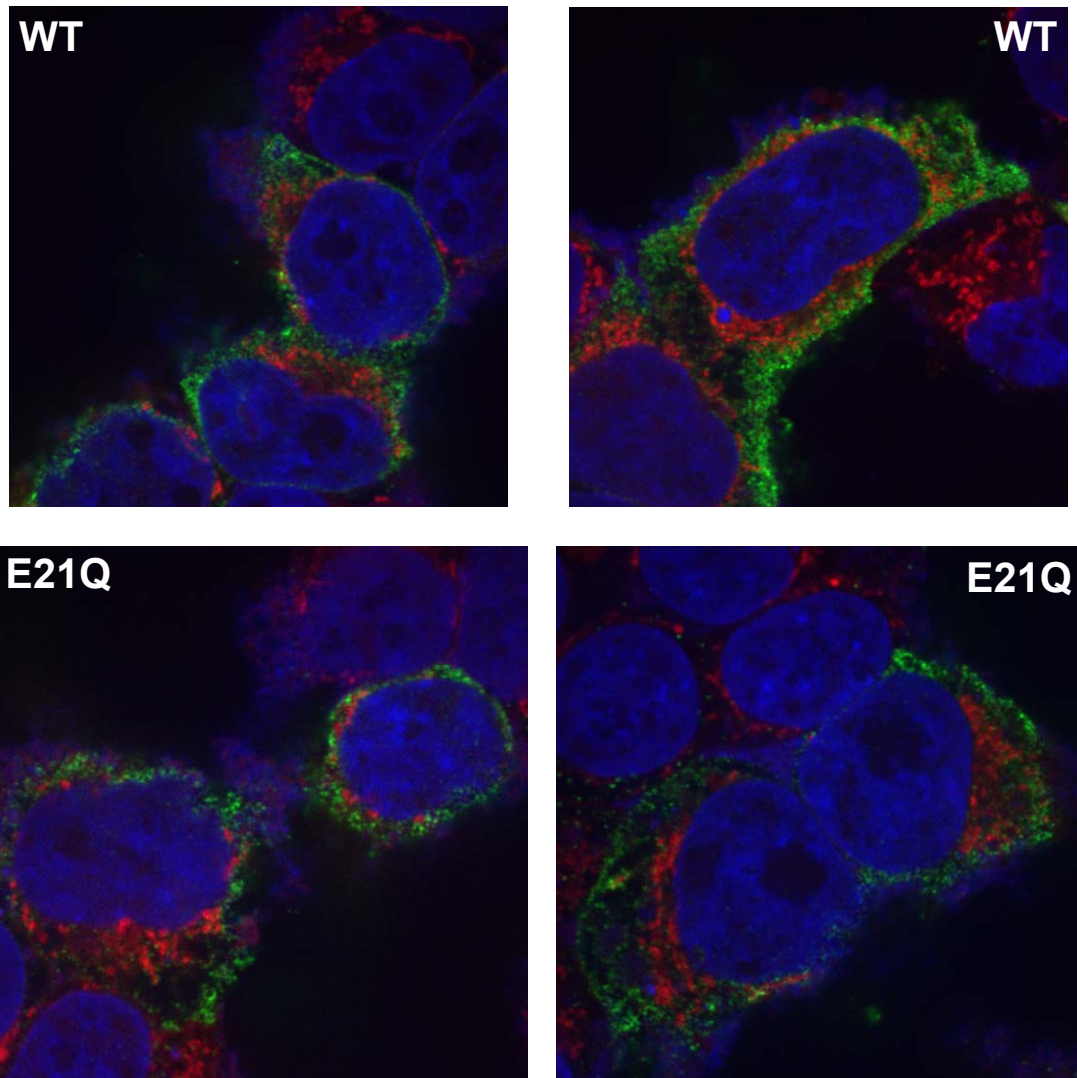


Figure 13. Neither WT nor E21Q NOL3-FLAG localize to mitochondria in HEK293 cells.

Cells were transiently transfected and visualized with confocal microscopy. DAPI, FLAG, and Mitotracker are stained blue, green, and red, respectively. Shown are results using an antibody to NOL3 protein itself; comparable results were obtained for FLAG antibody. There was no green signal visible in cells transfected with empty vector (note that some adjacent cells not expressing the transgene have no green visible).

The *E21Q* Mutation Alters Post-translational Modification of NOL3 Protein

Our next approach to investigating the functional consequences of the *E21Q* mutation was to generate HEK293 cell lines with stably-incorporated cDNA transgenes encoding FLAG-tagged *WT* or *E21Q* NOL3. To ensure that the lines were expressing

comparable amounts of transgene, we harvested protein and immunoblotted. We were immediately struck by the presence of two distinct bands in *NOL3*^{E21Q} cells but only a very faint second band in *NOL3*^{WT} cells (**Figure 14A**). By densitometry, the higher molecular weight species (henceforth referred to as the upper band) was ~10-fold enriched in *NOL3*^{E21Q} cells (**Figure 14B**). However, the total amount of NOL3 did not differ between *WT* and *E21Q* cell lines (**Figure 15**). This phenomenon held true for multiple independent HEK stable cell lines (**Figure 14A**), for transiently transfected HEK cells (data not shown), and for the COS7 cell line (data not shown). It was also observed when immunoblots were probed with either anti-FLAG (**Figure 14A**) or anti-NOL3 antibody (data not shown). The transgene encoded a cDNA, so the upper band could not have resulted from alternative splicing. It is unlikely that the upper band was a nonspecific stain because there was very little background staining, and we observed the upper band in a number of different cell lines and when staining with antibody to either the endogenous protein or the tag. Thus, we concluded that the *E21Q* mutation alters post-translational modification of NOL3 protein in cells.

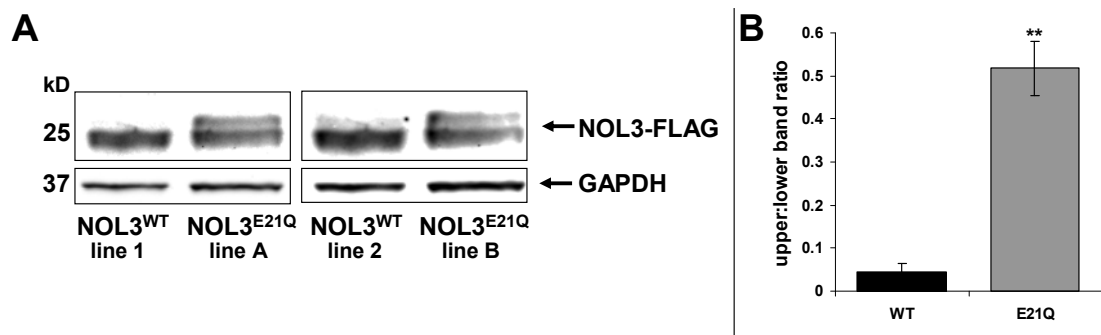


Figure 14. *NOL3*^{E21Q}-FLAG exhibits altered post-translational modification in HEK293 cells.

(A) Shown is representative experiment from four independently generated stable cell lines probed with anti-FLAG antibody. Glyceraldehyde-3-phosphate dehydrogenase (GAPDH) is loading control.

(B) Quantification of upper:lower ratio of FLAG bands in *NOL3^{WT}-FLAG* versus *NOL3^{E21Q}-FLAG* stable cell lines. Shown is the mean of 3 biological replicates; error bars denote standard deviation. **Paired 2-tailed t-test P-value was 0.0078.

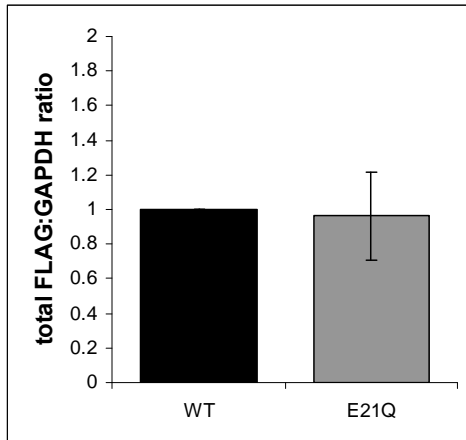


Figure 15. NOL3-FLAG protein is present at equal levels in WT and E21Q stable cell lines.

The E21Q FLAG:GAPDH ratio for each experiment was normalized relative to WT. Data represent three independent biological replicates. The paired two-tailed t-test P-value was 0.818.

Seeing as the upper, mutant-specific band was our only biochemical lead, it became a priority to identify it. The gel shift is ~2kD, NOL3 is known to be phosphorylated at 7 residues (**Figure 2**; Olsen et al. 2010), and phosphorylation at one of these residues, T149, is functionally important for NOL3 protein-protein interactions and consequent repression of apoptosis (see above; Li et al. 2002). Thus, our working hypothesis was that the upper band corresponds to a phosphorylated form of NOL3. We tested this hypothesis in multiple ways.

Presumably the two bands represent species in equilibrium, so any decrease in the upper band should commensurately enhance the lower band, and vice versa. If the upper band represents a phosphorylated form, then de-phosphorylation would be expected to

abrogate the upper band. Conversely, it is also possible that the upper band is a non-phosphorylated form and that the lower band instead corresponds to a phosphorylated form (proteins do not always run true to their molecular weight); in this case, de-phosphorylation would be expected to abrogate the lower band. We investigated these possibilities with in vitro phosphatase treatment, in which protein lysates from *WT* or *E21Q* cells were incubated with phosphatase and then immunoblotted. We experimented with different phosphatases (calf intestinal alkaline phosphatase, protein phosphatase 1, potato acid phosphatase), different amounts of each phosphatase, and various incubation times. We were cognizant that since a lysate contains the entire repertoire of phosphorylated proteins from a cell, the phosphatase enzyme may be so flooded with substrate as to consume its activity. Therefore, it is very unlikely that even large quantities of phosphatase would cause detectable changes in phospho-NOL3. To minimize interactions between phosphatase and nonspecific phosphorylated substrates, we repeated in vitro phosphatase experiments with immunoprecipitated NOL3-FLAG. Immunoprecipitation did not alter the banding patterns of *WT* or *E21Q* samples (**Figure 14A**). In all of these experiments, with lysate or immunoprecipitate, phosphatase treatment did not affect the banding pattern (**Figure 16**).

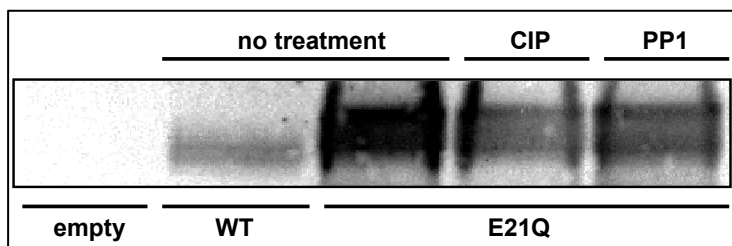


Figure 16. In vitro phosphatase treatment does not remove mutant-enriched upper band.

The same results were observed for a range of phosphatase doses and incubation times. CIP denotes calf intestinal alkaline phosphatase; PP1 denotes protein phosphatase 1.

However, it is possible that the *in vitro* phosphatase treatment was simply not sufficient to de-phosphorylate phospho-NOL3. For example, perhaps the enzyme was inactive, or phospho-NOL3 is refractory to de-phosphorylation except when catalyzed by one specific phosphatase. These possibilities are exceedingly unlikely, but, to our knowledge, cannot be disproved. In fact, it is impossible to dream up a positive control. When the experiment is performed on lysate, there is such a plethora of phosphorylated proteins present that no single phospho-protein can serve as positive control, since the probability is that the phosphatase will be overwhelmed with substrate before the positive control protein is appreciably de-phosphorylated. The melange of nonspecific phosphorylated proteins is removed by immunoprecipitation, but then there is no positive control protein that is co-immunoprecipitated. Conceivably, one could use as a positive control a phospho-protein that was separately immunoprecipitated, but that demolishes internal validity. Thus, despite using three different phosphatases, and many different phosphatase doses, and a range of incubation times, we cannot say for certain that the upper band is refractory to *in vitro* de-phosphorylation.

Next, we approached the hypothesis from a different angle: *in vivo* treatment with a phosphatase inhibitor. We reasoned that treatment with phosphatase inhibitor should drive the equilibrium towards the phosphorylated form. This in turn should be readily discernible by abrogation of the lower band (if the upper band represents phospho-NOL3), or abrogation of the upper band (if the lower band represents phospho-NOL3). Ellis et al. (2001) provided proof of principle. We utilized two phosphatase inhibitors, orthovanadate and fluoride, and incubated *WT* or *E21Q* cells for various time points (see **Methods**), then harvested protein and immunoblotted. The treatment did not alter the

banding pattern (data not shown). We considered extending this approach by treating cells with kinase inhibitors, or transfecting with phosphatase or kinase genes, but opted to not do so.

Instead, we created mutants of five of the seven published NOL3 phosphorylation sites (**Figure 2**; Olsen et al. 2010, Li et al. 2002). We individually mutated these residues to alanines, which are sterically neutral and cannot be phosphorylated. Four of the five alanine mutations had no effect, but one, *T114A*, abrogated the upper band (**Figure 17**). While this mutation did dramatically decrease the amount of upper band, it did not appear to completely abolish it (**Figure 17**). This suggested that T114 is critical to generation of the upper band but phospho-T114 does not constitute the upper band per se.

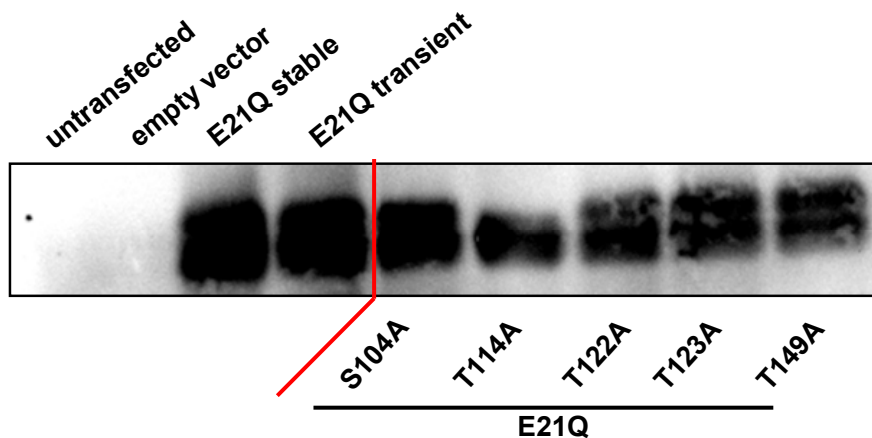


Figure 17. *T114A* mutation abrogates formation of upper band in mutant (*E21Q*) background.

The experiment was repeated at least five times. A representative image is shown.

To ensure that the upper band did not correspond to phospho-T114 – and if not, to identify the upper band once and for all – we pursued semi-quantitative mass spectrometry. We immunoprecipitated NOL3-FLAG from *WT* and *E21Q* protein lysates, then stained with Coomassie dye and excised the upper and lower bands (**Figure 18**). Purifi-

cation was robust. These samples were extensively analyzed by generic tandem mass spectrometry (MS/MS) as well as phospho-enrichment MS/MS. We observed dramatically increased T114 phosphorylation in both the *E21Q* upper band and the *E21Q* lower band, relative to the WT lower band (**Figure 19**). The measurement of increased phospho-T114 in the mutant lower band, along with low but detectable levels of phospho-T114 in the WT lower band, was not consistent with the hypothesis that the upper band corresponds to phospho-T114. To further rule out this possibility, we mutated *T114* to an aspartate, a residue that can mimic constitutive phosphorylation. In theory, if phospho-T114 is the upper band, then the *T114D* mutation should eliminate the equilibrium between non-phospho-NOL3 and phospho-NOL3—instead, all species should resemble phospho-NOL3 on Western blot. However, the banding patterns in *WT;T114D* and *E21Q;T114D* double mutants were unchanged from that of *WT* and *E21Q*, respectively (data not shown). Thus, we concluded that the upper band does not correspond to phospho-T114 per se. Rather, we propose that phosphorylation at T114 regulates the formation of the upper band, either by promoting the transformation from the lower to the upper band, or by inhibiting the transformation from the upper to the lower band.

One interesting question is whether T114 may be the “gatekeeper residue” for a kinase that phosphorylates NOL3 at multiple residues. Alternatively, one could posit that the *E21Q* mutation permits indiscriminate phosphorylation of NOL3. However, repeated MS/MS experiments, including phospho-enrichment, did not reveal any residues other than T114 that were phosphorylated (data not shown). [CONTINUED, p. 174]

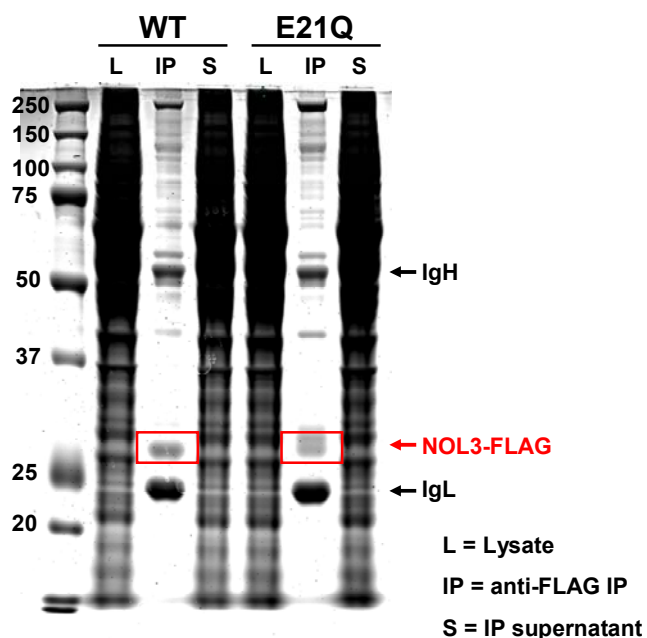


Figure 18. Coomassie staining demonstrates robust purification of NOL3-FLAG prior to mass spectrometry analysis.

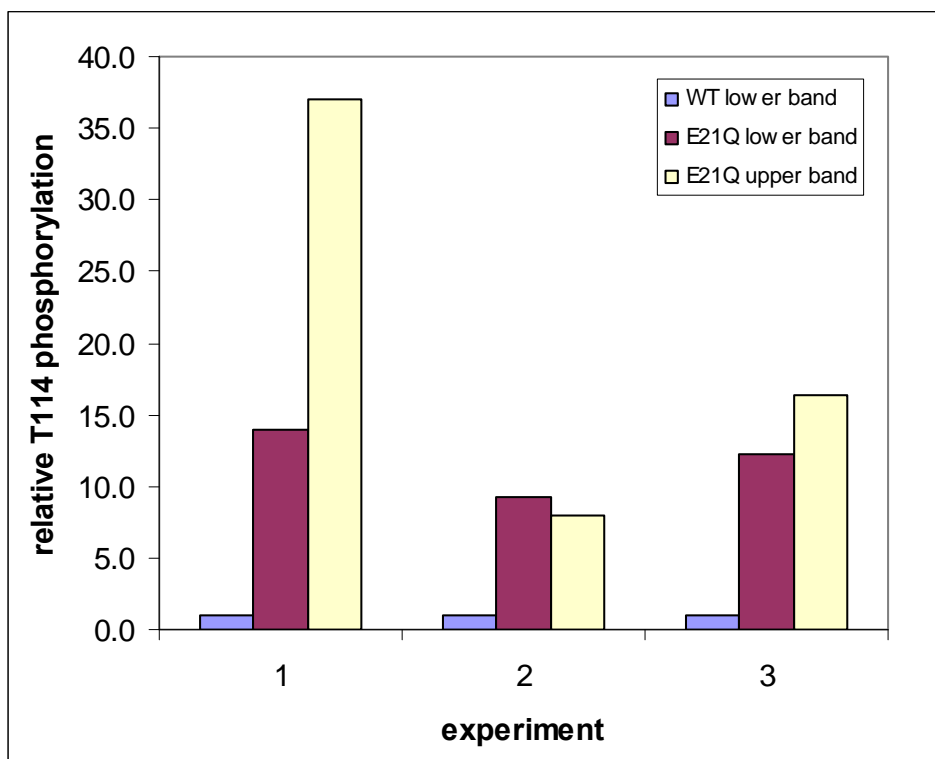


Figure 19. T114 is hyper-phosphorylated in both mutant upper and lower bands, relative to WT.

Having ruled out phosphorylation, we tested alternative identities for the mutant-enriched upper band. A reasonable guess was a ubiquitylated species because it was previously published that apoptotic stimuli trigger NOL3 ubiquitylation (Nam et al. 2007). Ubiquitylation occurs on lysine residues, which also happen to be the cleavage sites for trypsin. Ubiquitylation interrupts trypsin digestion and is thus easily detected by MS/MS. Indeed, semi-quantitative MS/MS suggested that peptides corresponding to tryptic cleavage at lysine residues were reduced in the mutant lower and upper bands. These peptides were enriched ~10-fold in the mutant upper band relative to the mutant lower band, and enriched ~50-fold in the mutant upper band relative to the WT lower band (data not shown). Furthermore, there was ~10-fold more ubiquitin per molecule of NOL3 in the mutant upper band versus the mutant lower band (data not shown). These measurements could be consistent with the upper band corresponding to a ubiquitylated NOL3 species, since there will inevitably be some contamination of the upper band species in the lower band samples. However, this hypothesis was contradicted by our repeated attempts at immunoblotting with anti-ubiquitin antibodies (see **Methods**), which did not stain either the upper or the lower band (data not shown). In parallel, we expressed tagged ubiquitin motifs to facilitate ubiquitin immunoblotting, but still did not detect any staining that colocalized with either NOL3 band (data not shown). Moreover, we mutated the three lysine residues on NOL3 to alanines, but there was no effect on the upper band (data not shown). If all lysines have been mutated to alanines, ubiquitylation cannot take place, so the persistence of the upper band indicated that it is not a ubiquitylated NOL3 species.

We entertained a number of other hypotheses regarding the upper band's identity. N-terminal cleavage is common in apoptotic signaling pathways, as is N-terminal acetylation (Yi et al. 2011). However, when we cloned a construct with distinct epitope tags at the N-terminus and the C-terminus, the banding pattern was identical upon immunoblotting with an antibody to either the N-terminal tag or C-terminal tag (data not shown). A species with N-terminal acetylation was detected by MS/MS, but the acetylated peptide was equally abundant in *WT* and *E21Q* samples (data not shown). Another species with N-terminal myristoylation was identified but again did not differ between *WT* and *E21Q* (data not shown). We also considered palmitoylation at residue C79 because MS/MS never detected a peptide containing this residue (data not shown). However, treatment with the reducing agent beta-mercaptoethanol, which should remove palmitoylation on cysteine residues (Valdez-Taubas & Pelham 2005), did not affect the upper band (data not shown). Furthermore, mutating C79 to alanine in a mutant background did not abolish the upper band, nor did it enhance the upper band in a *WT* background (data not shown). Another hypothesis was suggested to us by way of a very interesting paper in which a protein of the Bcl apoptotic family exhibited a ~2kD gel shift upon apoptotic stimulation, a gel shift that conferred the function of repressing apoptosis (Deverman et al. 2002). Deverman et al. ascribed these gel shifts to deamidation of two asparagine residues. Asparagine residues are most likely to be deamidated when followed by a glycine residue in an unstructured portion of the protein. In NOL3 (a 206 aa peptide) there is only a single asparagine residue, and it is not followed by a glycine. This alone would not be conclusive; however, the absence of a deamidated species by

MS/MS, and the presence of peptide fragments containing normal asparagine residues in the upper band, did rule out deamidation (data not shown).

There were yet more possibilities. Perhaps the mutation causes a failure to terminate translation, a phenomenon that is occasionally observed in expressed proteins. However, when we searched the MS/MS data for peptides containing the stretch of residues after the FLAG tag that would be translated if termination did not occur, none had been detected (data not shown). A second idea was that the upper band might correspond to a version of NOL3 that was not being fully denatured. We tested this hypothesis by using more concentrated SDS sample buffer and boiling for longer periods of times to ensure denaturation. We also tried adding TCEP, a reducing agent that breaks disulfide bonds. Neither treatment had any effect (data not shown). Our final approach was to digest with proteases other than trypsin. Again, there were no unassigned peptides with molecular weight of ~2kD different than the corresponding WT species (data not shown).

All of our attempts to identify the upper band by MS/MS or to alter the upper band with biochemical treatments were ineffectual. Out of ideas, we discontinued this line of investigation. We concluded that the *E21Q* mutation alters post-translational modification of NOL3, and that this process is regulated by the T114 residue. However, the identity of the modified species remains unknown, and in fact, we do not know for sure that the upper band represents a bona fide biochemical lead into FCM pathophysiology (see **Discussion**).

Apoptosis and Putative Pro-apoptotic Binding Partners

NOL3 binds five pro-apoptotic binding partners: Caspase-2, Caspase-8, Fas, FADD, and Bax (see **Introduction**). These interactions are necessary for *NOL3* to repress apoptosis. The *E21Q* mutation resides in the protein-protein interaction motif that is crucial for binding. Previously, point mutations in *NOL3* have been shown to abolish NOL3 binding to one of its pro-apoptotic binding partners (Li et al. 2002), and hence diminish *NOL3* inhibition of apoptosis (Li et al. 2002, Gustaffson et al. 2004). Thus, we sought to assess whether the *E21Q* mutation alters the known binding interactions, and/or whether it affects *NOL3* apoptotic function.

We began with apoptosis. The published experiments, which demonstrated that *NOL3* blocks apoptosis, employed microscopy to measure cellular viability. Cells are incubated with an inducer of apoptosis and then stained for markers of apoptosis, such as nuclear condensation, loss of mitochondrial membrane integrity, or chromatin fragmentation. We expended considerable effort attempting to replicate these experiments. Although some of our data did suggest that *NOL3* expression represses apoptosis, the data were inconsistent (data not shown). With practice, we ascertained what we feel is a fatal flaw of these experiments: cells which have already died will detach from the plate and are lost in the washes and incubations required to assess viability via imaging. The inability to include already-dead cells confounds the analysis.

To circumvent this shortcoming, we undertook fluorescence activated cell sorting (FACS) using a nuclear stain (PI, propidium iodide) and a phosphatidylserine stain (annexin V). The double stain approach (**Figure 20**) discriminates amongst the stages of apoptosis. An early apoptotic cell is annexin V-positive (since phosphatidylserine is

swapped from the inner plasma membrane to the outer membrane during early stages of apoptosis) but PI-negative (since plasma membrane integrity is intact, the PI dye does not penetrate into the cell and hence into the nucleus). During late apoptosis, the plasma membrane loses integrity, allowing penetration of PI, so these cells are annexin V-positive, PI-positive. Finally, a completely dead cell is defined as annexin V-negative, PI-positive, corresponding to a free-floating nucleus—the plasma membrane has effectively disintegrated. This double stain approach is considered the gold standard in apoptosis research. In addition to discriminating amongst the stages of apoptosis, FACS ensures that all cells are included, even those which have already died and would otherwise be lost in sample preparation.

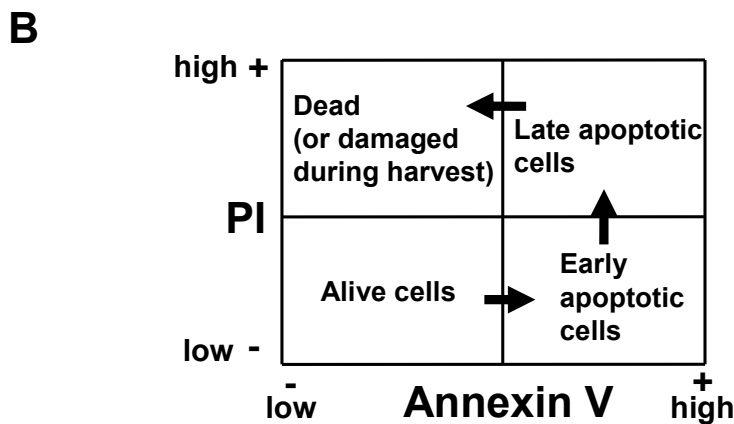
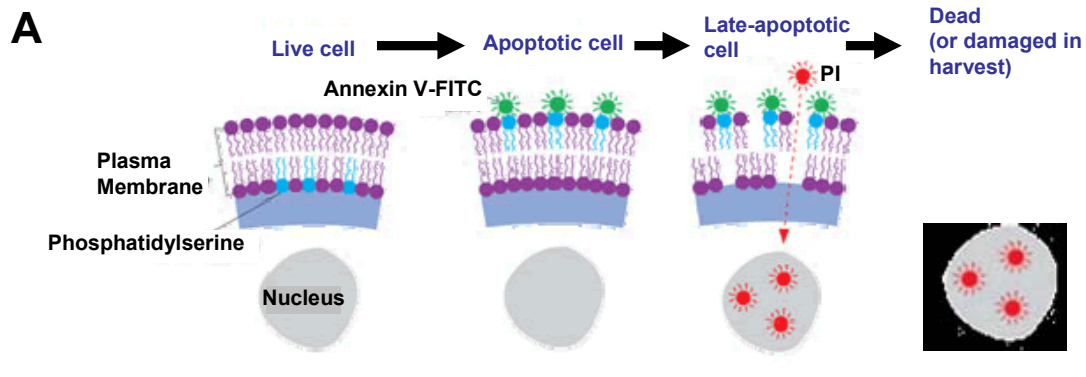


Figure 20. FACS double stain approach for apoptosis analysis.

(A) See text for explanation. Adapted from www.biomol.de/wiki/index.php?title=Annexin

n_V_Apoptosis_Detection_Kit.

(B) Schematic of cell viability as assayed by relative amounts of annexin V and PI. PI denotes propidium iodide.

These experiments revealed greater cell death at baseline (before treatment with apoptotic inducer) in cells expressing either *WT* or *E21Q NOL3* relative to vector (**Figures 21, 22**). After treatment, there were comparable levels of cell death between vector and the *NOL3* conditions (**Figures 21, 22**). Since there was increased apoptosis in *NOL3* cells at baseline, the relative increase in apoptosis upon treatment was smaller. The populations on FACS were less distinct than expected, but the placement of the FACS gates distinguished positively- or negatively-stained cells quite well, as is evident by comparing the unstained control to the PI-stained or annexin V-stained control (**Figure 21**). Moreover, there was clear progression in cell death after treatment (**Figures 21, 22**). On the basis of these data, we concluded that *NOL3* expression enhances apoptosis at baseline. This directly contradicts published findings (see **Discussion**). In any case, it is less important whether *NOL3* represses or enhances apoptosis. The more pertinent question, given our interest in FCM pathophysiology, is whether the *E21Q* mutation has any effect on this process. Upon close inspection with the double stain FACS analysis, the answer seems to be no. [CONTINUED, p. 181]

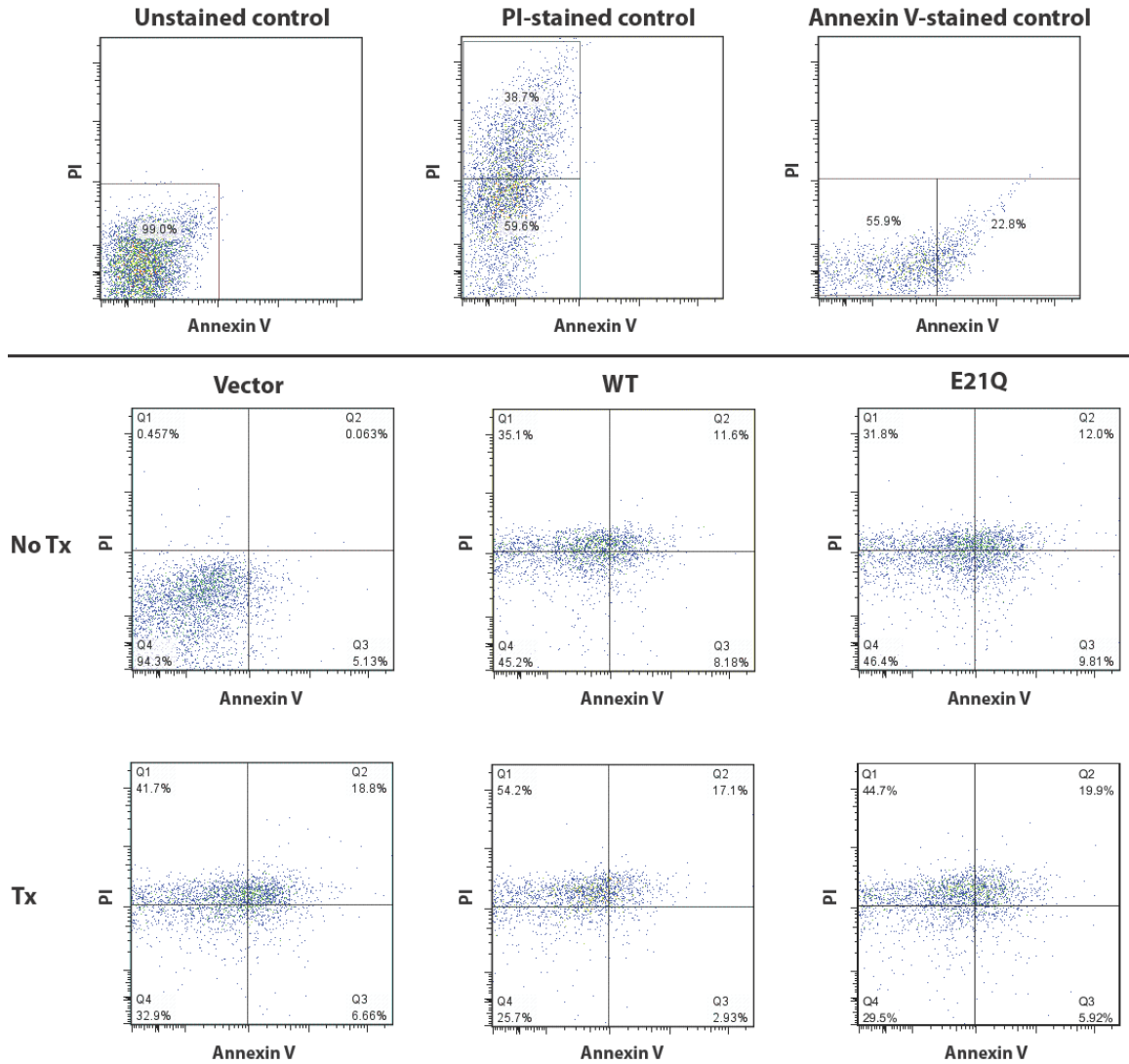


Figure 21. Expression of either *WT* or *E21Q NOL3* predisposes HEK293 cells to apoptosis at baseline.

PI denotes propidium iodide; Tx denotes treatment with staurosporine. See **Figure 20** for a schematic on interpreting these plots.

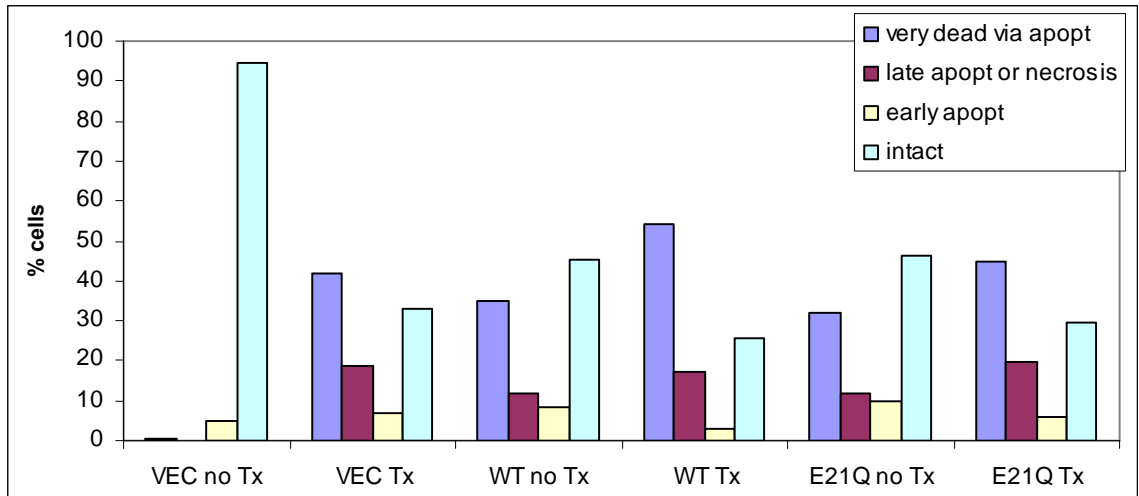


Figure 22. Quantification of FACS data confirms that *NOL3* expression predisposes to apoptosis at baseline.

Tx denotes treatment with an inducer of apoptosis; VEC denotes vector. Error bars are not shown because this data depicts a representative experiment.

What about the published claims of *NOL3* binding to pro-apoptotic proteins? Presumably, if *NOL3* expression predisposes to a higher basal rate of apoptosis, this mechanism may still be at play. Virtually all of the literature data comes from in vitro systems in which both the bait and the putative prey were highly overexpressed (e.g., driven by a cytomegalovirus [CMV] promoter). Since co-immunoprecipitations (co-IPs) are notoriously dependent upon protein overexpression and/or wash conditions, we sought to validate these interactions in more biologically relevant systems. First, we tried co-IPs with *WT* mice (*Nol3* knockout mice serving as a negative control). Unfortunately, the endogenous *NOL3* antibody worked very poorly for these IPs (data not shown). (We are currently generating a new endogenous *NOL3* antibody via the UC Davis/NIH NeuroMab project.) As a compromise, we used HEK293 cells to overexpress *NOL3* in the context of endogenous expression of putative prey proteins. We then co-IPed against the *NOL3* FLAG tag and probed for the prey using endogenous antibodies. We exper-

imented with many different antibodies, antibody concentrations, and wash conditions (see **Methods**). For two putative prey proteins, Caspase-2 and Bax, we were able to demonstrate via Western blot the lack of interaction between NOL3 and prey (**Figure 23**). Given these results, it is reasonable to conclude that the published protein-protein interactions either represent nonspecific phenomena implicit in double overexpression in vitro systems, or that these phenomena are not applicable to our more biologically relevant single overexpression in vitro system, and by extension, are unlikely to be biologically relevant in vivo.

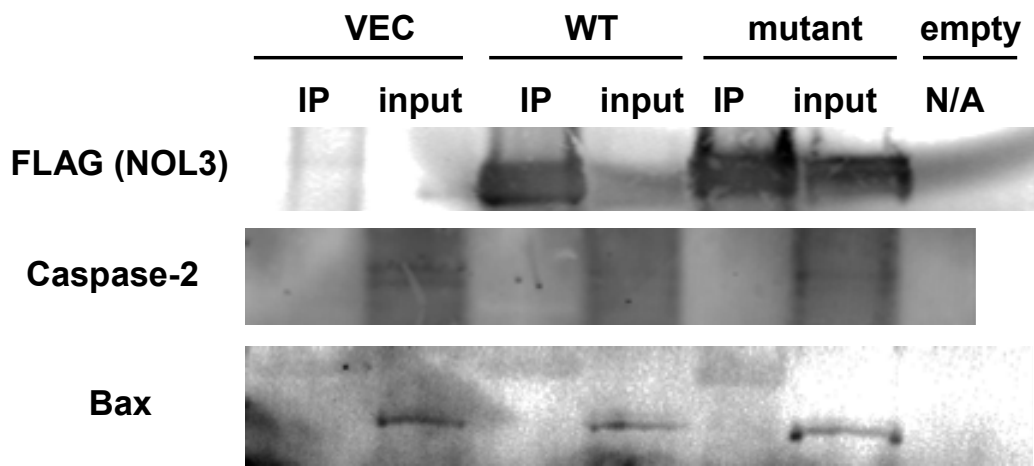


Figure 23. Putative pro-apoptotic binding partners do not interact with NOL3.

Shown are Western blots performed with antibodies to endogenous Caspase-2 or Bax. Enrichment of NOL3 via immunoprecipitation (IP) serves as a positive control. We tried many different antibodies and wash conditions of varying stringency, to no avail. All other putative pro-apoptotic binding partners could never be satisfactorily stained with endogenous Ab. VEC denotes vector.

A high-throughput protein-protein “interactome” project had previously used co-IP and MS/MS to identify two putative binding partners of NOL3, PACSIN3 and PNKP (Ewing et al. 2007). The study stated that these were high-confidence interactions. This hypothesis was attractive because PACSIN3 is involved in synaptic vesicle membrane

trafficking and endocytosis, and it also binds TRPV4 (Cuajungco et al. 2006), a calcium channel that tunes neuronal excitability in response to sensory stimuli (D'hoedt et al. 2008). *TRPV4* mutations in humans can cause neuropathy (Auer-Grumbach et al. 2010, Deng et al. 2010, Landoure et al. 2010), spinal muscular atrophy (Auer-Grumbach et al. 2010), and skeletal dysplasias (Rock et al. 2008, Krakow et al. 2009). The other putative binding partner, PNKP, is a DNA repair enzyme. *PNKP* is mutated in a microcephaly syndrome that includes severe seizures (Shen et al. 2010). Alas, repeated attempts to validate the interactions between NOL3 and PNKP or PACSIN3 through co-IPs were negative (data not shown).

Screen for Novel Binding Partners

Though we had ruled out the published binding partners, we nevertheless felt that since the *E21Q* mutation resides in the CARD domain, a known protein-protein interaction motif, it was still reasonable to hypothesize that FCM pathophysiology results from altered protein binding. For example, the *E21Q* mutation could cause loss-of-function in NOL3^{WT} binding interactions. Alternatively, the mutation could cause gain-of-function in NOL3^{E21Q}-specific binding partners. To identify novel NOL3^{WT} and NOL3^{E21Q} binding partners, we performed co-IP followed by MS/MS.

We aged *WT* and *Nol3* knockout littermate mice to one year, isolated brain, and performed co-IPs. Unfortunately, as mentioned above, the endogenous antibody was not effective, and we were unable to obtain sufficient protein for the screen (data not shown). Instead, we used HEK293 cells expressing either vehicle (vector), NOL3^{WT}-FLAG, or NOL3^{E21Q}-FLAG, and co-IPed against the FLAG tag. The bound proteins were eluted,

fluorescently labeled, run on a 2D SDS-PAGE gel, and identified by MS/MS (**Figure 24**). We focused on those proteins that were enriched relative to vehicle in the *WT* sample, the *E21Q* sample, or both. In both *NOL3* conditions, the positive control, *NOL3*, was very highly enriched. (None of the published interactors, discussed above, were identified by this method, which is further evidence against their biological relevance.) After removing hits that were likely nonspecific (actin, HSP70, Ig light chain), there were three candidates (**Table 2**).

Vehicle
WT

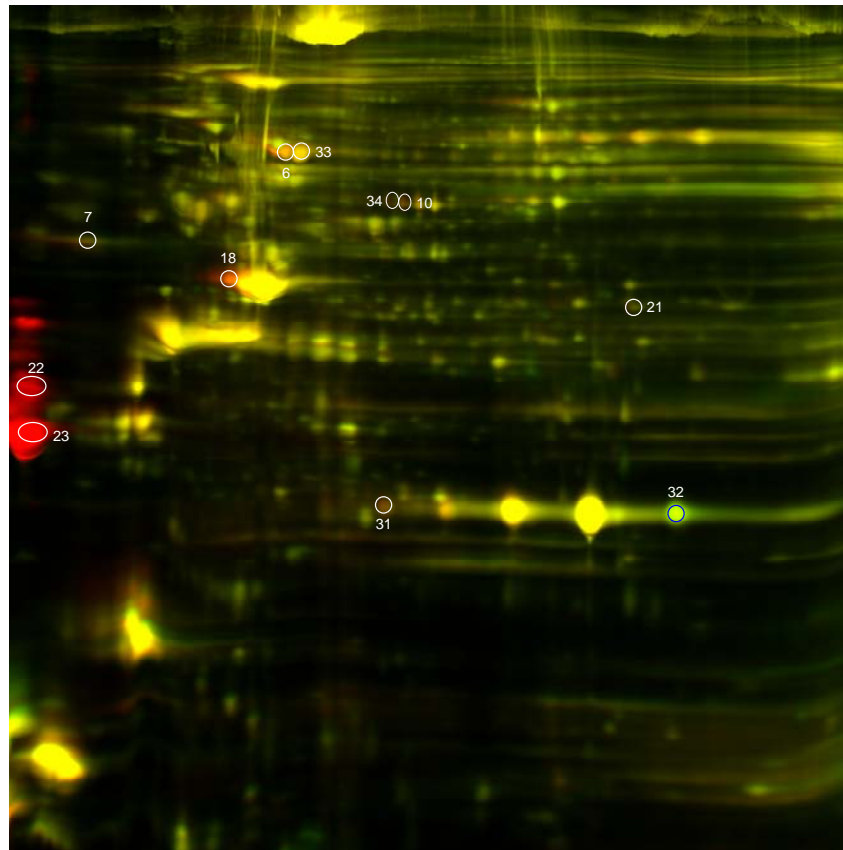


Figure 24. Two-dimensional gel electrophoresis of co-immunoprecipitates obtained from Vehicle or *WT NOL3* HEK293 cells.

The *E21Q* gel is omitted because no *NOL3*^{E21Q}-specific binding partners were identified. Spot numbers correspond to **Table 2**.

Table 2. Novel NOL3 binding partners identified by co-immunoprecipitation and differential two-dimensional gel electrophoresis.

The listed values represent relative spot intensity. The NOL3 lower and upper bands served as positive controls (since virtually no NOL3 was observed on the vehicle gel, the ratios were so high as to be meaningless). NOL3 upper band (spot 22) was much less abundant than the lower band in NOL3^{WT} (see **Figure 24**), in keeping with low but detectable levels observed by Western blot (**Figure 14A**). Spot numbers correspond to **Figure 24**.

Spot #	Gene	WT/Vehicle	Mutant/Vehicle	Other
23	<i>NOL3</i>	very high	very high	positive control
22	<i>NOL3</i>	very high	very high	positive control
18	<i>ACTIN</i>	4.08	no change	likely nonspecific
10	<i>PRPF19</i>	2.36	no change	presumably PRPF19 α
31	<i>IG light</i>	2.05	no change	low quality MS/MS
6	<i>HSP70</i>	2.00	1.40	likely nonspecific
34	<i>PRPF19</i>	1.63	2.28	presumably PRPF19 β
7	<i>ESRRA</i>	1.63	1.67	low quality MS/MS
33	<i>HSP70</i>	1.30	1.64	
21	<i>HNRNPD</i>	1.26	no change	likely nonspecific

The first candidate, ESRRA, is similar to estrogen receptor (ER)-alpha, but has no known endogenous ligand (Sladek et al. 1997). Little is known about its function, but it presumably modulates a bevy of transcriptional targets a la ER-alpha. The MS/MS data for ESRRA was relatively low quality (**Table 2**), so it was not identified with certainty and is less compelling than the other two candidates. The second hit was HNRNPD. Interestingly, HNRNPD functions in regulating expression of the peptide neurotransmitter enkephalin (Dobi et al. 2006), and in the proliferation and differentiation of cortical and cerebellar neural progenitors (Hambardzumyan et al. 2009, Lee et al. 2008). The third hit, PRPF19, modulates neural differentiation and neuronal/astroglial cell fate decisions (Urano et al. 2006).

PRPF19 is the most promising candidate for two reasons. First, the PRPF19 fold changes were highest of all the candidates, and second, two independent PRPF19 iso-

forms were enriched (**Table 2**). It is very unlikely that nonspecific binding would have led to enrichment of two distinct isoforms of the same gene. (The same argument could be made for HSP70, but HSP70 is known to function in protein folding and was probably enriched because of the CMV-mediated overexpression; this is corroborated by its enrichment in both *WT* and *E21Q*.) Interestingly, a previous paper identified two PRPF19 isoforms, PRPF19 α and PRPF19 β , one of which drives differentiation into neurons, and the other into astroglia (Urano et al. 2006). The MS/MS data did not enable determination of which gel spot corresponded to which isoform. Since PRPF19 α is 504aa and PRPF19 β is 523aa (Urano et al. 2006), we presume that spot 10, which ran at a smaller molecular weight, corresponds to PRPF19 α . Conversely, spot 34 likely represents PRPF19 β . The screen suggested that both NOL3^{WT} and NOL3^{E21Q} interact with PRPF19 β , but that NOL3^{E21Q} does not interact with PRPF19 α (**Table 2**). NOL3^{E21Q} loss-of-function in binding to PRPF19 α was accompanied by enhanced binding to PRPF19 β (**Table 2**), supporting the idea that there is an equilibrium in NOL3 binding that maintains the balance of PRPF19 α/β (see **Discussion**). NOL3^{E21Q} also did not interact with HNRNPD. Thus, we hypothesize that the *E21Q* mutation causes loss-of-function in binding to HNRNPD and PRPF19 α , and that these alterations ultimately affect CNS development (see **Discussion**).

Absence of Neuronal Hyperexcitability in *Nol3* Knockout Mice

Since the *NOL3* mutation causes a human disorder of neuronal hyperexcitability, we investigated the phenotype of a previously-generated *Nol3* knockout (*Nol3*^{-/-}) mouse line (Donath et al. 2006). On inspection, *Nol3*^{-/-} mice did not exhibit any overt motor

phenotype, including myoclonus (data not shown). To assess cortical excitability, we measured SSEPs in aged (5 months old) *Nol3*^{-/-} mice and littermate *WT* (*Nol3*^{+/+}) controls. SSEPs were recorded with cortical surface electrodes in response to stimulation with brief current pulses delivered via a needle electrode to the hindlimb. Mean SSEP time to peak (WT: 59.4±0.4msec [n=4]; KO: 58.3±0.1msec [n=3]; p=0.67 by t-test) and 10-90% rise time (WT: 41.8±0.1msec [n=4]; KO: 44.2±0.3msec [n=3]; p=0.21 by t-test) were statistically equivalent between genotypes (**Figure 25**). These data indicate normal conduction velocity of signals from the periphery to the cortex, and normal population responses of the somatosensory cortex to peripheral stimulation.

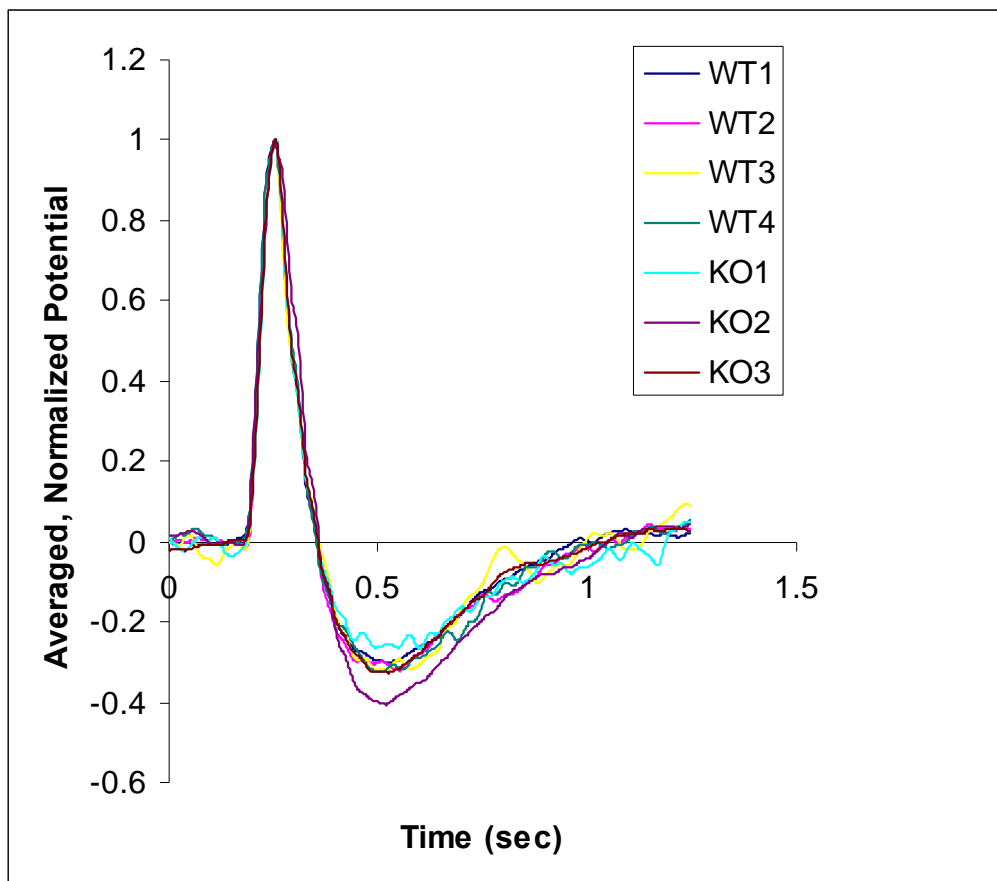


Figure 25. Somatosensory evoked potentials in aged *Nol3*^{-/-} (KO) and *Nol3*^{+/+} (WT) littermate control mice.

Generation of *E21Q* Mice

Since *Nol3* knockout mice do not recapitulate the human FCM phenotype (see above), we sought to test whether mice carrying the *E21Q* point mutation in *Nol3* would be a more faithful disease model. The *Nol3* gene contains 4 exons. Exons 2 and 3 encode the vast majority of the protein, with a few terminal amino acids encoded by exon 4. A targeting vector was constructed that matched the *WT* allele except for the addition of two *FRT* sites, three *LoxP* sites, a *Neo* cassette, and the *E21Q* point mutation (**Figure 26**). Placing the third *LoxP* site in the intronic region between exons 3 and 4 was a calculated gamble: placement in the intron could interfere with mRNA splicing, whereas insertion distal to that intron, in the 3'UTR, could interfere with mRNA stability. However, a location distal to the 3'UTR would have precluded efficient recombination, and bioinformatic analyses suggested that placement in the intron would not disrupt or create a splice acceptor site. Southern blot and PCR data to confirm successful construction of the targeting vector are presented in **Appendix 5**.

Upon electroporation of the targeting vector into embryonic stem (ES) cells, the 5' and 3' homology arms underwent recombination (**Figure 26**). After neomycin screening, ES cells were inserted into blastocysts, which were subsequently implanted into pseudopregnant females to generate chimeric mice. Chimeric mice will be bred to homozygosity, and then crossed to *Flp* mice to generate *Nol3^{E21Q}* knockin mice. It will then be possible to generate mice carrying a conditional knockout allele by crossing the *Nol3^{E21Q}* knockin allele to various *Cre* lines. The diversity of tissue-specific and temporal-specific *Cre* lines should allow us to interrogate the cell types and developmental stages that contribute to the phenotype of *Nol3^{E21Q}* mice.

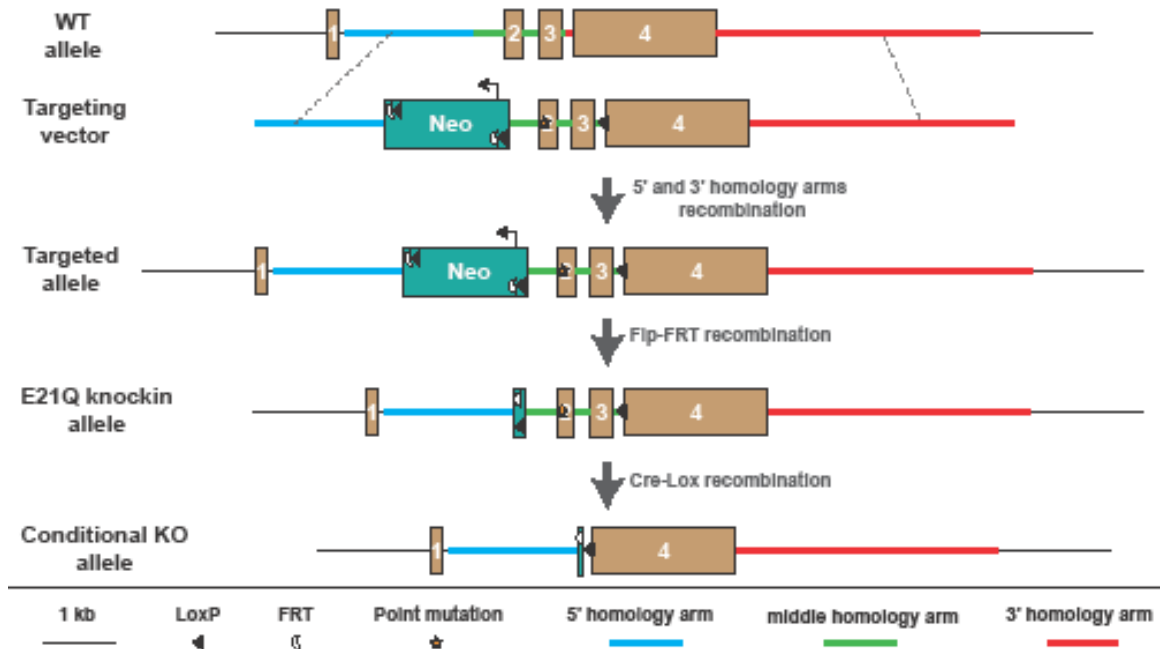


Figure 26. Generation of mice with knockin allele or conditional knockout allele at the *Ncl3* locus.

The depicted segments are the following lengths: 3' homology arm, 5809bp; 5' homology arm, 1798bp; *E21Q* point mutation, 1bp; *FRT*, 34bp; *LoxP*, 50bp; middle homology arm, 793bp; *Neo* cassette, 1712bp. See text and **Appendix 5** for more detail.

DISCUSSION

We have described our attempts to elucidate the mechanism by which *NOL3* mutation causes familial cortical myoclonus (FCM). We found that *NOL3* is broadly expressed in the CNS and that the *NOL3* mutation alters post-translational modification of *NOL3*. This modification is regulated by phosphorylation at the T114 residue, but its identity is still a mystery. We were unable to replicate the published claims that *NOL3* interacts with several pro-apoptotic binding partners, and, in further contrast to the literature, *NOL3* expression predisposed to apoptosis at baseline. In other work, a proteomic screen for novel binding partners suggested two tantalizing candidates: HNRNPD and PRPF19. Finally, we phenotyped *Nol3* knockout mice, and, since they did not have a phenotype akin to FCM, we generated *Nol3* knockin mutant mice. These experiments have a number of limitations and implications that are discussed in turn in the succeeding sections.

***NOL3* is Broadly Expressed in the Murine and Human Brain**

We demonstrated through various approaches that *NOL3* is expressed in many brain regions in both mice and humans (**Figures 7, 11**). Prior studies have demonstrated *Nol3* expression in the CNS of mice (see above), but our studies provide the first detailed characterization. We had hoped to detect expression in more limited subsets of the brain so as to aid in understanding FCM. Instead, *Nol3* is broadly expressed at low to moderate levels. The functional significance of this is not clear.

We had further hoped to glean some insight into pathophysiology if *Nol3* expression were restricted to particular CNS cell types. This was not the case: *Nol3* was

expressed in most or all cell types, at least in the mouse brain (**Figure 9**). We believe that **Figure 8** should be interpreted with circumspection—this experiment was a one-off. More stock can be placed in **Figure 9**. A major caveat is that all of these studies measured *Nol3* RNA. In point of fact, this is a shortcoming of nearly all contemporary gene expression studies. Since RNA is easy to measure, it is the only thing measured. However, with some notable exceptions (e.g., microRNAs), the primary matter of functional importance for the cell is the quantity of corresponding protein. Thus, we corroborated the RNA data by immunohistochemistry of NOL3 protein in *WT* mouse brain slices. This showed diffuse, low-level expression, with particular enrichment in the cell bodies of cortical pyramidal neurons and cerebellar Purkinje cells (data not shown). Given the relatively poor quality of the endogenous antibody, these findings are not definitive and have been omitted.

In Silico Homology Modelling and Bioinformatic Analyses

NOL3 is highly evolutionarily conserved, particularly around the mutated residue (**Figure 1**). Interestingly, we were unable to identify *NOL3* homologs in lower vertebrate species. It is tempting to speculate that the restriction of *NOL3* to higher vertebrates may somehow relate to the increasing complexity of their CNS. But correlation does not causation make, and for the time being this supposition remains just that—speculative.

To understand the structural ramifications of the *E21Q* mutation, in silico homology modelling was the only realistic option. Homology modelling is prone to error, and these analyses should be interpreted with due caution. This is particularly concerning because the CARD domain of Nod1, which served as the scaffold, is not especially ho-

mologous to the NOL3 CARD (**Figure 4**). If we were to select a scaffold based upon amino acid sequence homology, CARD6 would have been a much better choice (**Figure 4**), but its structure was not available. **Figure 4**, the alignment of all human CARD proteins, was illuminating—we were struck by their dissimilarity. When considered in concert with the fact that NOL3 lacks the 6 or 7 alpha-helices stereotypical of a CARD (**Figure 5**), it would not be unreasonable to conclude that *NOL3* may not even be a CARD after all. However, this assertion is contradicted by the substantial homology between NOL3 and CARD6. Nevertheless, we marvel at the influence that bioinformaticians can wield when assigning gene nomenclature to predicted coding sequences. We fear that nomenclature itself often biases investigation towards a functional direction that may be based solely on underwhelming sequence homology. Still, it cannot be disputed that the *E21Q* mutation changes a glutamate to a glutamine residue. If the homology modelling can be believed, then the E21 residue is positioned on the outer surface of the protein, and even if the modelling cannot be believed, having a polar side-chain the glutamate is unlikely to be positioned in the protein's hydrophobic core. As an exposed residue, a change from a glutamate (acidic) to a glutamine (neutral) residue will change the electrostatic surface potential. On balance, these analyses, in combination with the literature, support the hypothesis that the *E21Q* mutation alters protein-protein interactions (see below).

The Elusive Upper Band

When we first performed Western blots from cells expressing *NOL3*^{WT} or *NOL3*^{E21Q}, we were puzzled by the doublet banding pattern in *E21Q* samples. However,

this finding was robust and for a very long time was our only biochemical lead. We thus expended considerable time and effort attempting to identify it. In the end, we failed to identify it but did gain insight into the underlying biochemistry. We learned that mutating the T114 residue to an alanine (which prevents phosphorylation) abrogated the upper band (**Figure 17**). This was not true for the other phospho-site mutants that we tested (**Figure 17**). It should be noted that we only tested five of the seven known phospho-sites, but it would have been prohibitive to mutate all candidate phospho-sites (there are 17 serine, threonine, or tyrosine residues that we did not check), and by MS/MS we did not detect phosphorylation at any NOL3 residue other than T114. Despite the *T114A* mutation abrogating the upper band, we do not believe that the upper band corresponds to phospho-T114, for the following three reasons: phospho-T114 peptide was enriched in both the upper and lower bands from *E21Q* cells (**Figure 19**); a small amount of upper band was observed despite the *T114A* mutation (**Figure 17**); and repeated phosphatase manipulations – which should have modified the relative amounts of non-phospho-T114 and phospho-T114 – were ineffectual (**Figure 16**).

To reconcile these findings, we propose that phosphorylation at T114 regulates formation of the upper band, either by promoting the post-translational modification that converts the lower band to the upper band, or by inhibiting the modification that converts the upper band to the lower band. We cannot explain why the phospho-mimic *T114D* mutation and phosphatase manipulations, both of which would be expected to alter these processes, had no overt effect. It is even possible that the *T114A* mutation abrogates formation of the upper band by precluding some T114 modification other than phosphorylation. This would not, *prima facie*, accord with the mutant-specific MS/MS enrich-

ment of phospho-T114, but is nevertheless possible. We also do not know the exact identity of the upper band. As described in excruciating detail above, we considered many explanations for its identity and tested each using in vitro chemical treatments, mutagenesis, and MS/MS. Ultimately, it all proved fruitless.

The upper band's recalcitrance prompted us to doubt its biological relevance. These reservations are not intrinsic to its truculent nature—rather, it simply remains unclear whether the mutant-specific upper band represents a bona fide biochemical lead to understanding FCM pathophysiology or whether it is a red herring, a breadcrumb left by Mother Nature to induce us into a hopeless line of experimentation. If the latter, we fell for it hook, line, and sinker. On the other hand, the former would be supported by detection of the upper band in vivo. The upper band was not discernible by Western blot in samples from *WT* mice (Donath et al. 2006, and data not shown). Detection of the upper band would not necessarily be expected in vivo given that in *WT* cell lines the upper band is sometimes faint enough to be invisible (**Figure 14A**). Considering the low quality of the endogenous *NOL3* antibody, it may well be the case that the upper band is present in brain lysates but dilute enough to be below the limit of detection. Whether the upper band exists in vivo can be settled once and for all with the *E21Q* knockin mice. A complementary way to bolster the upper band's biological relevance would be if additional FCM-causative *NOL3* alleles are associated with a doublet banding pattern in vitro. Until either and preferably both of these developments come to pass, we refrain from passing judgment on the upper band's functional importance. We failed to identify it, and we failed to demonstrate its significance to FCM pathophysiology. The upper band was a fickle mistress indeed.

***NOL3* in Apoptosis**

When we had accumulated sufficient genetic evidence that *NOL3* is the FCM gene (Chapter III) and were ready to begin functional investigation, we were gratified to learn that *NOL3* was a relatively well-characterized gene (see **Introduction**). In retrospect, this was less of a blessing than a curse, for we were pigeonholed by the published claims that *NOL3* functions in apoptosis. Our data do support a role for *NOL3* in apoptosis, but that role is to enhance apoptosis at baseline. This conclusion is antithetical to the literature, which states that *NOL3* represses apoptosis. Using our data, one could, in theory, argue that *NOL3* represses apoptosis, but only if one calculates the relative cell death as a fold change, comparing pre-treatment to post-treatment values (**Figures 21, 22**). Any such calculation is confounded by the greater cell death at baseline (pre-treatment) in cells expressing *NOL3* (either *WT* or *E21Q*). Post-treatment, there are comparable levels of cell death in vehicle, *WT*, and *E21Q* (**Figures 21, 22**). In our view, to argue from these data that *NOL3* represses apoptosis is disingenuous. If a cell starts dead it is less likely that treatment will kill it, but that does not imply that starting dead represses apoptosis! As far as we can tell, the most accurate conclusion is that *NOL3* enhances basal apoptosis. Why an increase in apoptosis at baseline is not accompanied by a commensurate increase in apoptosis upon apoptotic induction is unclear. In any case, it is actually less important whether *NOL3* represses or enhances apoptosis, for our ultimate goal is to understand FCM pathophysiology, however that may come about. The more important question then becomes whether the *E21Q* mutation has any effect on this process. According to our double stain FACS analysis, the answer is no.

One does not blithely conclude that a stack of published papers are erroneous. And yet, it is impossible to adopt the party line when our data directly contradict it. We concede that our experiments are not definitive. One obvious limitation – among many – is that vehicle cells, while expressing an empty vector, did not overexpress protein via a CMV promoter, a la *WT* or *E21Q* cells. The robust *NOL3*-FLAG overexpression may have altered various cellular processes, including apoptosis. This limitation is not soluble, as overexpression of any other protein would confound the data. In that sense, utilizing both a *WT* and mutant *NOL3* construct serves as an internal control. In the end, we cannot say for sure that *NOL3* enhances apoptosis – though all evidence points in that direction – but it seems safer to conclude that the *E21Q* mutation has no effect on the role of *NOL3* in apoptosis, whatever that role may be (if any). Considered in isolation, this objection may be compelling. However, we must stress that the same shortcoming applies to the published experiments, experiments that we were unable to replicate despite using the exact same constructs, cell lines, apoptotic induction/measurement reagents, and methods. In retrospect, then, it is troubling that the published *NOL3* papers did not utilize the double stain FACS approach for assaying apoptosis. This assay is the gold standard method and has been established for well over a decade—for example, it was detailed in Current Protocols in 2001 (Zhivotovsky et al. 2001). Therefore, its omission as a validation step may be an indication that the data in those papers was, as is sadly all too common, massaged in order to generate conclusions that were expedient at the time but in the long view simply do not stand. At the very least, one could surmise that those groups performed FACS double staining and observed incompatible results.

Similarly, we were dismayed to find that we could not replicate the published NOL3 interactions with pro-apoptotic binding partners (**Figure 23**). Again, we are cognizant of the hubris in concluding that since we could not replicate the finding, the finding must be wrong. We may be wrong. All we can say for certain is that our laborious attempts to replicate the literature using the exact published methods were futile. Neither were we able to replicate the mitochondrial subcellular localization of NOL3 (**Figures 12, 13**) that was published in one paper (Li et al. 2002). We were also appalled to hear from a separate principal investigator that they had not used “yeast two-hybrid screening to identify interacting proteins with full-length [NOL3] as bait”, as was published in Nam et al. (2004). Instead, they “actually used an antibody array screen” (personal communication) to identify the putative NOL3 binding partners. Repeated requests to obtain pertinent reagents and primary data from both groups went unanswered. While we can never rule out confounding factors, we believe that if considerable effort is not sufficient to replicate what should be a straightforward finding, that finding must be called into question. At the minimum, the inability to replicate these interactions under slightly more biologically relevant conditions should raise doubts as to their importance in vivo.

PNKP19 and HNRNPD: a Potential Mechanism for FCM Pathophysiology?

Before expounding on the proteomics screen, we wish to touch on its disadvantages. (These partially apply to the apoptosis assays and co-IPs discussed above.) It is possible that the FLAG tag affects the binding properties of NOL3. We believe that this scenario is unlikely because the FLAG tag is a small epitope and is located at the C-terminus, whereas the protein-protein interaction motif is N-terminal; furthermore, since

the *E21Q* mutation is near the N-terminus, any alterations in NOL3 binding due to the FLAG tag will, presumably, equally affect both WT and mutant NOL3. Of greater concern is the choice of cell line. HEK293 cells, although they have been used extensively to characterize NOL3 (e.g., Koseki et al. 1998, Hong et al. 2003, Nam et al. 2004), obviously differ substantially from in vivo CNS cells. These differences could affect NOL3 function and could distort the pool of candidate binding partners. In other words, the screen may have been limited in detecting biologically relevant interactions. After all, if you fish all day long in a pool filled with minnows that bite at the lure, you may feel that the lure is attractive only to minnows, but you cannot know until you cast into the ocean—if the big fish bite, you were wrong all along. For technical reasons, we could not avoid this shortcoming. Nevertheless, the candidate binding partners identified by the screen present a legitimate starting point *if they can be validated in vivo*.

If they hold up, the HNRNPD and PRPF19 interactions intimate a seductive hypothesis. The hypothesis is as follows. NOL3^{WT} ordinarily interacts with HNRNPD, PRPF19 α , and PRPF19 β (**Table 2**). The *E21Q* mutation abolishes the interactions with HNRNPD and PRPF19 α (**Table 2**). Since PRPF19 α drives neuronal differentiation, whereas PRPF19 β promotes astroglial differentiation (Urano et al. 2006), the cessation of the PRPF19 α interaction should alter the balance of neuronal/astroglial differentiation. For now, we do not know whether NOL3's interactions with PRPF19 α/β serve to activate or inhibit, so it is impossible to predict the precise effects on differentiation. Similarly, we do not know whether this mechanism alters differentiation of excitatory versus inhibitory neurons. The same goes for differentiation of astroglia, which are becoming appreciated as critical modulators of CNS output in their own right (Coulter & Eid 2012,

Molofsky et al. 2012). At any rate, we predict that the ultimate effect of these abrogated interactions is cortical hyperexcitability, as manifested in stimulus-sensitive myoclonus (i.e., FCM). This hypothesis is testable (see Chapter V). In passing, we cannot help but remark that the data in the PRPF19 paper are, in our view, modest (Urano et al. 2006). Whether the findings can be replicated is an open question.

This hypothesis posits a loss-of-function, which, at first glance, does not seem to agree with the apparent absence of a phenotype in *Nol3* knockout mice (**Figure 26**), nor with the observation that one neurologically normal human has a heterozygous chromosomal deletion spanning *NOL3* (Park et al. 2010). However, these data need not contradict the HNRNPD/PRPF19 hypothesis, for the situation may be more complex than simple loss-of-function. For example, suppose that *NOL3* binding to both PRPF19 α and PRPF19 β maintains a balance of differentiation that ensures proper CNS development. When *NOL3* is mutated such that it can only bind PRPF19 β and not PRPF19 α , PRPF19 β is hyperactive and drives differentiation towards a mutant phenotype. Now, suppose that *NOL3* is absent altogether (e.g., in *Nol3* knockout mice). In this scenario, it is plausible that PRPF19 α and PRPF19 β remain in balance. That is to say, *NOL3* is not essential to maintain the balance—it is only when *NOL3* function is selectively disrupted that pathology ensues. Of course, the actual mechanism may be dramatically more complex than that. In any event, the presence or absence of an excitability phenotype in *E21Q* knockin mice should help to resolve at least some of these issues (see Chapter V).

In sum, we have shown that *NOL3* is highly conserved and broadly expressed in the brain. The *E21Q* mutation, which causes familial cortical myoclonus (FCM) in humans, alters post-translational modification of *NOL3* protein in vitro, although the iden-

tity and biological relevance of this change is not clear. In contrast to the literature, we did not observe NOL3 binding to pro-apoptotic proteins, nor did *NOL3* repress apoptosis. Be that as it may, we identified novel NOL3 binding interactions that are disrupted by the *E21Q* mutation and thus may explain FCM pathophysiology. This putative mechanism, some experiments required to test it, and the implications are more fully explored in Chapter V.

REFERENCES

- Abmayr S, Crawford RW, Chamberlain JS. 2004. Characterization of ARC, apoptosis repressor interacting with CARD, in normal and dystrophin-deficient skeletal muscle. *Hum Mol Genet* 13:213-21
- An J, Li P, Li J, Dietz R, Donath S. 2009. ARC is a critical cardiomyocyte survival switch in doxorubicin cardiotoxicity. *J Mol Med* 87:401-10
- Auer-Grumbach M, Olschewski A, Papic L, Kremer H, McEntagart ME, et al. 2010. Alterations in the ankyrin domain of TRPV4 cause congenital distal SMA, scapuloperoneal SMA and HMSN2C. *Nat Genet* 42:160-64
- Bouma W, Noma M, Kanemoto S, Matsubara M, Leshnower BG, et al. 2010. Sex-related resistance to myocardial ischemia-reperfusion injury is associated with high constitutive ARC expression. *Am J Physiol Heart Circ Physiol* 298:H1510-17
- Burrows NP, Nicholls AC, Richards AJ, Luccarini C, Harrison JB, et al. 1998. A point mutation in an intronic branch site results in aberrant splicing of COL5A1 and in Ehler-Danlos syndrome type II in two British families. *Am J Hum Genet* 63:390-98
- Cahoy JD, Emery B, Kaushal A, Foo LC, Zamanian JL, et al. 2008. A transcriptome database for astrocytes, neurons, and oligodendrocytes: a new resource for understanding brain development and function. *J Neurosci* 28:264-78
- Carter BZ, Qiu YH, Zhang N, Coombes KR, Mak DH, et al. 2011. Expression of ARC (apoptosis repressor with caspase recruitment domain), an antiapoptotic protein, is strongly prognostic in AML. *Blood* 117:780-87

- Chou JJ, Matsuo H, Duan H, Wagner G. 1998. Solution structure of the RAIDD CARD and model for CARD/CARD interaction in caspase-2 and caspase-9 recruitment. *Cell* 94:171-80
- Coulter DA, Eid T. 2012. Astrocytic regulation of glutamate homeostasis in epilepsy. *Glia* 60:1215-26
- Cuajungco MP, Grimm C, Oshima K, D'hoedt D, Nilius B, et al. 2006. PACSINs bind to the TRPV4 cation channel. *J Biol Chem* 281:18753-62
- D'hoedt D, Owsianik G, Prenen J, Cuajungco MP, Grimm C, et al. 2008. Stimulus-specific modulation of the cation channel TRPV4 by PACSIN3. *J Biol Chem* 283:6272-80
- de Alba E. 2009. Structure and interdomain dynamics of apoptosis-associated speck-like protein containing a CARD (ASC). *J Biol Chem* 284:32932-41
- Deng HX, Klein CJ, Yan J, Shi Y, Wu Y, et al. 2010. Scapuloperoneal spinal muscular atrophy and CMT2C are allelic disorders caused by alterations in TRPV4. *Nat Genet* 42:165-69
- Deverman BE, Cook BL, Manson SR, Niederhoff RA, Langer EM, et al. 2002. Bcl-x_L deamidation is a critical switch in the regulation of the response to DNA damage. *Cell* 111:51-62
- Dobi A, Szemes M, Lee C, Palkovits M, Lim F, et al. 2006. AUF1 is expressed in the developing brain, binds to AT-rich double-stranded DNA, and regulates enkephalin gene expression. *J Biol Chem* 281:28889-900

- Donath S, Li P, Willenbockel C, Al-Saadi N, Gross V, et al. 2006. Apoptosis repressor with caspase recruitment domain is required for cardioprotection in response to biomechanical and ischemic stress. *Circulation* 113:1203-12
- Doyle JP, Dougherty JD, Heiman M, Schmidt EF, Stevens TR, et al. 2008. Application of a translational profiling approach for the comparative analysis of CNS cell types. *Cell* 135:749-62
- Ekhterae D, Platoshyn O, Zhang S, Remillard CV, Yuan JXJ. 2003. Apoptosis repressor with caspase domain inhibits cardiomyocyte apoptosis by reducing K⁺ currents. *Am J Physiol Cell Physiol* 284:C1405-10
- Ekhterae D, Hinmon R, Matsuzaki K, Noma M, Zhu W, et al. 2011. Infarction induced myocardial apoptosis and ARC activation. *J Surg Res* 166:59-67
- Ellis CE, Schwartzberg PL, Grider TL, Fink DW, Nussbaum RL. 2001. α -synuclein is phosphorylated by members of the Src family of protein-tyrosine kinases. *Proc Natl Acad Sci U S A* 276:3879-84
- Engidawork E, Gulesserian T, Yoo BC, Cairns N, Lubec G. 2001. Alteration of caspases and apoptosis-related proteins in brains of patients with Alzheimer's disease. *Biochem Biophys Res Commun* 281:84-93
- Espinosa F, McMahon A, Chan E, Wang S, Ho CS, et al. 2001. Alcohol hypersensitivity, increased locomotion, and spontaneous myoclonus in mice lacking the potassium channels Kv3.1 and Kv3.3. *J Neurosci* 21:6657-65
- Ewing RM, Chu P, Elisma F, Li H, Taylor P, et al. 2007. Large-scale mapping of human protein-protein interactions by mass spectrometry. *Mol Syst Biol* 3:89
- Foo RSY, Nam YJ, Ostreicher MJ, Metz MD, Whelan RS, et al. 2007. Regulation of

- p53 tetramerization and nuclear export by ARC. *Proc Natl Acad Sci U S A* 104:20826-31
- Gulesserian T, Engidawork E, Yoo BC, Cairns N, Lubec G. 2001. Alteration of caspases and other apoptosis regulatory proteins in Down syndrome. *J Neural Transm Suppl* 61:163-79
- Gustafsson AB, Tsai JG, Logue SE, Crow MT, Gottlieb RA. 2004. Apoptosis repressor with caspase recruitment domain protects against cell death by interfering with Bax activation. *J Biol Chem* 279:21233-38
- Hambardzumyan D, Sergent-Tanguy S, Thinard R, Bonnamain V, Masip M, et al. 2009. AUF1 and Hu proteins in the developing rat brain: implication in the proliferation and differentiation of neural progenitors. *J Neurosci Res* 87:1296-1309
- Hawrylycz MJ, Lein ES, Guillozet-Bongaarts AL, Shen EH, Ng L, et al. 2012. An anatomically comprehensive atlas of the adult human brain transcriptome. *Nature* 489:391-99
- Heikaus S, Kempf T, Mahotka C, Gabbert HE, Ramp U. 2008. Caspase-8 and its inhibitors in RCCs in vivo: the prominent role of ARC. *Apoptosis* 13:938-49
- Heiman M, Schaefer A, Gong S, Peterson JD, Day M, et al. 2008. A translational profiling approach for the molecular characterization of CNS cell types. *Cell* 135:738-48
- Hiller S, Kohl A, Fiorito F, Herrmann T, Wider G, et al. 2003. NMR structure of the apoptosis- and inflammation-related NALP1 pyrin domain. *Structure* 11:1199-205
- Hong YM, Jo DG, Lee JY, Chang JW, Nam JH, et al. 2003. Down-regulation of ARC

- contributes to vulnerability of hippocampal neurons to ischemia/hypoxia. *FEBS Lett* 543:170-73
- Iuliano BA, Schmelzer JD, Thiemann RL, Low PA, Rodriguez M. 1994. Motor and somatosensory evoked potentials in mice infected with Theiler's murine encephalomyelitis virus. *J Neurol Sci* 123:186-94
- Joensuu T, Lehesjoki AE, Kopra O. 2008. Molecular background of EPM1-Unverricht-Lundborg disease. *Epilepsia* 49:557-63
- Kalviainen R, Khyuppenen J, Koskenkorva P, Eriksson K, Vanninen R, et al. 2008. Clinical picture of EPM1-Unverricht-Lundborg disease. *Epilepsia* 49:549-56
- Koseki T, Inohara N, Chen S, Nunez G. 1998. ARC, an inhibitor of apoptosis expressed in skeletal muscle and heart that interacts selectively with caspases. *Proc Natl Acad Sci U S A* 95:5156-60
- Krakow D, Vriens J, Camacho N, Luong P, Deixler H, et al. 2009. Mutations in the gene encoding the calcium-permeable ion channel TRPV4 produce spondylometaphyseal dysplasia, Kozlowski type and metatropic dysplasia. *Am J Hum Genet* 84:307-15
- Kuo CT, Zhu S, Younger S, Jan LY, Jan YN. 2006. Identification of E2/E3 ubiquitinating enzymes and caspase activity regulating *Drosophila* sensory neuron dendrite pruning. *Neuron* 51:283-90
- Landoure G, Zdebik AA, Martinez TL, Burnett BG, Stanescu HC, et al. 2010. Mutations in TRPV4 cause Charcot-Marie-Tooth disease type 2C. *Nat Genet* 42:170-74
- Lee C, Gyorgy A, Maric D, Sadri N, Schneider RJ, et al. 2008. Members of the NuRD

- chromatin remodeling complex interact with AUF1 in developing cortical neurons. *Cereb Cortex* 18:2909-19
- Lee HY, Xu Y, Huang Y, Ahn AH, Auburger GW, et al. 2004. The gene for paroxysmal non-kinesigenic dyskinesia encodes an enzyme in a stress response pathway. *Hum Mol Genet* 13:3161-70
- Lehtinen MK, Tegelberg S, Schipper H, Su H, Zukor H, et al. 2009. Cystatin B deficiency sensitizes neurons to oxidative stress in progressive myoclonus epilepsy, EPM1. *J Neurosci* 29:5910-15
- Lein ES, Hawrylycz MJ, Ao N, Ayres M, Bensinger A, et al. 2007. Genome-wide atlas of gene expression in the adult mouse brain. *Nature* 445:186-76
- Li PF, Li J, Muller EC, Otto A, Dietz R, et al. 2002. Phosphorylation by protein kinase CK2: a signaling switch for the caspase-inhibiting protein ARC. *Mol Cell* 10:247-58
- Li YZ, Liu XH, Zhu XM, Cai LR. 2007. ARC contributes to the inhibitory effect of preconditioning on cardiomyocyte apoptosis. *Apoptosis* 12:1589-95
- Li Z, Jo J, Jia JM, Lo SC, Whitcomb DJ, et al. 2010. Caspase-3 activation via mitochondria is required for long-term depression and AMPA receptor internalization. *Cell* 141:859-71
- Loan Le TY, Mardini M, Howell VM, Funder JW, Ashton AW, et al. 2012. Low-dose spironolactone prevents apoptosis repressor with caspase recruitment domain degradation during myocardial infarction. *Hypertension* 59:1164-69
- Manon F, Favier A, Núñez G, Simorre JP, Cusack S. 2007. Solution structure of NOD1

- CARD and mutational analysis of its interaction with the CARD of downstream kinase RICK. *J Mol Biol* 365:160-74
- Mercier I, Vuolo M, Jasmin JF, Medina CM, Williams M, et al. 2008. ARC (apoptosis repressor with caspase recruitment domain) is a novel marker of human colon cancer. *Cell Cycle* 7:1640-47
- Molofsky AV, Krencik R, Ullian EM, Tsai HH, Deneen B, et al. 2012. Astrocytes and disease: a neurodevelopmental perspective. *Genes Dev* 26:891-907
- Murtaza I, Wang HX, Feng X, Alenina N, Bader M, et al. 2008. Down-regulation of catalase and oxidative modification of protein kinase CK2 lead to the failure of apoptosis repressor with caspase recruitment domain to inhibit cardiomyocyte hypertrophy. *J Biol Chem* 283:5996-6004
- Nam YJ, Mani K, Ashton AW, Peng CF, Krishnamurthy B, et al. 2004. Inhibition of both the extrinsic and intrinsic death pathways through nonhomotypic death-fold interactions. *Mol Cell* 15:901-12
- Nam YJ, Mani K, Wu L, Peng CF, Calvert JW, et al. 2007. The apoptosis inhibitor ARC undergoes ubiquitin-proteasomal-mediated degradation in response to death stimuli: identification of a degradation-resistant mutant. *J Biol Chem* 282:5522-28
- Neuss M, Monticone R, Lundberg MS, Chesley AT, Fleck E, et al. 2001. The apoptotic regulatory protein ARC (apoptosis repressor with caspase recruitment domain) prevents oxidant stress-mediated cell death by preserving mitochondrial function. *J Biol Chem* 276:33915-22
- Olsen JV, Vermeulen M, Santamaria A, Kumar C, Miller ML, et al. 2010. Quantitative

- phosphoproteomics reveals widespread full phosphorylation site occupancy during mitosis. *Sci Signal* 3:ra3
- Park H, Kim JI, Ju YS, Gokcumen O, Mills RE, et al. 2010. Discovery of common Asian copy number variants using integrated high-resolution array CGH and massively parallel DNA sequencing. *Nat Genet* 42:400-405
- Prasad SS, Russell M, Nowakowska M. 2010. Neuroprotection induced in vitro by ischemic preconditioning and postconditioning: modulation of apoptosis and PI3K-Akt pathways. *J Mol Neurosci* 43:428-42
- Pyo JO, Nah J, Kim HJ, Chang JW, Song YW, et al. 2008. Protection of cardiomyocytes from ischemic/hypoxic cell death via Drbp1 and pMe₂GlyDH in cardio-specific ARC transgenic mice. *J Biol Chem* 283:30707-14
- Quadrilatero J, Bloemberg D. 2010. Apoptosis repressor with caspase recruitment domain is dramatically reduced in cardiac, skeletal, and vascular smooth muscle during hypertension. *Biochem Biophys Res Commun* 391:1437-42
- Rajandram R, Pat BK, Li J, Johnson DW, Gobe GC. 2009. Expression of apoptotic tumour necrosis factor receptor-associated factor, caspase recruitment domain and cell death-inducing DFF-45 effector genes in therapy-treated renal cell carcinoma. *Nephrology* 14:205-12
- Reed JC, Doctor KS, Godzik A. 2004. The domains of apoptosis: a genomics perspective. *Sci STKE* 239:re9
- Ren J, Babcock SA, Li Q, Huff AF, Li SY, et al. 2009. Aldehyde dehydrogenase-2 transgene ameliorates chronic alcohol ingestion-induced apoptosis in cerebral cortex. *Toxicol Lett* 187:149-56

- Renatus M, Stennicke HR, Scott FL, Liddington RC, Salvesen GS. 2001. Dimer formation drives the activation of the cell death protease caspase 9. *Proc Natl Acad Sci U S A* 98:14250-55
- Rizzo MA, Davidson MW, Piston DW. 2010. Fluorescent protein tracking and detection: fluorescent protein structure and color variants. *Live Cell Imaging, 2nd ed.* Cold Spring Harbor, NY: CSHL Press
- Rock MJ, Prenen J, Funari VA, Funari TL, Merriman B, et al. 2008. Gain-of-function mutations in TRPV4 cause autosomal dominant brachyolmia. *Nat Genet* 40:999-1003
- Shelke RR, Leeuwenburgh C. 2003. Lifelong caloric restriction increases expression of apoptosis repressor with a caspase recruitment domain (ARC) in the brain. *FASEB J* 17:494-96
- Shen J, Gilmore EC, Marshall CA, Haddadin M, Reynolds JJ, et al. 2010. Mutations in PNKP cause microcephaly, seizures and defects in DNA repair. *Nat Genet* 42:245-49
- Sladek R, Beatty B, Squire J, Copeland NG, Gilbert DJ, et al. 1997. Chromosomal mapping of the human and murine orphan receptors ERRalpha (ESRRA) and ERRbeta (ESRRB) and identification of a novel human ERRalpha-related pseudogene. *Genomics* 45:320-26
- Srimathi T, Robbins SL, Dubas RL, Hasegawa M, Inohara N, et al. 2008. Monomer/dimer transition of the caspase-recruitment domain of human Nod1. *Biochemistry* 47:1319-25
- Stoss O, Schwaiger FW, Cooper TA, Stamm S. 1999. Alternative splicing determines

- the intracellular localization of the novel nuclear protein Nop30 and its interaction with the splicing factor SRp30c. *J Biol Chem* 274:10951-62
- Sugino K, Hempel CM, Miller MN, Hattox AM, Shapiro P, et al. 2006. Molecular taxonomy of major neuronal classes in the adult mouse forebrain. *Nat Neurosci* 9:99-107
- Suzuki T, Miyamoto H, Nakahari T, Inoue I, Suemoto T, et al. 2009. Efhc1 deficiency causes spontaneous myoclonus and increased seizure susceptibility. *Hum Mol Genet* 18:1099-1109
- Tan WQ, Wang JX, Lin ZQ, Li YR, Lin Y, et al. 2008. Novel cardiac apoptotic pathway: the dephosphorylation of apoptosis repressor with caspase recruitment domain by calcineurin. *Circulation* 118:2268-76
- Trinidad JC, Thalhammer A, Specht CG, Lynn AJ, Baker PR, et al. 2008. Quantitative analysis of synaptic phosphorylation and protein expression. *Mol Cell Proteomics* 7:684-96
- Uhlen M, Oksvold P, Fagerberg L, Lundberg E, Jonasson K, et al. 2010. Towards a knowledge-based human protein atlas. *Nat Biotechnol* 28:1248-50
- Urano Y, Iiduka M, Sugiyama A, Akiyama H, Uzawa K, et al. 2006. Involvement of the mouse Prp19 gene in neuronal/astroglial cell fate decisions. *J Biol Chem* 281:7498-7514
- Valdez-Taubas J, Pelham H. 2005. Swf1-dependent palmitoylation of the SNARE Tlg1 prevents its ubiquitination and degradation. *EMBO J* 24:2524-32
- Vaughn DE, Rodriguez J, Lazebnik Y, Joshua-Tor L. 1999. Crystal structure of Apaf-1

- caspase recruitment domain: an alpha-helical Greek key fold for apoptotic signaling. *J Mol Biol* 293:439-47
- Wang JX, Li Q, Li PF. 2009. Apoptosis repressor with caspase recruitment domain contributes to chemotherapy resistance by abolishing mitochondrial fission mediated by dynamin-related protein-1. *Cancer Res* 69:492-500
- Wang M, Qanungo S, Crow MT, Watanabe M, Nieminen AL. 2005. Apoptosis repressor with caspase recruitment domain (ARC) is expressed in cancer cells and localizes to nuclei. *FEBS Lett* 579:2411-15
- Wu L, Nam YJ, Kung G, Crow MT, Kitsis RN. 2010. Induction of the apoptosis inhibitor ARC by Ras in human cancers. *J Biol Chem* 285:19235-45
- Yi CH, Pan H, Seebacher J, Jang IH, Hyberts SG, et al. 2011. Metabolic regulation of protein N-alpha-acetylation by Bcl-xL promotes cell survival. *Cell* 146:607-20
- Zaiman AL, Damico R, Thoms-Chesley A, Files DC, Kesari P, et al. 2012. A critical role for the protein apoptosis repressor with caspase recruitment domain in hypoxia-induced pulmonary hypertension. *Circulation* 124:2533-42
- Zhivotovsky B, Samali A, Orrenius S. 2001. Determination of apoptosis and necrosis. *Curr Protoc Toxicol* Chapter 2:Unit2.2
- Zhou P, Chou J, Olea RS, Yuan J, Wagner G. 1999. Solution structure of Apaf-1 CARD and its interaction with caspase-9 CARD: a structural basis for specific adaptor/caspase interaction. *Proc Natl Acad Sci U S A* 96:11265-70

CHAPTER V

Conclusion

We have described the characterization of a novel phenotype, familial cortical myoclonus (FCM), the identification of a mutation in *NOL3*, and functional investigations to elucidate the molecular pathophysiology by which *NOL3* mutation causes FCM. In the preceding chapters we presented ample evidence that FCM is a novel phenotype and that *NOL3* is the disease gene. On the other hand, the molecular mechanism is still speculative. In Chapter IV we laid out the hypothesis that the mutation alters the binding of *NOL3* to HNRNPD and PRPF19 α/β , thereby skewing neuronal/astroglial differentiation during development.

Given the panoply of reagents that we have generated, it should be relatively straightforward to test this hypothesis. First, the HNRNPD and PRPF19 interactions with *NOL3*^{WT} must be validated in vitro, then in vivo (in *WT* mice). Concomitantly, one can address whether the *E21Q* mutation alters HNRNPD and PRPF19 interactions both in vitro and in vivo (in *E21Q* knockin mice). *Nol3* knockout mice can serve as a negative control. The *E21Q* mice will, it is hoped, exhibit a myoclonus phenotype behaviorally and electrophysiologically. The next step would be a careful examination of neuronal proliferation and differentiation. This can be studied in vivo, using various *Cre* driver lines, because the *E21Q* allele is floxed. Moreover, since *Nol3* null mice are WT, we should be able to exploit the many existing *Cre* lines to perform tissue- and temporal-specific rescue of the *E21Q* myoclonus phenotype. Both HNRNPD and PRPF19 modulate RNA processing, so transcriptome sequencing (“RNA-seq”) should provide insight into the broader transcriptional changes. Finally, if the *E21Q* mice do faithfully recapitulate the FCM phenotype, it may even be possible to apply the knowledge gleaned from cellular and molecular studies by testing various compounds as possible treatments.

We are optimistic, but wish to emphasize in the most strenuous terms that the HNRNPD/PRPF19 hypothesis is a tentative one. Even if this hypothesis proves to be wrong, though, we predict that the *E21Q* knockin mice will confirm the assignment of *NOL3* as the disease gene. Granted, many bona fide human disease genes are not associated with similar phenotypes in mouse models, and sometimes there is no mouse phenotype at all. In that sense, a negative result would be less definitive than a positive one—that is, the absence of a myoclonus phenotype in the *E21Q* mice would not discredit *NOL3* as the disease gene. Ultimately, the claim that *NOL3* is the FCM gene can be best settled by the identification of independent *NOL3* mutations in patients with the same or a similar phenotype. As discussed in Chapter III, this long-awaited development may be nigh.

Were the HNRNPD/PRPF19 hypothesis to prove incorrect, what then is the mechanistic link between *NOL3* and neuronal hyperexcitability? The possibilities are, of course, legion. Given the published findings that *NOL3* inhibits apoptosis, an obvious possibility is that a mutation in an apoptosis repressor leads to increased apoptosis of neurons (e.g., inhibitory neurons). In the view of our results outlined in Chapter IV, this seems unlikely. It is also possible that *NOL3* functions in apoptotic signaling but not in apoptosis per se. Caspases and their inhibitors are expressed in healthy mature neurons and can regulate CNS functions other than apoptosis. For example, gain-of-function in a *Drosophila* apoptosis repressor abrogates caspase activity and dendritic pruning (Kuo et al. 2006, Rumpf et al. 2011). Caspase-3 activation promotes AMPA receptor internalization and associated long-term depression (Li et al. 2010). Caspase-3 also modulates glutamatergic synaptic transmission and plasticity (D’Amelio et al. 2010), and other cas-

pases control neuroinflammatory microglia (Burguillos et al. 2011) and pruning of axons (Nikolaev et al. 2009). Caspases are able to modulate these diverse activities without initiating apoptosis because they are active only in certain subcellular compartments (Feinstein-Rotkopf & Arama 2009). Returning to the dendritic pruning example, caspase activity is localized to those dendrites that are degenerating (Williams et al. 2006), thereby preventing widespread cellular damage. In total, these studies indicate that alterations in apoptotic pathway signaling may cause neurologic phenotypes by mechanisms other than apoptosis itself. However, since we observed relatively diffuse subcellular expression of WT and mutant *NOL3*, it is unlikely that this mechanism applies to FCM unless in vivo *NOL3* expression is more localized.

In fact, at this point it is still uncertain whether the *NOL3* mutation causes a loss-of-function, a gain-of-function, or a neomorph. The absence of an excitability phenotype in *Nol3* knockout mice, in concert with the observation of a neurologically normal patient with a heterozygous deletion of *NOL3* (Park et al. 2010), strongly argues against a loss-of-function mechanism. A gain-of-function seems more plausible, especially seeing as the *E21Q* mutation enhances *NOL3* post-translational modification. Liu et al. (2011) gives an illustrative example. They found that patients with chronic mucocutaneous candidiasis had mutations in *STAT1* that were gain-of-function: the mutations enhance phosphorylation of *STAT1* and thereby dampen IL-17 immunity. For FCM, a neomorphic mechanism is also possible, but a priori it is impossible to predict what that may be.

Moving beyond the molecular and cellular scale to the anatomical level, the pathophysiology of myoclonus is, to quote Churchill by way of Carr, “a riddle, wrapped in a mystery, inside an enigma” (2012). Even the anatomically tidy categories of sub-

cortical and cortical myoclonus have been called into question (Carr 2012). It turns out that cortical myoclonus may involve or derive from subcortical structures (Carr 2012). Other authors have argued for a cerebellar origin. For example, patients with familial adult myoclonic epilepsy, a classic disorder of cortical myoclonus, exhibit cerebellar pathology on autopsy and MRI (van Rootselaar et al. 2004, 2007, Striano et al. 2009, Buijink et al. 2012). Possible explanations include abnormal reciprocal interactions between the cerebellum and the motor cortex, or decreased cortical inhibition due to a dysfunctional cerebello-thalamo-cortical loop (Striano et al. 2012). Alternatively, the cerebellar pathology may be unrelated; under this model, the cortical hyperexcitability results from enhanced intrinsic rhythmicity in cortical generators (Striano et al. 2012). For now, we just do not know. For an elementary motor output – myoclonus – we have a very poor understanding of its etiology even at the broad anatomical level. In this regard, identifying a molecular culprit, *NOL3*, may be helpful.

In summary, we have identified a novel Mendelian phenotype characterized by autosomal dominant cortical myoclonus. We propose for this disorder the term familial cortical myoclonus (FCM). FCM is likely caused by a mutation in the gene *NOL3*. The mutation does not alter the published apoptotic *NOL3* functions. Instead, we hypothesize that the *NOL3* mutation disrupts *NOL3* interactions with HNRNPD and PRPF19, thus altering cortical development and culminating in neuronal hyperexcitability and disease. This hypothesis will be tested in the transgenic mice we generated. This work should facilitate diagnosis and genetic counseling in patients with myoclonus. Furthermore, as has proved the case for many other Mendelian diseases, we anticipate that further investigation to understand the role of *NOL3* in FCM pathophysiology will provide insight into

mechanisms of membrane hyperexcitability relevant to other forms of myoclonus and even epilepsy.

REFERENCES

- Buijink AW, Caan MW, Tijssen MA, Hoogduin JM, Maurits NM, et al. 2012. Decreased cerebellar fiber density in cortical myoclonic tremor but not in essential tremor. *Cerebellum* epub ahead of print
- Burguillos MA, Deierborg T, Kavanagh E, Persson A, Hajji N, et al. 2011. Caspase signalling controls microglia activation and neurotoxicity. *Nature* 472:319-24
- Carr J. 2012. Classifying myoclonus: a riddle, wrapped in a mystery, inside an enigma. *Parkinsonism Relat Disord* 18(Suppl 1):S174-76
- D'Amelio M, Cavallucci V, Middei S, Marchetti C, Pacioni S, et al. 2011. Caspase-3 triggers early synaptic dysfunction in a mouse model of Alzheimer's disease. *Nat Neurosci* 14:69-76
- Feinstein-Rotkopf Y, Arama E. 2009. Can't live without them, can live with them: roles of caspases during vital cellular processes. *Apoptosis* 14:980-95
- Kuo CT, Zhu S, Younger S, Jan LY, Jan YN. 2006. Identification of E2/E3 ubiquitinating enzymes and caspase activity regulating *Drosophila* sensory neuron dendrite pruning. *Neuron* 51:283-90
- Li Z, Jo J, Jia JM, Lo SC, Whitcomb DJ, et al. 2010. Caspase-3 activation via mitochondria is required for long-term depression and AMPA receptor internalization. *Cell* 141:859-71
- Liu L, Okada S, Kong XF, Kreins AY, Cypowyj S, et al. 2011. Gain-of-function human STAT1 mutations impair IL-17 immunity and underlie chronic mucocutaneous candidiasis. *J Exp Med* 208:1635-48
- Nikolaev A, McLaughlin T, O'Leary DDM, Tessier-Lavigne M. 2009. APP binds DR6

to trigger axon pruning and neuron death via distinct caspases. *Nature* 457:981-89

Park H, Kim JI, Ju YS, Gokcumen O, Mills RE, et al. 2010. Discovery of common Asian copy number variants using integrated high-resolution array CGH and massively parallel DNA sequencing. *Nat Genet* 42:400-405

Rumpf S, Lee SB, Jan LY, Jan YN. 2011. Neuronal remodeling and apoptosis require VCP-dependent degradation of the apoptosis inhibitor DIAP1. *Development* 138:1153-60

Striano P, Caranci F, Di Benedetto R, Tortora F, Zara F, et al. 2009. 1H MR spectroscopy indicates prominent cerebellar dysfunction in benign adult familial myoclonic epilepsy. *Epilepsia* 50:1491-97

Striano P, Louis ED, Manto M. 2012. Autosomal dominant cortical tremor, myoclonus, and epilepsy: is the origin in the cerebellum? Editorial. *Cerebellum* epub ahead of print

van Rootselaar AF, Aronica E, Jansen Steur EN, Rozemuller-Kwakkel JM, de Vos RA, et al. 2004. Familial cortical tremor with epilepsy and cerebellar pathological findings. *Mov Disord* 19:213-17

van Rootselaar AF, van der Salm SMA, Bour LJ, Edwards MJ, Brown P, et al. 2007. Decreased cortical inhibition and yet cerebellar pathology in “familial cortical myoclonic tremor with epilepsy”. *Mov Disord* 22:2378-85

Williams DW, Kondo S, Krzyzanowska A, Hiromi Y, Truman JW. 2006. Local caspase activity directs engulfment of dendrites during pruning. *Nat Neurosci* 9:1234-36

APPENDICES

Appendix 1. Microsatellite markers and primers for linkage analysis.

All references are to NCBI build 37.1. M13 denotes TGTAACGACGGCCAGT.

Marker	Start	End	Primers	Size range
16.6	64,999,636	64,999,785	(M13)GGTCTGCTGCTGTCCAAGAC TCCTAATTTCTCCCTCTTGTTCC	134-164
D16S3050	65,067,048	65,067,207	(M13)CATCTAATAAGTGATACACCCTGG CAAAGTGGCTTGTGATTTCT	168-186
16.16	65,206,748	65,206,293	(M13)CCAACCTTTTCCCAATGATG AATTGAATGTGGTGGTGGTG	227-243
16.3	65,285,223	65,285,462	(M13)TCCCCAGACAAATGTGTTTCA TCCCTTGGACTTTGCTGACT	249-267
D16S3043	65,492,263	65,492,559	(M13)AACCATGCCATCATAACTTTG AGATGCAGAAAGCAGGAGAGG	296-314
D16S3019	66,129,156	66,129,455	(M13)GGGCTGGAGGTCTAGTTCTAAG TTGAAGGGAGGAAATAACTGATG	308-324
D16S3086	66,935,898	66,936,081	(M13)CCTGCTGGGAAGTGACC CTAAGGACAAATGTAGATGCTCTGG	200-206
D16S3107	67,657,922	67,658,221	(M13)GGGAATAAGCCAGACAAGAGG AGCCTGGGCAAGAGAGTG	297-323
16.4	68,948,712	68,948,927	(M13)TTTGGCAGAAAGGCTACTTCA CGCCATCCTCCACTATCTA	224-234
D16S3141	69,105,838	69,106,120	(M13)AAACTCTTTGGAAGGGAGTGG CCTAAAGACTGCCCTTGTTCC	314-334
D16S3095	69,946,150	69,946,411	(M13)ACCACTGCACCACTCTAGCC CTGAGTTCATCCTGGCCTTC	270-282
16.1	70,306,725	70,306,969	(M13)CCCACACTAGGTCCCTGAAA GCTAGGATGCACTGAAGACACA	210-238
16.19	70,563,887	70,564,103	(M13)AATTAGCTGGGTGTGGTGGT AGCATTGTGAGATCCCCATC	230-242
16.21	70,779,308	70,779,507	(M13)GCAAAGTCCAGCCTACCACT AAACACAGCCAGCAGAAGGT	208-222
16.5	70,860,578	70,860,745	(M13)GATCTCACACTGCTGGATGC GCATTTGGAGCTAAGATGTGG	176-192
D16S752	71,335,127	71,335,354	(M13)GGGGTCACTGCATTTTCATCT AGGATCGCTCTTTCCTTGT	242-262
D16S3106	72,187,732	72,188,021	(M13)TGGACCTTATACCTCTTTGATAACC AGGAGAGCTTTGCAACATCC	209-219
D16S3139	72,711,582	72,711,821	(M13)AAGACAAGGATACCCCACTTACC TGACTTCTGAGTATGAACTTTGTATCC	256-258
D16S3066	73,329,816	73,330,063	(M13)TGCCTACATTATTTCCAAACAGAA AAGCCACCTGTGTCTCTTGC	205-213
D16S512	74,067,713	74,067,915	(M13)TGAGAGCCAAATAAATAAATGG TCACGTTGTGAATGCAAGT	214-220
D16S3115	74,530,429	74,530,674	(M13)GGAGAATGGCTTTCTTGC CAACTCTATGATGGGGTTTTATTAC	261-267
16.13	74,775,616	74,775,846	(M13)TCCCAAAGTGCTCGGATTAC AGGCATTTCCATGTATGATGTG	237-265
11.1	63,967,764	63,968,180	(M13)AAGGTGACGAGACCTGTGG ACCCACCTTCCAATGTACTGC	331-357

11.2	64,471,993	64,472,242	(M13)CCTAGCCAGAGTCCACCTACTG GATGATGCCTGACTGCTGTACT	259-277
11.3	65,211,716	65,211,986	(M13)CCACCTGGTAGTCCTCAGAC CCCCTCCTGCTAGTGCTAAG	274-292
11.4	65,705,974	65,706,129	(M13)TTCTAGTAGGCAAACCAGGATG CAAGACCTGAGCCAGTGTACC	164-182
11.5	65,903,669	65,903,957	(M13)GCTGTTGCTTTCAGTGTTTGG ATGGTGCTCATCACTCCTAGC	300-308
17.1	34,630,044	34,630,317	(M13)GAATTGAGGGTCCCAATAAAGA GGTGGTCAGTTTCCCAAAGA	250-260
D17S1867	35,379,394	35,379,489	(M13)AGTTTGACACTGAGGCTTTG TTTAGACTTGGTAACTGCCG	108-114
D17S1788	36,086,054	36,086,208	(M13)TGCAGATGCCTAAGAACTTTTCAG GCCATGATCTCCCAAAGCC	171-181

Appendix 2. Critical region contains 113 known or predicted genes.

Positions are via NCBI 37.1. Genes are listed in sequence order on chromosome 16q21-22.1.

Location		Gene	Description
start	end		
65,318,402	65,610,203	<i>LOC283867</i>	hypothetical protein LOC283867
66,400,525	66,438,686	<i>CDH5</i>	cadherin 5, type 2, VE-cadherin (vascular endothelium)
66,460,816	66,516,745	<i>BEAN</i>	brain expressed, associated with Nedd4
66,503,966	66,583,842	<i>TK2</i>	thymidine kinase 2, mitochondrial
66,516,775	66,519,747	<i>FLJ27243</i>	FLJ27243 protein
66,586,466	66,603,693	<i>CKLF</i>	chemokine-like factor
66,600,294	66,613,040	<i>CMTM1</i>	CKLF-like MARVEL transmembrane domain containing 1
66,613,351	66,622,178	<i>CMTM2</i>	CKLF-like MARVEL transmembrane domain containing 2
66,637,935	66,647,795	<i>CMTM3</i>	CKLF-like MARVEL transmembrane domain containing 3
66,648,653	66,730,610	<i>CMTM4</i>	CKLF-like MARVEL transmembrane domain containing 4
66,754,796	66,785,701	<i>DYNCL1L2</i>	dynein, cytoplasmic 1, light intermediate chain 2
66,788,879	66,835,523	<i>CCDC79</i>	coiled-coil domain containing 79
66,836,778	66,864,900	<i>NAE1</i>	NEDD8 activating enzyme E1 subunit 1 (amyloid beta precursor binding protein 1)
66,878,280	66,888,052	<i>CA7</i>	carbonic anhydrase VII
66,914,436	66,921,855	<i>PDP2</i>	pyruvate dehydrogenase phosphatase isoenzyme 2
66,942,025	66,952,860	<i>CDHI6</i>	cadherin 16, KSP-cadherin
66,955,582	66,959,547	<i>RRAD</i>	Ras-related associated with diabetes
66,958,781	66,959,438	<i>LOC100287719</i>	hypothetical protein LOC100287719
66,965,959	66,968,320	<i>FAM96B</i>	family with sequence similarity 96, member B
66,968,347	66,978,999	<i>CES2</i>	carboxylesterase 2 (intestine, liver)
66,995,138	67,008,999	<i>CES3</i>	carboxylesterase 3 (brain)
67,022,633	67,043,661	<i>CES8</i>	carboxylesterase 8 (putative)
67,063,050	67,134,961	<i>CBFB</i>	core-binding factor, beta subunit
67,143,915	67,182,442	<i>C16orf70</i>	chromosome 16 open reading frame 70
67,183,180	67,184,388	<i>B3GNT9</i>	UDP-GlcNAc:betaGal beta-1,3-N-acetylglucosaminyltransferase 9
67,188,083	67,193,812	<i>TRADD</i>	TNFRSF1A-associated via death domain
67,193,864	67,198,077	<i>FBXL8</i>	F-box and leucine-rich repeat protein 8

67,197,288		67,203,848	<i>HSF4</i>	heat shock transcription factor 4
67,207,772		67,209,624	<i>NOL3</i>	nucleolar protein 3 (apoptosis repressor with CARD domain)
67,209,507		67,217,883	<i>KIAA0895L</i>	KIAA0895-like
67,218,282		67,224,107	<i>EXOC3L</i>	exocyst complex component 3-like
67,226,068		67,232,821	<i>E2F4</i>	E2F transcription factor 4, p107/p130-binding
67,233,014		67,237,932	<i>ELMO3</i>	engulfment and cell motility 3
67,241,042		67,260,951	<i>LRRC29</i>	leucine rich repeat containing 29
67,261,016		67,263,182	<i>TMEM208</i>	transmembrane protein 208
67,263,292		67,281,561	<i>FHOD1</i>	formin homology 2 domain containing 1
67,282,853		67,306,093	<i>SLC9A5</i>	solute carrier family 9 (sodium/hydrogen exchanger), member 5
67,289,522		67,290,572	<i>LOC100289262</i>	hypothetical protein LOC100289262
67,311,413		67,323,402	<i>PLEKHG4</i>	pleckstrin homology domain containing, family G (with RhoGef domain) member 4
67,323,393		67,360,661	<i>KCTD19</i>	potassium channel tetramerisation domain containing 19
67,360,747		67,419,103	<i>LRRC36</i>	leucine rich repeat containing 36
67,423,631		67,424,540	<i>LOC100287746</i>	hypothetical protein LOC100287746
67,423,712		67,427,438	<i>TPPP3</i>	tubulin polymerization-promoting protein family member 3
67,428,322		67,450,377	<i>ZDHHC1</i>	zinc finger, DHHC-type containing 1
67,465,041		67,471,456	<i>HSD11B2</i>	hydroxysteroid (11-beta) dehydrogenase 2
67,471,922		67,515,140	<i>ATP6V0D1</i>	ATPase, H+ transporting, lysosomal 38kDa, V0 subunit d1
67,516,474		67,517,716	<i>AGRP</i>	agouti related protein homolog (mouse)
67,562,720		67,580,689	<i>FAM65A</i>	family with sequence similarity 65, member A
67,596,310		67,673,086	<i>CTCF</i>	CCCTC-binding factor (zinc finger protein)
67,679,030		67,691,456	<i>RLTPR</i>	RGD, leucine-rich repeat, tropomodulin and proline-rich containing protein
67,691,433		67,694,718	<i>ACD</i>	adrenocortical dysplasia homolog (mouse)
67,694,851		67,696,680	<i>PARD6A</i>	par-6 partitioning defective 6 homolog alpha (C. elegans)
67,696,848		67,700,667	<i>C16orf48</i>	chromosome 16 open reading frame 48
67,700,719		67,702,660	<i>C16orf86</i>	chromosome 16 open reading frame 86
67,708,436		67,753,324	<i>GFOD2</i>	glucose-fructose oxidoreductase domain containing 2
67,757,005		67,840,555	<i>RANBP10</i>	RAN binding protein 10
67,840,781		67,861,971	<i>TSNAXIP1</i>	translin-associated factor X interacting protein 1
67,862,064		67,869,241	<i>CENPT</i>	centromere protein T
67,876,213		67,878,097	<i>THAP11</i>	THAP domain containing 11
67,880,635		67,906,470	<i>NUTF2</i>	nuclear transport factor 2

67,906,975	<i>EDC4</i>	67,918,406	enhancer of mRNA decapping 4
67,918,781	<i>NRNIL</i>	67,920,275	neuritin 1-like
67,927,175	<i>PSKHI</i>	67,963,581	protein serine kinase H1
67,963,473	<i>CTRL</i>	67,965,770	chymotrypsin-like
67,968,405	<i>PSMB10</i>	67,970,990	proteasome (prosome, macropain) subunit, beta type, 10
67,973,653	<i>LCAT</i>	67,978,414	lecithin-cholesterol acyltransferase
67,978,230	<i>SLC12A4</i>	68,002,555	solute carrier family 12 (potassium/chloride transporters), member 4
68,009,566	<i>DPEP3</i>	68,014,713	dipeptidase 3
68,021,296	<i>DPEP2</i>	68,034,489	dipeptidase 2
68,047,986	<i>LOC100131303</i>	68,049,814	similar to hCG1775037
68,055,174	<i>DDX28</i>	68,057,959	DEAD (Asp-Glu-Ala-Asp) box polypeptide 28
68,057,183	<i>DUS2L</i>	68,113,223	dihydrouridine synthase 2-like, SMM1 homolog (<i>S. cerevisiae</i>)
68,119,375	<i>NFATC3</i>	68,263,162	nuclear factor of activated T-cells, cytoplasmic, calcineurin-dependent 3
68,259,871	<i>ESRP2</i>	68,270,487	epithelial splicing regulatory protein 2
68,279,247	<i>PLA2G15</i>	68,294,965	phospholipase A2, group XV
68,289,785	<i>LOC100289329</i>	68,293,697	hypothetical protein LOC100289329
68,298,423	<i>SLC7A6</i>	68,335,722	solute carrier family 7 (cationic amino acid transporter, y+ system), member 6
68,332,063	<i>SLC7A6OS</i>	68,344,848	solute carrier family 7, member 6 opposite strand
68,344,945	<i>PRMT7</i>	68,391,169	protein arginine methyltransferase 7
68,392,230	<i>SMPD3</i>	68,482,591	sphingomyelin phosphodiesterase 3, neutral membrane (neutral sphingomyelinase II)
68,573,661	<i>ZFP90</i>	68,601,039	zinc finger protein 90 homolog (mouse)
68,678,151	<i>CDH3</i>	68,732,971	cadherin 3, type 1, P-cadherin (placental)
68,679,211	<i>LOC100132515</i>	68,680,065	similar to hCG2045429
68,771,128	<i>CDH1</i>	68,869,444	cadherin 1, type 1, E-cadherin (epithelial)
68,877,509	<i>TMCO7</i>	69,119,083	transmembrane and coiled-coil domains 7
69,140,160	<i>HAS3</i>	69,152,622	hyaluronan synthase 3
69,151,913	<i>CHTF8</i>	69,166,484	CTF8, chromosome transmission fidelity factor 8 homolog (<i>S. cerevisiae</i>)
69,166,418	<i>CIRH1A</i>	69,202,924	cirrhosis, autosomal recessive 1A (cirhin)
69,221,032	<i>SNTB2</i>	69,342,955	syntrophin, beta 2 (dystrophin-associated protein A1, 59kDa, basic component 2)
69,345,279	<i>VPS4A</i>	69,358,951	vacuolar protein sorting 4 homolog A (<i>S. cerevisiae</i>)
69,360,816	<i>COG8</i>	69,373,513	component of oligomeric golgi complex 8
69,373,343	<i>NIP7</i>	69,377,014	nuclear import 7 homolog (<i>S. cerevisiae</i>)
69,377,151	<i>TMED6</i>	69,385,712	transmembrane emp24 protein transport domain containing 6

69,389,464	<i>TERF2</i>	69,419,859	telomeric repeat binding factor 2
69,458,428	<i>CYB5B</i>	69,500,169	cytochrome b5 type B (outer mitochondrial membrane)
69,598,997	<i>NFA75</i>	69,738,569	nuclear factor of activated T-cells 5, tonicity-responsive
69,743,304	<i>NQO1</i>	69,760,707	NAD(P)H dehydrogenase, quinone 1
69,775,770	<i>NOB1</i>	69,788,829	NIN1/RPN12 binding protein 1 homolog (<i>S. cerevisiae</i>)
69,796,209	<i>WWP2</i>	69,975,644	WW domain containing E3 ubiquitin protein ligase 2
69,984,810	<i>CLEC18A</i>	69,998,141	C-type lectin domain family 18, member A
70,147,529	<i>PDP1</i>	70,195,205	pyruvate dehydrogenase phosphatase regulatory subunit
70,207,928	<i>CLEC18C</i>	70,220,796	C-type lectin domain family 18, member C
70,284,134	<i>EXOSC6</i>	70,285,833	exosome component 6
70,286,290	<i>AARS</i>	70,323,409	alanyl-tRNA synthetase
70,328,749	<i>DDX19B</i>	70,369,186	DEAD (Asp-Glu-Ala-As) box polypeptide 19B
70,380,732	<i>DDX19A</i>	70,407,284	DEAD (Asp-Glu-Ala-As) box polypeptide 19A
70,413,338	<i>ST3GAL2</i>	70,472,991	ST3 beta-galactoside alpha-2,3-sialyltransferase 2
70,488,498	<i>FUK</i>	70,514,177	fucokinase
70,514,472	<i>COG4</i>	70,557,459	component of oligomeric golgi complex 4
70,557,691	<i>SF3B3</i>	70,608,820	splicing factor 3b, subunit 3, 130kDa
70,680,468	<i>IL34</i>	70,694,585	interleukin 34
70,695,107	<i>MTSSL</i>	70,719,954	metastasis suppressor 1-like
70,721,342	<i>VAC14</i>	70,835,071	Vac14 homolog (<i>S. cerevisiae</i>)

Appendix 3. Primers for Sanger sequencing select candidate genes in critical region.

Positions are via NCBI 37.1. Primers 12-23 overlap and in total cover *FLJ27243*, *BEAN* exons 5 and 6, *tk2* exon 11, and the pentanucleotide repeat insertion. Primers 25-30 overlap and in total cover *tk2* exon 10.

Primer	Locus	Primers	Size	Start	End
1	<i>LOC283867</i> ex 9	5'-GGGGGATAGAGGGGTGAGG-3' 5'-GAGGGAGGGGTGAGGTGTAG-3'	192 bp	65,319,230	65,319,421
2	<i>LOC283867</i> ex 8	GCCTCCTGAGAAAGCACAGT GGGATATCGCCCTTTGTGAT	355	65,345,204	65,345,558
3	<i>LOC283867</i> ex 7	AGGTGGCTGAACATGAGCTT TGATACCCATCTTCCACATTGA	234	65,388,072	65,388,305
4	<i>LOC283867</i> ex 6	CATGAA TGA AACTATGAGGCAAA TTAGGGAGGGCAATATGCTTT	246	65,390,246	65,390,491
5	<i>LOC283867</i> ex 5	GCTTCTCCATTACAGAGTATGTG GGGACATTTTGTGTCAGC	300	65,397,003	65,397,302
6	<i>BEAN</i> ex 1	CCGCATCTCGGAGTGACC TCGAGTTCAGGCAGAAAACCT	752	66,460,897	66,461,648
7	<i>BEAN</i> ex 2	CTAGGTGTCAATGAACACCCCTT CACTTCGGGAAGGGCTGATACAG	807	66,471,041	66,471,847
8	<i>BEAN</i> ex 3, <i>tk2</i> ex 14	GTGAGGTGCTGCTCTCCTTC CCCATCCATTCCTCTCTTCA	838	66,503,331	66,504,168
9	<i>tk2</i> ex 13	GATGCTCCCTCTGGGAAGTC GAGACGGAGTCTCTCACTGTCTG	795	66,509,219	66,510,013
10	<i>BEAN</i> ex 4	ACTGCC TAGTCCAGGTTATCC CCACGGAAATAGCCAGATACTCC	821	66,511,182	66,512,002
11	<i>tk2</i> ex 12	CAACTCCATCATGGGAAAGAGT GAAGTCTCACTGTCGCTAAGG	825	66,511,676	66,512,500
12	see legend	GAGACCAGGGTGTCTGGTAGC GTGTTATGAGTCACTGTGTCATC	821	66,514,116	66,514,936
13	see legend	GGCACCTCCGACTCAGGCAG CCTGGAATCGAGAGATAGGCAC	803	66,514,587	66,515,391
14	see legend	TTTCACGGAACGTGGAGCTCTC TGTCCTGCAACACCCACGCTG	809	66,515,077	66,515,885
15	see legend	GCTATCTCTGACCGTGCAGGC GCTGCACGCAGGATGCTACAG	843	66,515,540	66,516,382
16	see legend	GTAACAGAGGTGATTCTCTGAAGA	699	66,516,067	66,516,755

17	see legend	GGAACCTTATGCACCTCTCTGAAAAG AAGCAGTTCTGACCACCTTAGT GCTTCAATGGTGCTTAATCTTGAG GTATGAACAATAGCTCACTGTAG GCATCTAGGACTATGTTAGTGGG CAACTTCAGGACCTGACTCTAG CCATGCCTAGTGATGTTCAGAAC TGGCTCTGCTGGCCTATCAC CTCACTCCAATCTGGTACTCCTG GATGGTGTCCAGCCAATGIGCTG AGCCTTACTCTGTATCAACCCCTC CCAAAGCAGGTCAACCACTGCAG ACCGTTCATGCCAAGAGCCTG ACATGCACATACACACTGG AGAGGATCTCTTTGTTTGGATT TGTCCTTGAGCCTCAGTGACC AGGAACTGCATCCGAGACC ATGCCAACCGTGCCAGAGC CCTAACGTGGAGTGATGGGTC CACCAGCTCTGCCTGCCGCA AGAAACAGGCCACAGCCTCTC AAGATTCCTGGTAGCAAAGGTT AGGTCCTGCTTGAACCTGCTGC GCAGCCTCGCCTTCAATGCAG CCTGACACCAACGCTGGAGCT GACTGTCCTTGGGAACTGCTC GTCTCCAGCTGTGAAAGGAGGA GTCCCGTTTGTCATTTACCCAC TTGCCACGTTGCCCAAGCTGG AGCAAGAGAAAGGAGGATTACT CAGTGTTTGTGCCACGAACC AACACCACTAAGCATGAGCACC CCAAAATCCACTGTGATCTGATGG GCAAGTGCCTCACCCACTGC GCAGTGGCATGATCATGACC GAAGTGGACACCTGGGCTGG CTCACCCCTATTTAGGTCCTGG	726 762 839 821 838 716 950 897 809 828 833 817 810 829 864 869 810 835	66,516,426 66,516,820 66,517,288 66,517,765 66,518,192 66,518,626 66,519,077 66,526,673 66,543,114 66,543,734 66,544,236 66,544,744 66,545,231 66,545,679 66,547,108 66,550,581 66,551,588 66,562,535	66,517,151 66,517,581 66,518,126 66,518,585 66,519,029 66,519,341 66,520,026 66,527,574 66,543,922 66,544,561 66,545,068 66,545,560 66,546,040 66,546,508 66,547,972 66,551,450 66,552,398 66,563,370
18	see legend				
19	see legend				
20	see legend				
21	see legend				
22	see legend				
23	see legend, <i>BEAN</i> ex 7				
24	<i>BEAN</i> ex 8				
25	see legend				
26	see legend				
27	see legend				
28	see legend				
29	see legend				
30	see legend				
31	<i>tk2</i> ex 9				
32	<i>tk2</i> ex 8				
33	<i>tk2</i> ex 7				
34	<i>tk2</i> ex 6				

35	<i>tk2</i> ex 5	GGGCACTAGAGGCAGGTCAG GGATCCCATCACCTAGGTACTG	841	66,565,101	66,565,941
36	<i>tk2</i> ex 4	CCACTGGGAATAGTATGGGATA GTGAGACAGGGAGCGTACTAAAG	814	66,570,621	66,571,434
37	<i>tk2</i> ex 3	GCAATGCAATGGCGTGATCTCA GCTCTCGTTAAGGAGGCAGGAC	835	66,575,378	66,576,212
38	<i>tk2</i> ex 2	GCCCAAACTACCTGAAAGGATA TGCTCACACTCTGGTGCCAGC	859	66,582,635	66,583,493
39	<i>tk2</i> ex 1	GGGAAAAGAGTAGAGCAAAGGA TCTCCATCCCAGAACCAAAG	816	66,583,625	66,584,440
40	<i>CMTM4</i> ex 4	AGGGGAAAGAGATCAAGGAA TGGAATCTGACAGGACAAGG	395	66,655,879	66,656,273
41	<i>CMTM4</i> ex 3	AGGTTGGGTATCGTGGGTCT AGGGGGAGCAGGACACAT	288	66,657,220	66,657,507
42	<i>DYNCL12</i> ex 1	CATCGCAGACCTAGAGGACA GACAAATGGCAAGAGTGGTCA	399	66,785,258	66,785,656
43	<i>NAE1</i> ex 20	AAATGCAGCAGTAGGGTGTC TGACAAAGTAACTTIGAAATAGCAAGC	630	66,836,663	66,837,292
44	<i>LOC100287719</i>	CAGCAGCAGCACCTTGTA AGTGCCTGGCCCTCCTAATC	575	66,958,793	66,959,367
45	<i>CES3</i> ex 5	CTTGGGTCCTTCCAGGT GACTCTGCCACCACCTTGAAGA	500	67,006,511	67,007,010
46	<i>CBFB</i> ex 5	GATTACAGGCGTGAGCCACT CACAAAGCCAGAGATACAACTTT	364	67,115,993	67,116,356
47	<i>LOC100289329</i>	CCATCCAGTGTCCCTTGAGT GCAGCGGACACATCGAGA	293	68,293,488	68,293,780
48	<i>ZFP90</i> ex 1	TCCCCGGAGATGTGGTTTA GACTGCTCCAAACACCCCTTG	244	68,573,563	68,573,806
49	<i>ZFP90</i> ex 2	TGATAGCTCCTGCAGTATGTCC ACCTAAGCTCTGGGCACCAC	297	68,591,817	68,592,113
50	<i>ZFP90</i> ex 3	AGGGTTCITTTGTCCACTTGC CAGCTGCTGGAGGGTATCTC	235	68,592,320	68,592,554
51	<i>ZFP90</i> ex 4	TGTCCTTCTTCATTCCTACTTAGC CATGGTGTTCCTTCCAGGAT	586	68,596,869	68,597,454
52	<i>ZFP90</i> ex 4	GCAATTTGGGACATAATGCAG TCGACTAAAGGCTTCCAC	563	68,597,260	68,597,822
53	<i>ZFP90</i> ex 4	GGTCCITTAGGCATGGCAC	529	68,597,725	68,598,253

54	ZFP90 ex 4	CCAGTATGAAATTCGTGTGATGCTC CCCCTATGATTGTGAGCAGG GATCCTGAATCAGAAACATTTTAGC	543	68,598,119	68,598,661
55	LOC100132515 ex 2	GTCCACACC AAAATGGTCAC GACCAATCAGCACCCACCT	567	68,679,148	68,679,714
56	LOC100132515 ex 1	CTCAACCCGACCCACATC CTCCCCGGAACTGAGGT	683	68,679,093	68,679,775
57	CDHI ex 1	GAACTGCAAAAGCACCTGTGA GTGACGACGGGAGAGGAAG	250	68,771,206	68,771,445
58	CDHI ex 4	GGTAGGTTGGACTGTTAGACC CACTGGGTCTTTTCCCTTTC	299	68,842,252	68,842,550
59	CDHI ex 15	AACTGAACATAGCCCTGTGTGTAT TTTTTCTCATTTTTGACACAACTCC	293	68,863,484	68,863,776
60	CDHI ex 16	AGACTTCTTGCCCCAGATGA AAGGGAAGGGAGCTGAAAAA	366	68,867,123	68,867,488
61	SNTB2 ex 1	TCACCGTCCGTGTTACCTC CGCCTGTGAGTGGTAGGAAG	1863	69,220,461	69,222,323
62	SNTB2 ex 2	TCCCAAAGTCTGGGATTAC CCCCAAAATGCATCTCTCA	499	69,279,355	69,279,853
63	TERF2 ex 4	GCGCCTGGCTTTATAAATGTT CCTTTCCCTAATTCCTCCACA	294	69,406,101	69,406,394
64	TERF2 ex 1	GCTCGGAAACGCTGTTTCTAT GACAAGCAAAGCTGGGAGAG	517	69,419,380	69,419,896
65	CYB5B ex 1	CTCAGTTAGCGGTGGAGAGG TCCCTTCCCTCCCCACATACA	283	69,458,564	69,458,846
66	CYB5B ex 2	TTCTTCCCAATTGCATCCTGT ACTGGGATGACAGGTGTGAG	397	69,480,902	69,481,298
67	CYB5B ex 3	CAAGGGACTCTGATATGCTCA AACCACACAGGGCATAGCTT	466	69,481,846	69,482,311
68	CYB5B ex 4	TTCCCAGTCTATCCATTGCTT GCTACCTGTCCATGCATCCT	491	69,492,825	69,493,315
69	CYB5B ex 5	CCCCAACTACTTTGTGATAAAAAGC GATGCTGTGGCCAAATCGTCTT	378	69,496,188	69,496,565
70	NFAT5 ex 10	TCTGGTAAGTACGCATATTTGTGG GGTGGTCATGTTTACCATTAGGA	370	69,704,012	69,704,381
71	NFAT5 ex 12	CCCACCTTGGAGATTGGAGAA CAATATGAAGATACCCTGCAAG	377	69,718,619	69,718,995

72	EXOSC6 ex 1.1	GTCAGGGAGGACTTGGGTTTC CACATGTCAGCCACCAGAGA	700	70,284,822	70,285,521
73	EXOSC6 ex 1.2	CAGCTGCTCAGACACAGGAT AACCAGGCCCTGACTGACTA	617	70,285,264	70,285,880

Appendix 4. *NOL3* primers.

Positions are via NCBI 37.1

Primer	Regions amplified	Start	End	Primers	Size
exon 1	5'UTR	67,207,688	67,208,005	5'-TGGATAAACGGGGTCTGAAC-3' 5'-TCTGACCACTCCCTCAATGC-3'	318 bp
exon 2	coding	67,207,986	67,208,427	GCATTGAGGGAGTGGTCAG CCTTTTGTCTGCCCCAGC	442
exon 3	coding	67,208,468	67,208,931	GAGTGTGAAACCGCACAGG TGGTCAAAGAGGTGGGGTC	464
exon 4.1	8bp coding, 3'UTR	67,208,851	67,209,382	GTGAGTCCGCCCAAACC G TTCAGCTCAGGAACTTGCG	532
exon 4.2	3'UTR	67,209,222	67,209,684	CCTTAGGAGTCCAGGCTGC CCTTTGGCCTTAGTTTTCCC	463

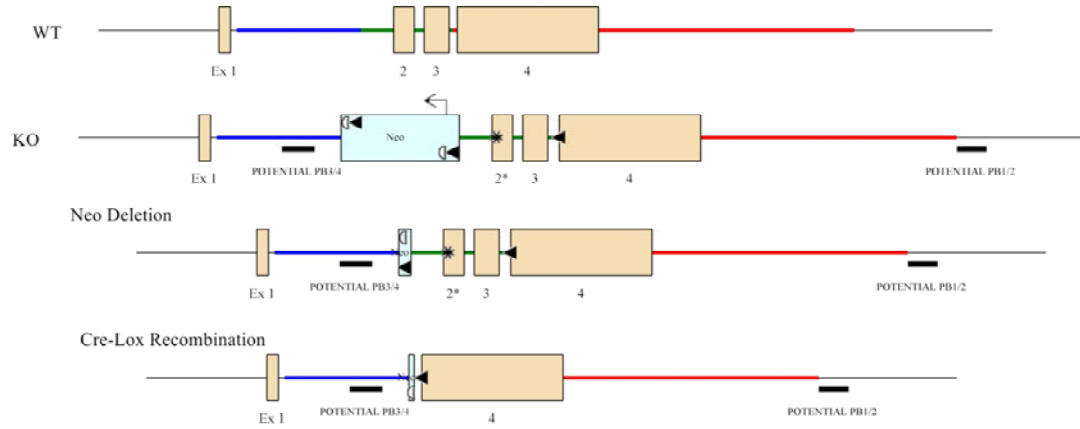
Appendix 5. Detailed characterization of knockin mouse generation.

A C57BL/6 BAC clone (RP23:80P23) was used to subclone an 8.94kb region into a 2.4kb backbone vector (pSP72, Promega) containing an ampicillin selection cassette. The construct was designed so that the 3' homology arm extended 5.81kb 3' to the 3' *LoxP* site. The 5' homology arm attaches to the 5' end of the *Neo* cassette flanked by *LoxP-FRT* sites. The 5' homology arm is 1.80kb. The *Neo* cassette was inserted 536bp upstream of the G→C point mutation in exon 2 of *Nol3*. The 3' *LoxP* site, which is located between exons 3 and 4, was engineered to contain Mfe I, BamHI, and BclI sites for Southern blot analysis; it is located 52bp downstream of exon 3.

The targeting vector was confirmed by restriction analysis after each modification step. P6 and T73 primers were used for sequencing the 5' and 3' ends of the BAC sub-clone, respectively. The N1 and N2 primers anneal within the *Neo* cassette and sequenced the 5' end of the target region and the 3' end of the short homology arm, respectively. The Lox1 and SQ1 primers ensured successful introduction of the G→C point mutation (see below) and ruled out the introduction of additional mutations by PCR.

<u>Primer</u>	<u>Sequence</u>
P6	5'-GAGTGCACCATATGGACATATTGTC-3'
T73	TAATGCAGGTAAACCTGGCTTATCG
N1	TGCGAGGCCAGAGGCCACTTGTGTAGC
N2	TTCCTCGTGCTTTACGGTATCG
Lox1	GGCAGTAGGTGTCTCGGTGC
SQ1	CTCCTGGTCAGCGTAGAGTAACGC

As shown below, Southern blots confirmed proper construction of the targeting vector. Moreover, successful introduction of the *E21Q* mutation was confirmed by Sanger sequencing of the G to C mutation (see below).

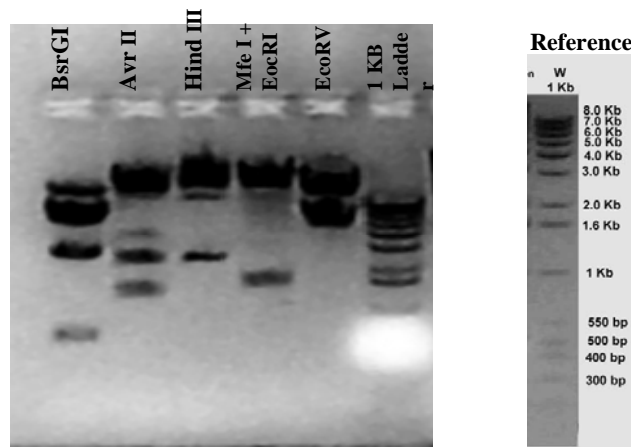


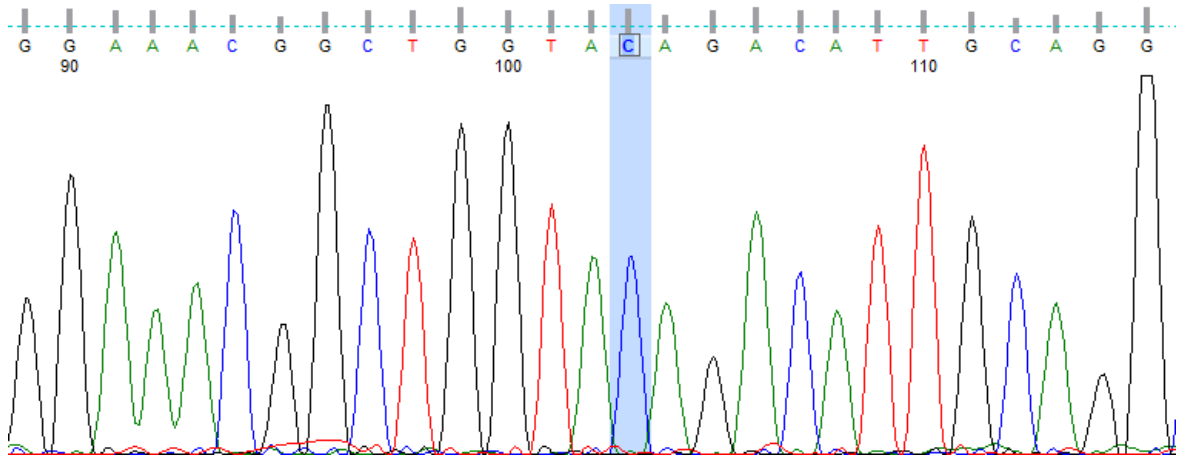
Long Arm External Probe		WT	KO	Neo Deletion (via FLP)	Cre Deletion of Target Region
Apa I	Neo cassette	14.55	13.12	11.59	10.15
Bcl I	Single LoxP	12.3	6.61	6.61	11.09
EcoRI	Neo cassette	10.99	7.7	7.7	9.79
Mfe I	Single LoxP	21.22	14.34	14.34	14.34
Xba I	Neo cassette	10.88	7.79	7.79	6.35

Short Arm Internal Probe		WT	KO	Neo Deletion (via FLP)	Cre Deletion of Target Region
Mfe I	Single LoxP	21.22	8.64	7.1	5.67
Bcl I	Single LoxP	12.3	7.46	5.92	11.09
Acc65I	Neo cassette	4.98	3.47	1.94	3.78
Stu I	Neo cassette	6.34	3.18	6.57	5.13
ApaI	Neo cassette	14.55	3.19	3.19	3.19

Expected Restriction Patterns

- Avr II:** 2124 1202 9710
- BsrG I:** 5580 513 2331 4612
- EcoR V:** 8802 4234
- Hind III:** 2149 10887
- Mfe I +EcoRI:** 1434 11602





UCSF LIBRARY RELEASE FORM

Publishing Agreement

It is the policy of the University to encourage the distribution of all theses, dissertations, and manuscripts. Copies of all UCSF theses, dissertations, and manuscripts will be routed to the library via the Graduate Division. The library will make all theses, dissertations, and manuscripts accessible to the public and will preserve these to the best of their abilities, in perpetuity.

I hereby grant permission to the Graduate Division of the University of California, San Francisco to release copies of my thesis, dissertation, or manuscript to the Campus Library to provide access and preservation, in whole or in part, in perpetuity.

Jonathan Foster Russell 3/4/2013
Author Signature Date